

**Photocatalytic and Biological Activities of Engineered Maize  
Biochar to Remove Aqueous Pollutants, Immobilize Soil Metals and  
Improve Plant Growth**



**Asif Kamal**

PhD

**Department of Plant Sciences  
Faculty of Biological Sciences  
Quaid-i-Azam University  
Islamabad Pakistan**

**2024**

**Photocatalytic and Biological Activities of Engineered Maize  
Biochar to Remove Aqueous Pollutants, Immobilize Soil Metals and  
Improve Plant Growth**



**A PhD dissertation submitted in the partial fulfillment for the degree of  
Doctor of Philosophy (PhD) in Plant Sciences**

**By**

**Asif Kamal**

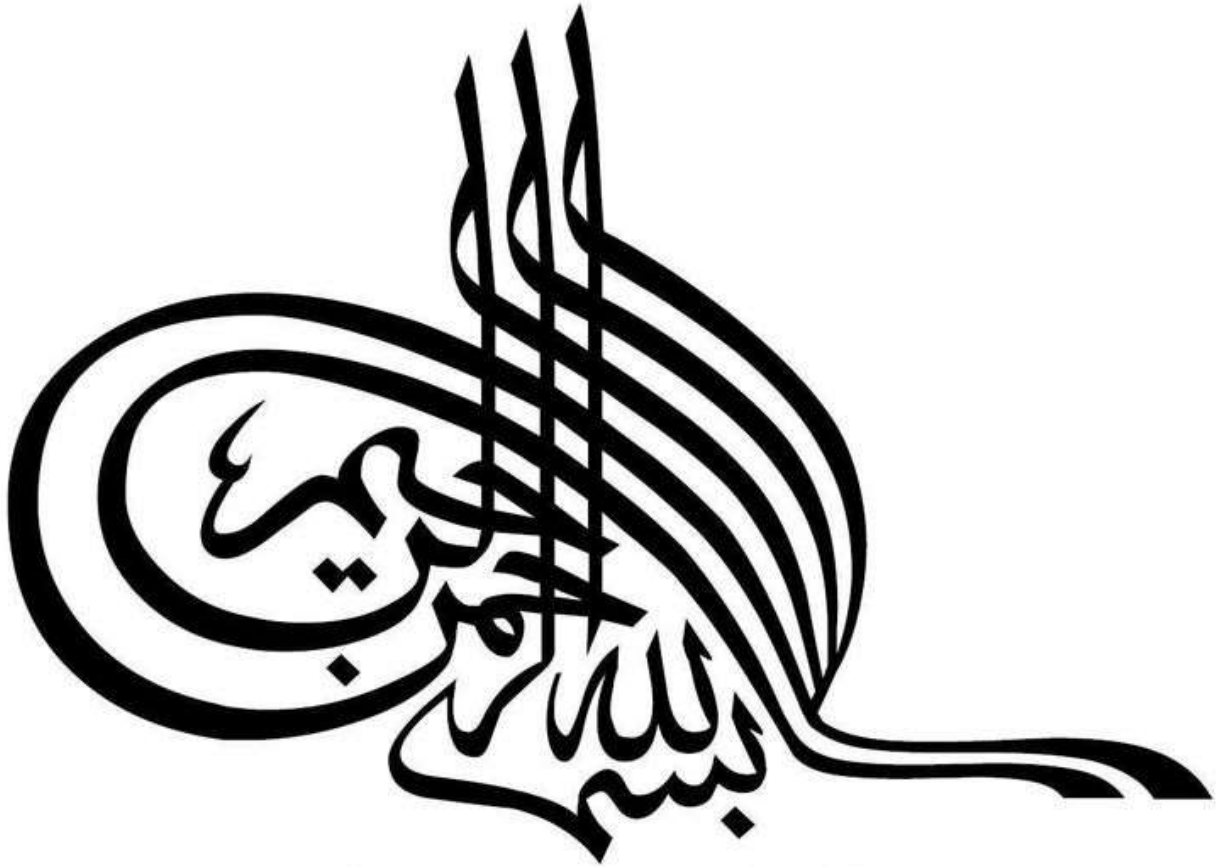
**Department of Plant Sciences**

**Faculty of Biological Sciences**

**Quaid-i-Azam University**

**Islamabad Pakistan**

**2024**



*In the name of Allah,  
the Most Beneficent,  
the Most Merciful*

*In the name of Allah, the Entirely Merciful, the Especially  
Merciful.*

*All the praise is due to Allah, Lord of worlds.*

*The Entirely Merciful, the Especially Merciful, Sovereign of  
the Day of Recompense.*

*It is You we worship and You we ask for help.*

*Guide us to the straight path. The path of those upon whom  
You have bestowed favour, not of those who have evoked Your  
anger or of those who are astray.*

*Surah Al-Fatiha*

## PLAGIARISM CERTIFICATE

It is certified that **Mr. Asif Kamal** (Registration No. **03042011004**) has submitted his PhD dissertation entitled “**Photocatalytic and Biological Activities of Engineered Maize Biochar to Remove Aqueous Pollutants, Immobilize Soil Metals and Improve Plant Growth**” and it has been checked on Turnitin for similarity index (plagiarism). Thesis plagiarism has been found to be 13%, which lies in the limit provided by HEC (19%).



**Prof. Dr. M. Farooq Hussain Munis**

Professor,

Department of Plant Sciences,

Quaid-i-Azam University,

Islamabad.

## DECLARATION OF ORIGINALITY

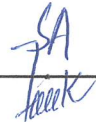
I hereby declare that the work accomplished in this thesis is the result of my own research carried out in the Molecular Plant Pathology Laboratory, Department of Plant Sciences, Quaid-i-Azam University, Islamabad. This thesis has not been published previously nor it contain material from the published resources that can be considered as violation of international copy right law. Furthermore, I also declare that I am aware of the terms “copyright” and “plagiarism”. If any copyright violation is found in this research work, I will be responsible for the consequences of any such violation.

  
**Asif Kamal**

## APPROVAL CERTIFICATE

This is to certify that the research work in this thesis, entitled “**Photocatalytic and Biological Activities of Engineered Maize Biochar to Remove Aqueous Pollutants, Immobilize Soil Metals and Improve Plant Growth**” was conducted by **Mr. Asif Kamal** under the supervision of **Dr. Muhammad Farooq Hussain Munis**. No part of this thesis has been submitted anywhere else for any other degree. This thesis is submitted to **Department of Plant Sciences, Faculty of Biological Sciences, Quaid-i-Azam University, Islamabad** in partial fulfilment of requirements for the degree of **Doctor of Philosophy** in the field of **Plant Sciences**.

Asif Kamal (Student)

Signature: 

### Examination Committee

a) **External Examiner 1:**

**Dr. Muhammad Ibrar Shinwari**  
Associate Professor  
Biosciences, CIRBS  
Alfarabi Research Complex,  
Islamic International University  
Islamabad, Pakistan

Signature: 

b) **External Examiner 2:**

**Dr. Muhammad Akmal**  
Associate Professor  
Institute of Soil and Environmental Sciences  
PMAS-Arid Agriculture University  
Rawalpindi, Pakistan

Signature: 

a) **Internal Examiner**

**Dr. M. Farooq Hussain Munis**  
Professor  
Quaid-i-Azam University, Islamabad


Signature: 

**Prof. Dr. M. Farooq Hussain Munis (Supervisor)**

Signature: 

Department of Plant Sciences

**Prof. Dr. Mushtaq Ahmad (Chairperson)**

Signature: 

Dated: 03/04/2024

## ***DEDICATED TO***

*My Most Loving Parents*

***Mr. Hamid Kamal & Mrs. Yasmin Bibi***

*Who opened up avenues for me to learn and their loving support in every aspect enabled me to achieve my goals. My success is all yours. I love you both the most. I don't have strength to write late in front of your name Ammi. You are alive in my heart always.*

*My Most Supportive Friend*

***Dr. Moona Nazish***

*Who, supported me gave and me courage to dream high.*

*My Most Beloved Grand Parents*

***Mr. Baid Ullah jan (Late) and Mrs. Bibi Ayesha***

*Whose selfless love will always be cherished but can never be repaid.*

*My Loving, Caring and Supportive Brothers and Sister*

***Engr. Anwar Kamal***

***Khalid Kamal***

***Wali Ullah***

***Yumna Kamal***

*My Very Dear Niece*

***M. Awais Khan***



## ACKNOWLEDGEMENTS

*Begin with Allah's name, who is the Most Merciful and the Most Gracious. "Almighty Allah" deserves all of the glory. Thank you, Allah, for providing me with the ability to seek knowledge and explore some of the numerous parts of His creation. I am grateful for my abilities and His guidance in completing this thesis. He has always lavished me with more than I deserve. Innumerable salutation to the **Holy Prophet (Peace Be Upon Him)**, wellspring of wisdom and benefits for all of creation, who has directed his Ummah to seek knowledge from cradle to grave and enabled me to gain honor in life.*

*First and foremost, I would like to express my heartfelt gratitude to my supervisor, **Prof. Dr. Muhammad Farooq Hussain Munis**, Department of Plant Sciences, Quaid-i-Azam University, Islamabad, for his supreme bearing, valiance, expert guidance, friendly advice, sympathetic attitude, enlighten supervision, vital assessment, brilliant comments, constant sponsorship in any more unfortunate situation, and providing an excellent atmosphere throughout the entire time. This dissertation would not have been completed without his guidance and active participation at every step. His guidance on both studies and my career has been invaluable. He has been a fantastic mentor to me. I credit his support and effort for my PhD degree. I could not have asked for a better or nicer supervisor. From the bottom of my heart, I shall be eternally grateful for your unwavering support.*

*I pay special gratitude to **Mr. Wahab Khan Shalmani**, manager of Zarai Taraqiati Bank Limited farm, Islamabad, Pakistan, for his continued guidance, encouragement, and critical suggestions and for providing samples for research. I am deeply indebted to **Dr. Qaiser Hussain** at the Institute of Soil and Environmental Sciences, PMAS-Arid Agriculture University Rawalpindi for their continuous support and for providing a good and friendly working atmosphere.*

*I express my thanks to **Dr. Sarwat Jahan**, Dean, Faculty of Biological Sciences, and **Dr. Mushtaq Ahmad**, Chairperson, Department of Plant Sciences, Faculty of Biological Sciences, Quaid-i-Azam University, Islamabad, for providing the support and equipment. I would like to special thanks to **Dr. Hassan Javed Chaudhary** and **Dr. Umar Masood Quraishi** for their guidance and very nice attitude and also thankful to **Dr. Imran** (Department of Microbiology) for provision of equipment facility.*

*My special thanks to my sister **Farzana** for being my constant supporter. For all your efforts, love, and support. Without your contribution, this would never be possible. Thank you for trusting me and standing by my side always. I cannot thank Allah Pak enough for having a partner like you. Most notably, it would not have been achieved without the support and patience of you who has been a regular source of support, my success is dedicated to you.*

*Most importantly, none of this would have been possible without the love and patience of my family to whom this dissertation is dedicated to, has been a constant source of love, concern, support and strength all these years. I would like to express my heart-felt gratitude to my family, they have aided and encouraged me throughout this endeavor. I have no suitable word that can fully describe their everlasting love for me. Special thanks to **Ami and Abu** for their prayers, endless love and sincere support. They have helped me financially, morally, and spiritually. They always gave me words of encouragement. I wish I could have achieved this degree in my mother's life. May his soul rest in eternal peace. I miss her existence everywhere in my life. I am also grateful to my dear brothers **Anwar Kamal, Khalid Kamal, and Wali Ullah**, sweet and loving sisters **Farzana, Nadia, and Yumna**, and my niece **M. Awais Khan** for always feeling proud of me, for always supporting me, for always loving me unconditionally, for always boosting me up. I love you all.*

*My sincere thanks and deep appreciations go to my most supportive friend **Dr. Moona Nazish** Who supported me always and gave me courage to dream high and also to other friends **Asif kamal, Khushdil Khan, Shabir Ahmed, Abdullah, Nabeel ur Rehman, M. Sameer Shehzada, and M. Kaleem** who had the utmost confidence in my abilities and with whom I spent a lot of time discussing my work. Who helped me throughout my research work. Who stood with me in every thick and thin. They helped me to face my failures. Special thanks to **Dr. Kinza** who helped me to initiate my work. Special prayers for her.*

*No acknowledgment could ever adequately express my feelings to my affectionate and adorable friends plus sisters. It's my fortune to gratefully acknowledge the support of some special individuals. Words fail me to express my appreciation to **Dr. Munazza Yousra** and **Dr. Anila Iqbal** for their support. They always push me and motivate me. Thank you doesn't seem sufficient, but it is said with appreciation and respect to both for their support, encouragement, and understanding.*

*Thank you dear for being with me. The good times spent with them can never be erased from my memories.*

*Very special and deepest thanks to my seniors and juniors and my lab family members **Mahnoor, Farhan, Maryam Anar, Dr. Musrat Ali, M. Asad Farooq, Kinza, Zimen Ahmed, Syeda Gul Nisa, Rabia Nawab, Mohammad Sameer Zubair, Junaid Ahmed, Fareeha Anwar, Faryal Niazi, Meekal Mustafa, Saamia Sajid, Saira, Amna Zahid, Afia, Hira Saleem, Hassna, Aatra, Hira Jabeen, Kanwal, Abdul Rehman, Hassaan, Sidra, Mishal, Namra, Nosheen, Tooba Idrees and Sohail** for their support, motivation and cooperation, and for helping me in very tough time without their assistance I could never complete this task.*

*In the end I want to present my unbending thanks to all those hands who prayed for my betterment and serenity.*

***Asif Kamal***

# CONTENTS

## CHAPTER 1

## INTRODUCTION

	<b>Page no.</b>
1.1 Biochar	01
1.2 Production of Biochar	02
1.2.1 Pyrolysis	02
1.3 Sources for Biochar production	03
1.3.1 Forest and Agricultural Residues	04
1.3.2 Industrial and Municipal Waste	04
1.3.3 Nonconventional materials	04
1.4 Preparation of Engineered Biochar	05
1.4.1 Biochar-based Hybrid Nanomaterials	06
1.4.1.1 Zinc oxide and Zinc oxide-nanocomposite	07
1.4.1.1.1 Synthesis of Biochar-Zinc Oxide Nanocomposite	08
1.4.2 Production of <i>Trichoderma harzianum</i> Loaded Biochar	11
1.5 Pollution	12
1.5.1 Water Pollution	13
1.5.2 Soil Pollution	13
1.5.3 Causes of Water and Soil Pollution	14
1.5.3.1 Agricultural Pollutants	14
1.5.3.2 Heavy Metals	16
1.5.3.3 Industrial and Laboratory Effluents	17
1.6 Application of Engineered Biochar	19
1.6.1 Photocatalysis against Environmental Pollutant	19
1.6.2 Biomedical and Therapeutic Application	20
1.6.3 Application in Crops Disease Control	21
1.6.4 <i>Trichoderma harzianum</i> Loaded Biochar for metal immobilization of Heavy Metals (HMs)	22
1.6.5 Use of Nanocomposite in Cd-Cu Immobility	23
1.7 Egyptian Riverhemp ( <i>Sesbania sesban</i> Linn.)	25
1.7.1 Habitat	25

1.7.2	Distribution	26
1.7.3	Morphological Description	26
1.7.4	Uses of <i>S. sesban</i> Linn.	27
1.7.5	Medicinal Usage	27
1.7.6	Antioxidant and Phytochemical Properties	27
1.8	Aims and Objectives	28

## **CHAPTER 2 MATERIALS AND METHODS**

### **2.1 EXPERIMENT 1: BALL-MILLED SYNTHESIS OF MAIZE BIOCHAR-ZNO NANOCOMPOSITE (MB-ZnO) AND ESTIMATION OF ITS PHOTOCATALYTIC ABILITY AGAINST DIFFERENT ORGANIC AND INORGANIC POLLUTANTS**

2.1.1	Plant Material	29
2.1.2	Synthesis of Biochar	29
2.1.3	Preparation of Nanocomposite	29
2.1.4	Characterization of MB-ZnO Nanocomposite	30
2.1.5	Adsorption and Photocatalysis Performances against Organic and Inorganic Pollutants	30
2.1.5.1	Stock Solutions of Pollutants	30
2.1.5.2	Adsorption experiments in dark conditions	30
2.1.5.3	Photocatalysis Experiment	31
2.1.5.4	Total Organic Carbon Analysis (TOC)	32
2.1.5.5	Kinetic Study	32

### **2.2 EXPERIMENT 2: BIOLOGICAL APPLICATIONS OF BALL-MILLED SYNTHESIZED BIOCHAR-ZINC OXIDE NANOCOMPOSITE USING *ZEA MAYS* L.**

2.2.1	Biocompatibility Assays	33
2.2.2	Protein Kinase Inhibition Potential (PK)	34
2.2.3	Alpha-amylase (AA) Inhibition Potential	34
2.2.4	Antileishmanial Assay of MB-ZnO nanocomposite	35

2.2.5	Anti-inflammatory Assay	35
2.2.6	Antioxidant Activities	36
2.2.6.1	Total Antioxidant Capacity Determination (TAC)	36
2.2.6.2	Total Reducing Power Determination (TRP)	36
2.2.6.3	Free Radical Scavenging Assay (FRSA)	36
2.2.7	Antifungal Assay	37
2.2.8	Statistical Analysis	37

### 2.3 EXPERIMENT 3: DIAGNOSIS AND CONTROL OF BROWN LEAF SPOT OF KIWI (*ACTINIDIA DELICIOSA*) USING BIOCHAR-ZINC OXIDE (MB-ZnO) NANOCOMPOSITE AS A NON-TOXIC BIO-FUNGICIDES

2.3.1	Field Observation	38
2.3.2	Isolation of Disease-Causing Agent from Infected Leaves	39
2.3.3	Microscopic Recognition	39
2.3.4	Molecular Analysis	39
2.3.5	Phylogenetic study by MEGA 7.0	40
2.3.6	Pathogenicity Assessment	40
2.3.7	Synthesis of MB-ZnO	40
2.3.8	In vitro antifungal activity of MB-ZnO	40

### 2.4 EXPERIMENT 4: *TRICHODERMA HARZIANUM* SUPPLEMENTED BIOCHAR PRODUCTION TO ENHANCE METAL STABILIZATION AND ENZYMATIC ACTIVITY IN CONTAMINATED SOIL

2.4.1	Synthesis of Biochar	42
2.4.2	Preparation of <i>Trichoderma harzianum</i> Loaded Biochar	42
2.4.3	Soil Incubation Testing	42
2.4.4	Tessier Sequential Extraction of Heavy Metals from the Soil	43
2.4.5	Phyto-availability of Heavy Metals in the Contaminated Soil	43
2.4.6	Bio-accessibility of Heavy Metals in the Soil	44
2.4.7	Soil Enzymatic y Study	44
2.4.8	Data Analysis	45

### 2.5 EXPERIMENT 5: USE OF ENGINEERED BIOCHAR AGAINST THE MOBILIZATION OF Cd-Cu AND INVESTIGATION OF BIOCHEMICAL AND

ENZYMATIC ALTERATIONS INDUCED BY THESE TWO HEAVY METALS IN *SESBANIA SESBAN* (L.) Merr.

2.5.1	Collection of Soil and Amendments	46
2.5.2	Preparation of Soil	46
2.5.3	Characterization of Soil	46
2.5.4	Amendments of Soil	46
2.5.5	Preparation of Maize Straw Biochar	47
2.5.6	Preparation of Engineered Biochar	48
2.5.7	Experimental Design	48
2.5.8	Application of MB-ZnO Nanocomposite	48
2.5.9	Harvesting of Plants for Experimental Analysis	48
2.5.10	Physiological Parameters	49
2.5.11	Biochemical Parameters	49
2.5.11.1	Total Soluble Sugar	49
2.5.11.2	Protein Content of Leaves	49
2.5.11.3	Estimation of Proline Content	49
2.5.11.4	Estimation of Chlorophyll Content	50
2.5.11.5	Relative Water Content (RWC)	50
2.5.11.6	Relative Electrolyte Leakage	50
2.5.12	Antioxidant Assay	50
2.5.12.1	Peroxidase (POD)	50
2.5.12.2	Superoxide Dismutase (SOD)	51
2.5.12.3	Hydrogen Peroxide Content (H <sub>2</sub> O <sub>2</sub> )	51
2.5.12.4	Malondialdehyde (MDA) Content	51
2.5.13	Anatomical Parameter	51
2.5.13.1	Leaf Epidermal Anatomical Study (LM)	51
2.5.14	Statistical Analysis	52

## CHAPTER 3

## RESULTS

3.1	Experiment 1	
	3.1.1. Graphical Abstract	53

3.1.2	Characterization of Synthesized Nanocomposite	53
3.1.2.1	SEM and EDX Study	53
3.1.2.2	XRD Analysis	55
3.1.2.3	FTIR Analysis	55
3.1.2.4	Thermogravimetric Analysis	56
3.1.2.5	Optical Properties Analysis	57
3.1.3	Removal of Saf and MC via MB-ZnO nanocomposite	59
3.1.3.1	Degradation Rate of Pollutants	63
3.1.3.2	Comparison of Photodegradation of Saf and MC in various Light Conditions	65
3.1.3.3	Mineralization of Pollutants	66
3.1.3.4	Reaction kinetics	67
3.2	Experiment 2	
3.2.1	Graphical Abstract	69
3.2.2	SEM and EDX Analysis	69
3.2.3	XRD Study	70
3.2.4	FTIR Spectroscopy	71
3.2.5	Thermogravimetric Analysis	72
3.2.6	UV Analysis	73
3.2.7	Antioxidant activity of MB-ZnO Nanocomposite	74
3.2.8	Anti-Inflammatory Assay	75
3.2.9	Enzyme Inhibition Activities	77
3.2.10	Biocompatibility Assay	78
3.2.11	Antileishmanial Potential	80
3.2.12	Antifungal Assay	81
3.3	Experiment 3	
3.3.1	Graphical Abstract	83
3.3.2	Isolation and Identification of the Disease-Causing Pathogen	83
3.3.3	Pathogenicity test	84
3.3.4	Molecular confirmation and Phylogenetic Study	84
3.3.5	Illustrations of MB-ZnO	86
3.3.5.1	SEM and EDX Study	86



3.3.5.2	XRD Study	87
3.3.5.3	FTIR Spectroscopy	88
3.3.5.4	UV Analysis	89
3.3.5.5	Thermo Gravitational Analysis	89
3.3.6	Antifungal Assay of MB-ZnO	89
3.4	Experiment 4	
3.4.1	Graphical Abstract	92
3.4.2	Properties of Soil	92
3.4.3	Characterization of Fungus ( <i>T. harzianum</i> ) Loaded Biochar (MBT)	92
3.4.4	Fluctuations in Soil pH	94
3.4.5	Cd and Cu Fractionation in a Treated Soil	95
3.4.6	Phyto-availability of Cu and Cd	98
3.4.7	Bio-accessibility of Cd and Cu	99
3.4.8	Effect of Biochar Amendments on Enzymatic Activities of Soil	101
3.4.9	Mechanisms and Effects	103
2.5	Experiment 5	
3.5.1	Graphical Abstract	104
3.5.2	Physiological Parameters	104
3.5.2.1	Root and Shoot Length	104
3.5.2.2	Fresh and Dry Weight	105
3.5.3	Biochemical Parameters	106
3.5.3.1	Chlorophyll a,b and Carotenoids	106
3.5.3.2	Relative Water Contents (RWC) and Relative Electrolyte Leakage (REL)	107
3.5.3.3	Malondialdehyde (MDA) and Hydrogen peroxide (H <sub>2</sub> O <sub>2</sub> )	107
3.5.3.4	Total soluble sugar, leaf protein contents and Proline Content	108
3.5.3.5	Cadmium and Copper Level in <i>Sesbania</i>	109
3.5.4	Antioxidant Enzyme Assays	109
3.5.5	Anatomical Assay	111

<b>CHAPTER 4</b>	<b>DISCUSSION</b>	113
5.1	Conclusion	124
5.2	Future Prospectus	126
<b>CHAPTER 5</b>	<b>REFERENCES</b>	129

## LIST OF TABLES

<b>S. no.</b>	<b>Title</b>	<b>Page No.</b>
1.1	Classification of <i>Sesbania sesban</i> Linn.	26
2.1	Properties of the pure biochar and soil	47
3.1	Assessment of Saf and MC removal efficacies attained in the present work and already available literature	60
3.2	Selected properties of the pure biochar and soil	93

## LIST OF FIGURES

S.no.	Title	Page No.
1.1	Chemical structure of Mancozeb	16
1.2	Chemical structure of Safranin	18
2.1	Sample collection area	38
3.1	Schematic Demonstration of Complete Experiment	53
3.2	SEM images of pure biochar (A) and MB-ZnO nanocomposite (B)	54
3.3	EDX spectra and elemental analysis of MB-ZnO nanocomposite	54
3.4	XRD analysis of MB-ZnO nanocomposite	55
3.5	FTIR spectra of MB-ZnO nanocomposite	56
3.6	TGA of pure biochar (A) and MB-ZnO nanocomposite (B)	57
3.7	UV study of pure biochar (A), ZnO alone and MB-ZnO nanocomposite (B)	58
3.8	Band gap study of MB-ZnO	59
3.9	Plot of Saf removal at various time duration in dark conditions (A), UV light (B), and visible light (C) sources	61
3.10	Pure Saf and treated solution at different time duration	62
3.11	Plot of Mancozeb removal at various time duration in dark condition (A), UV light (B), and visible light (C)	63
3.12	Pure MC and treated solution at different time duration	63
3.13	Efficiency-time degradations of MB-ZnO nanocomposite as a photocatalyst against Saf (A), and MC (B), in various light conditions	65

3.14	Degradation efficacy of MB-ZnO in various light conditions against Saf (A) and MC (B)	66
3.15	Plot of TOC removal efficacy vs irradiation time of Saf (A) and (B) MC	67
3.16	Plots $\ln C_t/C_0$ versus time (A) absorbance of Saf and (B) MC	68
3.17	Schematic Illustration of Complete Experiment	69
3.18	SEM images of pristine biochar (A) and MB-ZnO (B)	70
3.19	XRD patterns of MB-ZnO nanocomposite	71
3.20	FTIR analysis of MB-ZnO	72
3.21	Thermogravimetric Analysis of biochar (A) and MB-ZnO (B)	73
3.22	UV study of pristine biochar (A), pure ZnO and MB-ZnO (B)	74
3.23	Antioxidant potential of MB-ZnO	75
3.24	Anti-inflammatory activity of MB-ZnO nanocomposite	76
3.25	Inhibition activity of MB-ZnO nanocomposite against PK (A) and AA activities (B)	78
3.26	Biocompatibility of MB-ZnO in case of human RBCs and macrophages	79
3.27	Antileishmanial potential of MB-ZnO at various concentrations	81
3.28	Antifungal potential of MB-ZnO nanocomposite	82
3.29	Schematic Representation of Complete Experiment	83
3.30	Leaf spots were examined on the Kiwi leaves (A). Disease causing pathogen was grown in plates and observed from front side (B) and reverse side (C). A microscopic study was performed at magnification of 40× (D). Healthy leaves were injected with the isolated pathogen, and disease symptoms were developed after 3 days (E) and 5 days (F) of inoculation. Disease causing pathogen was re-isolated and observed from front (G) and back (H) side of plates	85
3.31	Phylogenetic analysis of isolated <i>R. oryzae</i> sequence with 14 closely associated ITS sequences after BLAST study	85
3.32	Phylogenetic analysis of isolated <i>R. oryzae</i> sequence with 16 closely related EF-1 $\alpha$ sequences after BLAST analysis.	86

Subsequent from 1,000 replicates, bootstrap values are presented at the branch points

3.33	SEM micrograph of pure MB (A) and MB-ZnO (B)	87
3.34	XRD spectroscopy of MB-ZnO	88
3.35	FTIR analysis of MB-ZnO	88
3.36	UV spectra of ZnO NPs and MB-ZnO nanocomposite	89
3.37	Antifungal activity of MB-ZnO nanocomposite. C (control), T1 (6 mg/ml), T2 (12 mg/ml), T3 (19 mg/ml)	91
3.38	Effect of different application rates of MB-ZnO nanocomposite on the growth of <i>R. oryzae</i> . (A) Control, (B) 19 mg/mL application rate, (C) 12 mg/ML application rate, (D) 6 mg/mL application rate	91
3.39	Schematic Diagram of Complete Experiment	92
3.40	SEM images of pure biochar (A), <i>T. harzianum</i> (B), and <i>T. harzianum</i> loaded biochar (C)	93
3.41	Fluctuations in soil pH after the addition of maize biochar (MB) and fungus-loaded biochar (MBT). CT shows control sample; MB1, MB5, MBT1 and MBT5 indicates the soil samples treated with 1% MB, 5% MB, 1% MBT and 5% MBT, respectively	95
3.42	Cd (A) and Cu (B) speciation in the contaminated soil	98
3.43	Fluctuations in DTPA-Cu (A) and DTPA-Cd (B) in a treated soil	99
3.44	Bio-accessibility of Cd (A) and Cu (B) in stomach phase, and Cd (C) and Cu (D) in intestinal phase after 90 days of incubation	101
3.45	Impact of MB and MBT on the activities of urease (A) and catalase (B) in the soil	103
3.46	Schematic Depiction of Complete Experiment	104
3.47	Effects of MB-ZnO on Root and Shoot of <i>S. sesban</i> in Cd-Cu stressed soil; C (Control), T1 (0 mg/L), T2 (50 mg/L), T3 (75 mg/L), T4 (100 mg/L)	105
3.48	Effects of MB-ZnO on Fresh and Dry weight of <i>S. sesban</i> in Cd-Cu stressed soil. C (Control), T1 (0 mg/L), T2 (50 mg/L), T3 (75 mg/L), (100 mg/L)	105

3.49	Effects of MB-ZnO on Chlorophyll a, Chlorophyll b, and Carotenoids contents of <i>S. sesban</i> in Cd-Cu stressed soil. C (Control), T1 (0 mg/L), T2 (100 mg/L), T3 (150 mg/L), (200 mg/L)	106
3.50	Effects of MB-ZnO on RWC, and REL of <i>S. sesban</i> in Cd-Cu stressed soil. C (Control), T1 (0 mg/L), T2 (50 mg/L), T3 (75 mg/L), (100 mg/L)	107
3.51	Effects of MB-ZnO on MDA, and H <sub>2</sub> O <sub>2</sub> of <i>S. sesban</i> in Cd-Cu stressed soil. C (Control), T1 (0 mg/L), T2 (50 mg/L), T3 (75 mg/L), (100 mg/L)	108
3.52	Effects of MB-ZnO on Sugar, Proline and H <sub>2</sub> O <sub>2</sub> of <i>S. sesban</i> in Cd-Cu stressed soil. C (Control), T1 (0 mg/L), T2 (50 mg/L), T3 (75 mg/L), (100 mg/L)	108
3.53	Effects of MB-ZnO on Cd concentration in Roots and Shoots of <i>S. sesban</i> in Cd-Cu stressed soil. C (Control), T1 (0 mg/L), T2 (50 mg/L), T3 (75 mg/L), (100 mg/L)	109
3.54	Effects of MB-ZnO on Cu concentration in Roots and Shoots of <i>S. sesban</i> in Cd-Cu stressed soil. C (Control), T1 (0 mg/L), T2 (50 mg/L), T3 (75 mg/L), (100 mg/L)	110
3.55	Effects of MB-ZnO on POD, SOD and CAT of <i>S. sesban</i> in Cd-Cu stressed soil. C (Control), T1 (0 mg/L), T2 (50 mg/L), T3 (75 mg/L), (100 mg/L)	110
3.56	Effects of MB-ZnO on leaf anatomy of <i>S. sesban</i> in Cd-Cu stressed soil; C (Control), T1 (0 mg/L), T2 (50 mg/L), T3 (75 mg/L), (100 mg/L)	112

---

## LIST OF ABBREVIATIONS

AA	Alpha-amylase
ATP	Adenosine triphosphate
BC-ZnO	Biochar-ZnO nanocomposite
BLAST	Basic local alignment search tool
BSA	Bovine serum albumin
CaCO <sub>3</sub>	Calcium Carbonate
CaCl <sub>2</sub>	Calcium Chloride
CAT	Catalase
CB	Carbonate bound
Cd	Cadmium
CEC	Cation exchange capacity
Chl	Chlorophyll
cm	Centimeter
CO <sub>2</sub>	Carbon dioxide
CTAB	Cetyltrimethyl ammonium bromide
Cu	Copper
°C	Degree Celsius
dNTP	Deoxyribonucleotide triphosphate
DMSO	Dimethyl sulfoxide
DNA	Deoxyribonucleic acid
DPPH	2,2-diphenyl-1-picrylhydrazyl
DTPA	Diethylenetriamine penta acetic acid
DW	Dry weight
°E	Degrees east



EBDC	Ethylene bisdithiocarbamate
EC	Electrical conductivity
EDX	Energy-dispersive X-ray spectroscopy
EDTA	Ethylenediamine tetraacetic acid
EF-1 $\alpha$	Elongation factor 1-alpha
EPA	Environmental Protection Agency
ETU	Ethylenethiourea
EX	Exchangeable
FDA	Food and drug administration
FRSA	Free radical scavenging assay
FT-IR	Fourier transform infrared spectroscopy
FW	Fresh weight
g	Gram
Hb	Hemoglobin
Hcl	Hydrochloric acid
HMs	Heavy metals
H <sub>2</sub> O <sub>2</sub>	Hydrogen peroxide
ITS	Inter transcribed region
L	Litre
LM	Light microscopy
MB	Maize biochar
MBT	<i>Trichoderma</i> loaded biochar
MB-ZnO	Maize biochar-ZnO nanocomposite
MC	Mancozeb
MDA	Malondialdehyde
MEGA	Molecular evolutionary genetic analysis

mg	Milligram
MgCl <sub>2</sub>	Magnesium chloride
min	Minute
mL	Millilitre
mM	Millimolar
MMT	Million metric tons
°N	Degrees north
NaCl <sub>2</sub>	Sodium chloride
nm	Nanometer
NO <sub>x</sub>	Nitrogen Oxide
NPs	Nanoparticles
OD	Optical density
PAHs	Polycyclic Aromatic Hydrocarbon
PCR	Polymerase chain reaction
PCRWR	Pakistan Council of Research in Water Resources
%	Percentage
PDA	Potato dextrose agar
PK	Protein kinase
POD	Peroxidase
RAA	<i>R. arrhizus</i>
RBCs	Red blood cells
REL	Relative electrolytic leakage
RNA	Ribonucleic acid
ROS	Reactive oxygen species
rpm	Rotation per minute
rRNA	Ribosomal ribonucleic acid

RS	Residual portion
RWC	Relative water content
Saf	Safranin
SEM	Scanning electron microscope
SOD	Superoxide Dismutase
SO <sub>x</sub>	Sulfur Oxide
TAC	Total antioxidant capacity
TGA	Thermogravimetric analysis
TOC	Total organic Carbon
TRP	Total Reducing Power
μg	Microgram
μL	Microliter
μm	Micrometer
UNO	United Nation Organization
UV-Vis	Ultraviolet visible
XRD	X-ray diffraction
ZnO	Zinc oxide



## ABSTRACT

Industrial and agricultural processes produce different types of dyes, metals, and pesticides in water and soil. Removal of these contaminants is essential to elude environmental and health issues. Biochar is a pyrolyzed black color mass containing a high amount of carbon, and it has been reported to enhance soil fertility and improve plant growth. In this study, ZnO-loaded maize biochar nanocomposite (MB-ZnO) and *Trichoderma harzianum* loaded maize biochar (MBT) have been synthesized and used to remove different aqueous pollutants, immobilize toxic metals of soil, and improve the growth of a fast-growing model plant (*Sesbania sesban*).

In the first part of this study, biochar with unique physicochemical characteristics, like increased surface area, high carbon contents, and electron-conductive behaviors was synthesized from maize straw, using free ball-milling technology. Synthesized MB-ZnO was characterized via thermogravimetric analysis (TGA), ultraviolet-visible (UV) spectroscopy, Fourier-transform infrared (FTIR) spectroscopy, X-ray powder diffraction (XRD), scanning electron microscopy (SEM) and energy-dispersive X-ray (EDX) spectroscopy. The average size of the MB-ZnO nanocomposite was determined (43 nm) by means of the X-ray line broadening technique. FTIR spectroscopic results depicted the presence of different functional groups on MB-ZnO to confirm its reduction and successful formation. Successfully produced MB-ZnO was applied as a photocatalyst to degrade pollutants present in aqueous medium pollutants in different light conditions. The degradation potential (adsorption potential and photocatalytic performance) of MB-ZnO nanocomposite was analyzed against Mancozeb (MC) and Safranin O (Saf) in a closed container in the dark and under various light sources including visible and UV light. The reaction kinetics were calculated by applying the pseudo-first-order kinetic study model to elaborate the procedure of MC and Saf amputation from the solution. MB-ZnO composite showed different photocatalytic activities to degrade Saf invisible light (83.5 %), UV radiation (81.0 %), and dark environments (78 %) in a time duration of 60 minutes. The highest degradation of MC via MB-ZnO was determined in visible light (56.5 %), followed by UV radiation (27.5 %) and dark environment (25.2 %). These results proved that the

prepared nanocomposite can be applied as an efficient catalyst to eliminate pollutants from aqueous medium, in both light sources and dark environments.

In the second section of this study, MB-ZnO nanocomposite was assessed in different *in vitro* biological activities, including anti-inflammatory assay, biocompatibility activity against RBCs and macrophages, cytotoxicity assays of leishmanial parasites, enzymes inhibition assay against protein kinase, alpha-amylase, antifungal assay, and antioxidant assays. Results of this study revealed that MB-ZnO did not create any harm in the biocompatibility and the cytotoxic activity, and it achieved better in the antioxidant and anti-inflammatory assays. MB-ZnO nanocomposite produced modest enzyme inhibition and was more powerful against fungal pathogens. These findings directed that MB-ZnO might be useful as an efficient catalyst in different practices. This study has provided the latest and most valuable information to researchers and readers working on nanocomposites and biopolymers.

This study was further extended to apply MB-ZnO nanocomposite for the control of a novel fungal disease of the Kiwi plant. Kiwi worked as an excellent natural source of vitamin C and has multiple uses. During the month of October-November 2021, tiny brown spots were observed on the leaves of Kiwi. For diagnosis, the affected leaf samples were collected and placed on potato dextrose agar (PDA) nutrient media. Morphological and anatomical characterization has shown this disease-causing pathogen to be *Rhizopus oryzae*. For the molecular study of the isolated pathogen, partial sequences of elongation factor (EF-1 $\alpha$ ) and inter-transcribed sequence (ITS) were amplified and sequenced. BLAST analyses of the resultant ITS sequence revealed >99% similarity with *R. oryzae* (MT603964.1), whereas the EF-1 $\alpha$  sequence exhibited 100% resemblance with the elongation factor-1 $\alpha$  gene of *R. oryzae* (MK510718.1). The attained ITS sequence was deposited to the NCBI database (MW603842.1). Koch's postulates confirmed the pathogenicity of the isolated pathogen and verified that *R. oryzae* was the leaf spot pathogen of Kiwi. For eco-friendly control of Kiwi leaf spot, MB-ZnO nanocomposite was used. MB-ZnO nanocomposite revealed considerable mycelial growth inhibition and the maximum of 79% inhibition was examined at 19 mg/mL dose rate of MB-ZnO nanocomposite. These results highlighted the efficacious use of MB-ZnO for the control of plant pathogens.

In the fourth part of this study, simple maize straw biochar (MB) and fungus (*Trichoderma harzianum*) loaded biochar (MBT) were used at various rates, for the immobilization of Cd and Cu from polluted soil. Throughout the remediation time of 90 days, the dynamic effects of MB and MBT on the physiochemical properties and function of the soil were observed. The findings of this study showed that the application of 5% MBT considerably increased soil pH at an early stage of incubation, which decreased later to a neutral-alkaline level. The application of MBT promoted residual bound Cu-Cd fractions and decreased carbonate and exchangeable bound fractions in the treated soil. These bindings reduce the bio-accessibility of plants, animals, and humans to heavy metals. The addition of MBT also enhanced catalase and urease activities of soil, in the later phase of the experiment, indicating the retrieval function of soil for the post-stabilization of metal. The findings of this research offered new understandings of the production of functional substances and skills for the sustainable reclamation of heavy metal-polluted soil with the amalgamation of biochar and functional microbes.

In the last part of this study, both types of engineered biochar (MB-ZnO nanocomposite and MBT) were applied to influence the growth of a fast-growing model plant (*Sesbania sesban*). In a greenhouse, *S. sesban* plants were grown in pots, containing Cd-Cu-contaminated soil. These plants were sprayed with various doses (0, 50, 75, 100 mg/L) of MB-ZnO nanocomposite and 1.0% (w/w) MBT. The findings of these applications showed that the combined application of MB-ZnO nanocomposite and MBT enhanced the physiological, biochemical, anatomical, and antioxidant enzyme activities of *S. sesban* and diminished Cd and Cu meditations. Foliar application of 100 mg/L MB-ZnO nanocomposite significantly reduced Cd and Cu content in the shoots of *S. sesban* by 30% and 31%, respectively. Combined application of MB-ZnO nanocomposite and MBT diminished Cd and Cu content by 39% and 38%, respectively, and increased the pH of soil from 8.03 to 8.23 units. These results signify the importance of the application of engineered biochar for plant growth under a metal-stress environment.

Conclusive findings of this study proved that the application of engineered biochar (MB-ZnO nanocomposite and MBT) is an environment-friendly and efficient way to remove aqueous pollutants, immobilize toxic metals from the soil, control plant foliar

diseases, and improve plant growth. There is a need to channelize the large-scale production and application of these products for a sustainable ecosystem.



# CHAPTER 1

# INTRODUCTION

## 1. INTRODUCTION

The rapid increase in industrialization has polluted the environment and affected our life. Industrial technologies are resulting in various ecological problems and the deterioration of natural resources (Brillas and Martínez-Huitle, 2015). Different pollutants released by various industries and other anthropogenic activities disturb the ecosystem and eventually living bodies. The outflows of various industries like leather, paper, textile, cosmetics, and different laboratories, mostly hold different types of heavy metals, dyes, and chemicals, which are one of the key causes of ecological pollution (Xu et al., 2019). The occurrence of these pollutants, mainly in fresh water and agricultural soil, creates a worldwide issue, and the integration of these pollutants into the food chain might affect plants, animals, and the human body. In the current era, industrial effluents and chemical fungicides used in agriculture for crops are the major pollutants. Different industries utilize dyes, and their dregs are esthetically disgusting and disturb light conduction, which is important for photosynthetic and many other processes. Scientists are seriously working to address these issues by applying different natural and synthetic products.

### 1.1 BIOCHAR

Biochar is simply a term used for black color mass having high carbon contents that are formed after the combustion of biological resources at high temperatures in an anaerobic condition. Biochar is an economical, and eco-friendly approach and it can be applied for multiple purposes, like waste management, soil remediation, greenhouse gas declination, plant growth, and production of energy. Due to a large number of benefits in various fields of life, biochar is often termed as “Black Gold”.

Fossil fuels combustion releases CO<sub>2</sub>, which results in climate change and global warming and along with the development of air pollutants, like nitrogen and sulfur oxides (Zhang et al., 2007). Organic material are complexes of inorganic and organic substances originating from living organisms are communally termed as biomass, which not just include living organisms (animals and plants) but also the waste of animals, waste wood, and sludge (Tripathi et al., 2016). Thermal and chemical decomposition procedures convert

biomass to biochar. Biomass is considered carbon neutral and it has very less adversarial properties on the atmosphere as it contains small nitrogen (N) and Sulphur (S), resulting in a small amount of NO<sub>x</sub> and SO<sub>x</sub> emissions, as compared to fossil energy sources (Zhang et al., 2007).

Biochar is a black color solid mass obtained during the pyrolysis of biomass, is described by the International Biochar Initiative as “a solid substance formed from the biomass carbonization”. Different studies has been directed for to develop modern application of biochar (Lehmann and Joseph, 2015). Chemical composition of the biochar diverges depends on the raw material (biomass), and properties of the of the carbonization process (Cha et al., 2016). Though the key component of biochar include carbon (C), oxygen (O), hydrogen (H), ash, and other small quantity of sulfur and nitrogen (Liu et al., 2015a). Due to its greater surface area, porous morphology, various functional groups, and large contents of mineral, biochar has been considered as an adsorbent for air and water pollutants (Ahmad et al., 2014; Mohan et al., 2014), removal of tar, biodiesel production (Konwar et al., 2015; Shen, 2015), and as a soil health enhancer (Ahmad et al., 2014; Najar et al., 2015).

## **1.2 PRODUCTION OF BIOCHAR**

Several practices like gasification, hydrothermal carbonization, pyrolysis, flash carbonization (Antal et al., 2007; Nunoura et al., 2006) and torrefaction (Chen et al., 2016; Chiou et al., 2016) are applied for the synthesis of biochar. Among these processes, pyrolysis is preferred over others and is mostly used for biochar production due to easy handling and unhazardous effects.

### ***1.2.1 Pyrolysis***

Pyrolysis is a method of thermally breaking organic materials in an anaerobic environment, at high temperature ranges from 300 °C to 900 °C (Han et al., 2017; Lee et al., 2016a; Shafaghat et al., 2016). In thermal breakdown, cellulose, hemicellulose, and lignin create gaseous, liquid, and solid products. The production of the pyrolysis material are associated with the source of biomass materials and the applied pyrolysis procedures.

The factors inducing the processes of pyrolysis and its products include the range of the temperature, rate of heating, and temperature duration. Usually, the production of biochar declines and the yield of syngas rises with enhancing the temperature (Cha et al., 2016; Demirbas, 2004). Some studies have described that the biochar yields and its acidic properties are reduced with rising pyrolysis temperature, while those of the basic properties, such as , pH, ash content and carbon stability is improved (Cha et al., 2016; Zhang et al., 2015a). The rise in pH with rising pyrolysis temperature has been credited to the declination of organic functional groups, like –OH and –COOH.

Pyrolysis methods are classified into fast and slow pyrolysis, conditional to the degree of the increase in temperature. During slow pyrolysis process, the pyrolyzed materials is heat up for large duration in the reactor at low temperatures and the remaining vapor-phase reactions enhance the yield of biochar (Ayllón et al., 2006; Chen et al., 2003). Inguanzo et al. (2001) evaluated the synthesized biochar at the higher temperature having a less volatile materials with a large ash and determined that a high temperature increasing rate has better quality of the products in biochar. Lu et al. (1995) documented that the yield biochar declines with rising residence time at the same pyrolysis temperature. Lu et al. (1995) indorsed the findings of Pavlovic et al. (2012) to a diminishing and cessation of the pore entrances due to the biochar sintering, leading to the declination of the surface area. Prior to usage, thermally treated biochar is normally stimulated to either increase its surface area, pore number or create functional groups in biochar. The activation processes are classified into chemical and physical activation (Hui and Zaini, 2015; Jung and Kim, 2014; Manocha et al., 2010). The pore size and fraction dissemination of the activated biochar differs depending on the nature and amount of biomass and stimulating gas.

### **1.3 SOURCES FOR BIOCHAR PRODUCTION**

Various kinds of biomasses possess their own chemical constituents and structures, resulting in corresponding pyrolyzed products with various structures and characteristics. According to various sources, these feedstocks of biomass feedstock can be categorized into the multiple classes includings: i) forest and agricultural residues, ii) municipal waste material and industrial by-products and iii) nonconventional ingredients.

### ***1.3.1 Forest and Agricultural Residues***

Forest and agricultural residues are the utmost extensively applied biomasses for biochar synthesis. They are extensively used for their environmental friendly, economical nature, and having abundant natural constituents (Singh et al., 2015). Every year, logging, agriculture, and other anthropogenic actions produce millions of tons of different forms of residues, including rice husk, straws, and wood chips. Large levels of cellulose and lignin in the biomass resource provide strong security for producing affordable biochar. The pyrolysis and vaporization of cellulose results in the formation of pores on biochar, which assist in the removal of impurities (Kumar et al., 2011). For illustration, woody biomass, like wood of pine, typically has rigid and solid structure, which require high temperature and large pyrolysis time. In contrast, straw biomass has a loose structure that makes it break readily when it is pyrolyzed, resulting in a structure that is very porous (Sewu et al., 2017).

### ***1.3.2 Industrial and Municipal Waste***

Industrial and municipal trashes are another key sources for production of biochar (Inyang et al., 2016). Industrial byproducts and municipal wastes, in contrast to agriculture and forestry residues, include waste released from a variety of sources, including the sewage treatment plant, paper industry, food industries, and compact waste material from anthropogenic activities (Mo et al., 2018; Takaya et al., 2016). This form of biomass is a blender of organic and inorganic substances, comprising various kinds of chemicals compounds, mineral salts, viruses and bacteria etc (Zhou et al., 2019). Therefore, biochar prepared from industrial and municipal trashes, like wastewater treatment slush and press cake from anaerobic digestate, generally contain large quantity of ash contents and inorganic compounds.

### ***1.3.3 Nonconventional materials***

Nonconventional materials majorly comprise of different waste material, except the aforementioned, like waste cardboard, animal dung, waste bones, waste tire rubber, plastics, and so on (Sánchez-Olmos et al., 2020; Shah et al., 2022). The properties of the

biochar formed from various biomass materials are extremely diverse because of the stark differences in chemical compositions and structures. Lonappan et al., (2016) have documented a type of biochar prepared from dung of pig, and the amount of ash was determined approximately 65%.

In conclusion, forest and agriculture residues generally have greater amounts of cellulose and lignin, in comparison to slush and animal waste, which means that pyrolytic products have greater yield, greater carbon amount, and relatively greater surface areas in a similar pyrolysis environment. The lignin content of woody biomasses is often higher than that of leaves, grasses, straws, and herbaceous flora, which are generally composed of cellulose and hemicellulose. High amount of cellulose and lignin content in agricultural and forest biomass produces a large amount of oxygen and carbon. Furthermore, a high oxygen and carbon content in biomass might result in a large production of biochar and the development of multiple functional groups (such as  $-C-O-R$ ,  $-COOH$ ,  $C-OH$ ,) on biochar (Li et al., 2017; Takaya et al., 2016). The aforementioned groups can work as additional active positions to enhance the biochar efficacy. In comparison, biochar prepared from industrial municipal trashes and other nonconventional resources (e.g., animal waste, press cake from digestate, and sewage sludge, fossil bones) generally contain larger amount of ash and different inorganic substances with small amount of energy (Li et al., 2017). Moreover, it is also documented that high amount of ash would decrease the adsorption capability of biochar toward organic pollutants by creating the active adsorption positions (Zheng et al., 2013).

In the current work, maize straw was used for biochar synthesis due to its porous nature, easy availability, and economical value. For better efficacy, the biochar was modified by loading various materials and the prepared material is described as “engineered biochar”.

#### **1.4 PREPARATION OF ENGINEERED BIOCHAR**

Biochar can be engineered to make it suitable for planned application by alteration of its physio-chemical characteristics like surface area, morphology, functional groups, and pore size and structures. This engineering may be achieved via different procedures

stretching from physical to biochemical techniques. Biochar can be modified into various forms conditional to the purpose of use. Biochar can be utilized in the creation of hybrid material for the removal of pollutants, like biochar-supplemented biofilters, permeable barriers, and biochar-based membrane purification (Palansooriya et al., 2020). In 2019, a new chem-bio hybrid method was developed from wheat straw biochar Fe-S nanocomposite and *Corynebacterium*. This engineered biochar could proficiently eliminate and degrade pollutants from polluted water while displaying a greater stability and lesser hydrodynamic diameter, in comparison to pure biochar (Lyu et al., 2018).

An organic-inorganic composite system has been created by loading soft wood biochar with TiO<sub>2</sub>. The modified biochar considerably increased the photocatalytic efficiency of phenol in comparison to the pure biochar and TiO<sub>2</sub> alone, i.e., achieving 64% in UV light and 34% in visible light (Lisowski et al., 2017). Generally, engineering biochar via hybridization method could significantly enhance their removal efficacy of pollutants from contaminated water. In present work, we modified the biochar by physical and biological method including Zinc oxide nanocomposite and *Trichoderma* loaded biochar. The engineered biochar is a hybrid material of two or more substances.

#### ***1.4.1 Biochar-based Hybrid Nanomaterials***

The preface “nano” in nanotechnology states a billionth ( $1 \times 10^{-9}$ ). Nanotechnology is concerned with the configuration of matter having size of the order of the billions of a meter called nanomaterial or nanoparticle. Currently, nanotechnology has become one of the most significant and exhilarating leading fields in Chemistry, Physics, Engineering, and life sciences. It reveals prodigious potential of providing us with various innovations that will transform the track of technological progresses in a diverse range of application. The recent extensive attention in nanotechnology dates to the year 1996 to 1999. However, it is not clear when humans started to take benefits of nanoparticles (NPs). NPs is defined as a tiny particle that is produced from the conversion of matter via chemical, physical, and biological methods, and practices with or without including other constituents that has at least one of its dimensions and having size less than 100 nm. Therefore the prepared NPs are different from the bulk size materials, as they reveal distinctive optical,

electrochemical, and thermal properties, along with a considerably greatly surface area to volume ratio (Sokhal et al., 2018).

The inimitable characteristics of NPs are liable for their attractiveness and extensive applications in different fields such as agriculture, chemistry, biotechnology, communications, electronics, consumer goods, defense, energy, environmental remediation, material science, industries, microbiology, medicine, optics, and many fields of engineering (Solaymani et al., 2017). Metals oxides are widely transformed into NPs and nanocomposites via physical, chemical and biological procedures (Ghaedi et al., 2013; Ghosh et al., 2013; Raul et al., 2012). The advantages and outstanding characteristics of green-synthesized methods include the dual efficacy of active natural constituent, like the extract, both as a capping and reducing agent. The distinctive properties of nanomaterial include their large surface area, small size, and high surface atomic fraction (Amara et al., 2022). Although, there is extensive variety in the chemical nature and structures of nanomaterial's.

Simple biochar is designated as pristine biochar and it having from some weaknesses like limited surface functional groups and small anti-interference capacity, resulting to restricted uses in the ecological problems management (Tan et al., 2016). To overawed the weakness of pristine biochar, and more expand their uses in the environmental pollution treatment, different approaches are being established to increase its performance (including surface area, pore size, functional groups, etc.) via modification. Now a days, for the efficient performance of biochar and biochar-hybrid materials, it is converted into nano-size material, with altered physical and chemical nature. The use of various modification tactics, such as biomass pretreatment and chemical amendment of biochar surface, has fabricated different kinds of novel biochar-based composite substances. These hybrid substances mainly involve magnetic-biochar composites, nanometal oxides/nanometallic oxides/hydroxide-biochar composites and several additional kinds of usual functionalized composites.

#### ***1.4.1.1 Zinc oxide and Zinc oxide-nanocomposite***

Incredible functions of zinc oxide (ZnO) NPs, such as photocatalytic activity,

---



physical and chemical stability, and nontoxic characteristics to the human body have been reported, earlier (Ifijen et al., 2022). In recent years, ZnO has got better attention concerning potential electronic uses because its holding a distinctive optical, chemical, physical and electrical properties and being an extensive band-gap semiconductor (3.36 eV) (Baxter and Aydil, 2005). The accessibility of a wide range of ZnO nanostructures makes an perfect material for nanoscale optoelectronics (Yi et al., 2005), nanogenerators (Song et al., 2006) and other applications in the field of biotechnology (Wang, 2004). Additionally, ZnO acts strongly to resist microorganisms (Sawai et al., 1996). Many studies (Sawai and Yoshikawa, 2004) have documented the substantial antibacterial potential of ZnO, which is credited to the creation of ROS on the surface of these oxides, which cause the death of microorganism. The benefit of using this ZnO as antimicrobial agents is that they hold micronutrients necessary to men and reveal good efficiency even when managed in minor quantities. The efficacy is quantitatively assessed by investigating the fluctuations in growth medium, produced by bacterial metabolism. ZnO are particularly interesting as they can be prepared with very high surface areas and are more appropriate for biological activities. Inorganic antibacterial constituents show greater stability, less toxicity, greater selectivity and heat resistance, when compared with organic antibacterial materials.

Recently, the status of bio-polymer-functioned ZnO nanohybrid materials has got devotion in the different fields of medical sciences and treatment due to their toxic-free and eco-friendly behavior (Pooresmaeil and Namazi, 2023). A recent study on nanocomposite describes that cellulosic material accumulated with ZnO shows antimicrobial characteristics (Qi et al., 2022). Among the cellulose based material, biochar has got more connotation due to its unique characteristics, like biodegradability, biocompatibility, and antimicrobial potential (Das and Panda, 2022). The prepared biochar-ZnO composites possess the properties of both ZnO NPs and biochar (Song et al., 2022).

#### ***1.4.1.1.1 Synthesis of Biochar-Zinc Oxide Nanocomposite***

Generally, biochar nanometallic oxides composites not only have the functional properties of biochar, but also the distinctive physio-chemical characteristics of NPs (Chen

et al., 2018b; Rajapaksha et al., 2016; Wang et al., 2018b; Zhang et al., 2016). The amalgamation of biochar and metal oxides might endow biochar more functionalities and support its own benefits via synergetic effects. Subsequently, combining biochar with different metallic oxides has been observed as a sagacious idea in the production of very effective biochar-hybrid materials.

Loading ZnO on the biochar is an auspicious tactic for enhancing the multi-performances of biochar (Chen et al., 2019). The amalgamated ZnO NPs must be uniformly distributed on the biochar surface to increase its efficiency. The basic purpose of producing a nanocomposite of biochar and ZnO (BC-ZnO) is to reduce the value of band gap energy, enhance surface area, improve pores number, increase pore size, attain excellent reusability, and increase its recovery (Ahmaruzzaman, 2021; Gonçalves et al., 2020). All these practices will improve the nanocomposites to have greater efficacy in comparison to pure biochar and ZnO NPs individually. Biochar-ZnO nanocomposite is awarded with intrinsic properties of the material which are pretty changed from individually precursor substances. BC-ZnO nanocomposites have the great photocatalytic ability, low accumulation, greater pollutant adsorption ability, and few electron-hole pairs recombination (Leichtweis et al., 2020).

The Plant-based nanocomposites have ominously drawn the interest of the scientist because of its simple nature (Iqbal et al., 2019; Song and Kim, 2009). The plant material, such as maize straw biochar, can work as a stabilizing, strong reducing, and capping agent and has gained the interest of the researcher because of its simplicity, fast, eco-friendly and cost effective nature (Singh et al., 2016a; Song and Kim, 2009). The phytochemicals present in the raw material of plant behave as a durable reducing material and leads to the synthesis of capped nanoparticles. So, plant feedstock work as both natural capping and reducing agents, eradicate many stages and lessen charges and chemical consumption (Ahmed et al., 2016; Iqbal et al., 2019). Maize straw has medicinal importance because of the existence of various phytochemicals like flavonoids, alkaloids, polyphenols, terpenoids, vitamins and amino acids (Ahmed et al., 2016; Iqbal et al., 2019).

BC-ZnO nanocomposites can be created by both chemical and physical processes. Among the ordinarily used synthesis methods for biochar-ZnO nanocomposite, metallic

oxides and biomass are blended initially and then heat up it. While, in the next method, the metallic oxides are loaded over the pre-synthesized biochar. In the primary method, the treatment efficacy is narrow because of the multifarious stepwise synthesis, weak adherence of the oxides, and random dissemination of metallic oxide on the biochar (Yu et al., 2021). The most frequently applied approaches to fabricate BC-ZnO hybrid material are hydrothermal process, sol-gel preparation, thermal poly-condensation, ultrasound-assisted synthesis, and solvothermal procedure (Ahmaruzzaman, 2021). These approaches need metallic solution impregnation and co-pyrolysis processes, which emits wastewater and gas emission, and hence increase contamination threats to the ecosystem. Furthermore, ball milling preparation has been considered as an auspicious method for preparation of biochar metallic oxide nanocomposites utilized in the elimination of inorganic and organic substances (Yu et al., 2021).

Ball-milling technique has been utilized to transform the wholesome biochar, by reducing the particles magnitude, increase functional groups and improve the biochar surface area to enhance its adsorption ability without the addition or release of impurities (Namazi and Belali, 2016). Ball-milling of metal oxides results in even-sized NPs, without disturbing the enhanced accomplishments (Pudełko et al., 2021). Ball milling amendment is the frequently used physical approach for the enhancement of the properties of biochar. It has been documented by researchers that amended biochar shows greater adsorption ability for organic, inorganic pollutants, and heavy metal elements because of the enhanced surface properties and small particle size after physical amendments (Zhou et al., 2017). However, the dispersibility of biochar in the aqueous medium depends upon the ball mill procedure intensity, limiting ball milled biochar used in water and soil remediation. The physical methods are safer and cheaper approach of biochar production because of impurities free nature easily controllable in comparison to chemical method. It has been determined that ball milling method could be an excellent practice to synthesize biochar-metal oxide hybrid material for enhanced photocatalytic activity. The aforementioned physical tactic is preferred over others, because of eco-friendly, chemicals free, high productivity and cost effective nature low cost (Javanbakht et al., 2019).

In the existing study, properties of the final product (MB-ZnO nanocomposites) were investigated through the characterization of MB-ZnO nanocomposites by XRD, TGA, FT-IR, SEM, EDX, and UV–Vis DRS method (Fazal et al., 2020; Hu et al., 2019a). The complete differences in MB surface areas are most possibly emanated from the differences in pyrolysis temperature and the feedstock used for MB preparation. Moreover, this study includes the exploration of the industrial potential of MB-ZnO in various sectors of applications.

#### ***1.4.2 Production of *Trichoderma harzianum* Loaded Biochar***

Microorganisms own various metabolic mechanisms (Mohammadipanah and Dehghani, 2017; Wink et al., 2017), make them able to change different types of organic products, such as pollutants and discarded materials, into useful substances (Dehghani et al., 2019) and even valuable daily substances (Sajedi et al., 2018). Because of their small size, they can breach through small cracks and result in biofilm, which is a hard structure, able them to maintain during washing out. Microbes can change the biochemistry of pristine biochar by settlement and biofilm production on its larger surface area. This modification procedure permits engineering biochar with desired characteristics. More precisely, a synchronized adsorption of organic substances and their removal through biochar framework and inoculated microbes could be examined, correspondingly. It has been reported that certain microbes are able as bio-adsorbent of a different types of heavy metals (Hamedi et al., 2015). It was determined that filter prepared of biochar-active-biofilm could proficiently adsorb and degrade pollutant (carbamazepine up to 98%). The by-products from anaerobic breakdown of feedstock could be effectively applied for engineered biochar preparation because of more appropriate pH and oxidation reduction ability. Actually, the biochar prepared from anaerobic breakdown of feedstock has better worth in terms of specific surface area, surface charges, more alkaline pH, anion exchange capacity, and cation exchange ability, in comparison to pure biochar (Yao et al., 2018). Commonly, this biologically stimulated biochar might be proficiently used as ion exchangers in ecological remediation approaches for requisitioning both positively and

negatively charged ions such as phosphate and heavy metals. The integration of such practices could extraordinarily enhance ecological and economic viability.

The carrier substances applied for the immobilization of microbial cells are usually synthetic macromolecule and composite materials (Bouabidi et al., 2019; Partovinia and Rasekh, 2018). Currently, biochar has been applied as the best carrier substance for the crop growth-enhancing microorganisms, and the enhanced productivity of hyperaccumulating plants natural substances (e.g., zeolite, diatomite, activated sludge), artificial inorganic substances in the Cadmium contaminated soil (Wu et al., 2019). The possible relations strategies between soil native microorganism and biochar reported by many scientists, are (i) biochar provide accommodation for microbes; (ii) biochar work as a nutrients source for microorganism; (iii) biochar can alter soil basic properties, soil microbial population, and enzyme activity of soil; and (iv) biochar increase the conversion and degradation of pollutants with the help of sorption, free radicals, and electron transfer (Bandara et al., 2020; Zhu et al., 2017). Though the combined working procedure that how exactly soil microorganisms interact with biochar is not clearly acknowledged, the individual role of biochar and applied microbes is indistinguishable.

## **1.5 POLLUTION**

Industries and chemicals are significant components of modern society. Various pharmaceuticals, petrochemicals, and agrochemicals industries are contributing to the welfare of humanity. As an outcome, all these discharges injurious substances to the environment that change the environment's physical, chemical, and biological characteristics and it is termed as "pollution". The harmful substances that cause changes in ecosystem are called "pollutants". These may be biodegradable or non-biodegradable. Among these, non-biodegradable pollutants are the major source of pollution. These pollutants are progressively dissolved in the environment and cross-national boundaries and do not remain confined to a specific territory. Due to market outcomes and personal benefits, everyone ignores the harmful effect of pollution. Among different kinds of pollution, water and soil are very lethal in developing and underdeveloped countries due to lack of proper management, unavailability of technical knowledge and financial issues.

### ***1.5.1 Water Pollution***

Water is a vital constituent for living organisms. Fresh water constitutes 3% of the entire water present on earth's surface. Just a small amount (0.01%) of the fresh water is accessible for human consumption (Hinrichsen and Tacio, 2002). Unluckily, even this little quantity of drinking water is under massive pressure because of the fast population growth, habitat destruction, urbanization, and unmanageable usage of fresh water in agriculture and industries. According to a United Nation Organization (UNO) report, the global population is increasing exponentially whereas the availability of this water is decreasing. This problem is more serious in emerging nations due to the unavailability of facilities (Azizullah et al., 2011). Like other developing nations, Pakistan is also facing a precarious water pollution issue and freshwater shortage. The country has basically exhausted its available fresh water assets (Azizullah et al., 2011). Pakistan is thought to be water-stressed country and will have water scarcity in the near future (Hashmi et al., 2009; Pakistan, 2007). This reduction in freshwater amount, coupled with growing demand, lead to severe freshwater scarcities in almost every sector of the country. This combined effect of decreasing quantity and increasing consumption in numerous sectors has badly affected the quality of water and led to a serious water pollution issue. Pakistan Council of Research in Water Resources (PCRWR) conducted a comprehensive survey on the quality of water in 23 main areas of Pakistan and determined that an average of 84–89% of the country's water sources fall short of the criteria for human consumption (Azizullah et al., 2011).

### ***1.5.2 Soil Pollution***

Soil is a natural habitat for growth and development of plants and contains a mixture of organic and inorganic materials existing in gaseous, liquid, and solid forms. Environmentally and genetically, soils varies ominously, however, they perform the task of store house of water and nutrients, essential for the appropriate development and growth of the plant roots and microbes (Ndiaye et al., 2000). Soil has the potential of holding different pollutants, like heavy metals, fungicides, pesticides, or PAHs (Polycyclic Aromatic Hydrocarbon), hence, it functions as a pollutant's absorber. They participate to

the contamination of the food chain, which can also possibly intimidate human health (Borkar, 2015). Soil is an important natural reservoir and plays an effective role in different biochemical pathways, water filtration, recycling of materials and food chain. It is an important medium through which people are exposed to a range of pollutants and dangerous substances, which has a substantial impact on the inhabitant's quality of life (Guagliardi et al., 2012; Lu et al., 2017).

Fast urbanization and robust industrialization over the past two decades have seriously polluted the soil with several harmful chemicals and hazardous substances (Liu et al., 2013; Ngole-Jeme and Fantke, 2017). Destruction of quality of soil in metropolitan areas due to human accomplishments have resulted to many health and environmental issues (Chonokhuu et al., 2019; Ye et al., 2019). Due to inadequate waste management systems, heavy metal pollution-related environmental issues are particularly severe and harmful in developing nations like Pakistan (Alsbou and Al-Khashman, 2018; Bhat et al., 2022). Serious toxicological consequences on the human body are being caused by exposure to the lethal metals available in the soil (Antoniadis et al., 2019; Kamunda et al., 2016). Various research projects on soil contamination and associated health risks have been carried out recently, all around the world (Karimi et al., 2020; Ye et al., 2019).

### ***1.5.3 Causes of Water and Soil Pollution***

Numerous constituents are considered as active pollutants. The most common among them are fungicides, pesticides, inorganic pollutants, metals, dyes, and water-soluble radioactive substances. All these materials, if they surpass a threshold limit, are lethal and result in severe human's health problems and other living organisms in the environment. All these substances are posing serious threats to quality of fresh water in Pakistan.

#### ***1.5.3.1 Agricultural Pollutants***

The global consumption of pesticides has greatly increased due to ever-increasing demands for food with the growing human population. Pesticides were first used in agricultural field, around the world in 1950s, to provide essential protection against pests

(Jin et al., 2019). Pesticides are broadly utilized in agricultural and veterinary practices across the globe. The entire pesticides consumption is about two million tons per year, across the globe (Singh et al., 2016b). Pakistan is an agricultural nation, with approximately 70% of the population living in villages and associated with agriculture, either directly or indirectly (Azmi et al., 2006). Pesticides are utilized as herbicides, fungicides, and insecticides. Each year fungi produces excessive damages to different types of crops and farmers applies a fungicide for the purpose to provoke fungal pathogens and get better production (Karlsson et al., 2014; Patel et al., 2015).

Among fungicides, Mancozeb is extensively used in agricultural fields, so ultimately becoming the major cause of water and soil pollution. Mancozeb, is an ethylene bisdithiocarbamate (EBDC) based fungicide having de-gradated ethylenethiourea (ETU), and it was first listed in 1948 in the United States, as a wide spectrum fungicide (Saha et al., 2022). Mancozeb has since established nearly 75 years of fungicidal efficiency in a broad range of application in agricultural and industries, including its application as a fungicide of main agricultural crops such as tomato, turnip, potato, and fruit crops for almost 400 plant pathogens. Mancozeb is presently recorded as a common use pesticide by the Environmental Protection Agency (EPA). Mancozeb production is predicted to continue to rise quicker than normal, because of the low purchase price, amassed global demand for vegetables and fruits, and constant non-selective fungicidal ability. According to EPA, above 50% of the water problems of the streams, rivers and sea is resulted due the leaking of different chemicals, applied in agriculture processes (Nigam and Kumar, 2022). Fungicides and their constituents after degradation flow into the water, soil, and ecosystem and result in the aggregations of hazardous chemicals in the environment. The longer-term toxicity of the Mancozeb and its products cause endocrine disorders, , mutagenic, and teratogenic, carcinogenic risks (Nigam and Kumar, 2022; Qadir and Malik, 2011). The environmental pollution caused due to the consumption of fungicides is now a very serious issue in Latin America, Asia, Africa, Middle East, and Eastern Europe.



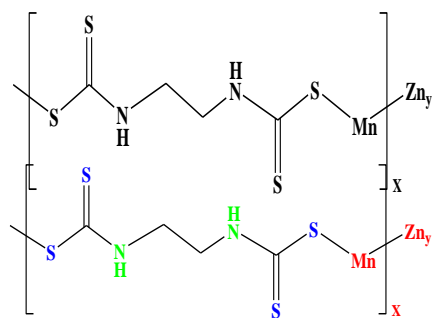


**Fig.1.1** Chemical configuration of Mancozeb

### 1.5.3.2 Heavy Metals

Soil contamination, particularly heavy metal contamination, is an alarming global ecological problem. Heavy metal contamination has been renowned as a serious matter at the local, regional, and global levels due to its intimation on the health of man (Qadir and Malik, 2011). The occurrence of heavy metals (HMs) in the water and soil causes severe problems because of the low biodegradable nature, high toxicity, extensive last effect, irretrievable nature of the contamination, and accumulation in the food chain. Risk assessment showed that the overall results for the carcinogenic risk were trivial. Cd, Al, Pb, Cu, Br, and Ar so forth are included in the list of heavy metals. Higher amounts of these metal ions are extremely lethal to living organisms including humans, animals, and plants. Their water-soluble nature is recognized as one of the main environmental concerns (Azizullah et al., 2011; Wei and Yang, 2010). According to their harmfulness to living systems, they can be prescribed in the following manner : Hg > Cu > Zn > Cd > Ni > Pb > Cr > Sn > Mn > Fe > Al (Filipiak-Szok et al., 2015; Pueyo et al., 2004).

Various metal-contaminated sites in various sites have been identified in various countries throughout the world. In the United States, more than 100,000 polluted localities have been recognized (Connell et al., 2005), whereas, in the European Union nations, 250,000 locations turned out to be contaminated and need to be remediated, urgently (Mench et al., 2010). The environmental issues of Pakistan are primarily linked to unprovoked social and economic situations in recent times. All main towns of Pakistan

face chaotic, unexpected increases because of the shifting of people from villages to cities which deteriorates the situation to manage this contest. Since the municipal department and other departments have limited resources, slapdash urban congestion is the main cause for the decline of natural assets like soil, water, and air quality. In view of a large amount of a broad range of soil pollution in Pakistan and globally, there is a must to adopt sustainable, and eco-friendly remediation methods and practices, especially for the elimination of heavy metals in polluted soil.

### ***1.5.3.3 Industrial and Laboratory Effluents***

The quality of surface and ground water is badly affected by the effluents from different industries, which has an impact on soil, human health, and the ecosystem (Setia et al., 2020). It was documented that almost two million tons of sewage and other effluents are deposited in water reservoirs, globally. The effluents contain a kind of dangerous substances, including by-products, anilines, organics, dye compounds, and hazardous trace elements; several of these substances are stubborn and difficult to degrade (Fahmi et al., 2010). Additionally, the chemicals found in these effluents are changed into mutagenic and carcinogenic ones (Paz et al., 2017). Regarding these various chemicals, dye pollution poses a significant risk to the environment (Ong et al., 2011). These dyes are employed in several industrial practices, including those involving leather, paper, fabrics, cosmetics, pharmaceuticals, and food, and they are eventually released into the environment (Ajmal et al., 2014). Industries discharge dyes into the aquatic ecosystem, where the contaminated water increases water turbidity, reduces penetration of sunlight in the water, and changes soil properties, all of which have an impact on the photosynthetic activity and transport system of the floral community existing in both the terrestrial and aquatic environment. Dyes contain large amount of chemicals, COD, reactive residues, particulates, and chemical dissolved solids (Malakootian and Heidari, 2018). Many industries in Pakistan have been documented to release dyes into the ecosystem and result in water and soil pollution (Hussain et al., 2013; Sial et al., 2006).

One of the most popular used azine-type dyes is Safrarin (SF). SF is, in fact, one of the ancient synthetic dyes. Safranin O, also recognized as basic red II, is extensively

applied to color leather, wool, silk, cotton, jute, and paper. Safranin is also utilized in printing inks and paints (Ekka et al., 2019). Specifically, Safranin O possess a planar structure having a positive charge that intercalates with macromolecules. So, this chemical has been applied as a staining agent in microscopic study of cells and tissues (Schmitz et al., 2010). Safranin O also contributes in energy transfer processes and as redox indicators in chemistry. Additionally, it is also applied in a Gram staining process to differentiate between bacterial strains (Beveridge, 2001). Numerous studies have discovered the interaction of Safranin O with deoxyribonucleic acid (DNA), based on electrochemical processes (Jyske, 2008), and spectroscopic study (Saha and Kumar, 2011). This artificial dye is alkaline in nature and it is very dangerous to the environment (Mohamed et al., 2018). SF is very dangerous that causes the eye infection, skin problems, respiratory tract infection and mutation in the human body (Abukhadra and Mohamed, 2019).

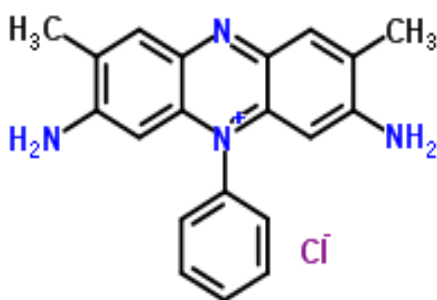


**Fig.1.2** Chemical structure of Safranin

It is necessary to minimize the environmental risks of synthetic Safranin, Mancozeb and Heavy metals, before final discharge. Numerous procedures such as ozonation, advanced oxidation, coagulation, microbiological decaying, and ion exchange are applied, for the aforementioned purposes (Bhatnagar and Sillanpää, 2010; Ramakrishnan and Nagarajan, 2009). These techniques are expensive, and their implementation is very challenging. There is a dare need to introduce novel substitute environmental-friendly procedures for the degradation of these lethal fungicides (Brito et al., 2010).

## 1.6 APPLICATION OF ENGINEERED BIOCHAR

Applications of pristine-biochar are well investigated and described by several researchers. However, in the current work, engineered biochar has been explored for several applications.

### *1.6.1 Photocatalysis against Environmental Pollutants*

Due to the incredible potential of biochar, it was used for various activities but due its certain limitation, different types of amendments have been tried, including physical, chemical, mineral loading, and magnetic amendments (Sun et al., 2019; Premarathna et al., 2019). Therefore, the current experiment was intended to determine the efficacy of Biochar-zinc oxide (MB-ZnO) nanocomposite for the removal of safranin and Mancozeb from the contaminated wastewater. Use of biochar nanocomposites is the utmost auspicious tool for the degradation of evolving pollutants and different conventional contaminates by photocatalysis practices (Arkaan et al., 2020; Do Minh et al., 2020). This is a decent changing opportunity from the single wastewater purification technology into a multi-component tactic.

ZnO is an extensively utilized and auspicious photocatalyst with decent photosensitivity, low price, stability, and eco-friendly nature. ZnO has a broad energy band gap (3.37 eV), which needs UV light to indorse an electron from the valence to the conduction band and create electron-hole pairs (Gonçalves et al., 2020). These difficulties can be overawed by fixing the ZnO nanomaterials on carbonaceous skeleton. In line with this technology, photocatalysis, which is the photodegradation technique, has been effectively practiced by using MB-ZnO nanocomposites. MB-ZnO nanocomposites have synergetic effect of MB and ZnO. The major active species is the hydroxyl radical in photodegradation, along to its corresponding electron-hole pairs. The chemical bond developed (C-O-Zn) is a good prerequisite to reduce the rapid recombination of the electron-hole pairs (He et al., 2021). The combined effect of MB-ZnO performs a greater photocatalytic removal of the contaminants in contaminated water. BC-ZnO nanocomposite has high photocatalytic potential against pollutants in contaminated water

(Leichtweis et al., 2020). Usually, BC-ZnO nanocomposite has been successfully utilized for the elimination of contaminants from water and other bodies.

### ***1.6.2 Biomedical and Therapeutic Application***

Among various kinds of metal oxide NPs, ZnO NPs are repeatedly used due to their less toxic nature. Currently, the food and drug administration (FDA) has confirmed ZnO as a non-toxic material, in comparison used as packaging antimicrobial agents in, textile stuff, food parcels, ointments, mouth spray, and lotions for inhibition of microbial growth (Moustafa et al., 2019; Youssef et al., 2018). NPs show their contributions in various fields, mainly in nanomedicine, and in the treatment of various contagious diseases. For using it as a therapeutic agent, the agent must be analyzed, prior to its application. MB-ZnO has been developed as auspicious technology for a broad range of biomedical use, and their widespread application depends on the evaluation of their biosafety. There is an increasing demand to assess the health effect of these substances and to expand information of their toxicity and biocompatibility (Carnovale et al., 2019). When a new nanomaterial develops, its cytotoxic impact, i.e., the possible changes in the primary cellular functions, is generally assessed at first. In this study, the synthesized nanocomposite was tested for biocompatibility potential assay of Red MTT, at various concentrations.

It is well accepted that reactive oxygen species (ROS), including superoxide anion ( $O_2^{\cdot-}$ ), singlet oxygen ( $O^{\cdot-}_2$ ), hydroxyl radicals ( $OH^{\cdot}$ ), and hydrogen peroxide ( $H_2O_2$ ), perform a key function in the oxidative stress development that may cause to several problems such as cardiovascular problems, inflammation, diabetes, degenerative disorders, cancer, anemia, and ischemia (Luo et al., 2004). In this research, synthetic antioxidant agents have been prepared against the oxidative stress. Though, the features like lack of availability, expensive nature, and side effects exist as key setbacks in fighting oxidative stress. In this direction, MB-ZnO got a prominence due to their non-toxic nature, less expensive and having the synergetic effect of plant source and metals (Luo et al., 2004). Plant origin antioxidant compounds (Dragland et al., 2003) show a protective role by inhibiting the production of free radicals and therefore they are very useful to control the diseases as a result of oxidative stress (Akinmoladun et al., 2010). Besides to these classes

of organic compounds, current studies confirmed that minor metals including Zn, Cu, Mn, Mg, and Se perform a useful part in antioxidant mechanism (Deng et al., 2019).

Inflammation is a defensive response to a number of factors, like, chemical and physical agents, microbial infections, immunological reactions, hypoxia, toxins, and tissue damage (Nagajyothi et al., 2015). Different researchers have discovered that flavonoids and phenolic based constituents work as outstanding anti-inflammatory agents (Talhok et al., 2007). The anti-inflammatory assets of flavonoids was comprehensively investigated and its useful role have been described in several animal models (Talhok et al., 2007). Excess creation of pro-inflammatory particles like TNF- $\alpha$  and nitric oxide are supposed to be accountable for moderating inflammation along with their vital role in immune-inflammatory mechanism. These inflammatory substances are also recognized to cause cell necrosis and damage of tissue as nitric oxide can react with the free radicals like superoxides to generate peroxynitrite, that can result to irreversible damage to cell membranes (Lee et al., 2005). For the purpose to examine an effective anti-inflammatory agent, recent study has applied MB-ZnO nanocomposite.

The prepared MB-ZnO nanocomposite was tested at various doses to determine the potential against alpha-amylase (AA) and protein kinase (PK). PK is recognized to be a crucial enzyme, having anticancer potential. Alpha-amylase performs a vital role in the hydrolysis of polysaccharides to treat diabetes. Antileishmanial Activity was also performed to determine its anti-parasitic potential. *Leishmania* is hosted by macrophages. *Leishmania* prevent the enzymatic process of Macrophages and can live inside the cells without being visible to any harm (Mehta and Shaha, 2006). Hence, it might be recommended to inhibit *Leishmania* parasites via physical way, such as through MB-ZnO, as an alternative of in an enzymatic way that can be blocked by parasites. The researcher hypothesizes that MB-ZnO, with their distinctive characteristics can be applied as an effective agent in the leishmaniasis treatment.

### ***1.6.3 Application in Crops Disease Control***

Different types of pathogens cause diseases in agriculture crops. Among them, fungus is one of the major causes of diseases that results in great economic loss.

Nowadays are mostly used for disease control. Many reports have described the application of biochar to control diseases in plants. Pathogenic microbes and nematodes induce systemic resistance resulting from the association of soil microbes (like species of *Trichoderma*, and *Bacillus*), and plant roots (Ramadan and Abd-Elsalam, 2020). In MB-ZnO nanocomposite, the ZnO component powerfully inhibits the pathogenic microbes action even in small amount and the biochar component provide a large surface area for the ZnO to interact with the microbes. Additionally, these are resilient and show great selectivity and heat resistance (Haque et al., 2022). Further, application of MB-ZnO nanocomposite as antifungal agent does not cause harm to environment as compared to traditional antifungal agents but increases the soil fertility. Furthermore, the FDA has confirmed that ZnO is a free of harmful constituents in comparison to different other nanoparticles (Kamal et al., 2022a).

The current study has characterized *Rhizopus oryzae*, and its control through nanocomposite which is a very harmful plant pathogen. The genus *Rhizopus* has been re-categorized into 7 varieties and 10 species (Liu et al., 2007). With the passage of time, the phylogenetic relationships study developed better, and scientists initiated analyzing the phylogeny of various genes like actin (act1), translation elongation factor 1  $\alpha$  (EF-1 $\alpha$ ) and rDNA ITS (Abe et al., 2010). *R. oryzae* is found everywhere in universe and some scientists have designated it as a synonym of *R. arrhizus* (Jennessen et al., 2005). *R. oryzae* belongs to the phylum Zygomycetes and resulted in huge loss of crops (Battaglia et al., 2011). It has been documented to cause diseases in different staple crops such as *Oryza sativa* (Lanoiselet et al., 2007), *Citrus medica* (Naz et al., 2015), *Ipomoea batatas* (Wang et al., 2017), *Cascabela thevetia* (Arif et al., 2017), and *Brassica campestris* (Arif et al., 2019). *R. oryzae* exists throughout the world and it looks in the form of white to gray mycelia with many spores producing sporangia (Kwon et al., 2012).

#### ***1.6.4 Trichoderma Harzianum Loaded Biochar for metal immobilization of Heavy Metals (HMs)***

The loading of biochar with useful microbial strains (fungal and bacterial species) and its use in bioremediation is considered as the best and evolving tactic for the doable

reclamation of contaminated soil (Chen et al., 2019; Wu et al., 2019). For HMs immobilization in the polluted soil, different microorganism species having resilient metal tolerance and adsorption competence have been isolated and inoculated to the contaminated soil, as microbial agents either directly or with a specific exporter material. Fungi release a large range of organic acids extracellular proteins, and different metabolites, which helps in the adaptation of the organism to environmental changes (Cochrane, 1958). Some Species of *Trichoderma* have been isolated from polluted soils and have analyzed, their capability to survive in the existence of various HMs (Zafar et al., 2007). They are of prodigious interest in agricultural science.

Species of *Trichoderma* are abundant in soils, grow fastly, having a high reproduction ability and a possess great competitive saprophytic potential (Williams et al., 2003). Further, few species *Trichoderma* having excellent antagonistic potential against pathogenic fungi of plants and have useful impact on the growth of plants (Benítez et al., 2004). Moreover, *Trichoderma Spp* are greatly resistant to a number of toxins and xenobiotic compounds (fungicides, antibiotics), and HMs (Harman et al., 2004a). HMs, apart from for mercury, do not affect the inhibition of enzyme development in the mycoparasite *T. harzianum*, proposing that mycoparasitism is effective even in the stress of heavy metal (Kredics et al., 2001). Though, little evidence is accessible on the mechanism of tolerance of HMs in this genus.

### ***1.6.5 Use of Nanocomposite in Cd-Cu Immobility***

The effect of Cd and Cu on plants depends on their bioaccessible fraction in the soil, especially on the surface of the root (Li et al., 2020). High amount of Cd and Cu in soil results in toxic effects on plants, including root growth reduction, fluctuations in mineral nutrition, carbohydrate and protein metabolism, chlorosis, and might result huge reduction of biomass (Varun et al., 2017). Decrease of biomass due to Cu and Cd toxicity could be the direct consequence of the synthesis of chlorophyll inhibition and photosynthesis. Traditional cleanup methods involve soil digging, carrying to clean sites, stations, or soil purification by physical and chemical treatment, followed by the return of processed soil to the site.



The accumulation of metals by roots could be declined by diminishing the bioavailable components of metals in the soil, which can be attained through different metal immobilizing tactics in the soil (Abbas et al., 2017). The Engineered biochar can reduce metal accumulation in plants via several processes including enhancing metal immobility in the contaminated soil and shifting the soil's basic characteristics and the response be contingent on the nature of biochar, soil type, and species of crops (O'Connor et al., 2018). The reported research revealed that a large amount of biochar was applied in several experiments for the declining metals in plants (O'Connor et al., 2018). Though, it may not be possible to apply a large amount of biochar in the field, particularly in a Pakistani soil due to its alkaline nature. Hence, a small amount of biochar, along with other treatments may be an appropriate method to decrease metal intake via crops.

Use of biochar to soil can not only isolate carbon in soil, but also enhance the quality of soil through neutralizing acidic soil, increasing the soil CEC, and enhancing the activity of soil microbes. In general, the CEC increases with increasing pH of the soil. Cha et al., (2016) documented that the CEC of biochar rises when the pH was rised from 5.1 to 8.6. Biochar having large amount of N, Ca, P, and K, which might add nutrients to the soil or may be used as a source of nutrients to microorganisms. The use of biochar to the soil increases the pore fraction. Every pore offers the space where the microbes can grow and rises the quantity of moisture, air and the residence time of nutrients, resulting in the boosted activity of microbes and enhanced growth rate of plants in that soil. The isolation of biochar in soil can decline the carbon emissions as biochar is barely decomposed by microorganisms.

The attachment of fungus to the biochar surface neutralizes the pH of soil by secreting acidic substances. Fungus-biochar composite may decrease the available fraction of the Cd and Cu to the plants by attaching on its surface due to the synergistic effect of both biochar and *T. harzianum*. This composite could also play vital part in the immobility of metals and plant growth (Cakmak and Kutman, 2018). Due to resemblance between zinc and heavy metals (Cd and Cu), this composite interacts with Cd and Cu in the soil, at the surface of the root and translocate within the plant (Shen et al., 2020). Because of the antagonistic nature in the soil-plant system, investigations have shown that Zn may reduce

plant accumulation of Cd and Cu (Ali et al., 2019). Various techniques have been applied for Zn supply the plants (Rizwan et al., 2019a). Currently, the use of nutrients the in the field of agriculture in the NPs form is determined as an effective way to enhance growth of crops (Rizwan et al., 2017).

Many studies have documented the influence of Zinc oxide in soil and plant growth (Hussain et al., 2019). Soil pH, nature of soil, and plant variety are among the major features effecting the availability of Zn in the soil and toxicity of ZnO nanoparticles to the crops (García-Gómez et al., 2018). It has been demonstrated that foliar application of Zn is effective in reducing metals absorption by plant to that of soil application (Ali et al., 2019). It has been documented that Zn use efficiency was increased in wheat plant when Zn was sprayed in nano form (Dapkekar et al., 2018). The poisonousness of NPs particularly at greater concentration might be a main problem (Sturikova et al., 2018). It is also documented that the high amount of ZnO (> 500 mg/kg) are harmful to plants whereas lower amount are useful, depends on plant variety and growth conditions (Sturikova et al., 2018). Hence, to avoid high dose, ZnO can be used in combined form with MB-ZnO, so that plants get suitable amount of micronutrients like Zn for normal growth, which justifies the use of MB-ZnO for proper plant growth.

### **1.7 EGYPTIAN RIVERHEMP (*Sesbania sesban* Linn.)**

This plant species has multiple local names in various localities such as Sesaban in Arabic, Egyptian river hemp, Jainti or Jaiyant in Bengali, Sesban in English, Añil francés or tamarindillo in Spanish.

#### **1.7.1 Habitat**

*S. sesban* is an indigenous crop of semi-arid to sub-humid regions and monsoonal places. They grow under 500-2000 mm rainfall per annum. It grows alongside streams, marshy, and moist places. The habitat of the *S. sesban* is indicative of its moisture, salinity, and alkalinity tolerance capacity (Orwa et al., 2009). China has naturalized *S. sesban* at roadsides, wastelands, stream-sides, riversides and mountain slopes, at lower than 300-

1300 m altitude (Committee, 2014). The plant is ideally suitable for flooded areas as they can survive in floods (Orwa et al., 2009).

### 1.7.2 Distribution

*S. sesban* Linn. belongs to the family Fabaceae. Its origin is not clear, however it is commonly found and cultivated in Asia and Tropical Africa. It has a wide dissemination ranging in Africa from Egypt to South Africa and west to Nigeria and Senegal. The plant is also native to southeastern Arabian Peninsula, Western Asia, Pakistan, India, Southeast Asia and northern Australia (Orwa et al., 2009).

**Table 1.1:** Classification of *Sesbania sesban* Linn.

Rank	Classification
Domain	Eukaryota
Kingdom	Plantae
Phylum	Spermatophyta
Sub-Phylum	Angiospermae
Class	Dicotyledonae
Order	Fabales
Family	Fabaceae
Genus	<i>Sesbania</i>
Species	<i>S. sesban</i>

### 1.7.3 Morphological Description

The leaves of the *Sesbania* are compound, peri-pinnate, made of 6-27 pair of leaflets, narrow, oblong, asymmetrical, with minute or absent stipules. The flowers are

yellow with white raceme inflorescence. Pods are yellow (10-20 cm long) and up to 40 seeds are present in a pod (Evans and Macklin, 1990).

#### **1.7.4 Uses of *S. sesban* Linn.**

*Sesbania* is a fodder crop, and it is also used for soil improvements. The leaves and shoots have protein (25-28%) and they are easily digestible by the cattle and goats (Evans and Macklin, 1990). *Sesbania* is a nitrogen fixing plant, and the species is grown in scattered form in the annual crop field for nitrogen fixation. It is experimentally grown in between different crops for mulching and leaf manure. The wood of *S. sesban* is used to make charcoal in India and used for firewood purposes in both India and Africa. This wood is very light in weight and cannot be used as timber. The *S. sesban* grows faster, and 10,000 trees can produce up to 15-20 tons of woody dry biomass, in one year. The flowers of *S. sesban* can be added to stews and in egg dish in certain regions, may be mainly as decor element (Kathiresh et al., 2011).

#### **1.7.5 Medicinal Usage**

Parts of *S. sesban* plants are utilized as conventional medicine. The seeds of plant are applied to treat inappropriate menstrual flow, decrease the spleen enlargement, skin diseases and diarrhea. Leaves are used as Anthelmintic (Gomase, 2012) and show different potential anti-fertility activities (Priya et al., 2012), CNS stimulant effect (Naik et al., 2011), anti-inflammatory (Faris and Singh, 1990), anti-diabetic (Pandhare et al., 2011) and adjuvant induced arthritis (Dande et al., 2010).

#### **1.7.6 Antioxidant and Phytochemical Properties**

The anthocyanin, extracted from the flowers of *S. sesban* has dose dependent free radical scavenging activity against superoxide anions, hydroxyl ions and DPPH radicals, which prove it can deal with stress conditions such as heavy metal stress (Kathiresh et al., 2011). Upon the prelude phytochemical screening, it divulges the presence of tannis, amino acids, pyruvic acid, carbohydrates, triterpenoids, guaiacyl and alpha-ketoglutaric acid (Pandhare et al., 2011).

The current study was designed to engineer biochar via eco-friendly methods and its application in various fields including environmental problems, biomedical and agriculture for disease control and plant growth and to provide an insight into the mechanisms.

## 1.8 AIMS AND OBJECTIVES

The current study was envisioned with the following objectives:

- Synthesis and characterization of biochar-nanocomposite with solvent free and environmental-friendly procedures.
- To investigate the adsorption and photocatalytic potential of the nanocomposite for the elimination of inorganic and organic pollutants under various light and dark environments.
- To study the effect of the prepared MB-ZnO nanocomposite in different biological assays.
- Isolation and identification of disease-causing agent of the Kiwi leaf spot and its control using MB-ZnO nanocomposite.
- Use of Biochar and *Trichoderma harzianum* loaded biochar in the immobilization of Cd-Cu dual polluted soil and to elaborate their effects on the physiochemical properties and function of soil.
- Application of engineered biochar for the growth enhancement of *S. sesban* in metals-contaminated soil.

# CHAPTER 2

# **MATERIALS AND METHODS**

## 2. MATERIAL AND METHODS

### 2.1 EXPERIMENT 1: BALL-MILLED SYNTHESIS OF MAIZE BIOCHAR-ZNO NANOCOMPOSITE (MB-ZnO) AND ESTIMATION OF ITS PHOTOCATALYTIC ABILITY AGAINST DIFFERENT ORGANIC AND INORGANIC POLLUTANTS

The objectives of this study were obtained by the following methodology.

#### 2.1.1 *Plant Material*

Maize straw was collected from the local farmland of Islamabad capital territory (ICT) and crushed to 1–1.5 mm for the preparation of biochar. All chemicals used in this work (Safranin, Mancozeb, ZnO, NaOH, and HCl) were purchased commercially. Deionized water was used for the synthesis of chemical solutions.

#### 2.1.2 *Synthesis of Biochar*

Maize biochar (MB) was synthesized according to a standard protocol (Yu et al., 2016). Concisely, the maize straw was cut into small pieces, splashed with deionized water, desiccated in a shade, creased, and sieved. Then the powder that was obtained from sieving was filled in china dishes (10 g) and positioned in a vacuum furnace. The powder was pyrolyzed at 600 °C for 6 h. The attained biochar was sieved through an 80-mesh sieve and deposited till more application.

#### 2.1.3 *Preparation of Nanocomposite*

MB-ZnO was prepared by merging ZnO with synthesized maize straw biochar (MB) via the ball-milling apparatus. Usually, about 6 g of each ZnO and MB mixture (50:50 ratio by mass) were shifted to an agate jar of 500 mL, having 180 g agate balls (6 mm), and placed in a planetary ball milling apparatus. The agate balls and material (ZnO and MB) were present with a ratio of 15:1 (by mass). The physical milling was executed in a horizontal oscillatory mill in a water-free environment for 72 hours. The physically milled constituents were utilized directly, with no using any solvent medium.

#### **2.1.4 Characterization of MB-ZnO Nanocomposite**

The surface morphology of the MB-ZnO was inspected via scanning electron microscopy (SEM, JEOLJSM 25910). The FT-IR analysis was studied by using a spectrophotometer (SPECTRUM, 65). The crystalline properties of prepared MB-ZnO was studied at 0–80° by X-ray diffraction (XRD, Bruker, D8). The thermal assessment was performed in a thermogravimetric analyzer (Mettler Toledo TGA/SDTA851e). The element study was done with the help of energy-dispersive X-ray spectroscopy (EDX, UKINCA 200). Optical properties of the MB-ZnO nanocomposite were determined through UV–Vis diffused reflectance spectroscopy ranges from 200–800 nm. The value of band gap energies of the prepared MB-ZnO were calculated from diffuse reflectance UV–Vis. The band gap of the MB-ZnO was calculated according to the following formula:

$$(\alpha h\nu)^2 = K(h\nu - E_g) \quad (1)$$

In the above equation  $\alpha$  represent the absorption coefficient,  $h\nu$  shows photon energy (eV),  $K$  is the absorption index and  $E_g$  indicates band gap energy.

#### **2.1.5 Adsorption and Photocatalysis Performances against Organic and Inorganic Pollutants**

##### **2.1.5.1 Stock Solutions of Pollutants**

To check the adsorption and photodegradation efficiency of MB-ZnO under different light conditions against organic and inorganic pollutants, a stock solution of each pollutant was prepared. For the synthesis of Safranin stock solution, 15 mg of Safranin (Saf) was dissolved in 300 ml water. For further analysis, this solution was equally divided into 3 different flasks, each containing 100 ml solution and 5 mg of MB-ZnO was added to each flask. The pH of each solution was recorded and adjusted to 6.8. In parallel, Mancozeb stock solution (MC) was prepared under the same conditions and concentrations.

##### **2.1.5.2 Adsorption experiments in dark conditions**

To check the activity of biochar nanocomposite in dark, the adsorption tests



of Safranin (Saf) and Mancozeb (MC) were conducted separately in dark conditions, at 25 °C. Adsorption of Saf and MC by biochar-nanocomposite (MB-ZnO) was conducted, separately. For the adsorption study of Saf, a solution of one 100 mL flask was homogenized in a sonicator for 1 hour. The suspension was then stirred and after the interval of each 10 minutes, 3 ml of the solution was collected for the concentration measurements. All the sampling solutions were immediately centrifuged for 5 minutes at 4000 rpm and filtered through a 0.45 µm syringe filter. The concentrations of Saf in the collected samples were measured by UV-Vis spectrophotometer (Evolution 300 UV-Vis spectrophotometer) at a wavelength of 660 nm. The same procedure was followed for the estimation of MC.

### ***2.1.5.3 Photocatalysis Experiment***

Photocatalytic activities of the ball-milled synthesized MB-ZnO nanocomposite were assessed through the photodegradation of Saf and MC under different light sources (visible light and UV). Based on previous protocol of Yu et al., (2016), 5 mg/100 mL dose of MB-ZnO nanocomposite was applied. To assess the valuation of photodegradation of Saf, two flasks of 100 mL of synthesized solution were placed in a sonicator for 60 minutes to prepare a homogeneous mixture. These flasks were exposed to various light sources. The first flask was kept in visible light (in the 500 W Xe Lamp) and stirred for one hour. The second flask was placed in UV radiation (400 W) in a separate sealed container and stirred for one hour. In each case, the light source was almost 10 cm away from the solution. In the whole photodegradation process, the pH and temperature were sustained at 6.8 and 25 °C, correspondingly.

To analyze the degradation efficacy of the MB-ZnO in both light conditions, 3 mL sample were collected from both stirred solutions, after the break of every 10 min. All the samples (3 mL) were directly centrifuged at 4000 rpm for 5 minutes and filtered via a 0.45 µm syringe filter. The amount of Saf was measured with a UV-Vis spectrophotometer at a wavelength of 660 nm. A similar protocol was adopted for the MC assessment.

The percentage of degradation rate of individually Saf and MC through MB-ZnO nanocomposite was calculated according to the mentioned formula:

$$\eta = \frac{C_0 - C_t}{C_0} \times 100 \quad (2)$$

Where  $\eta$  (%) indicates the degradation percentage of pollutants.  $C_0$  and  $C_t$  (mg/L) stand for the primary concentration and equilibrium concentration of pollutants, respectively. The photocatalytic activities of prepared biochar nanocomposites were measured by studying the discoloration of Saf and MC solutions.

#### **2.1.5.4 Total Organic Carbon Analysis (TOC)**

Total organic carbon was analyzed according to the reported literature (Radich et al., 2014). Concisely, for determination of TOC, 1 mL HCl was mixed to 10× diluted samples, for the purpose to remove carbonates and residues of CO<sub>2</sub>. TOC study was done by means of TOC-analyzer and IR detector. The temperature was increased to 700 °C in the catalytic furnace, progressively to convert the intermediate products to CO<sub>2</sub>, entirely.

#### **2.1.5.5 Kinetic Study**

In all the experiments, the pollutants withdrawal throughout the irradiation under light sources followed pseudo-first-order kinetics. The kinetics of the photocatalytic decolorization rate of the pollutants were calculated by applying the following Langmuir–Hinshelwood kinetics model:

$$\ln (C_0/C_t) = \text{Kappa} \quad (3)$$

Initial decolorization rate constants were calculated from the slope of  $\ln (C_t/C_0)$  vs  $t$  (min.) plots. Where,  $C_t$  is the concentration of Pollutant (Saf and MC) at any given time,  $C_0$  is the concentration of a pollutant at zero-time, and  $t$  is the irradiation time and Kappa is the apparent kinetic constant. The whole light-driven degradation rate of Saf and MC by the photocatalyst followed pseudo-first-order kinetics.

## 2.2 EXPERIMENT 2: BIOLOGICAL APPLICATIONS OF BALL-MILLED SYNTHESIZED BIOCHAR-ZINC OXIDE NANOCOMPOSITE (MB-ZnO) USING ZEA MAYS L.

The core aim of this experiment was to evaluate the application of MB-ZnO nanocomposite in various biological processes. To accomplish this study, MB-ZnO nanocomposite was synthesized, as described under heading 2.1.1 to 2.1.4, and used for the following assays:

### 2.2.1 Biocompatibility Assays

The biocompatible nature of the prepared nanocomposite was investigated against human RBCs and macrophages. Hemolytic assay was implemented to evaluate the biocompatible behavior of the prepared nanocomposite with fresh isolated RBCs, according to the a earlier described procedure (Khalil et al., 2018). In the assay, 2mL of blood was collected in an EDTA tube from a healthy person. To extract RBCs, blood sample (1 ml) was centrifuged at 12000 rpm for six min. RBCs suspension of was prepared by adding 200  $\mu$ L of extracted RBCs with 9.8 ml phosphate buffer saline having pH of 7.2. Then, RBCs suspension of 100  $\mu$ L was amended with MB-ZnO nanocomposite and placed in at 40 °C for one hr. After that sample was centrifuged for 15 min at 12000 rpm. To examine hemoglobin (Hb) comes out from the RBCs, the supernatant was transported to a 96-well plate and its absorbance was sedate at 540 nm. DMSO was applied as a negative control and triton X-100 was used as a positive control. The data was summarized as percentage hemolysis and calculated using the following equation:

$$\text{Hemolysis (\%)} = 100 \times (\text{Abs} - \text{Abnc}) / (\text{Abpc} - \text{Abnc}) \quad (4)$$

The: Abs denotes the sample absorbance, Abpc shows positive and Abnc represents negative control.

To investigate the biocompatible behavior of the nanocomposite against phagocytes, MTT cytotoxicity was implemented against healthy isolated phagocytes (Ali et al., 2017). Macrophages were extracted following the standard procedure (Malagoli, 2007). After extraction, the macrophages were treated with multi

concentration of MB-ZnO nanocomposite (1.95–250 µg/ml) for 24 hours. Pure phagocytes culture (without MB-ZnO) was utilized as a positive control. Inhibition percent was determined using to the following equation:

$$\text{Inhibition} = 1 - \text{sample absorbance} \times 100 / \text{control absorbance} \quad (5)$$

### 2.2.2 Protein Kinase Inhibition Potential (PK)

Protein Kinase inhibition via the prepared nanocomposite was executed, according to previous standard protocol (Fatima et al., 2015). For PK, *Streptomyces* 85E strain was kept in a tryptone soya broth medium for 96 h at 30 °C. To synthesize a bacterial lawn, the fresh colonies of bacteria were dispersed on sterilized plates containing ISP4 medium. The MB-ZnO nanocomposite (15 µl) was scattered on filter discs of 6 mm and placed on the Petri dishes, to investigate the PK inhibition potential of bacterium. Surfactin was applied as a positive control and DMSO as a negative control. To examine the growth of *Streptomyces* 85E was incubated for 72 hr at 30 °C. After the incubation of 24 hours, clear and bald zones could be examined around the discs, which proved the spore inhibition and mycelial growth. Afterward, the inhibition zone was recorded.

### 2.2.3 Alpha-amylase (AA) Inhibition Potential

Alpha-amylase inhibition potential of MB-ZnO nanocomposite was assessed, using the previous protocol, with slight adulterations (Ebrahiminezhad et al., 2018). In this activity, the reaction mixture, consisting of 85 µl phosphate buffer, 80 µl AA enzyme (0.14 U/ml), 10 µl MB-ZnO (1 mg/ml DMSO), and 40 µl starch solution (2 mg/ml in deionized water), was incubated in 96 well plates for 35 min at 45 °C. To cease the reaction, 20 µl HCl (1 M) was added to it. To every well, 20 µl of iodine reagent (5 mM potassium iodide and 5 mM iodine in phosphate buffer) was added. For the preparation of the blank well, phosphate buffer and DMSO were added in place of the sample and α-amylase enzyme solution, respectively. DMSO was used as a negative control and acarbose was taken as a positive control. The absorbance was measured at 540 nm. The activity was described as percentage of α-amylase inhibition and was determined using the formula below.

$$\alpha\text{-amylase inhibition (\%)} = (O_s - O_n) / (O_b - O_n) \times 100 \quad (6)$$

Where:  $O_n$  is the absorbance of negative control,  $O_s$  is the absorbance of the sample and  $O_b$  is the absorbance of the blank.

#### 2.2.4 Antileishmanial Assay of MB-ZnO nanocomposite

The antileishmanial activity of the nanocomposite was assessed against *Leishmania tropica* promastigotes, following the previously documented protocol (Ahmad et al., 2016). All test tubes contain 3 mL of medium with  $1 \times 10^5$  parasites/mL of *L. tropica* promastigotes. In separate tube, 5 mL of each dose (10  $\mu\text{g/ml}$ , 50  $\mu\text{g/ml}$ , 100  $\mu\text{g/ml}$ , and 150  $\mu\text{g/ml}$ ) of MB-ZnO nanocomposite was decanted and placed in incubator at 28 °C. During this experiment, amphotericin-B was taken as a positive control and DMSO as a negative and. Parasites numbers were counted via hemocytometer separately in control and MB-ZnO nanocomposite amended samples at various time duration (24, 48, 72 and 96 h) of incubation experiment and the percentage inhibition was measured through the following formula:

$$\text{Inhibition (\%)} = 100 \times \text{Absampl}/\text{Abcontrol} \quad (7)$$

Where, Absample refers to the absorbance of the treated sample and Abcontrol shows to the absorbance of the negative control.

#### 2.2.5 Anti-inflammatory Assay

Anti-inflammatory potential of MB-ZnO nanocomposite and biochar nanoparticles (MB NPs) was assessed by the Heat-induced Albumin denaturation procedure (Ahmad et al., 2016). Reaction cocktail bovine serum albumin (BSA) was synthesized in saline Tris buffer (pH 6.8). Stock solution (1 mg/ml) of treated samples was more diluted in methanol to get the anticipated concentration. The 900  $\mu\text{l}$  of BSA solution was blended with 100  $\mu\text{L}$  of different doses (1000, 500, 250, 125, and 62.5  $\mu\text{g/ml}$ ) of MB-ZnO nanocomposite. Diclofenac sodium ( $\mu\text{g/ml}$ ) was taken as a standard (Ismail and Mirza, 2015). Primary heating of samples was executed at 37 °C for 30 minutes, followed by final heating for 30 minutes at 50 °C. Samples were cooled down for 10 minutes at room temperature and their absorbance was measured at 660 nm. The

activities was implemented thrice, and the protein breakdown was calculated according to the below mentioned formula:

$$\text{Protein inhibition (\%)} = 100 \times (\text{Abs. (control)} - \text{Abs. (sample)}) / \text{Abs. (control)} \quad (8)$$

### **2.2.6 Antioxidant Activities**

Following the methodology of Ali et al. (2021), various antioxidant activities including total antioxidant capacity (TAC), total reducing power (TRP), and DPPH-free radical scavenging (FRSA) were performed to assess the antioxidant assays of the prepared nanocomposite at different doses (1–200 mg/mL).

#### **2.2.6.1 Total Antioxidant Capacity Determination**

To evaluate TAC, MB-ZnO nanocomposite (100  $\mu\text{L}$ ) was mixed with a reagent, following the standard methodology (Javed et al., 2016a). The mixture was cooled down to room temperature and then the absorbance was recorded at 660 nm, via a microplate reader. Ascorbic acid (AA) was taken as a positive control and DMSO was applied as a negative control. TAC was measured as  $\mu\text{g}$  ascorbic acid equivalent per mg dry weight ( $\mu\text{g AAE/mg DW}$ ).

#### **2.2.6.2 Total Reducing Power Determination**

TRP of the synthesized nanocomposite was determined by potassium-ferricyanide method (Baqi et al., 2018). DMSO was taken as a negative control and AA was applied as a positive. The solution absorbance solution was measured at 620 nm, and the TRP of MB-ZnO nanocomposite was recorded as AA equivalents per milligrams (AAE/mg).

#### **2.2.6.3 Free Radical Scavenging Assay**

To evaluate FRSA, DPPH (2, 2-diphenyl-1-picryl hydrazyl) was synthesized in methanol and utilized as a reagent solution. Briefly, a reagent solution of 180 mL was poured to the test concentrations of 20 mL and placed in incubator for 60 mins. FRSA (%) was observed at 515 nm (Ali et al., 2021). AA was taken as a positive, whereas DMSO was utilized as a negative control. % was measured using the following formula:

$$\text{FRSA (\%)} = 100 \times \text{Ab sample/Abs negative Control} \quad (9)$$

### 2.2.7 Antifungal Assay

The antifungal activity of the prepared nanocomposite was performed against the pathogenic fungi, *Alternaria alternata* (accession no. MH553296). The preserved *A. alternata* culture was freshen on potato dextrose agar (PDA) media for for one week at  $26 \pm 1$  °C. The antifungal potential of MB-ZnO nanocomposite was assessed using the “food poisoned” technique. PDA media was amended with different doses (6 mg/mL, 12 mg/mL, and 19 mg/mL) of MB-ZnO nanocomposite. The 4mm disc of *A. alternata* was inoculated and positioned in the middle of MB-ZnO amended PDA containing plates via the Cork borer. PDA lacking of MB-ZnO nanocomposite was taken as a positive control. Inoculated Petri plates were placed in incubator at  $26 \pm 1$ , for one week and the inhibition was calculated using the following formula:

$$\text{Growth Inhibition (\%)} = 100 \times (C - T) / C \quad (10)$$

Where C refers to the average mycelial growth in the positive control plate, and T denotes the average growth of mycelia in a MB-ZnO nanocomposite treated plate.

### 2.2.8 Statistical Study

The statistic ta were evaluated by one-way ANOVA with the help of statistical software SPSS (SPSSversion16.0). Whole experiments were performed in triplicate, and means were studied. Graphical representation of different activities were studied by using the Origin (4.5).

## 2.3 EXPERIMENT 3: DIAGNOSIS AND CONTROL OF BROWN LEAF SPOT OF KIWI (*ACTINIDIA DELICIOSA*) USING BIOCHAR-ZINC OXIDE (MB-ZnO) NANOCOMPOSITE AS A NON-TOXIC BIO-FUNGICIDES

The part of study was directed to identify the Kiwi leaf spot pathogen and MB-ZnO was tested for the control of Kiwi leaf spot disease.

The experiment was conducted using the following materials and methods.

### 2.3.1 Field Observation

In the period of October-November 2021, minute brown color spots were observed on the leaves of Kiwi plant, in the Islamabad capital territory (33.6844° N, 73.0479° E) and adjacent areas (Fig. 2.1). The samples (effected leaves) were collected, tagged, and packed separately in sterilized polythene bags and brought to the laboratory of Molecular Plant Pathology, for further analyses.

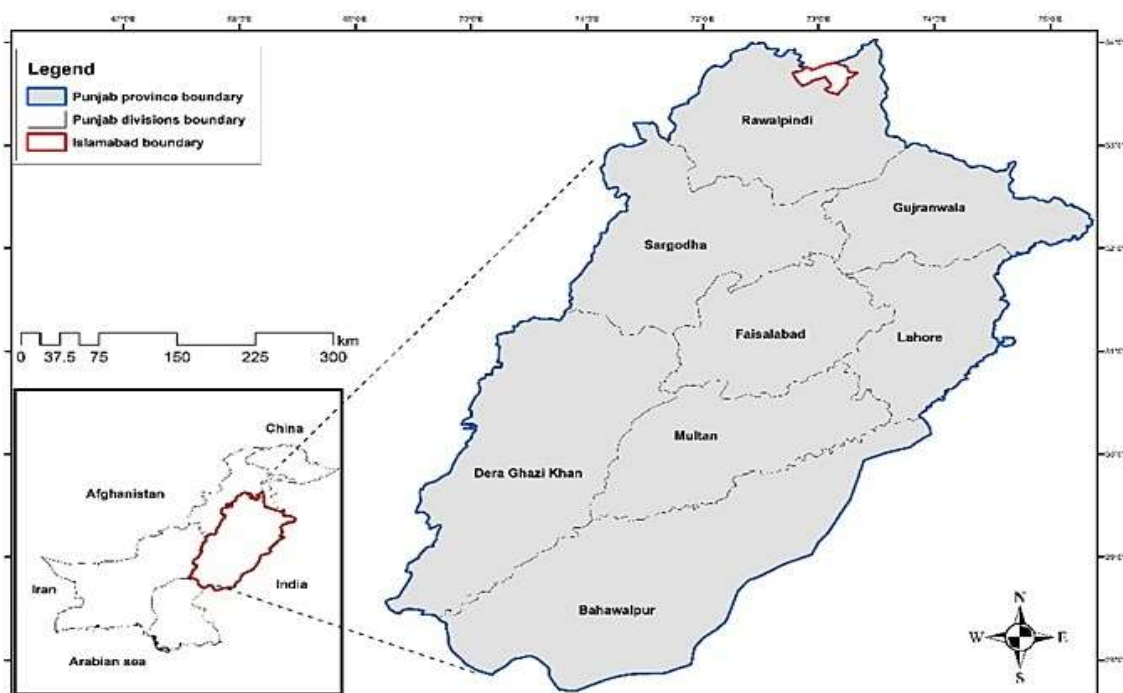


Fig. 2.1 Sample collection area.



### 2.3.2 Isolation of Disease-Causing Agent from Infected Leaves

Surfaces of collected diseased leaves were sterilized with 75% ethanol and rinsed three times with autoclaved distilled H<sub>2</sub>O. From each sterilized leaf, minor diseased portions (<1 cm<sup>2</sup>) were excised and placed on Petri plates containing potato dextrose agar (PDA). The Petri plates were placed in an incubator at 28°C for three days. After visible mycelial growth, single spore cultures were produced on PDA and incubated again. After one week of incubation, protrusive mycelial growth was examined and photographed from both the front and back sides of Petri plates.

### 2.3.3. Microscopic Recognition

For light microscopy, 1 to 2 droplets of lactophenol blue were positioned on the slide, and from the edges of the fungus growth medium; mycelial fragments were transferred to the slide. Mycelia were torn apart swiftly, and a drop of lactic acid was positioned on the slide. To evade bubbles, the coverslip was placed cautiously, and the slide was examined under microscope at 40× magnification.

### 2.3.4 Molecular Analysis

As all isolates revealed indistinguishable morphology, only one isolate was randomly selected and used for more analyses including molecular study and pathogenicity tests. For genomic examination, DNA was extracted via CTAB method (Cullings, 1992). Briefly, for isolation of DNA, 2% CTAB, 100 mM Tris-HCl (pH 8), 20 mM EDTA, 1.4 M NaCl, and 1% PVP was utilized. Forward ITS1 primer (FTCCGTAGGTGAACCTGCGG) and reverse ITS4 primer (TCCTCCGCTTATTGATATGC) were utilized to amplify 1 ITS regions (White et al., 1990). Concisely, the reactions were executed in 0.2-mL tubes in 100 µL reaction volume, having the following ingredients: 10 mM Tris-HCl, 2.5 mM MgCl<sub>2</sub>, 200 µM dNTP, 0.02 U/µL *Taq* DNA polymerase, 1 ng/µL genomic DNA (template) and 1 pmol/µL of each oligonucleotide primer. Furthermore, forward EF1 primer (GTTGTCATCGGTCACGTCGATTC) and reverse EF2 primer (ATGACACCRACAGCGACGGTTTG) were applied to amplify the gene sequence of elongation factor 1-alpha (EF-1α). Polymerase chain reaction (PCR) was performed having 25 µL of total volume containing DNA template of 1 µL, 10 µL of master mix,

10 mM of each forward and reverse primer, and 13  $\mu\text{L}$  of sterilized distilled water. The reaction was executed at 94 °C for 3 minutes, with a entire of 35 cycles of 94 °C for 30 seconds, 56 °C for 30 seconds, 72 °C for 1 minute, and a last step of 72 °C for 7 minutes. Amplified PCR product was sequenced and exposed to a BLAST analysis (<https://blast.ncbi.nlm.nih.gov/Blast.cgi>).

### **2.3.5 Phylogenetic study by MEGA 7.0**

For the creation of the phylogenetic tree, the sequences of nucleotide were aligned by MEGA (version 7.0) (Howell et al., 1999). Using 1,000 bootstrap replications, the phylogenetic tree was created via the maximum composite method.

### **2.3.6 Pathogenicity Assessment**

To authenticate the pathogenicity of the isolated pathogen Koch's postulates were followed. Twenty different fresh Kiwi leaves were detached and then sterilized their surface. Ten healthy leaves were inoculated with 10  $\mu\text{L}$  conidial suspension ( $10^6$  conidia  $\text{mL}^{-1}$ ) of isolated pathogen after wounding. The additional ten leaves were inserted with sterilized distilled water and used as control treatment. All the leaves were placed in incubator at 26°C and having relative humidity of 75-80%. After the growth of lesions, the pathogen was re-isolated on PDA media and morphology of the fungus was analyzed.

### **2.3.7 Synthesis of MB-ZnO**

MB-ZnO was synthesized, as described under heading 2.1.1 to 2.1.4, and used for the following assay.

### **2.8 Antifungal activity of MB-ZnO**

Using the food poisoned technique, the antifungal activity of MB-ZnO was studied. For the assessment of the antifungal potential of the nanocomposite, PDA media was treated with various doses of (6 mg/mL, 12 mg/mL, and 19 mg/mL) of the MB-ZnO. A 4 mm disc of *R. oryzae*, was positioned in the center of the PDA plates via Cork borer. PDA without M-ZnO used as a control sample. These injected Petri plates were located in an incubator at  $26 \pm 1$  °C for 7 days and the inhibition was calculated through the following formula.

$$\text{Growth Inhibition \%} = (C-T) / C \times 100 \quad (11)$$

In the above formula, C denotes average mycelial growth in control treatments, and T shows average mycelial growth in MB-ZnO-nanocomposite amended samples. The activity was accomplished in triplicate.

## **2.4 EXPERIMENT 4: *TRICHODERMA HARZIANUM* SUPPLEMENTED BIOCHAR PRODUCTION TO ENHANCE METAL STABILIZATION AND ENZYMATIC ACTIVITY IN CONTAMINATED SOIL**

In this section, engineered biochar was used for the immobilization of cadmium and copper. For this purpose, the following materials and methods were used.

### ***2.4.1 Synthesis of Biochar***

The maize straw was utilized for the preparation of biochar (MB), according to the protocol of Liu et al. (2017). Earlier studies have described their potential in the immobilization of metals (Li et al., 2016). Biochar was prepared by gradual pyrolysis for 5 h, in a vacuum furnace at 600 °C, in an anaerobic environment. The elementary characteristics of the MB were recorded (Table 1). Prior to usage, the prepared biochar was crushed and passed through the sieve of 0.30 mm pores size.

### ***2.4.2 Preparation of *Trichoderma harzianum* Loaded Biochar***

The fungal strain of *Trichoderma harzianum* was attained from the preserved culture of laboratory. *T. harzianum* has been reported to exhibit strong potential to tolerate heavy metals in polluted soil (Tu et al., 2020). For the synthesis of *T. harzianum* loaded biochar (MBT), the fungus was grown on PD media and mixed with autoclaved sorghum seeds, for 10 days. Subsequently, fungus-coated sorghum seeds were mixed with synthesized biochar in 1:1 ratio (w/w) and placed at room temperature for one week. The sorghum seeds were removed from the biochar after one week of incubation and the synthesized MBT was examined under scanning electron microscope (SEM) (JEOLJSM 25910). The pristine biochar (without fungus) was also examined under SEM.

### ***2.4.3 Soil Incubation Testing***

The samples of soil were collected from the topsoil (0–20 cm) of the unpolluted field. The basic soil properties like pH, soil texture, electrical conductivity (EC), cation exchange capacity (CEC), organic substances, and elemental composition (C, K, P,

and Na) were measured (RK, 1999). The soil was shade-dried and sieved to eradicate various scums like nuggets and organic remains. Later, the solutions of Cu (NO<sub>3</sub>)<sub>2</sub> and Cd (NO<sub>3</sub>)<sub>2</sub> were variegated in soil, carefully, and placed for 2 weeks at room temperature. The treated soil contained 60 mg kg<sup>-1</sup> and 258 mg kg<sup>-1</sup> of Cd and Cu, correspondingly.

The incubation trial was executed in a thermostatic chamber for 90 days at room temperature (25 °C). Cd and Cu amended soils were treated with both 1% and 5% concentrations of MB and MBT and designated as MB1, MB5, MBT1, and MBT5, correspondingly. Throughout the incubation span, the soil humidity was maintained at 35%. After 90 days of incubation, the sample of soil was dried in a shade and then sieved before subsequent assessment.

#### ***2.4.4 Tessier Sequential Extraction of HMs from the polluted Soil***

Using “Tessier sequential extraction procedure” fluctuations in Cd and Cu speciation and redistribution in contaminated soil samples were investigated (Tessier et al., 1979). Five diverse components nominated through this process were exchangeable (EX), carbonate bound (CB), matter bound (OM), Fe-Mn oxide bound (OX), and an organic and residual portion (RS). The first four of them were isolated through 1.0 mol L<sup>-1</sup> NaOAc (pH 5), 1.0 mol L<sup>-1</sup> MgCl<sub>2</sub>, 0.04 mol L<sup>-1</sup> NH<sub>2</sub>OH·HCl, and 0.04 mol L<sup>-1</sup> HNO<sub>3</sub> (in 30% H<sub>2</sub>O<sub>2</sub>), correspondingly. The fifth fraction was collected by digesting the residual part with the mixture of HNO<sub>3</sub>-HF-HClO<sub>4</sub>.

#### ***2.4.5 Phyto-availability of HMs in the Contaminated Soil***

Soil heavy metals take out through diethylenetriamine penta acetic acid (DTPA) are used as the easily accessible portion for the intake of the plant (Fellet et al., 2014). DTPA extraction assessment is also applied to determine the level of heavy metals and to recognize bioavailability and ecotoxicity in polluted soils (Conder et al., 2001; Otomo et al., 2011). DTPA extraction protocol was used to evaluate the impacts of MB and MBT amendments on the phyto-availability of Cu and Cd. Soil samples were mixed with the extract suspension comprising 0.005 mol L<sup>-1</sup> DTPA, 0.1 mol L<sup>-1</sup> triethanolamine (pH 7.3), and 0.01 mol L<sup>-1</sup> CaCl<sub>2</sub> with a solid-to-water ratio of 1:2 (m/v). The solutions were rotated on a shaker for 2 h at 25 °C at 180 rpm, centrifuged,

and then filtered through 0.45  $\mu\text{m}$  polyethersulfone filter paper. Cu and Cd concentrations in the filtrates of the above-mentioned sequential extraction were quantified through an atomic absorption spectrophotometer.

#### ***2.4.6 Bio-accessibility of Heavy Metals in the Soil***

A unified bio-accessibility method (UBM) was utilized to analyze the consumption of Cu and Cd by the body of human through oral intake (Wragg et al., 2011). The bio-accessible portion of Cd and Cu in the gastric juice is usually more than that of the intestinal juice (Zhong and Jiang, 2017). Concisely, every amended soil sample of 2 g was blended using 45 mL artificial stomach solution, prepared using the modified UBM procedure (Wragg et al., 2011). The pH of the solution was brought to 1.1.

For the assessment of Cd and Cu in the intestine of humans, the intestinal juice was prepared according to the U.S. Pharmacopeia procedure. Briefly, the intestinal solution was synthesized from the gastric solution through the addition of pancreatin and neutralization with solid sodium hydrogen carbonate to gain pH 7. Then 2 g of soil from every treatment was blended with the simulated intestinal solution (45 mL) and the suspension was agitated slowly for 1 h at 35 °C. After that, the suspensions were centrifuged, passed over a filter, and preserved at 4 °C. Cu and Cd contents in the filtrates of the gastric and intestine phases were quantified through an atomic absorption spectrophotometer. The bio-accessibility was shown as a ratio of the concentration of Cu and Cd in the simulated extract to their entire amount in the contaminated soil.

#### ***2.4.7 Soil Enzymatic y Study***

Catalase activity was estimated, according to the standard protocol (Kumar et al., 2016). Concisely, 2 g of soil was blended with 40 mL of distilled water and 5 ml of 0.3 %  $\text{H}_2\text{O}_2$ . The mixture was agitated for 20 min at 25 °C and mixed with 5 mL  $\text{H}_2\text{SO}_4$  (1.5 mL). The suspensions were titrated with 0.1 M  $\text{KMnO}_4$ .

The urease activity was recorded using the protocol of Tabatabai et al., (1986). For the assessment of urease activity, moist soil of 5 g was incubated at 35 °C for 2 h in 20 ml of borate buffer. Later to incubation, 50 ml of 1 M KCl solution was mixed and shaken for 30 min. Absorbance of the mixture was determined by UV-visible spectrophotometer at 690 nm.

#### ***2.4.8 Data Analysis***

The whole experiment was carried out in triplicate. Results were shown as means with standard deviations. The statistical studies were done using SPSS Statistics 19.0 software. ANOVA was applied to measure the repercussion of various treatments on the evaluated factors.

## **2.5 EXPERIMENT 5: USE OF ENGINEERED BIOCHAR AGAINST THE MOBILIZATION OF Cd-Cu AND INVESTIGATION OF BIOCHEMICAL AND ENZYMATIC ALTERATIONS INDUCED BY THESE TWO HEAVY METALS IN *SESBANIA SESBAN* (L.) Merr.**

The principal aims of the current experiment was to analyze the influence of engineered biochar on growth attributes of *S. sesban*. The following protocols were adopted to assess these parameters.

### ***2.5.1 Collection of Soil and Amendments***

The samples of soil for the current work were brought from the topsoil (0–20 cm) of the unpolluted field with 25 years long-term cultivation history in Islamabad capital territory (33° 44' 16.9620" N, 73° 5' 4.1568" E), 507 meters (1,663 ft) above sea level.

### ***2.5.2 Preparation of Soil***

Any annoying material like roots was removed from the sample of soil and dried in air and sieved through 2 mm mesh. Thorough mingling of soil was ensured for the soil homogenization.

### ***2.5.3 Characterization of Soil***

Basic soil properties like soil texture, pH, CEC, EC, organic substance, and total C, K, P, Na were measured (Bajpai et al., 2006).

### ***2.5.4 Amendments of Soil***

The soil was dried in a shade and sieved to eradicate various impurities like nuggets and organic remains. Solutions of Cu (NO<sub>3</sub>)<sub>2</sub> and Cd (NO<sub>3</sub>)<sub>2</sub> were mixed carefully in the soil and placed for two weeks at room temperature. Cd and Cu level of treated soil were maintained at 60 and 258 mg kg<sup>-1</sup>, correspondingly. The basic characteristics of the soil (Table 2.1) revealed that the soil was only polluted with Cd and Cu and additional elements were present in low concentration. The soil structure



and texture was determined by the methodology of Bouyoucos (1962). Selected physicochemical properties of the soil and amount of trace element were recorded following standard methods. A pH meter was used to measure the soil pH of a 1:2.5 soil-to-water ratio solution. The organic matter content and CaCO<sub>3</sub> concentrations in the soil were determined, following the methodologies of Walkley and Black, (1934), and Stocks-Fischer et al. (1999), respectively. Total and bioavailable metal amount were measured after digesting the soil with concentrated HClO<sub>3</sub> and HNO<sub>3</sub>, and ammonium bicarbonate diethylene triamine penta acetic acid (AB-DTPA), correspondingly (Amacher, 1996).

### 2.5.5 Preparation of Maize Straw Biochar

The maize straw biochar was prepared (as discussed in section 2.1.2) and characterized by via chemical procedures, like the protocol applied for soil analysis. Basic comprehensive properties of the biochar was determined according to the methodology of Abbas et al. (2017).

**Table 2.1:** Properties of the pure biochar and soil.

Properties	Biochar	Soil
Ash contents	1.50%	–
pH	9.30	7.6
Texture	–	Silty clay
Organic matter (g kg <sup>-1</sup> )	98.41	5.8
Total C (g kg <sup>-1</sup> )	57.8	-
Total N (g kg <sup>-1</sup> )	8.46	0.57
Total P (g kg <sup>-1</sup> )	1.40	0.113
Total K (g kg <sup>-1</sup> )	11.8	6.37
Total Na (g kg <sup>-1</sup> )	–	0.09%
CEC (cmol kg <sup>-1</sup> )	10.72	5.41
E.C	–	0.261 dS/m

### **2.5.6 Preparation of Engineered Biochar**

In this experiment, both MB-ZnO nanocomposite and MBT were prepared according to section 2.1.3 and section 2.4.2, respectively and used by the following way.

### **2.5.7 Experimental Setup**

A pot culture experiment was executed in the growth chamber at Laboratory of Molecular Plant Pathology, Quaid-i-Azam University, Islamabad under ambient climatic conditions (32 °C and 40% RE). The seeds of *S. sesban* were disinfected with 1% sodium hypochlorite for 2 min. For this experiment, plastic pots (18 cm height and 32 cm diameter) were filled with 700 g of soil. These pots worked as control. For other treatment, MBT (2% w/w) was mixed in separate pots (Albuquerque et al. 2013) and the soil was incubated under dry environment for seven days before the transplantation of the seedlings of *S. sesban*. Five seedlings were transplanted in each pot and kept under controlled conditions.

### **2.5.8 Application of MB-ZnO Nanocomposite**

Foliar applications of 4 levels of MB-ZnO nanocomposite (0, 50, 75, and 100 mg/L) were performed using a hand spray on 14 days, 28 days, 42 days, and 56 days old seedlings. The solutions of specific amount of the MB-ZnO nanocomposite were prepared individually from the measured quantities of the salt in distilled H<sub>2</sub>O of 500 mL of, and the solutions were sonicated for 30 min. A total of 1.0 L volume was used in all replications of each treatment. For the selection of concentration levels and application method of MB-ZnO nanocomposite, methodology of Hussain et al., (2018) was followed.

### **2.5.9 Harvesting of Plants for Experimental Analysis**

All cultivated *S. sesban* plants were harvested after 60 days of sowing and their following physiological, biochemical, antioxidant and anatomical parameters were measured.

### **2.5.10 Physiological Parameters**

Growth attributes of harvested plants including root length, shoot length, fresh weight, and dry weight of each treatment were noted. The root and shoot lengths were measured using measuring tape and fresh weight was measured using an electrical weighing balance. For the measurement of dry weight, plant parts were placed in an oven at 70 °C for 48 hours and dry weight was measured using an electrical weighing balance (El-Sharkawy et al., 2021).

### **2.5.11 Biochemical Parameters**

Following biochemical parameters were studied to investigate the possible reaction of plant seedlings against metals stress conditions.

#### **2.5.11.1 Total Soluble Sugar**

The methodology of Ahmet et al. (2009) was used to determine the total soluble sugar of the leaves of each treatment. Using the following formula, total sugar contents were measured:

$$\text{Sugar Content} = k \text{ value} \times \text{dilution factor} \times \text{absorbance} / \text{sample weight}$$

Where  $k = 20$

#### **2.5.11.2 Protein Content of Leaves**

Protein contents of fresh leaves were measured following the standard protocol of Lowry et al. (1951).

#### **2.5.11.3 Estimation of Proline Content**

A standard procedure was used to determine proline contents of harvested plants (Günes et al., 1996). Proline content was determined by following formula:

$$\text{Proline Content} = k \text{ value} \times \text{dilution factor} \times \text{absorbance} / \text{fresh sample weight}$$

Where,  $k \text{ value} = 17.52$ ,  $\text{Weight of sample} = 0.5 \text{ g}$ ,  $\text{Dilution factor} = 2$

#### **2.5.11.4 Estimation of Chlorophyll Content**

For the estimation of photosynthetic pigments including chlorophyll a, chlorophyll b and carotenoids, the protocol of Lichtenthaler (1987) was followed.

#### **2.5.11.5 Relative Water Content (RWC)**

To calculate RWC, the standard protocol of Peñuelas et al. (1993) was used. Relative water content was derived by the given formula,

$$\text{RWC (\%)} = [(\text{FW} - \text{DW}) / (\text{TW} - \text{DW})] \times 100$$

Where FW shows fresh weight of leaves, TW represents turgid weight and DW indicates dry weight of leaves.

#### **2.5.11.6 Relative Electrolyte Leakage**

Relative electrolytic leakage (REL) was calculated by using standard protocol of Lutts et al. (1996).

#### **2.5.12 Antioxidant Assay**

##### **2.5.12.1 Peroxidase (POD)**

Peroxidase activity was assayed by following a previously optimized protocol (Vetter et al., 1958). For peroxidase activity analysis, 0.2 gram of plant material from each amendment was ground in 3 ml of 100 Mm phosphate buffer using pre-cooled mortar and pestle and centrifuged at 10,000 rpm for 15 mins at 4 °C. Supernatant was taken and 100 µl was mixed with reference solution and absorbance was checked at 436 nm. POD was calculated according to the following formula:

$$\text{POD (U/I)} = V_r \times V_t \times 1000 / \epsilon \times L \times \Delta t \times 0.100$$

Where,  $V_r$  shows total volume of reaction mixture,  $V_t$  indicates Crude enzyme solution in cuvette,  $\epsilon$  shows extinction coefficient at 436 nm ( $6.39 \text{ cm}^2 / \mu\text{mol}$ ),  $L$  shows Light path, and  $\Delta t$  shows the time duration mandatory for expansion in extinction to 0.100.

0.100 = 1 unit of POD defined as amount of enzyme that rises 0.100 of absorbance at 436 nm/minute.

#### **2.5.12.2 Superoxide Dismutase (SOD)**

Using the method of Beauchamp et al. (1971), Superoxide dismutase contents of *S. sasban* leaves was determined. .

#### **2.5.12.3 Hydrogen Peroxide Content (H<sub>2</sub>O<sub>2</sub>)**

To determine the amount of H<sub>2</sub>O<sub>2</sub> in a freshly harvested leaves of *S. sasban*, standard procedure of Kapoor et al. (2019) was followed. At 390 nm, the absorbance of the supernatant was measured.

#### **2.5.12.4 Malondialdehyde (MDA) Content**

MDA was assessed using method of Tulkova and Kabashnikovam (2022). Optical density of the supernatant was checked at 440 nm, 550nm and 660nm.

#### **2.5.13 Anatomical Parameter**

##### **2.5.13.1 Leaf Epidermal Anatomical Study (LM)**

Leaf anatomy was studied following the maceration technique of Shultze's with little modification (Brennan and Subrahmanyam, 1996). The mature and dried leaves of different plants from different treatments were examined under the light microscope. The leaf epidermis was isolated following the method of Kigkr (1971). The properly cut leaf section was retained in a test tube with 1 ml distilled water, 4 ml concentrated Nitric acid, and 2 g Potassium chloride and heated at 100 °C for 8 mins to make the leaves transparent. The samples of leaf were then placed in the Petri plate and splashed twice with double distilled water. The adaxial and abaxial dermis layers of softened leaves were isolated with the help of lax camel brush. The collected epidermal layer fragments were mounted on a slide and amended with one drop of lactic acid to clear the surface. The slide was then concealed with a cover slip. Nail polish was applied to coat the cover slip margins to prepare the permanent slide. Four different leaves samples (control and treatments) were taken and their adaxial and abaxial surfaces were studied. To obtain the consistency of epidermal characteristics, five foliar samples were taken from each treatment and about five slides of adaxial and abaxial surface of each treatment were prepared.

Leaf epidermis qualitative characteristics were examined using a Nikon light microscope and micrographs were taken via microscope (XSP-45LCD). The observed characters were the shape of epidermal cells, subsidiary cells and guard cells shape, a cell wall pattern, and stomata type.

#### ***2.5.14 Statistical Analysis***

All the experimental study was done in triplicates. The results were compiled by using excel software, for further database processing. Standard deviation and mean values were also calculated, and the graphs are formed by using Origin Lab 2021. Statistic 8.1 was used for the analysis of variance for statistical analysis. The difference among mean values of treatments ( $p \leq 0.05$ ) was measured using Tukey's Honest Significant difference test (HSD test).

# CHAPTER 3

# RESULTS

### 3. RESULTS

#### 3.1 EXPERIMENT 1

##### 3.1.1. Graphical Abstract

For initial understanding, schematic representation of the experiment has been presented in Figure 3.1.

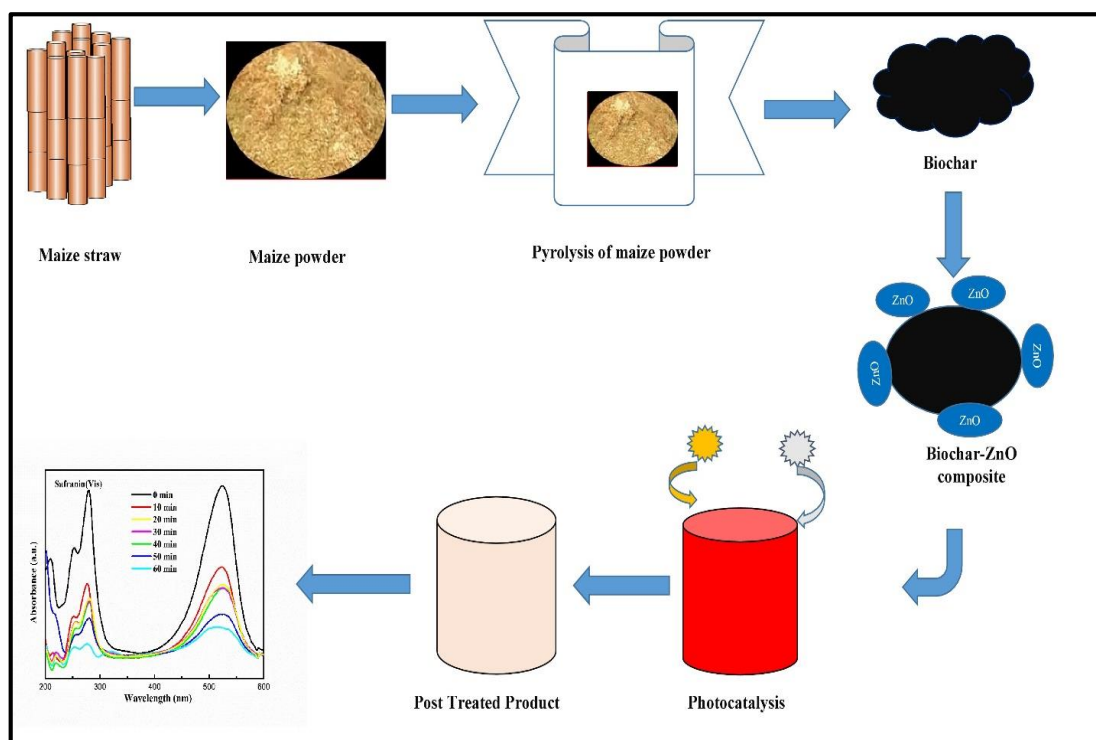


**Fig. 3.1** Schematic Demonstration of Complete Experiment.

##### 3.1.2 Characterization of Synthesized Nanocomposite

Characterization of nanocomposite revealed the following results.

###### 3.1.2.1 SEM and EDX Study

The effect of zinc oxide on the morphological properties of biochar was studied via SEM study. SEM analysis helped us to examine the porosity and shape of ZnO nanoparticles, loaded on the biochar surface of biochar. SEM image also revealed the porous and rough structure of pristine biochar (Fig. 3.2 A). This porous and rough structure might be due to the removal of volatile substances during pyrolysis. These



structural properties of MB proved its ability to adsorb and support nano-sized particles. The SEM of MB-ZnO nanocomposite exhibited ultrafine white particulates of ZnO, in the form of clusters on the whole biochar surface (Fig. 3.2 B). The EDX was performed for the quantification of attached particles (Yu et al., 2021). EDX microanalysis of MB-ZnO nanocomposite showed the existence of C, O, Ca, Si, K, Mg, Na, P, and Zn elements (Fig. 3.3 A). Additionally, a strong peak of Zn in the EDX spectrum indicated the successful interpretation of ZnO by the ball-milling process. The results were additionally investigated via the elemental exploration (Fig. 3.3 B).

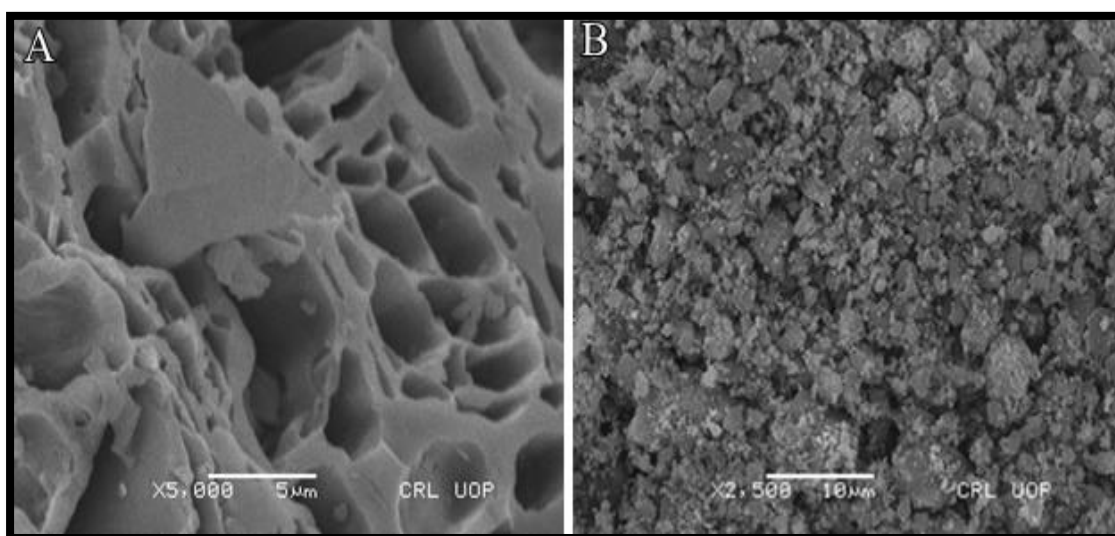


**Fig. 3.2** SEM images of pure biochar (A) and MB-ZnO nanocomposite (B).

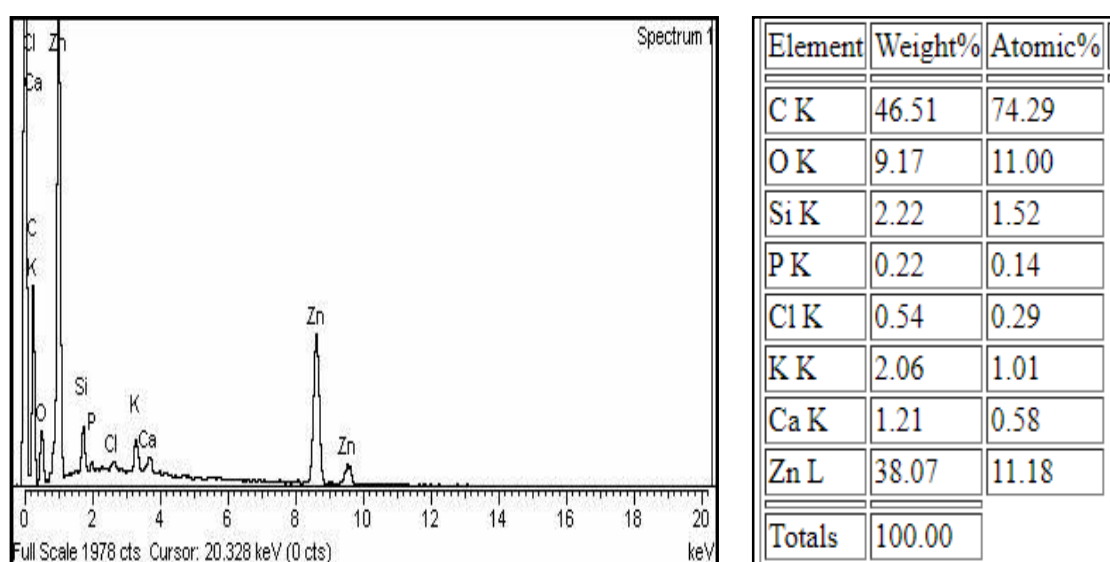


**Fig. 3.3** EDX spectra and elemental analysis of MB-ZnO nanocomposite.

### 3.1.2.2 XRD Analysis

XRD was achieved at a scanning rate of  $1^\circ$  per minute in  $0.013^\circ$  steps, casing the  $2\theta$  angle from  $10^\circ$  to  $70^\circ$ . The XRD spectrum divulged six distinctive peaks of MB-ZnO (Fig. 3.4). It revealed a low-intensity peak at  $63^\circ$ , recommending squat crystallinity. XRD pattern of MB-ZnO confirmed different peaks at  $31.85$ ,  $34.51$ ,  $36.36$ ,  $47.62$ ,  $56.65$ , and  $62.93^\circ$ , conforming to (100), (002), (101), (102), (110), and (103), respectively, which revealed crystallographic planes of hexagonal arrangement of synthesized ZnO NPs, according to JCPDS (no. 036–1451) (Duo et al., 2018). Following the Scherrer formula, the normal MB-ZnO particle size was calculated as 47 nm, which confirmed their successful synthesis.

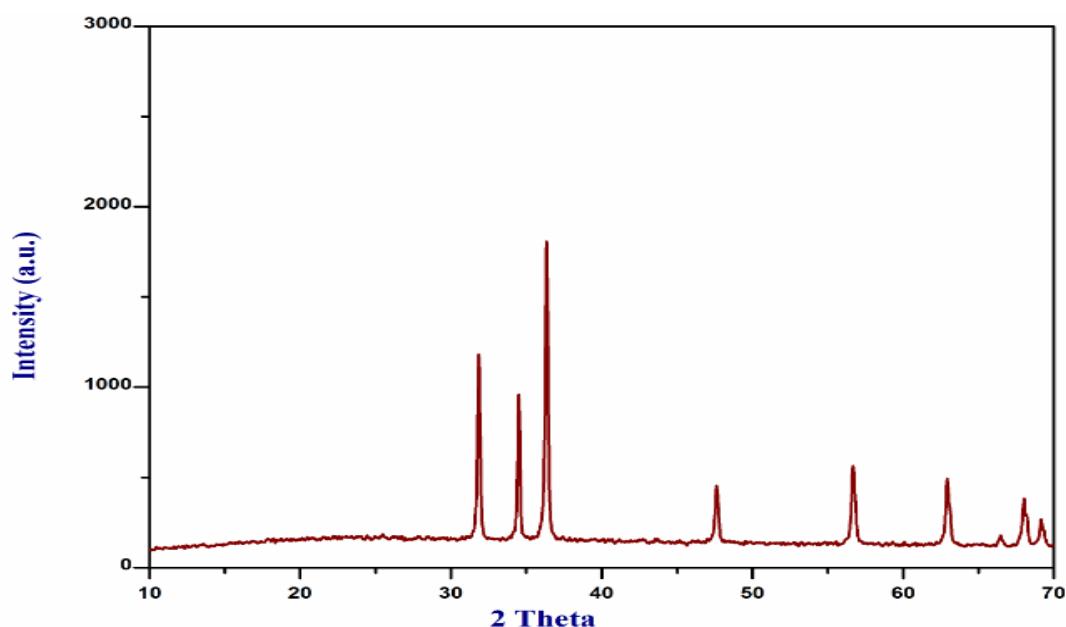


**Fig. 3.4** XRD analysis of MB-ZnO nanocomposite.

### 3.1.2.3 FTIR Analysis

FTIR study is commonly used to identify functional groups that might participated to the stabilization and reduction of nanocomposite (Batra et al., 2012; Chu et al., 2012). FTIR analysis successfully determined various dominant functional groups of the nanocomposite (Fig. 3.5). In the FTIR analysis, nine different peaks were observed in the range of  $500\text{--}4000\text{ cm}^{-1}$ . The peaks observed at  $520\text{ cm}^{-1}$  and  $556\text{ cm}^{-1}$  recognized the bending vibration of C-I stretching and C-Br stretching, respectively. The peaks located at  $799\text{ cm}^{-1}$  represented medium C=C bending of alkene. Similarly,

the peak at  $1091\text{ cm}^{-1}$  and  $1571\text{ cm}^{-1}$  indicated the strong stretching of C-O and medium stretching of C=C. The appearance of a broad peak at  $3244\text{ cm}^{-1}$  showed strong and broad O-H stretching of alkyne. Interestingly, the highest peak observed at  $520\text{ cm}^{-1}$  in FTIR spectra was similar to the previous results (Batra et al., 2012). Another peak was observed at  $556\text{ cm}^{-1}$  in MB-ZnO nanocomposite, which suggested the existence of ZnO nanoparticles at the MB surface (Arfin and Rangari, 2018).

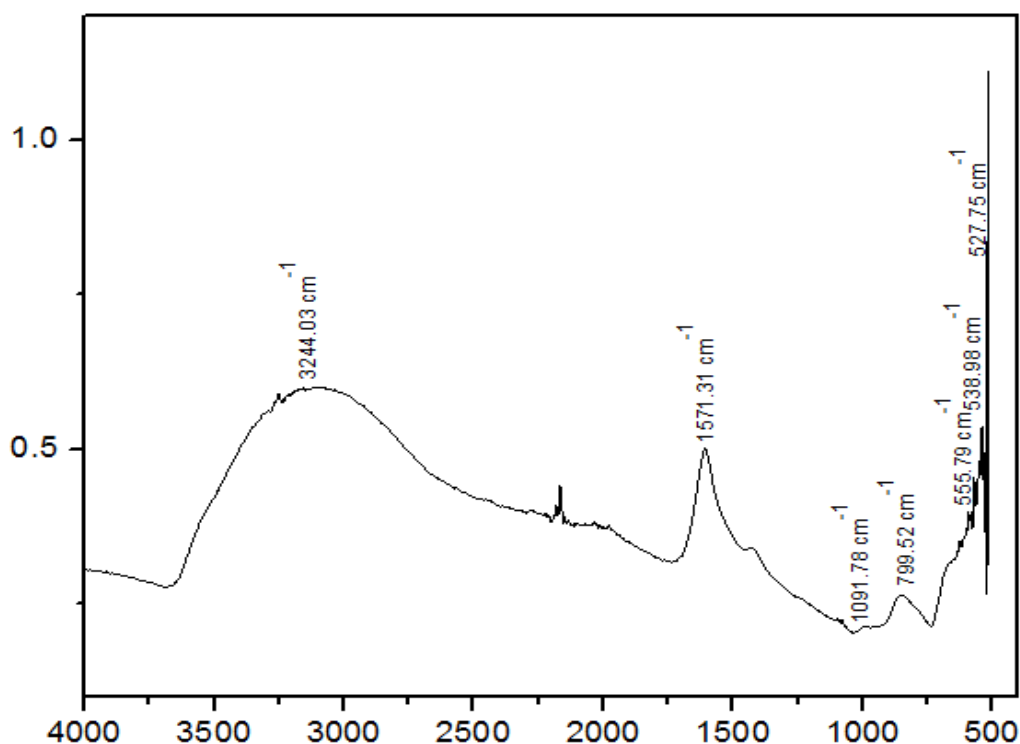


**Fig. 3.5** FTIR spectra of MB-ZnO nanocomposite.

#### 3.1.2.4 Thermogravimetric Analysis

Thermogravimetric analysis was performed to investigate thermal characteristics and ranges where biomass removal of different matters such as water vapors and additional residuals found in the samples (Pietro and Paola, 2004). TGA analysis showed the declination in weight with rising temperature. The first reduction in mass at low temperature suggest to the water droplets evaporation reserved in the pore of particles (Teo et al., 2016a).

This curve was produced because of 5% weight loss due to the vaporization of water molecule (at  $50\text{--}100\text{ }^{\circ}\text{C}$ ), additional 5-8% mass loss of hemicelluloses in plant

material (at 150 °C–350 °C), more 10–12% loss by cellulose (at 300 °C–500 °C), and another 20–25% loss by lignin (at 700 °C). In comparison to the pristine biochar (Fig. 3.6 A), MB-ZnO nanocomposite (Fig. 3.6 B) degraded fast, to some extent. It shows a considerably low thermal stability of MB-ZnO nanocomposite in comparison to pure biochar. Generally, pristine biochar has low thermal stability in comparison to MB-ZnO, but at this time biochar was synthesized at high temperature which may enhanced the thermal characteristics of the pure biochar. These findings confirmed better thermal constancy of individually pure biochar and the nanocomposite.

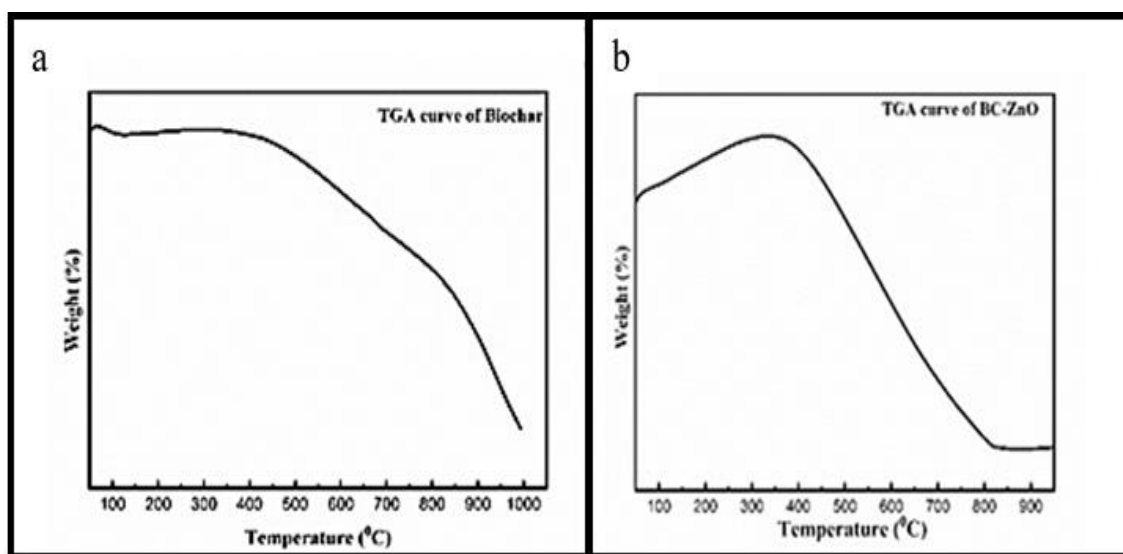


**Fig. 3.6** TGA of pure biochar (A) and MB-ZnO nanocomposite (B).

#### 3.1.2.5 Optical Properties Analysis

The excitation developed through a light source at a specific wavelength result into a distinctive peak at that wavelength and it is known as surface plasmonic resonance (SPR) in UV–visible studies. For the determination and comparison of optical behavior, a small quantity of each sample (MB, ZnO, and MB-ZnO) was dispersed in deionized water under ultrasound irradiations for 5 minutes and then the adsorption spectrum was observed by UV-Vis spectrometer. MB revealed a peak at 450 nm (Fig. 3.7 A), while the peaks of ZnO and MB-ZnO nanocomposite were observed at 350 and 400 nm, respectively (Fig. 3.7 B) indicating the reduction of ZnO on the

biochar surface. The data of absorption spectra stands as a practical appliance for determination of for valve of band gap energy.

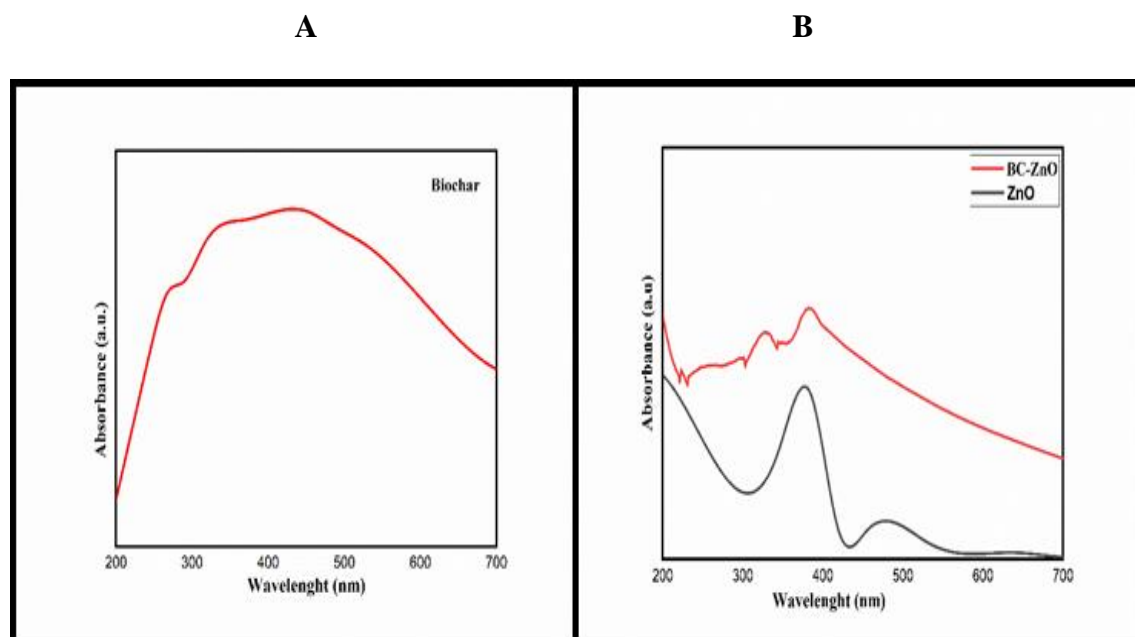


**Fig. 3.7** UV study of pure biochar (A), ZnO alone and MB-ZnO nanocomposite (B).

Using the UV–Vis spectra, the bandgap energy values were calculated. ZnO nanoparticles and biochar-ZnO nanocomposite had average band gaps of 3.04 and 2.77 eV, respectively, as documented previously (Duo et al., 2018).

The ball milled synthesized nanocomposite revealed band gap values of almost 1.71 eV. The procedure was executed by smearing the Tauc Plot technique which is pulling extrapolation at the linear area from  $h\nu$  and  $(ah\nu)^2$  correlation graph up to its cut energy axis (Teo et al., 2016a), as shown in Fig. 3.8. The Fig. 3.8 illustrates the association between band gap energy ( $h\nu$ ) and the coefficient it was absorbed in photon  $(ah)^2$  as the ordinate till it cut energy axis, and therefore the value of band gap energy can be attained.

The decrease of band gap in MB-ZnO nanocomposite may because of the creation of some fresh energy statuses in MB-ZnO produced due to the interaction of ZnO and MB in the MB-ZnO or might because of the certain elements constricting the band gap existing in the synthesized carbon biomass, which reduce energy requisite for

the electrons to transition from the valence to the conduction band of ZnO (Zhang et al., 2012).

Many researcher has described that the charging of semiconductors like zinc oxide on the surface of non-metallic particles (like carbon, Sulphur, nitrogen and calcium) can elevate their photocatalytic ability, because the band gap reduction and enhance the range of absorption to the visible light (Ahn et al., 2007; Zhang et al., 2014b). Further, it also escalate electron, due to the great dual conductivity between ZnO and carbon containing substance (Ahn et al., 2007). Various other elements that can contributed in the band gap reduction were elucidated comprehensively in the preparation of biochar-ZnO nanocomposite (Zhang et al., 2012).

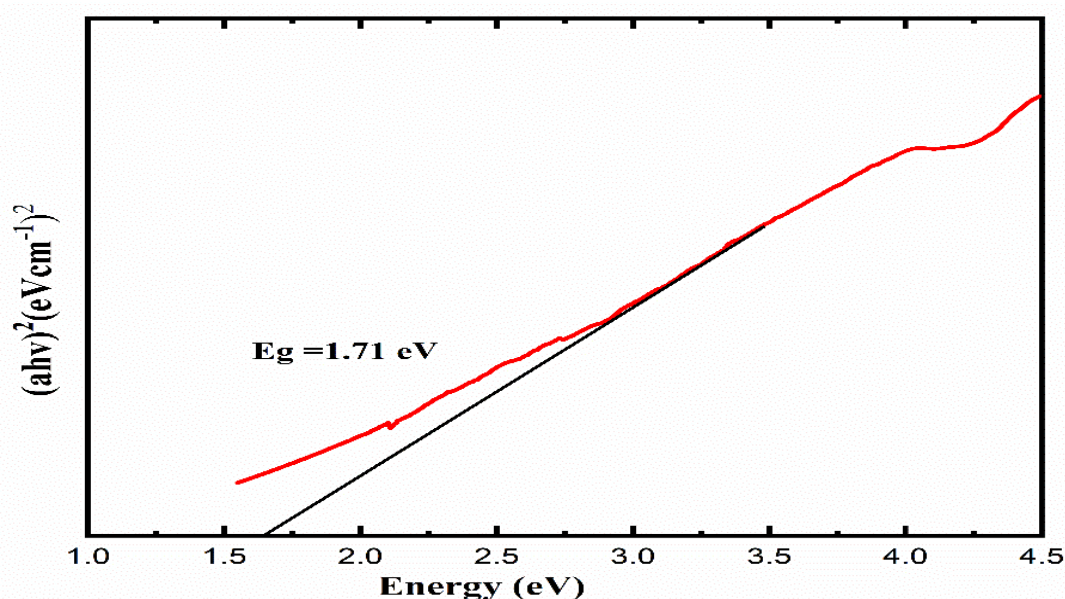


**Fig. 3.8** Band gap study of MB-ZnO.

### **3.1.3 Removal of Saf and MC via MB-ZnO nanocomposite**

The adsorption and photocatalytic potential of the prepared nanocomposite was evaluated in dark and various light sources by examining the elimination of MC and Saf from aqueous medium. The entire MB-ZnO doses show decent removal of Saf in the UV and visible lights and dark (Fig. 3.9). Use of MB-ZnO into the assay tubes efficaciously degrades Saf by shifting the solution color from pink to transparent in an aqueous medium (Fig. 3.10). A comparative analysis of Saf and MC degradation proficiencies attained in the present study and by various other studies has been mentioned in Table 3.1. The entire MB-ZnO nanocomposite treated samples showed

virtuous removal of fungicides (MC) in the different light sources and dark (Fig. 3.12). A transparent solution was obtained after the application of MB-ZnO nanomaterial into the flask, which confirmed the efficacious degradation of MC via MB-ZnO (Fig. 3.12).

The degradation of the Saf and MC in an aqueous medium by MB-ZnO nanoparticle can be designated following the standard protocol (Lee et al., 2016b; Saravanan et al., 2013; Silvestri et al., 2019). After the aforementioned findings, it was determined that MB-ZnO has superior decaying efficacy against Saf as compared to MC. The most appraisable thing is that the ball-milled prepared MB-ZnO revealed excellent photodegradation against both pollutants under visible light, maybe owing to its virtuous photocatalytic activity or the activation of free radicals through UV light (Huang et al., 2020; Liang et al., 2023; Yu et al., 2021).

**Table 3.1:** Assessment of Saf and MC removal efficacies attained in the present work and already available literature.

Pollutant	Reference	Nanomaterial	Conditions	Efficiency (%) / Time
Imidacloprid	(Yari et al., 2019)	C-ZnO	100 mg/L, catalyst dosage 100 mg/L, UV lamp	80%/20 min
Diazinon	(Moussavi et al., 2014)	C-ZnO	10 mg/L, catalyst dosage 15 mg/L, UV lamp	57%/30 min
Safranin	(El-Berry et al., 2021)	Cu <sub>N</sub> NPS	20 mg/L, catalyst dosage 10 mg/L, UV lamp	95%/70 min
Safranin	(Nenavathu et al., 2018)	GS/ZnO	$2.2 \times 10^{-4}$ M, catalyst dosage 20 mg/L, Vis	20%/60 min
Safranin	(Hayat et al., 2011)	WO <sub>3</sub>	200 mg/L, catalyst dosage 100 mg/L, Laser	93%/30 min
Safranin	Current work	MB/ZnO	catalyst dosage 5 mg/L, Vis	87%/60 min
Mancozeb	Current work	MB/ZnO	catalyst dosage 5 mg/L, Vis	57%/50 min

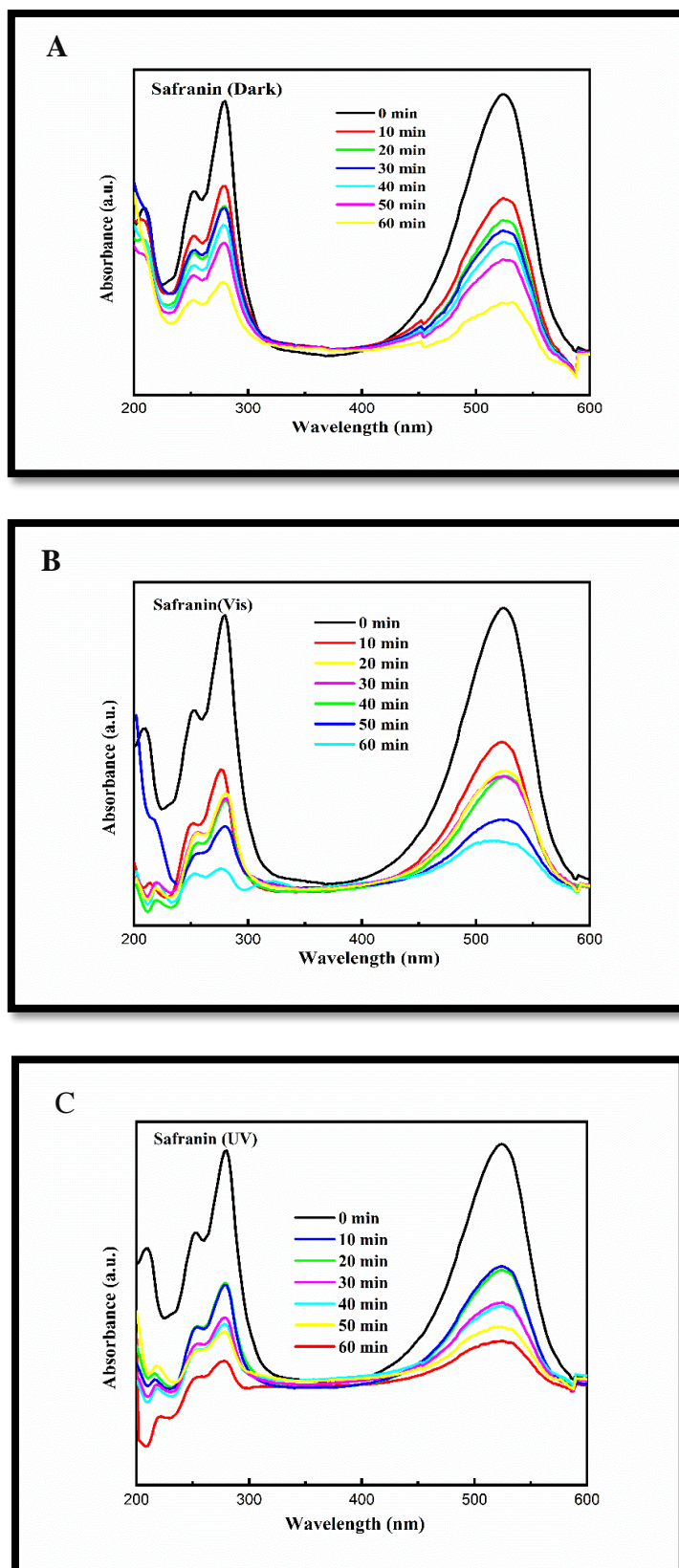


**Fig. 3.9** Plot of Saf removal at various time duration in dark conditions (A), UV light (B), and visible light (C) sources.



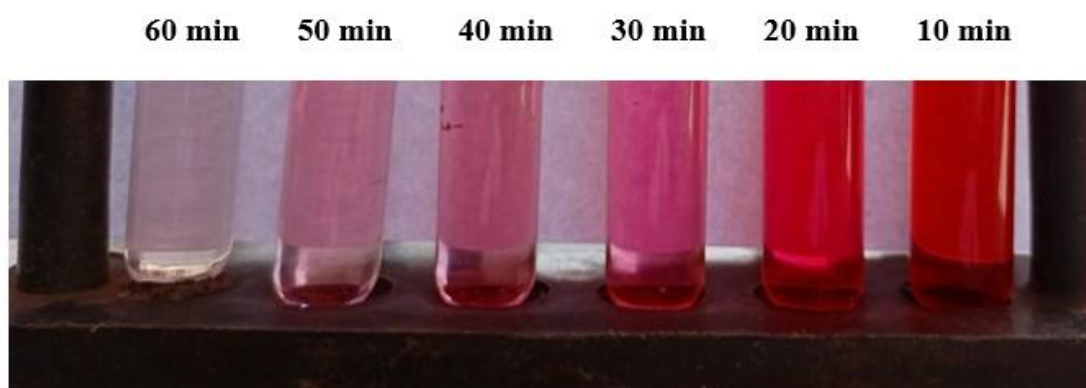
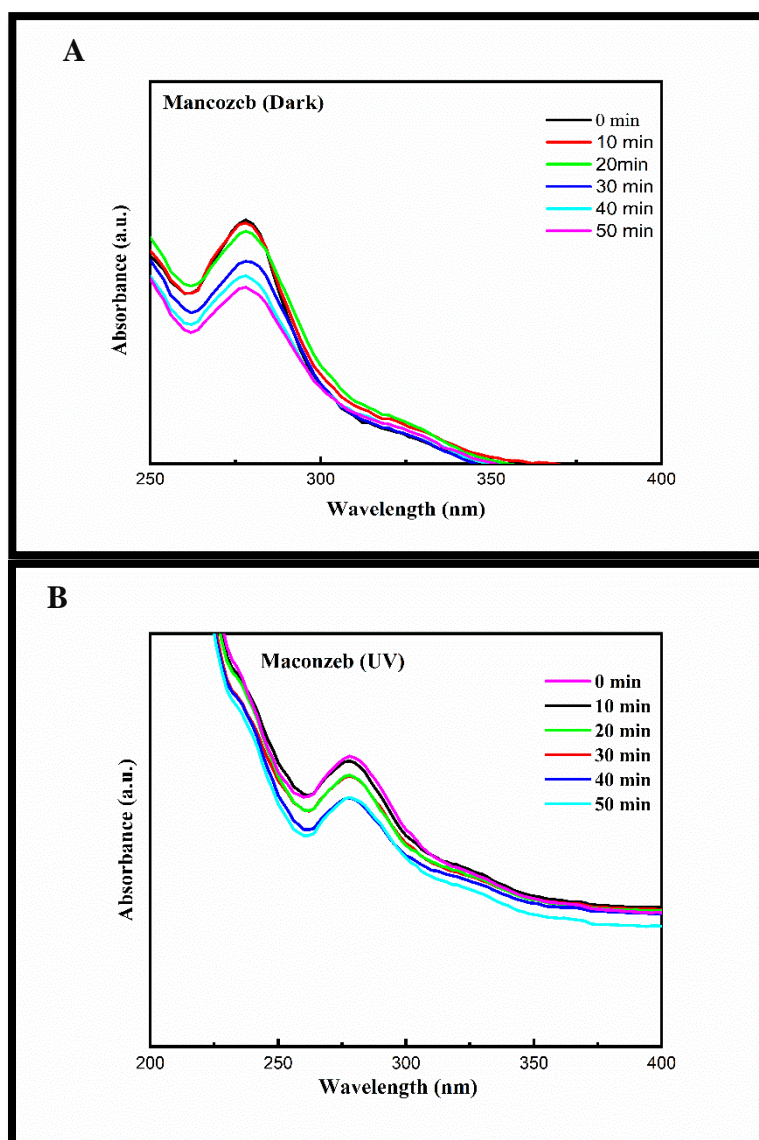
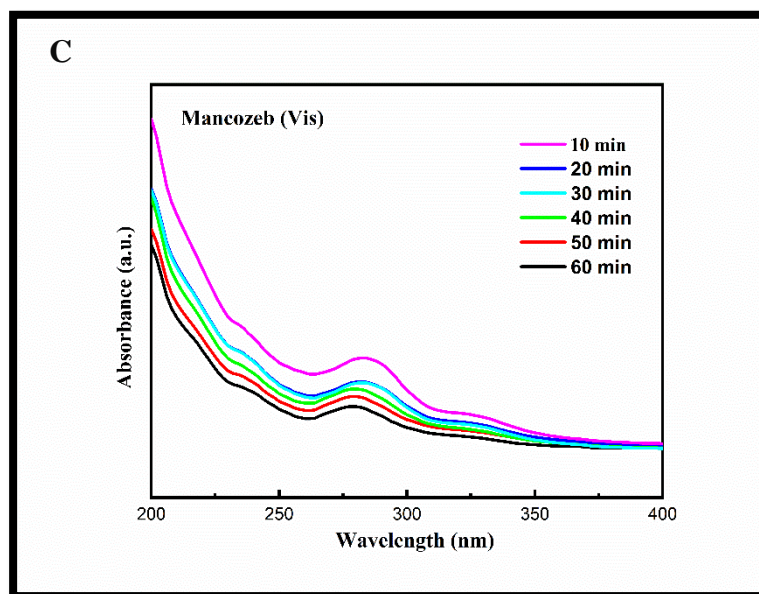
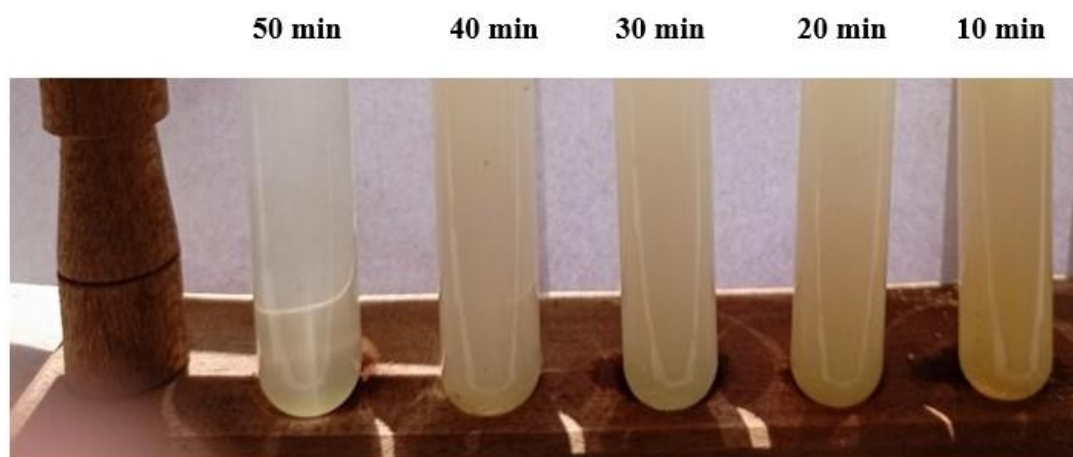


Fig. 3.10 Pure Saf and treated solution at different time duration.





**Fig. 3.11** Plot of Mancozeb degradation at various time duration in dark condition (A), UV light (B), and visible light (C).



**Fig. 3.12** Pure MC and treated solution at different time duration.

### 3.1.3.1 Degradation Rate of Pollutants

A sequence of experiments was performed to assess the photocatalytic performance of the MB-ZnO nanocomposites under dark, UV, and visible light sources at various irradiation times (0–60 min). The absorbance curves revealed the reduction of Saf concentration over time under dark, UV, and Visible light conditions (Fig. 3.13

A). The Saf degradation showed steeper curves under Vis and UV light than dark conditions. The graph showed that the irradiation was performed with various rates in different mediums, but the removal of Safranin-O was higher in the visible light. The biochar-ZnO nanocomposite revealed good photocatalytic performance, achieving a Saf degradation efficacy of 83.5%, only in 60 min in visible light. The degradation efficiencies of the composite in other environments were estimated to be 81.0% (UV light) and 78% (dark). Similarly, the reduction of MC concentration over time under different conditions is presented in Fig. 3.13 B. The efficiency of MB-ZnO nanocomposite was greater in visible light than that of VU and dark conditions. Moreover, the biochar-ZnO nanocomposite exhibited the best photocatalytic performance for MC degradation (56.5%) in only 50 min in visible light. The degradation efficiencies of the composite in other environments were estimated to be 27.5% (UV light) and 25.2% (dark).

Zinc oxide is an n-type semiconductor having bandgap energy value of 3.37 eV and has absorption capacity at room temperature (Ryu et al., 2017). When photo-induced by energy equivalent to or greater than its band gap electron ( $\bar{e}$ ) is released from the valence shell and transfers to the conduction band, producing a positive gap ( $h^+$ ) at the valence band. Therefore, this rehearsal produces photogenerated electron-hole pairs ( $\bar{e}/h^+$ ). When ZnO molecules were irradiated through light with energy greater than the bandgap energy, the conduction-band electrons ( $e^-_{CB}$ ) and valence-band holes ( $h^+_{VB}$ ) are generated on the ZnO particles surface (Singh et al. 2016b). Holes could react with  $H_2O$  molecules present to the ZnO surface to generate hydroxyl radicals ( $\cdot OH$ ) which is highly reactive in nature (Karlsson et al. 2014). Ultimately, oxygen behave as an electron acceptor by generating a superoxide radical anion ( $O^{\cdot-2}$ ) (Patel et al. 2015). Pollutants was considered to be battered through direct oxidation via the  $\cdot OH$  radicals and  $O^{\cdot-2}$  radicals (Ranjith et al. 2022). Earlier studies also confirmed that the electrostatic forces might strongly disturb the contaminants degradation on biochar-based composites (Zhang et al., 2020).



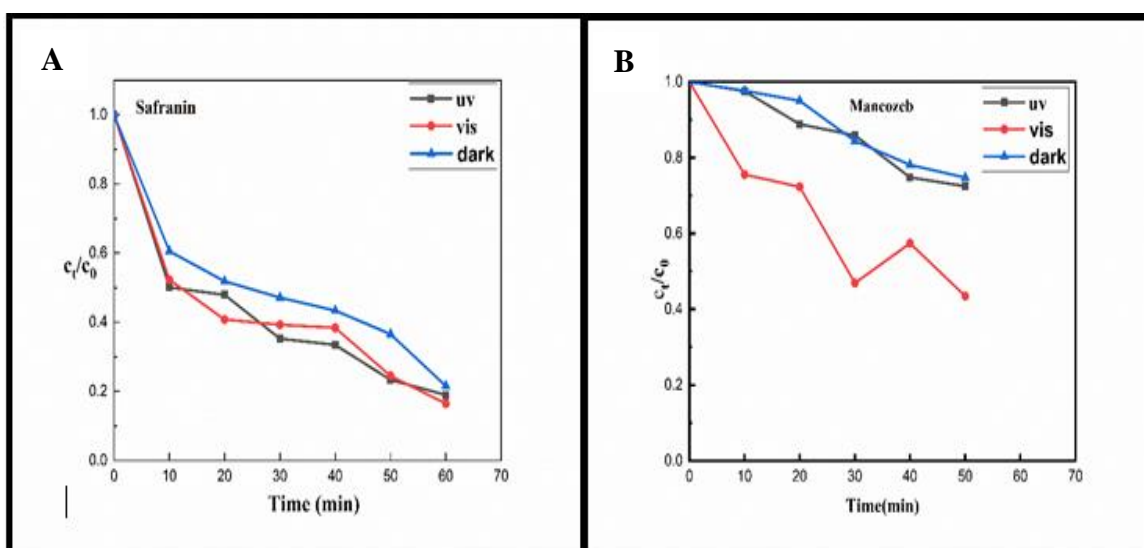


**Fig. 3.13** Efficiency-time degradations of MB-ZnO nanocomposite as a photocatalyst against Saf (A), and MC (B), in various light conditions.

### 3.1.3.2 Comparison of Photodegradation of Saf and MC in various Light Conditions

Findings of the present study revealed the best activity of optimum catalyst dose (5 mg/100 mL) for the removal of both Saf and MC pollutants. The degradation of both Saf and MC was preferred at constant temperature and pH. Results of current study also revealed that MB-ZnO to be an effective catalyst in all dark and light against both Saf and MC (Fig. 3.14). The highest degradation of Saf was examined after 50 min in visible light (84%). In the case of MC, 57% degradation was observed in presence of visible light, which is greater to that of UV and dark condition in the equal time duration (50 mins).

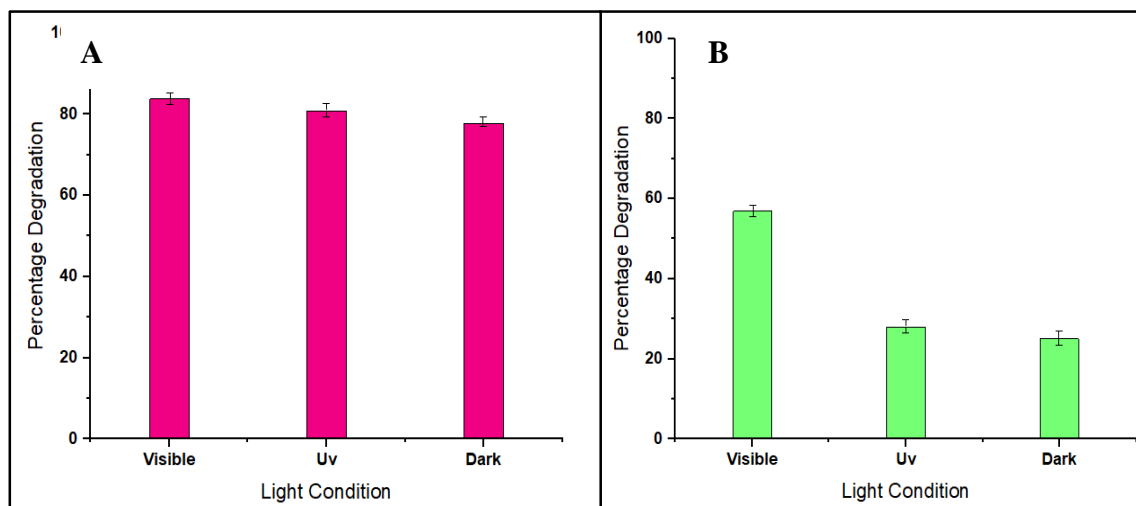


**Fig. 3.14** Degradation efficacy of MB-ZnO in various light conditions against Saf (A) and MC (B).

### 3.1.3.3 Mineralization of Contaminants

For a well description of the overall degradation reaction of pollutants in various light conditions, TOC was premeditated. TOC analysis was performed to evaluate the degradation of pollutants to CO<sub>2</sub>, water, and mineral ions in various light conditions. The values of TOC of the solution were measured as a function of time. Samples were used for analyses after the irradiation periods. The declination in the rate of absorption with a reduction in TOC level was observed. Declination in the absorbance peaks (Fig. 3.15 A and B) indicated the decaying of the Saf and MC molecules to smaller molecules. All the absorption peaks were also gradually diminished, and no fresh absorption peaks produced during the whole reaction. Transitional molecules produced in the degradation were also productively degraded to whole mineralization.

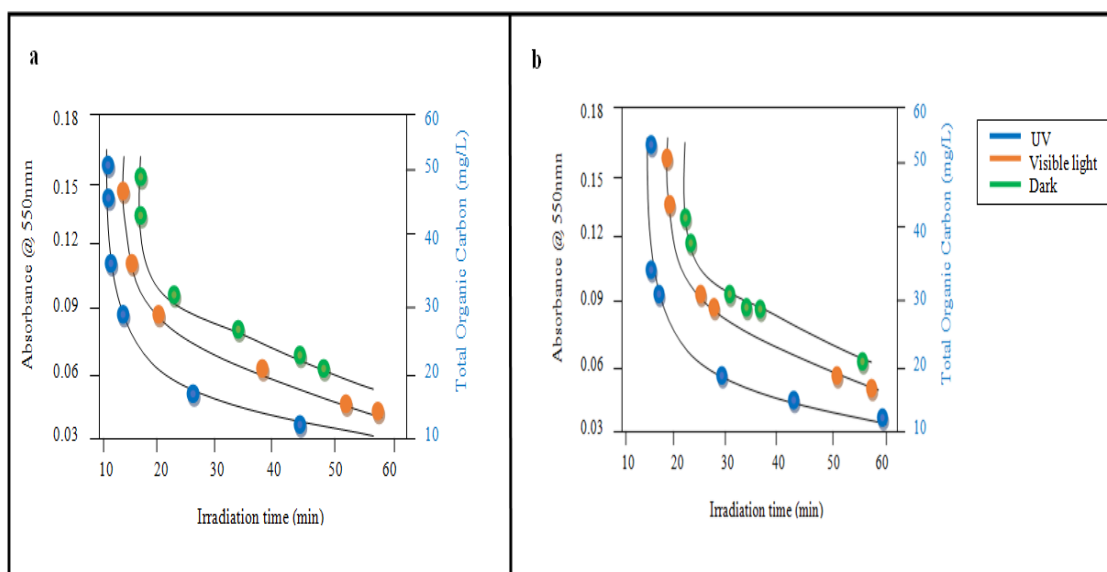


**Fig. 3.15** Plot of TOC removal efficacy vs irradiation time of Saf (A) and (B) MC.

### 3.1.3.4 Reaction Kinetics

Kinetics supports to understand procedure of pollutant degradation in various conditions. It is well accepted that the photo-catalytic degradation of organic pollutants follows the Langmuir–Hinshelwood (L-H) pseudo-first-order kinetic (Fu et al., 2012), which shows a linear relationship between  $\ln(C_0/C_t)$  and the reaction time. The first-order reaction can be written as:

$$\ln C_0/C_t = K_{app}t \quad (7)$$

For the calculations of reaction kinetics of Saf;  $C_0$  shows the initial amount of Saf,  $t$  is the time of reaction and  $C_t$  is the amount of Saf at reaction time  $t$ . Thus, based on the pseudo-first-order equation, the activities of the photocatalyst were calculated by assessing the absorbance of Saf in solution. This analysis was executed at different time durations, in various light sources containing a similar amount of photo-catalyst to determine the solitary effect of different light sources. It is confirmed from the findings of this experiment that the Saf removal was less in absence of light and the photocatalyst had excellent degradation activity of Saf in the visible and UV light for 60 mins (Fig. 3.16 A).

The association between the apparent reaction constants ( $K_{app}$ ) for the photo-degradation of Saf in the existence of MB-ZnO at room temperature exposing to various lights sources is presented in Fig. 3.16 A. From the slopes, it can be examined that the

apparent rate constant enhanced considerably for MB-ZnO nanocomposite i.e.,  $0.93 \text{ min}^{-1}$  in dark,  $0.94 \text{ min}^{-1}$  in UV, and  $0.95 \text{ min}^{-1}$  in visible light. These findings proved effective and rapid photocatalytic degradation of Saf in Visible light by MB-ZnO nanocomposite. Concluding's showed that MB-ZnO is one of the infectious photocatalysts in visible light to degrade Saf with good rate.

The potential of MB-ZnO and the effect of different factors like dark, visible and UV light on the MC degradation kinetics were also investigated, effectively. The degradation rate constant for MC was the maximum ( $0.882 \text{ min}^{-1}$ ) in visible light, followed by UV ( $0.884 \text{ min}^{-1}$ ), and dark conditions ( $0.920 \text{ min}^{-1}$ ) (Fig. 3.16 B). It can be concluded from the findings that MB-ZnO NPs has also showed an effective photocatalytic decaying of MC, in presence of Visible light.

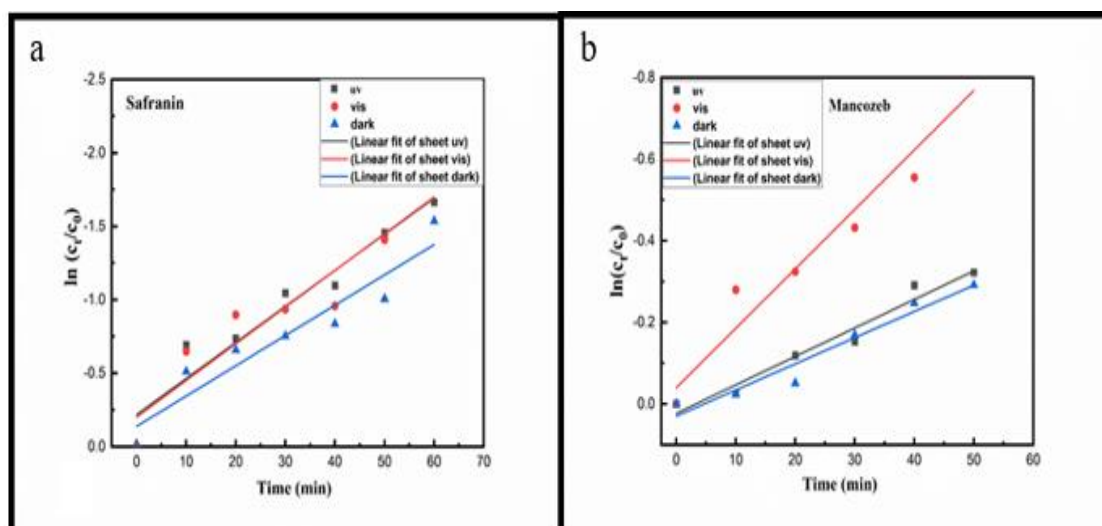


**Fig. 3.16** Plots  $\ln C_t/C_0$  versus time (A) absorbance of Saf and (B) MC.

## 3.2 EXPERIMENT 2

### 3.2.1 Graphical Abstract

For initial understanding, schematic representation of the experiment has been presented in Figure (3.17).

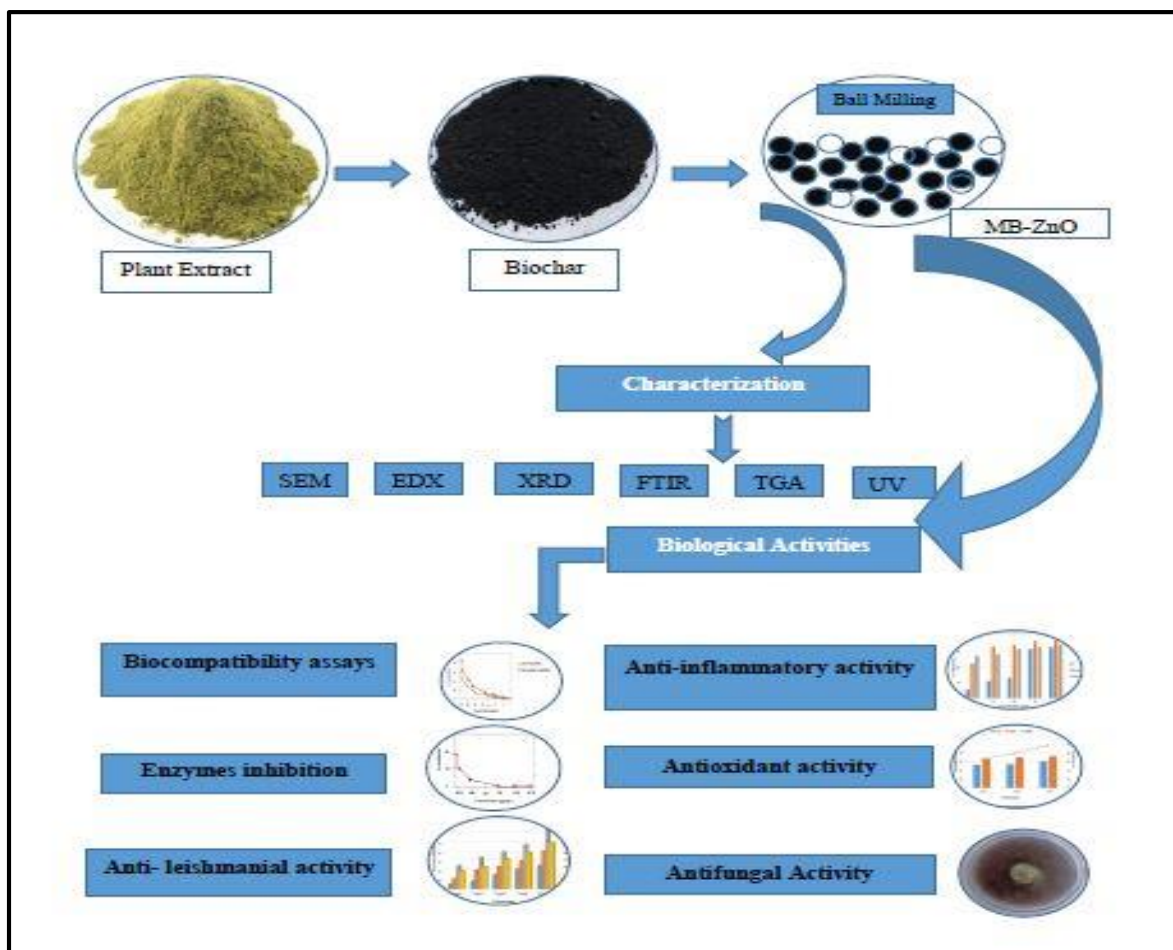


**Fig. 3.17** Schematic Illustration of Complete Experiment.

### 3.2.2 SEM and EDX Analysis

SEM was successfully used to observe the texture of maize biochar (MB) (Fig. 3.18 A). SEM micrographs declared the porous a rough surface of pure biochar. The rough and porous configuration of the MB is produced thru the elimination of unstable materials, in the pyrolysis process. As these ingredients vanished, pores and claps created on the MB, and it viewed rough. The aforementioned structural description of MB confirmed its ability to behave as the good support for nano-sized substance. After



the process of ball-milling, ultrafine white particles (ZnO) seemed in form of cluster, along the biochar surface (Fig. 3.18B). SEM study revealed that the loading of raw substances not only altered the products composition but also exhibited a huge influence on their texture (Fig. 3.18 B).

The MB-ZnO nanocomposite elemental composition of was assessed by EDX analysis (Kamal et al., 2022a). This microanalysis confirmed the presence of Zn, C, K, O, Na, P, Ca, and Si elements in MB-ZnO nanocomposite (Fig. 3.3). SEM and EDS analysis of MB-ZnO established the attachment of ZnO on the skeleton of biochar, which indicates that biochar-ZnO is successfully prepared (Yu et al., 2021).

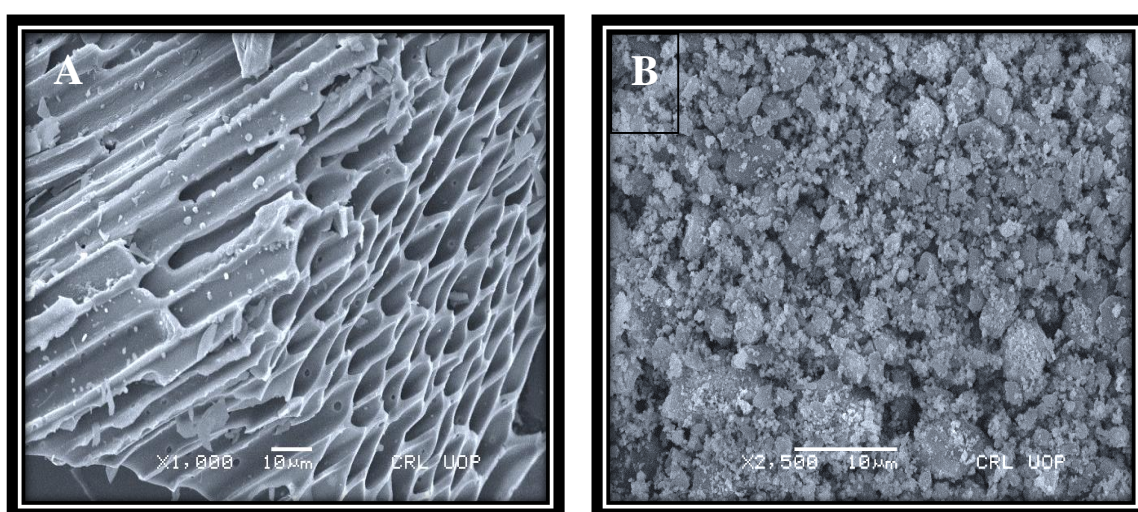


**Fig. 3.18** SEM images of pristine biochar (A) and MB-ZnO (B).

### 3.2.3 XRD Study

XRD analysis was accomplished at a scanning rate of  $1^\circ$  per minute in  $0.013^\circ$  steps, covering 2-theta angle between  $10^\circ$  to  $80^\circ$ . The XRD pattern showed nine major peaks of the prepared nanocomposite (Fig. 3.19). XRD spectrum of MB-ZnO showed low-intensity peak at  $67.5^\circ$ , representing low crystallinity. XRD spectrum shown various peaks at  $31.82$ ,  $34.50$ ,  $36.33$ ,  $47.62$ ,  $56.69$ ,  $62.95^\circ$ ,  $66.42^\circ$ ,  $67.54^\circ$  and  $69.01^\circ$  (Fig. 3), indicating to (100), (002), (101), (102), (110), (103), (200), (112) and (201) planes, independently. These findings specified crystallographic planes of hexagonal arrangement of MB-ZnO nanocomposite, according to JCPDS no. (036–1451). The average size of the MB-ZnO particle was calculated as 47 nm through the X-ray line broadening method through the Scherrer equation, using the highest peak of MB-ZnO.

These XRD findings confirmed that the MB-ZnO was nano-sized and these results are aligned to earlier documented findings (Lourenço et al., 2021).

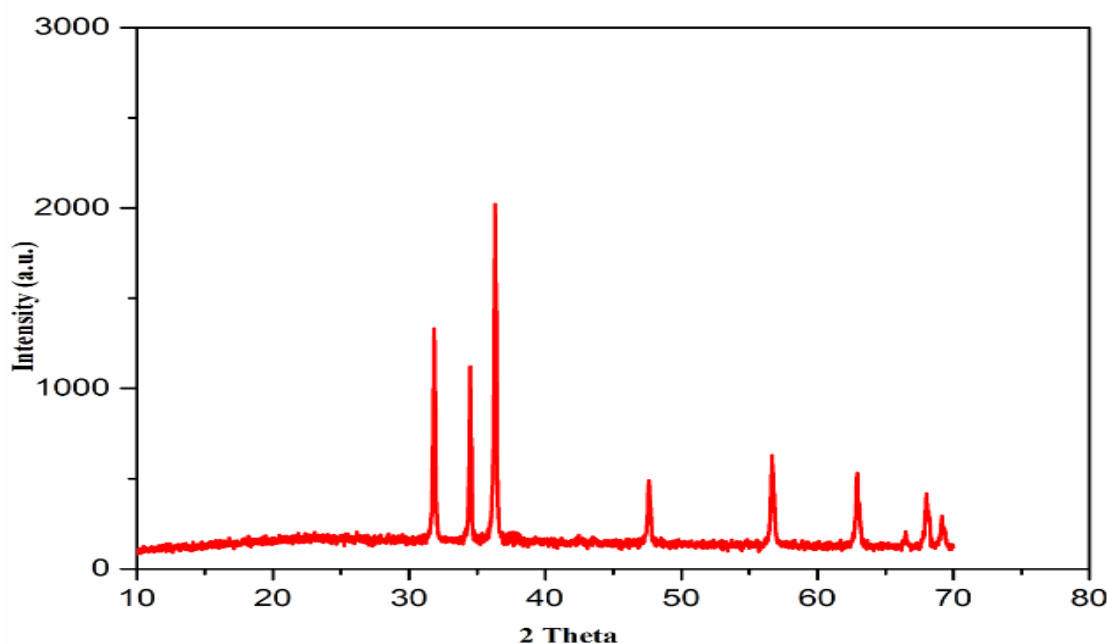


**Fig. 3.19** XRD patterns of MB-ZnO nanocomposite.

### 3.2.4 FTIR Spectroscopy

FTIR study revealed distinctive peaks of different principal functional groups (Fig. 3.20). FTIR spectroscopy showed nine characteristics peaks stretching from 500-4000  $\text{cm}^{-1}$ . The peak detected at 2163  $\text{cm}^{-1}$  represented strong bonding of N=C=N and the peak 1124  $\text{cm}^{-1}$  demonstrates to the C-O stretching. The peak at 1037  $\text{cm}^{-1}$  and 799  $\text{cm}^{-1}$  indicated strong S=O stretching of alkene and C=C bending of alkene respectively. The existence of peak at 626  $\text{cm}^{-1}$  documented the  $\text{CO}_3^{2-}$  stretching (Bakr et al., 2018). Similarly, the peak at 580  $\text{cm}^{-1}$  was recognized to the ZnO vibration and confirmed the existence of ZnO nanoparticle on the biochar surface (Arfin and Rangari, 2018). The occurrence of a broad peak at 3440  $\text{cm}^{-1}$  represented wide and strong stretching O-H of alkyne (Chu et al., 2012). Additional strong peak at 524  $\text{cm}^{-1}$  accredited to Zn-O stretching (Batra et al., 2012a). Previous researchers have also documented the identical peaks for the presence of ZnO on the surface of MB-ZnO (Gholami et al., 2019).

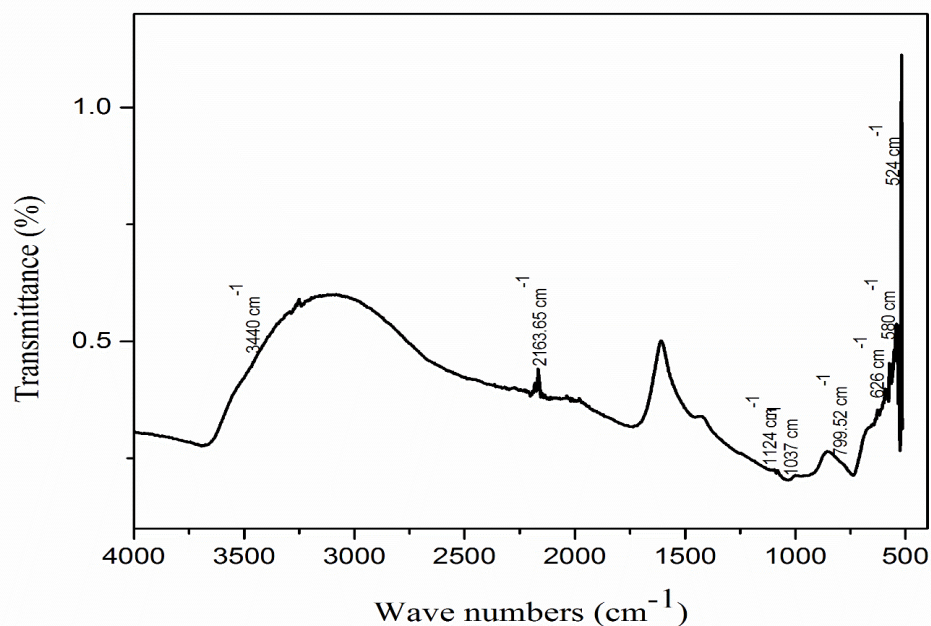


**Fig. 3.20** FTIR analysis of MB-ZnO

### 3.2.5 Thermogravimetric Analysis

Thermogravimetric Analysis was executed for finding the thermal properties of MB-ZnO along with their ranges due to the removal of biomass samples (Pietro and Paola, 2004). TGA description have been documented in an inclusive pattern in our earlier published research work (Kamal et al., 2022b). TGA findings showed the association of mass fluctuations with temperature ranges (Fig. 3.21). The mass declination started with the rise in temperature, from initial temperature ( $T_i$ ) to final temperature ( $T_f$ ), and these weight alterations were due to various thermal courses, such as vaporization, oxidation, reduction, absorption and desorption (Law, 2020). The early mass loss at low T linked to the evaporation of water molecules existing in the rough surface of particles (Teo et al., 2016). The curve imitates weight loss due to the vaporization of water (at 50–100 °C), hemicelluloses volatilization (at 150–350 °C), cellulose degradation (at 300–500 °C), breakdown of lignin (till 700 °C) and later phases, through the gradual decaying of the remains of pyrolysis.

TGA of pure biochar (Fig. 3. 21 A) and the MB-ZnO nanocomposite (Fig. 3.21 B) showed that degradation of MB-ZnO nanocomposite initiated a little earlier as in comparison to pure biochar, which indicates a little lower thermal stability of MB-ZnO. Usually, the individual biochar has low thermal stability in comparison to biochar-ZnO nanocomposite, but due to the preparation of biochar at high temperature (600 °C), the thermal nature of the pristine biochar may have enhanced. These findings established that pristine biochar and MB-ZnO nanocomposite have decent thermal firmness. The loss of weight of pure ZnO NPs at higher temperatures to be very high has been recognized (Moharram et al., 2014). In general, the thermal decay curve of pristine biochar MB-ZnO and was nearly identical to each other.

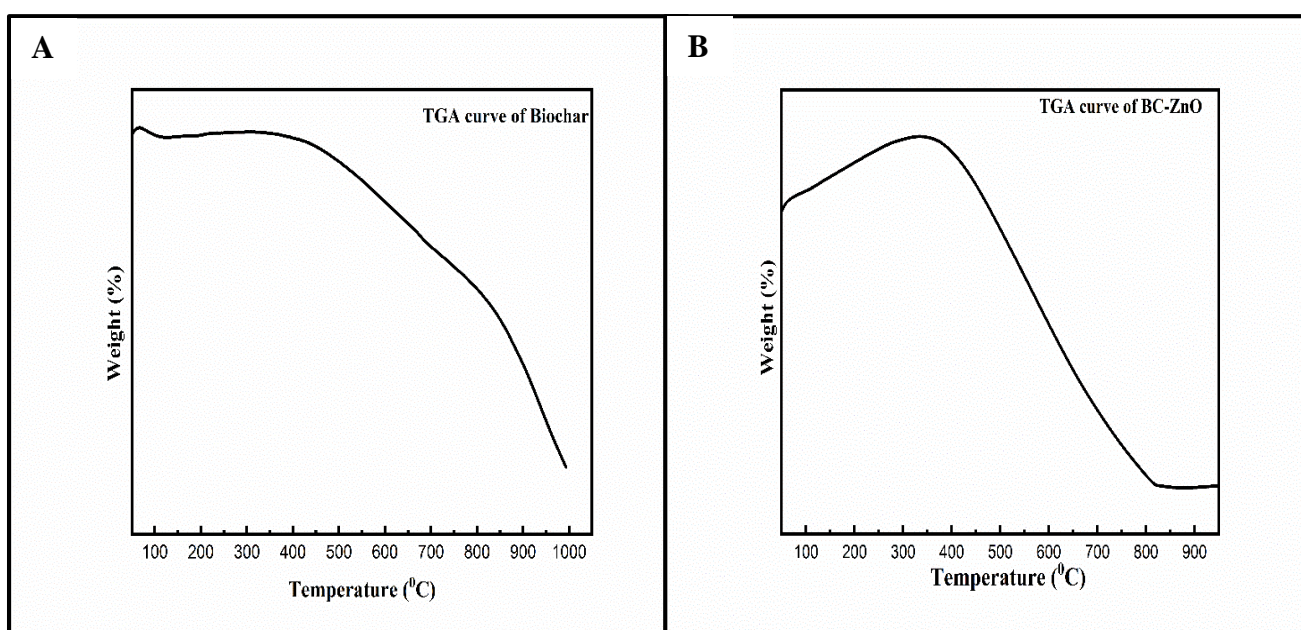


**Fig. 3.21** Thermogravimetric Analysis of biochar (A) and MB-ZnO (B).

### 3.2.6 UV Analysis

UV-Vis study provided an edifying adsorption spectrum of pure biochar (Fig. 3. 22 A), and pristine ZnO and the MB-ZnO nanocomposite (Fig. 3. 22 B). Distinct peaks were observed at 450 nm (MB), 350 nm (ZnO), and 400 nm (MB-ZnO nanocomposite) determined the band gaps effectively.

The value of band gap energy was achieved through UV–Vis spectra. Usual band gap energy values for biochar-ZnO nanocomposite (2.77 eV) and pristine ZnO

NPs (3.04 eV) have been documented previously (Gholami et al., 2019). In this study, we have calculated a band gap values 1.71 eV of the MB-ZnO as reported in a comprehensive way in our previous work (Kamal et al., 2022a). Different researchers have acknowledged that loading ZnO on the non-metallic particles surface (like carbon, phosphorus, sulfur, and nitrogen) improve their efficacy with decreasing the band gap band (Ansari et al., 2016; Zhang et al., 2014a). The complete mechanism of reduction of the band gap has been reported in several articles (Ul-Haq et al., 2012).

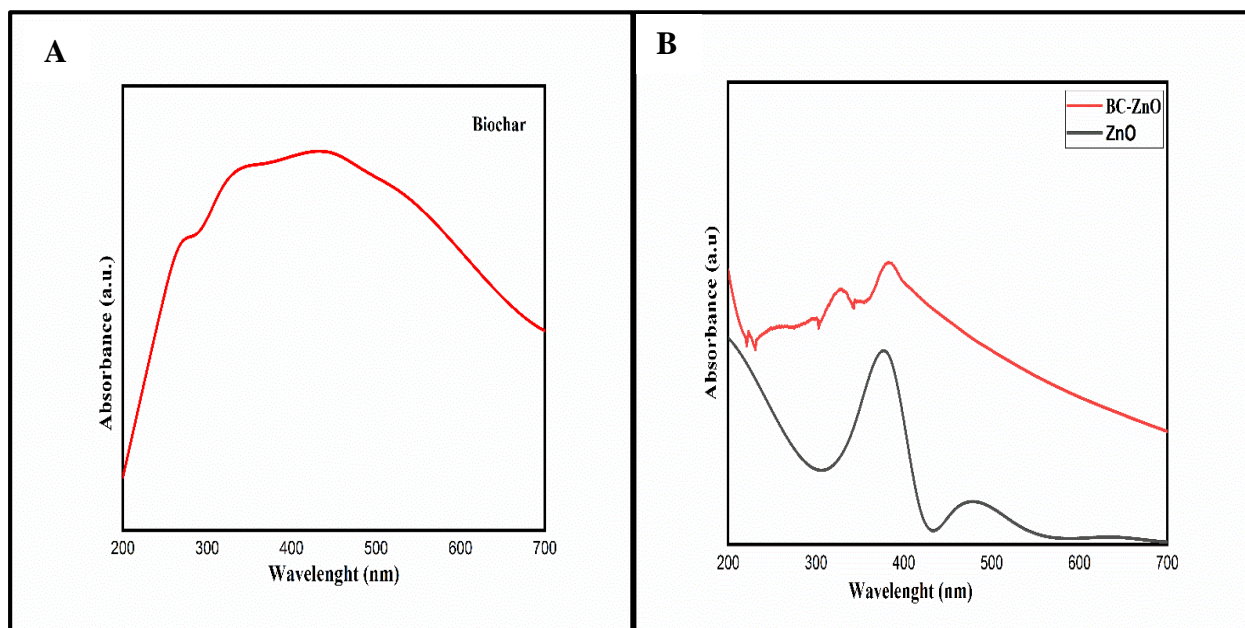


**Fig. 3.22** UV study of pure biochar (A), pure ZnO NPs and MB-ZnO (B).

### 3.2.7 Antioxidant activity of MB-ZnO Nanocomposite

Antioxidant assays were studied at various dosage rates (1.95–200  $\mu\text{g/ml}$ ). MB-ZnO nanocomposite has never been studied before for antioxidant assays, earlier. The maximum activity for TAC of MB-ZnO nanocomposite, in terms of AA equivalent/milligrams, was calculated as 30.09% at application rate of 200  $\mu\text{g/ml}$ . The oxidation process generally occurs in all living cells, ensuing in the creation of reactive oxygen species (ROS), which can disrupt the normal metabolic processes of the living cell. An insufficient number of antioxidants can result in awful concerns, like lipid peroxidation, inactivation of enzyme, and DNA, RNA and protein annihilation. More assessment of the antioxidant activities of the nanocomposite was supported via analyzing their TRP test. This activity was executed to observe the reductones that play

a vigorous role in the antioxidant assay via creating H-atoms and producing harm to free radicals (Tamer et al., 2021). TRP of the nanocomposite was decreasing with a declination in the concentration of the nanocomposite. The maximum TRP score (36.29%) was examined at the highest concentration of 200  $\mu\text{g}/\text{ml}$  (Fig. 3.23). Maximum DPPH radicals scavenging efficiency (49.19%) was observed for MB-ZnO nanocomposite at the highest concentration of 200  $\mu\text{g}/\text{ml}$ . The antioxidant activity is due to the presence of different functional groups in the nanocomposite and combined functions of both Zn and MB. The differences in the antioxidant assays of MB-ZnO nanocomposite as compared to the NPs might be due to different factors e.g., experimental setup, nature of nanoparticles, size of nanoparticles, and plant species.

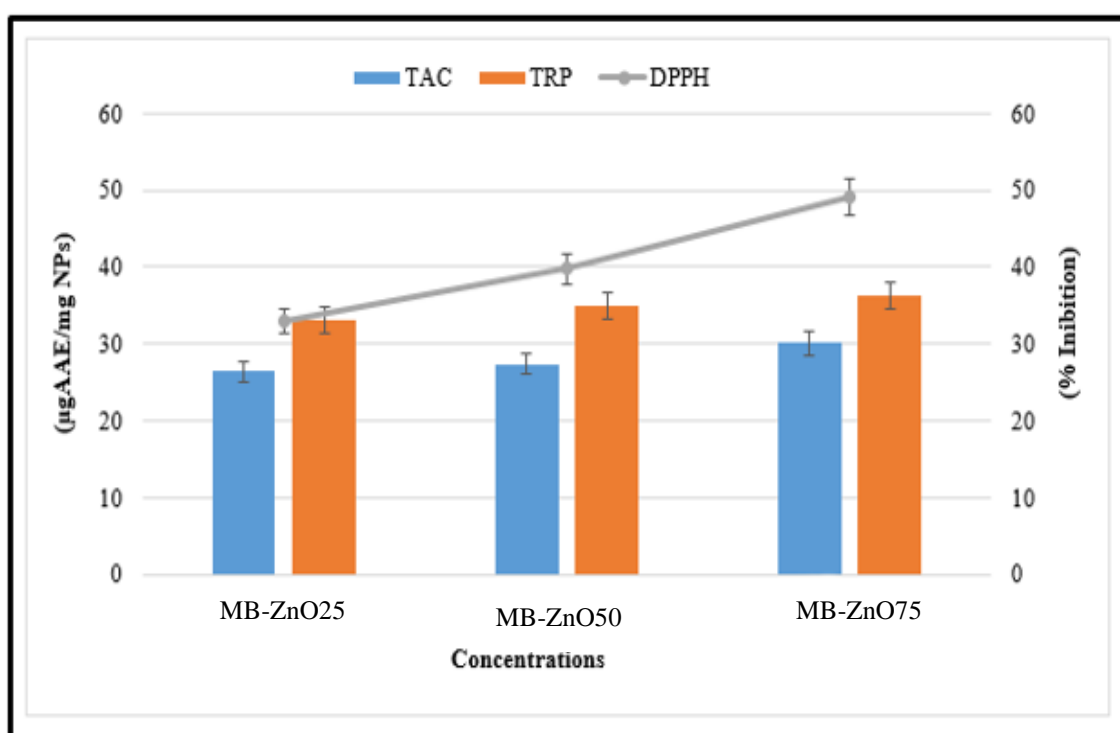


**Fig. 3.23** Antioxidant potential of MB-ZnO.

### 3.2.8 Anti-Inflammatory Assay

The physically prepared pristine biochar nanoparticle (BC NPs) and the MB-ZnO nanocomposite revealed parallel anti-inflammatory potential comparison to standard diclofenac sodium. MB-ZnO behaved as an excellent anti-inflammatory agent (Figure 3.24). Both BC NPs and MB-ZnO nanocomposite assist to reduce inflammation, *in vitro* study. The growth inhibition of MB-ZnO nanocomposite was recorded 45%, 67%, 69%, 75%, and 76% at concentration of at 62.5  $\mu\text{g}/\text{mL}$ , 125  $\mu\text{g}/\text{mL}$ ,

250  $\mu\text{g/mL}$ , 500  $\mu\text{g/mL}$ , and 1000  $\mu\text{g/mL}$  correspondingly. The dose more than 1000  $\mu\text{g/mL}$  revealed more than 78% growth inhibition. The highest inhibition percentage achieved via BC NPs was 11% at application rate of 62.5  $\mu\text{g/mL}$ , 23% at 125  $\mu\text{g/mL}$ , 26% at 250  $\mu\text{g/mL}$ , 64% at 500  $\mu\text{g/mL}$ , and 66% 1000  $\mu\text{g/mL}$ , correspondingly. Rising the application rate of both particles was directly related to the inhibition. Comparative study showed that the MB-ZnO nanocomposite is a better anti-inflammatory agent in comparison to pristine BC nanoparticles in a similar experimental setup. These results revealed that MB-ZnO nanocomposite has increased anti-inflammatory potential compared to individual metal oxide. The excellent activity of the MB-ZnO nanocomposite may develop because of the smaller size and greater surface-to-volume ratio. Moreover, the combined function of both ZnO and MB is an additional key element that might enhance its efficacy.

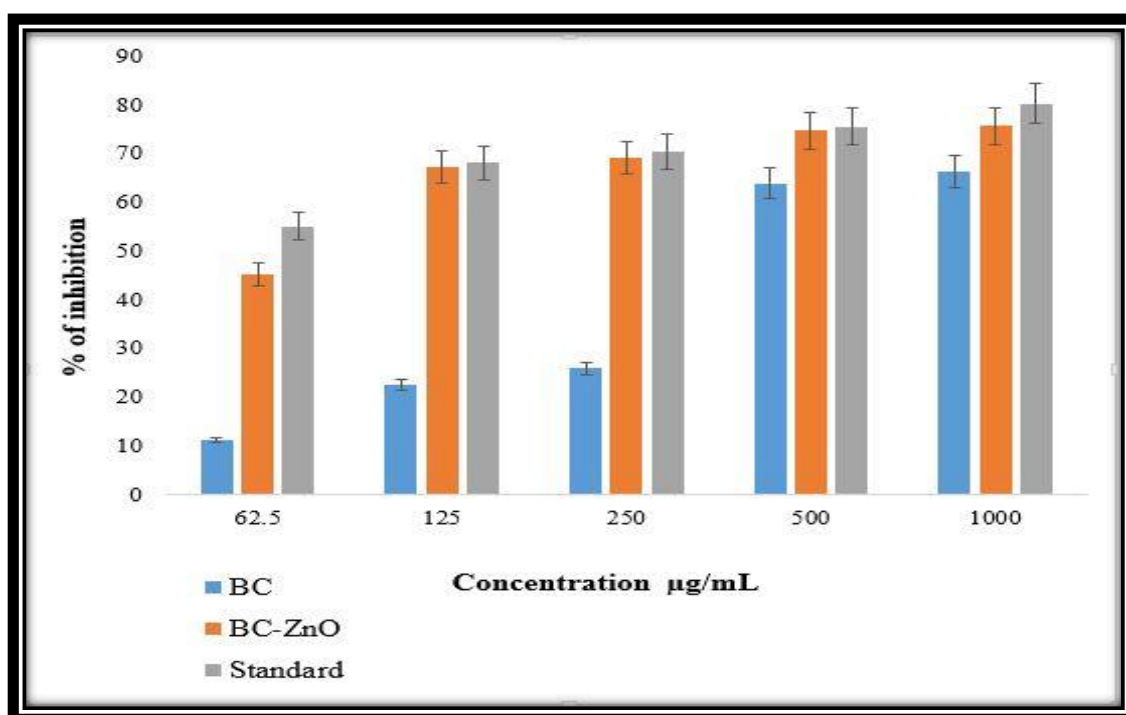


**Fig. 3.24** Anti-inflammatory activity of MB-ZnO nanocomposite.

### 3.2.9 Enzyme Inhibition Activities

At various tested doses, MB-ZnO nanocomposite showed excellent potential against protein kinase inhibition (Fig. 3.25A) and alpha-amylase (Fig. 3.25B) activities. PK is an enzyme, having potential for anticancer activities. PK phosphorylate serine-

threonine and tyrosine amino acid residues sustain different organic processes, such as cell division, cell elongation, cell differentiation, and cell demise. Uncontrolled phosphorylation via PK at serine-threonine and tyrosine remnants can lead to production of tumor. Therefore, PK inhibition can be acknowledge as possible cancer remedial target (Gholami et al., 2019). Additionally, chemical constituents devouring the potential to inhibit PK enzymes is important. PK phosphorylation has been documented to be a vital element in the *Streptomyces* hyphal growth, and therefore it has been repeatedly used to recognize the inhibitors of PK. *Streptomyces* 85E strain was used to study PK inhibition activity of MB-ZnO nanocomposite. The bald zones were calculated in mm and the largest zone of 19 mm was observed at concentration of 1 mg/ml. All experimented concentrations created bald zones (till 250 µg/ml). Additional dilutions did not produce inhibition (Fig. 3.25 A). These results revealed that MB-ZnO nanocomposite could be used as a signal transductor inhibitor in the production of cancer. Surfactin was applied as a positive control which revealed highest inhibition of 23 mm at concentration of 1000 lg/ml and 7.4 mm at 31.25 lg/ml of application rate.

In addition, AA inhibition potential was analyzed at various concentrations (62.5 to 1,000 µg/ml) of the prepared nanocomposite (Fig. 3.25 B). AA perform a substantial part in the cessation of polysaccharides (starch) into monosaccharaides (glucose) (Oyedemi et al., 2017). This inhibiting potential of alpha amylase can decrease the glucose concentration in blood, consequently creating a new field of research to use nano-size particle for the diabetes treatment (Dobrovolskaia et al., 2008). In the present study, ball-milled prepared MB-ZnO showed a good inhibition of AA. The utmost inhibition activity (45%) was perceived at the maximum dosage rate (1,000 µg/ml). Though, this AA inhibition potential steadily decreased with reducing in MB-ZnO nanocomposite application rate (Fig. 3.25 B). The inhibiting activity of AA can reduce the level of glucose, hence creating a latest field of research to use nano-size particle for the diabetes treatment (Dobrovolskaia et al., 2008).



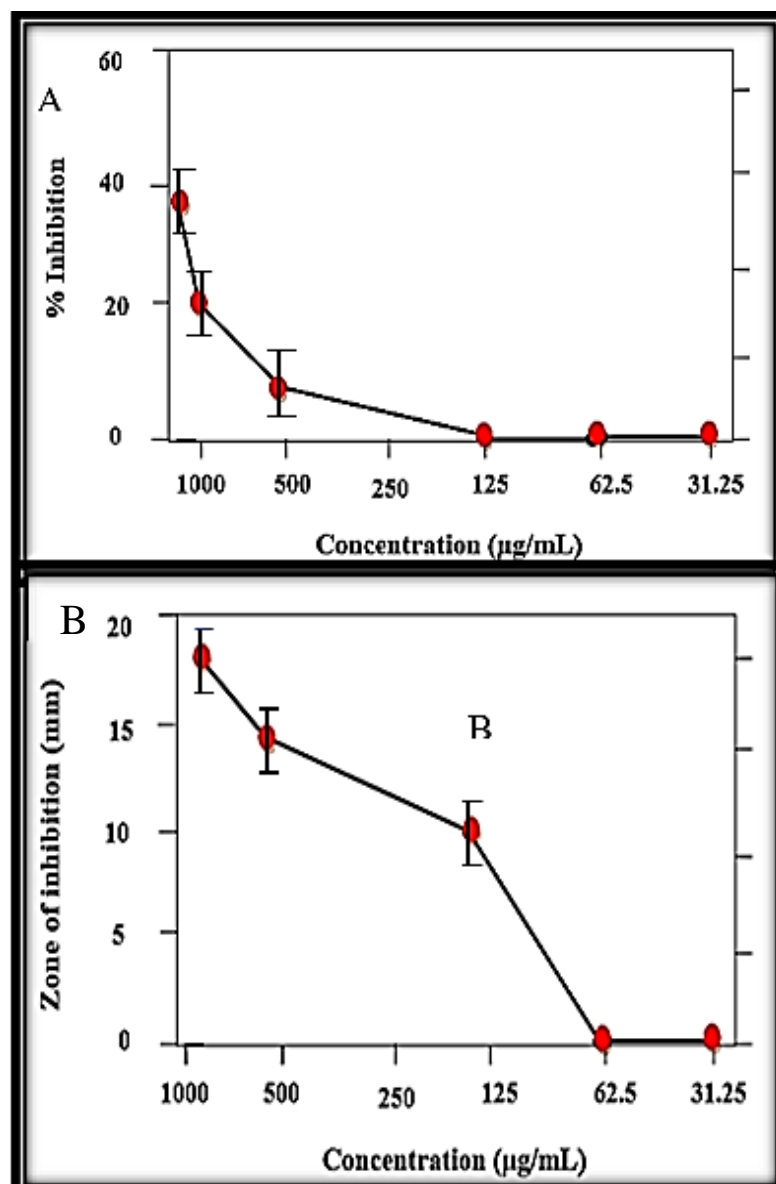


**Fig. 3.25** Inhibition potential of MB-ZnO nanocomposite against PK (A) and AA activities (B).

### 3.2.10 Biocompatibility Assay

Usually, among various *in vitro* assays of red blood cells nanocomposite (RBCs-nanocomposite), hemolysis is the commonly practiced biological activity. It confirms toxicity, which is determined by the release of hemoglobin from the bursting red blood cells. It is measured from the data of absorbance at the 530 nm wavelength (Dash et al., 2010). Similarly, many *in vitro* experiments have documented

the interactions of cells-nanoparticles, most of them had tested RBCs with usual nano-sized material, not with nanocomposite. Results of this study were calculated in the range of 1 – 200  $\mu\text{g/ml}$  and the hemolytic behavior was assessed using the American Society scale (Yang et al., 2019). The cytotoxicity potential of MB-ZnO nanocomposite was analyzed against the RBCs (Fig. 3.26). The findings of the hemolytic study confirmed the less cytotoxic behavior of the nanocomposite to the RBCs of human. Highest hemoglobin breakdown (28%) was observed at the highest dose (200  $\mu\text{g/ml}$ ); however, no hemolysis was analyzed at the concentration of 5  $\mu\text{g/ml}$  and below that.

For additional study of the biocompatible behavior of the nanocomposite, an MTT cytotoxicity activity was performed against human macrophages. Our results have confirmed that the MB-ZnO nanocomposite is less-toxic to human phagocytes (Fig. 3.26). Our results revealed that MB-ZnO is non-toxic at a small amount (2  $\mu\text{g/ml}$ ), while it is a slight toxic at 5–100  $\mu\text{g/ml}$  dosage rate. At 200  $\mu\text{g/ml}$  concentration, a 42% of macrophages death rate was examined. The IC<sub>50</sub> value of MB-ZnO nanocomposite was examined to be >200  $\mu\text{g/ml}$  against RBCs and macrophages. Generally, MB-ZnO nanocomposite can be established as non-toxic and safe in small concentrations (Fig. 3.26). Positive control sample (0.5% Triton X-100) revealed 73% hemolysis.

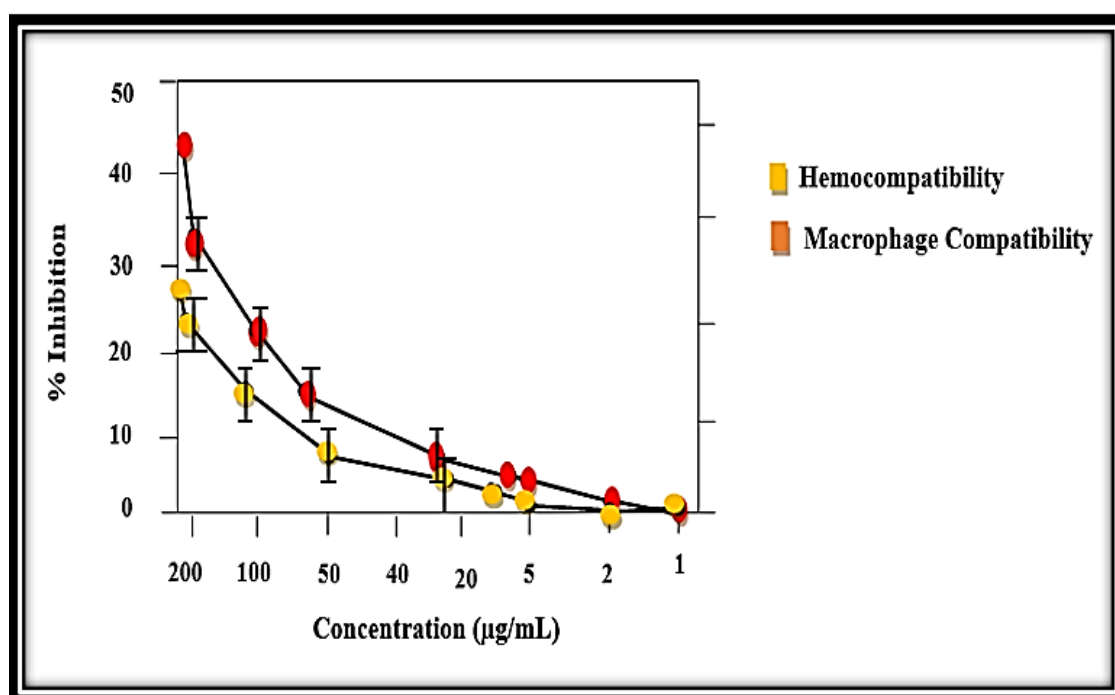


**Fig. 3.26** Biocompatibility of MB-ZnO in case of human RBCs and macrophages.

### 3.2.11 Antileishmanial Potential

The efficacy of MB-ZnO nanocomposite as an antileishmanial agent was studied for 96 h and designated by means of percent inhibition (Fig. 3.27). To collect the results, promastigotes numbers were sum up in both control and experimental groups at different time duration (24, 48, 72, and 96 h). After amendments with different doses of the MB-ZnO nanocomposite, the parasites number was calculated in both control and experimental samples at constant time duration extending from 24 to 96 hours. Antileishmanial efficacy increased with the rising concentration of MB-ZnO nanocomposite. The antileishmanial efficacy was examined to be 18%, 25%, 31%, and 35% at concentration of 25 µg/ml, 50 µg/ml, 75 µg/ml and 100 µg/ml, respectively in the initial incubation for 24 h. After 48 h of incubation, the cells count was decreased in the MB-ZnO treated samples.

MB-ZnO nanocomposite exhibited antileishmanial efficiency of 34% at application rate of 25 µg/ml, 45% at 50 µg/ml, 57% at 75 µg/ml, and 68% at 100 µg/ml, respectively, after the incubation for 72 hours. Later, a little reduction in activity was perceived. This reduction in efficacy might be because of the consumption of reactive ions present in the MB-ZnO nanocomposite. Moreover, biochar-metal oxides having the potential of ROS production, which kill the pathogens via causing holes in the cell wall and disturbs morphological characteristics of the cell membrane, resulting in the interruption of the membrane and leakage of intracellular constituents (Wang et al, 2021).

It is also recognized that Leishmania is very susceptible to these ROS, and the medicine that could generate ROS will be used a productive antileishmanial agent. The noteworthy findings of our judgments hence clearly examine that MB-ZnO nanocomposite might be an auspicious agent for therapy of leishmaniasis.

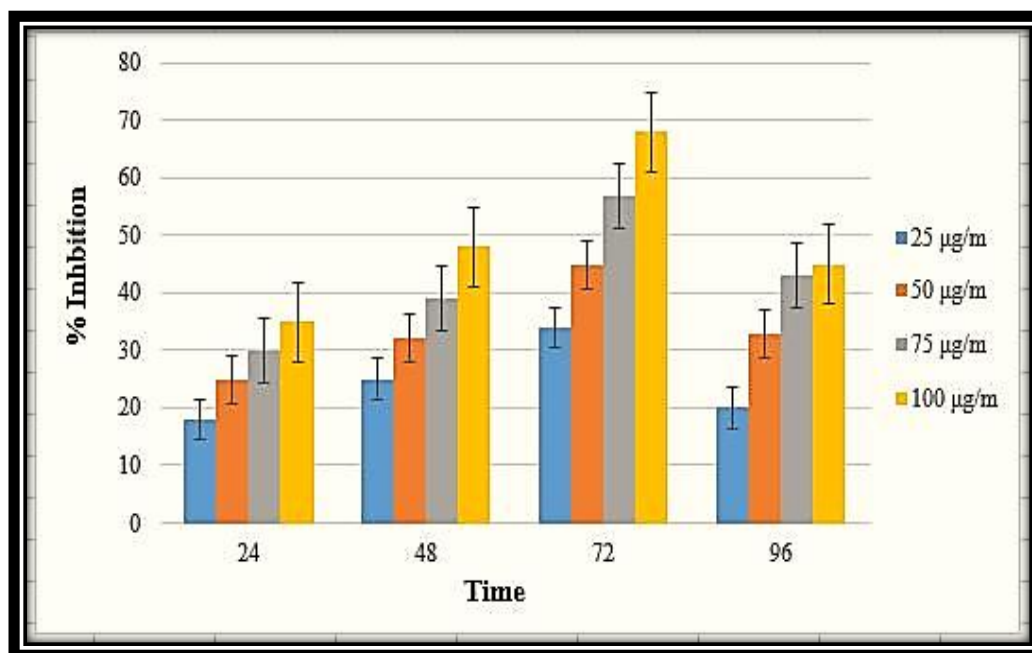


**Fig. 3.27** Antileishmanial potential of MB-ZnO at various concentrations.

### 3.2.12 Antifungal Assay

The inhibition potential of MB-ZnO nanocomposite at various doses was assessed on PDA media (Fig. 3.28). The fungal inhibition potential of synthesized MB-ZnO nanocomposite was examined at various doses, following to the formerly documented protocol (Zhang et al., 2014b). The highest inhibition ( $73 \pm 2.1\%$ ) was observed at 19 mg/ml dosage rate, followed by 12 mg/ml application rate ( $60 \pm 1.7\%$  GI), and 6 mg/ml concentration ( $52.77 \pm 0.5$ ). More rise in the MB-ZnO concentration did not increase growth inhibition, which may be due to rising in concentration results in the aggregation of nanocomposite. Nanoparticles has a smaller size but larger surface-to-volume ratios, enable them highly unstable and reactive (Hoseinzadeh et al., 2016). The physiochemical attributes like Brownian movement, size, and surface properties could also influence aggregation.

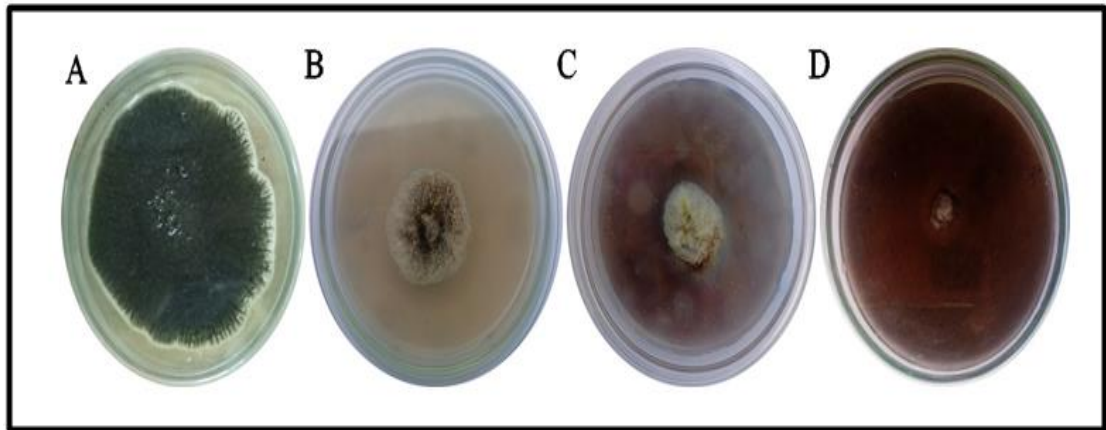


**Figure 3.28** Antifungal potential of MB-ZnO nanocomposite.

### 3.3 EXPERIMENT 3

#### 3.3.1 Graphical Abstract

For initial understanding, schematic representation of the experiment has been presented in Figure (3.29).

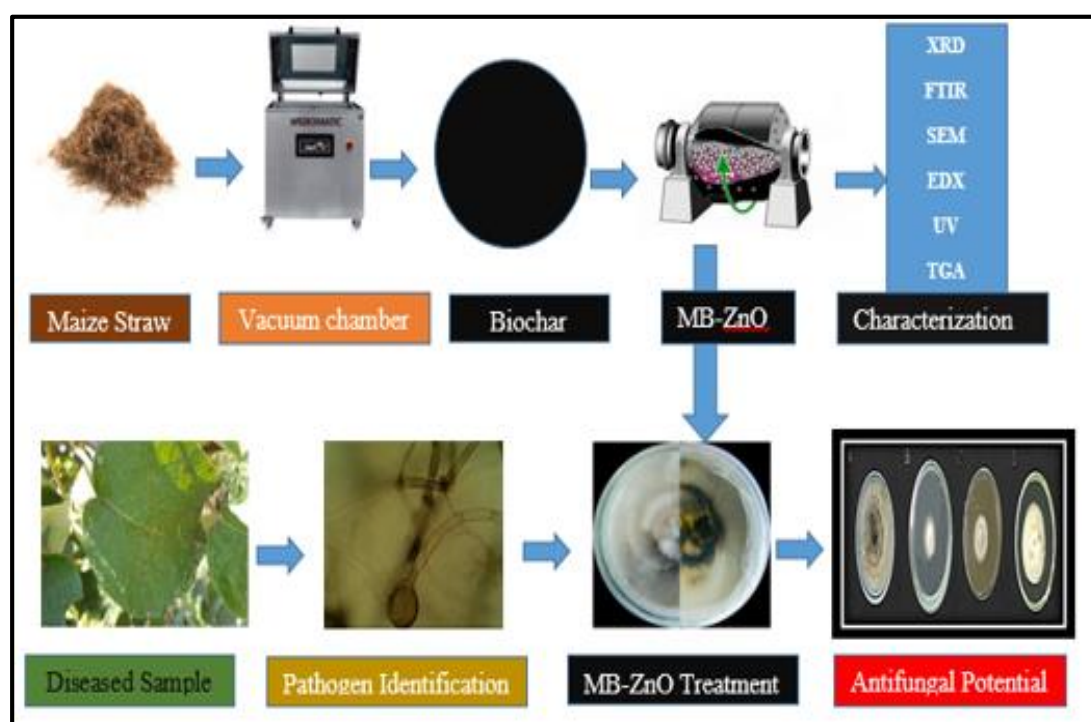


**Fig. 3.29** Schematic Representation of Complete Experiment.

#### 3.3.2 Isolation and Identification of the Disease-Causing Pathogen

In this experiment, brown spots were detected in an irregular manner on Kiwi leaves (Fig. 3.30 A). The size and number of these spots gradually enlarged and changed into dark brown, eventually. The disease-causing organism was isolated productively from the effected leaves, having an isolation frequency of 84%. After incubation for 5-6 days, white color mycelia were perceived, which shifted to grayish black with net-like appearance (Fig. 3.30 B). On the reverse side of the petri plates, the pattern was dark brown in appearance (Fig. 3.30 C). The color, appearance, and pattern of growth were similar to previously documented features of *R. oryzae* (Zhang et al., 2013). Microscopic analysis also delivered profound understanding into the

identification of pathogen isolated from the Kiwi leaves. Sporangiohores were usually straight, and they exist in single or in cluster form. They had a brownish color, varied in length from 220 to 1100  $\mu\text{m}$ , and in width from 7 to 12  $\mu\text{m}$  (Fig. 3.30 D). Sporangia were dark brown in color and ranged in size from globule to sub-globule, with a diameter of between 70 to 170  $\mu\text{m}$  (Fig. 3.30 D). The sporangiospores were angular, unseptate, or hardly septate, and brownish in color (Fig. 3.30 D). These description established the studied pathogen to be *R. oryzae* (Park et al., 2014).

### 3.3.3 Pathogenicity test

Injected healthy leaves displayed grayish lesions to to inoculation of 3 days (Fig. 3.30 E), which changed to dark after 5 days (Fig. 3.30 F). No lesion was established, on control leaves, and they stayed healthy. The pathogen was re-isolated from these lesions and displayed an identical mycelial appearance on PDA (Fig. 3.30 G and H). These results established the link of this pathogen to the Kiwi leaf spot.

### 3.3.4 Molecular confirmation and Phylogenetic Study

For the confirmation of the *R. oryzae* identity, phylogenetic study of the symbolic isolates was executed by amplified sequences of ITS, and EF-1 $\alpha$ . BLAST exploration of the resultant sequence from ITS1-ITS4 revealed >99% similarity with *R. oryzae* strain RAA. The internal transcribed spacer 1, partial sequence; 5.8S ribosomal RNA gene and internal transcribed spacer 2, whole sequence; and large subunit ribosomal RNA genes, partial sequence (MT603964.1). The sequence of EF-1 $\alpha$  showed 100% resemblance with translation elongation factor-1 $\alpha$  gene of *R. oryzae* (MK510718.1). The attained sequence from ITS1-ITS4 of *R. oryzae* was deposited to NCBI (MW603842.1). The Phylogenetic study competently elaborates the association of amplified ITS1/ITS4 sequence (Fig. 3.31) and EF-1 $\alpha$  sequence (Fig. 3.32), with closely associated genes, available in the NCBI database and confirmed BLAST analysis results. This is the first study of *Rhizopus oryzae* causing disease on leaves of Kiwi plant in Pakistan.

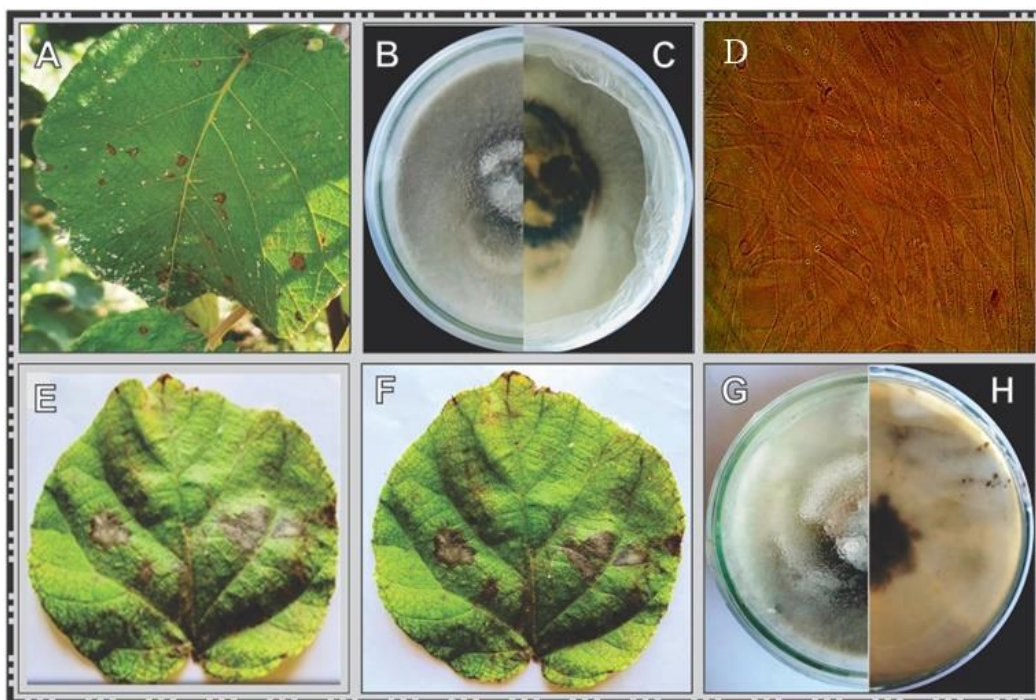


**Fig. 3.30** Leaf spots were examined on the Kiwi leaves (A). Disease causing pathogen was grown in plates and observed from front side (B) and reverse side (C). A microscopic study was performed at magnification of 40 $\times$  (D). Healthy leaves were injected with the isolated pathogen, and disease symptoms were developed after 3 days (E) and 5 days (F) of inoculation. Disease causing pathogen was re-isolated and observed from front (G) and back (H) side of plates.

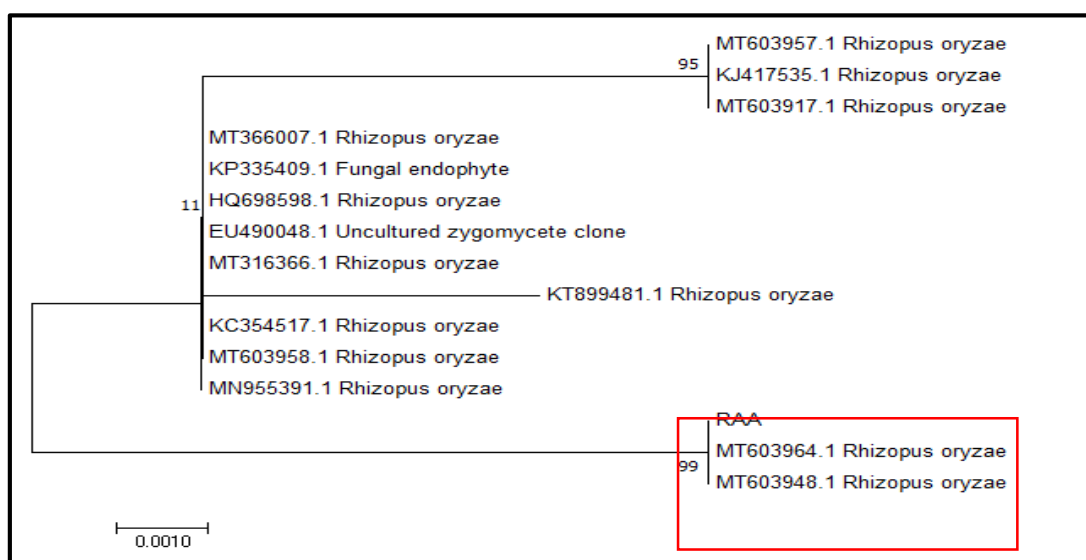


**Fig. 3.31** Phylogenetic analysis of isolated *R. oryzae* sequence with 14 closely associated ITS sequences after BLAST study.



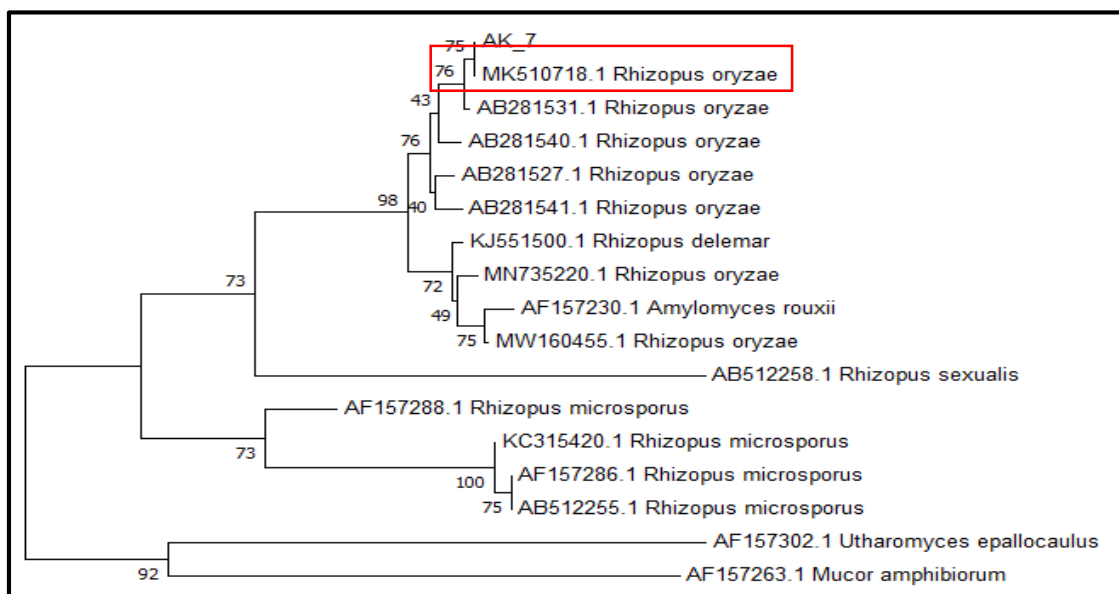


**Fig. 3.32** Phylogenetic analysis of isolated *R. oryzae* sequence with 16 closely related EF-1 $\alpha$  sequences after BLAST analysis. Subsequent from 1,000 replicates, bootstrap values are presented at the branch points.

### 3.3.5 Illustrations of MB-ZnO

#### 3.3.5.1. SEM and EDX Study

SEM analysis magnificently described the surface characteristics of pure biochar (Fig. 3.33 A) and MB-ZnO (Fig. 3.33 B). Micrographs through SEM revealed a coarse and porous outline of pristine biochar. The pyrolysis produced biochar with a porous and rough shape by vaporizing unstable substances. These textural properties of pure biochar established its ability as a superb support for nano-size material. After milling process, a white fine powder like of mass ZnO was examined on the surface of biochar, in assembled pattern (Fig. 3.33 B). SEM analysis shown that the attachment of raw materials on the biochar surface modified their surface configuration as well as altered the chemical composition of biochar (Fig. 3.33 B). These findings established the successful synthesis of MB-ZnO nanocomposites (Tu et al., 2020).

The elemental analysis of MB-ZnO nanocomposite were analyzed by EDX, which established the occurrence of C, O, Zn, Si, Ca, K, P, and Na in the

nanocomposite (Kamal et al., 2022b). EDX and SEM analysis of the prepared revealed the existence of ZnO on the MB skeleton.

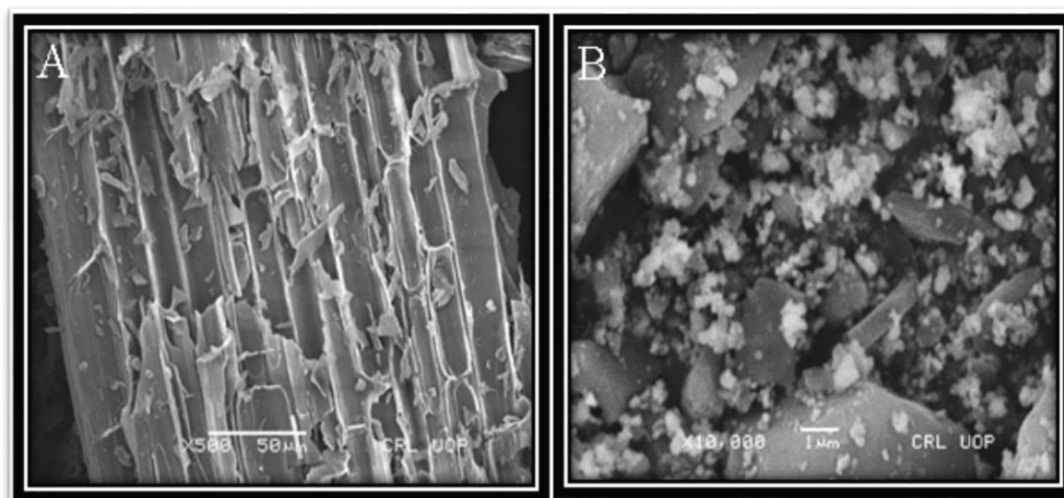


**Fig. 3.33** SEM micrograph of pure MB (A) and MB-ZnO (B).

### 3.3.5.2 XRD Study

The study of the crystal nature of MB-ZnO nanocomposite was investigated at a scanning rate of  $1^\circ$  per minute in  $0.013^\circ$  steps, covering a 2-theta angle extending from  $10^\circ$  to  $70^\circ$ . XRD analysis showed nine major peaks of MB- ZnO (Fig. 3.34). The various peaks at  $2-\theta=31.78, 34.43, 36.26, 47.55, 56.6, 62.9, 66.8, 67.9, 68.9, 72.7^\circ$  corresponded to (100), (002), (101), (102), (110), (103), (200), (112), (201), (004), (202), planes, separately (Duo et al., 2018) MB-ZnO showed the multiple diffraction peaks gives confirmation of hexagonal configuration according to the JCPDS no. (036-1451) and the intense and small peak proposed no enormous effect of the occurrence of Carbon on the crystalline nature of ZnO (Kamal et al., 2022a). The average MB-ZnO NPs size was determined as 46 nm, by an X-ray line broadening technique (Lourenço et al., 2021).

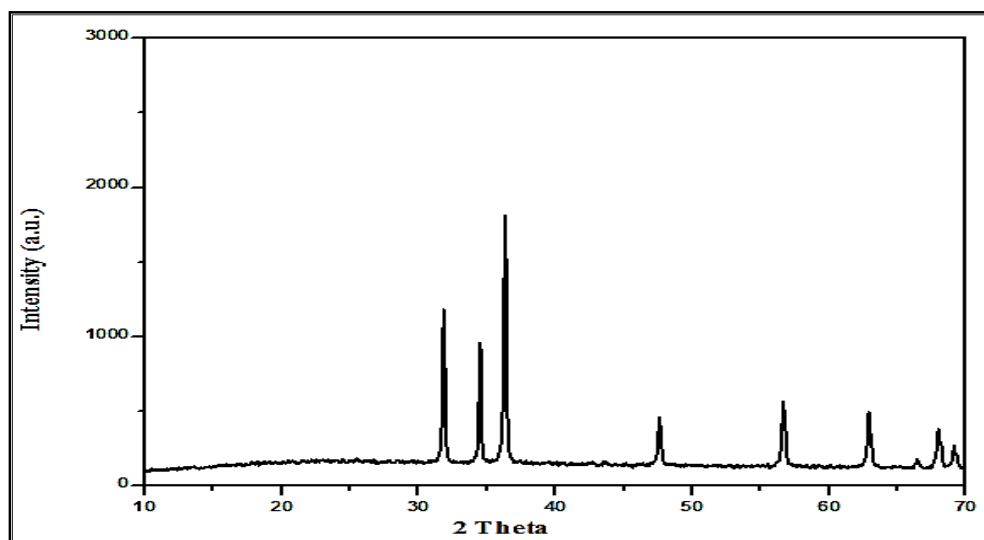


Fig. 3.34 XRD spectroscopy of MB-ZnO.

### 3.3.5.3 FTIR Spectroscopy

FTIR spectroscopy confirmed several functional groups found in the MB-ZnO (Fig. 3.35). Moderate bands are observed at  $1650\text{ cm}^{-1}$  confirming the bending of H-O-H and the peak at  $3440\text{ cm}^{-1}$  representing the O-H bonding. The peaks at  $2850$  and  $2940\text{ cm}^{-1}$  describes symmetric and asymmetric types of vibration of C-H bond, respectively (Chu et al., 2012). Bands at  $1037$ ,  $1124$ ,  $1325$ ,  $1417$ , and  $1452$  credited to the stretching of Si-O-Si, C-H, C-C,  $\text{CH}_2$  group, and  $\text{COO}^-$ , correspondingly (Jung et al., 2018; Saleh et al., 2018). Notably, a strong peak at  $524\text{ cm}^{-1}$  is ascribed to the Zn-O bonding (Batra et al., 2012). Another peak observed at  $580\text{ cm}^{-1}$  portrayed vibration of Zn and established the existence of ZnO on the MB-ZnO surface.

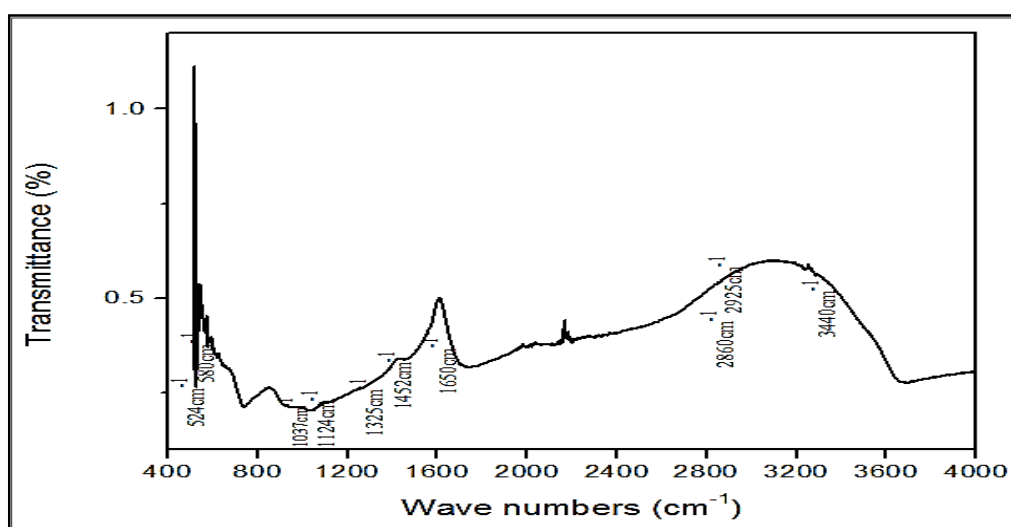


Fig. 3.35 FTIR analysis of MB-ZnO.

### 3.3.5.4 UV Analysis

UV-vis pattern of pure ZnO NPs and MB-ZnO presented sharp peaks extending from 200-800 nm (Fig. 3.36). Pristine ZnO nanoparticles revealed robust absorption in the ultraviolet spectra (200 to 250 nm) however not any peak was examined in visible region, which is similar with previous documented studies (Monticone et al., 1998). The absorption peaks of MB-ZnO nanocomposite were evaluated in the wavelength of 250 nm to 320 nm. The variations in the peaks is attributed to the chemical bonding between the ZnO NPs and pristine biochar (Akir et al., 2017).

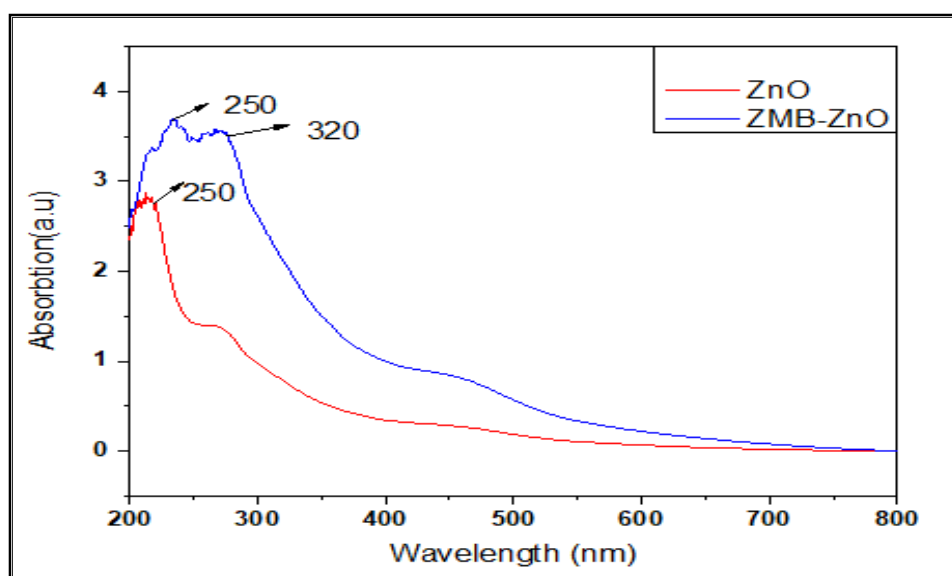


Fig. 3.36 UV spectra of ZnO NPs and MB-ZnO nanocomposite.

### 3.3.4.5 Thermo Gravitational Analysis

TGA was executed to analyze the thermal characteristics of MB-ZnO nanocomposite. Results of the current study exposed decent thermal stability of ball-milled prepared MB-ZnO, which confirm that the prepared nanocomposite can work in different environmental conditions with efficiency.

### 3.3.6 Antifungal Assay of MB-ZnO

Different mycelial inhibitions were examined at various dosage rates of MB-ZnO nanocomposite on PDA media (Fig. 3.37). A same pattern of fungal inhibition was examined previously (Lourenço et al., 2021). The maximum inhibition of growth ( $79 \pm 2.1\%$ ) was examined at 19 mg/ml application rate (Fig. 3.38), followed by moderate growth inhibition ( $67 \pm 1.7\%$ ) at 12 mg/ml concentration, and little growth inhibition

( $57.77 \pm 0.5$ ) at 6 mg/ml dosage. More rising in the dosage rate of MB-ZnO did not escalate fungal inhibition, which may be due to increase in concentration leading to the assembling of the MB-ZnO nanoparticles. Previous research establishes that nanocomposite materials are highly unstable and reactive due to their small size but high surface-to-volume ratios (Bakr et al., 2018). The physiochemical properties like size, shape, Brownian movement, and surface properties might be influencing their aggregation.

In the last decade, nanotechnologists have successfully used ZnO nanocomposite to inhibit the growth of several fungi like *Pythium uttimum*, *Ascochyta rabiei*, *Candida albicans*, *Aspergillus niger*, *Botrytis cinerea*, and *Fusarium graminearum* (Hoseinzadeh et al., 2016; Omar et al., 2016; Zhang et al., 2014a). It is also suggested by some nanotechnologists that in the antimicrobial assay, ZnO NPs creates  $Zn^{+2}$  which destroy the pathogens membrane (Naraginti and Li, 2017). The most recent antimicrobial efficacy of metal-oxide based NPs comprises of the generation of noxious ions to abolish cells (Thaya et al., 2016). It has been documented that nanoparticles powerfully interact to the surface of microorganism and show antimicrobial potential (Nguyen et al., 2019). Metals nanocomposites produce holes by cracking the cell wall and changes morphological properties such as polarity and permeability of the cell membrane and leading to the interruption of the plasma membrane and hence easily entered into the cell and resulting in damage of DNA, RNA, and proteins constituents present in the cytoplasm of the target cell (Pereira et al., 2014). This devastation creates a leakage of various components such as DNA, RNA, proteins, and enzymes, and leads into necrosis. Due to several useful applications, scientists have used various approaches to control the pathogens of kiwi (Chen et al., 2022).

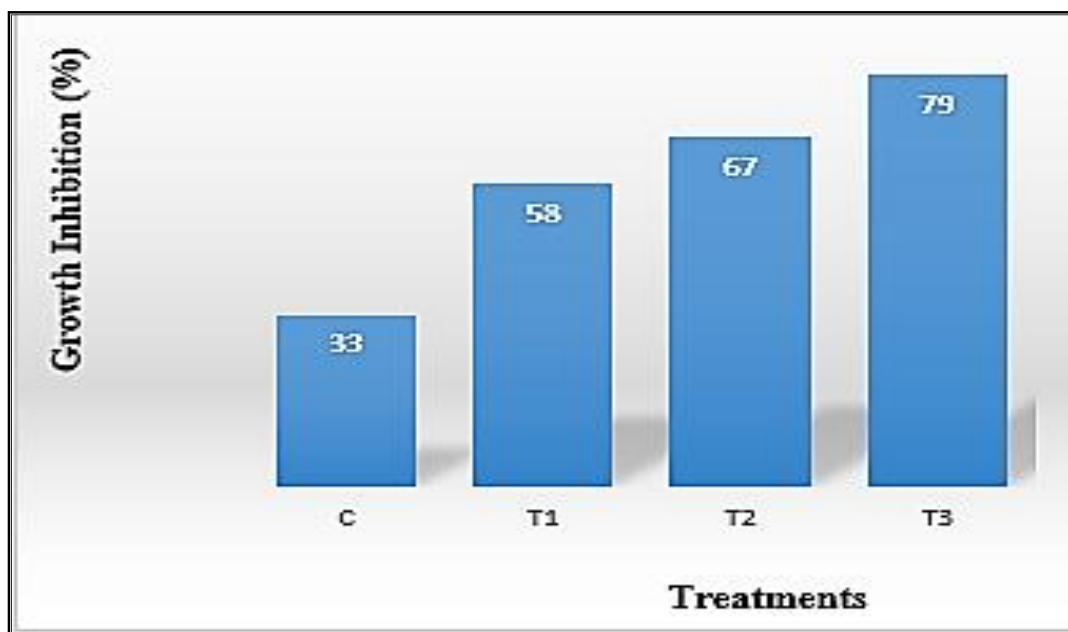


**Fig. 3.37** *In vitro* antifungal activity of MB-ZnO nanocomposite. C (control), T1 (6 mg/ml), T2 (12 mg/ml), T3 (19 mg/ml).



**Fig. 3.38** Effect of different application rates of MB-ZnO nanocomposite on the growth of *R. oryzae*. (A) Control, (B) 19 mg/mL application rate, (C) 12 mg/mL application rate, (D) 6 mg/mL application rate.

### 3.4 EXPERIMENT 4

#### 3.4.1 Graphical Abstract

For initial understanding, schematic representation of the experiment has been presented in Fig. 3.39.

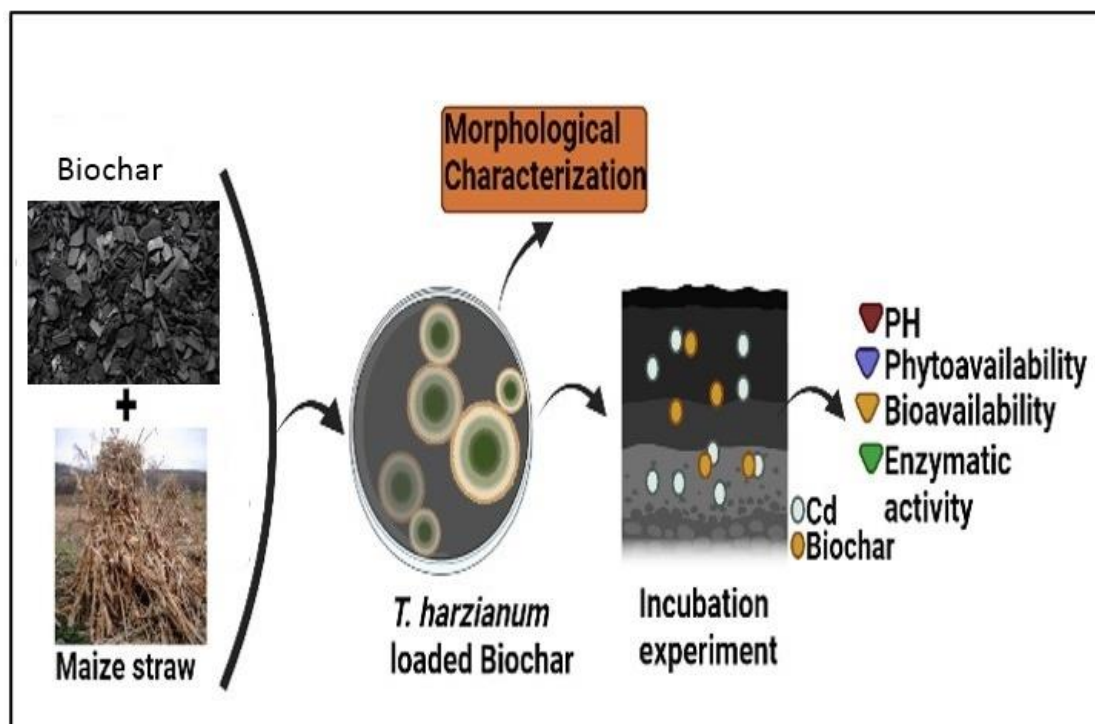


Fig. 3.39 Schematic Diagram of Complete Experiment.

#### 3.4.2 Properties of Soil

Soil used in this experiment was slightly alkaline with silty clay texture. Complete soil properties have been pronounced in (Table 4.2).

#### 3.4.3 Characterization of Fungus (*T. harzianum*) Loaded Biochar (MBT)

SE microscopy of MB revealed rough and porous morphology of MBT (Fig. 3.40 A). This kind of morphology might help the addition and propagation of fungus. Strain of *T. harzianum* (Fig. 3.40 B) stuck well to the biochar and most hyphae were colonized or disseminated on the surface of biochar (Fig. 3.40 C). It is equitable that certain hyphae pass in through the pores in the surface of biochar. The settlement of microbial strain on the surface of biochar and its roughness is based on its

morphological characteristics (Zhu et al., 2017). Earlier studies have also described the attachment of microorganisms to the biochar skeleton (Quilliam et al., 2013). These studies concluded that the existence of polycyclic hydrocarbons and many minerals might prevent the attachment of microorganisms to the surface of biochar. In contrast, some researchers have reported the attachment of microorganisms on the biochar surface, for a very short period of 10 days (Kappler et al., 2014).

**Table 3.2:** Selected properties of the pure biochar and soil.

Properties	Biochar	Soil
Ash contents	1.50%	–
pH	9.30	7.6
Texture	–	Silty clay
Organic matter (g kg <sup>-1</sup> )	98.41	5.8
Total C (g kg <sup>-1</sup> )	57.8	–
Total N (g kg <sup>-1</sup> )	8.46	0.57
Total P (g kg <sup>-1</sup> )	1.40	0.113
Total K (g kg <sup>-1</sup> )	11.8	6.37
Total Na (g kg <sup>-1</sup> )	–	0.09%
CEC (cmol kg <sup>-1</sup> )	10.72	5.41
Electrical conductivity (E.C.)	–	0.261 dS/m

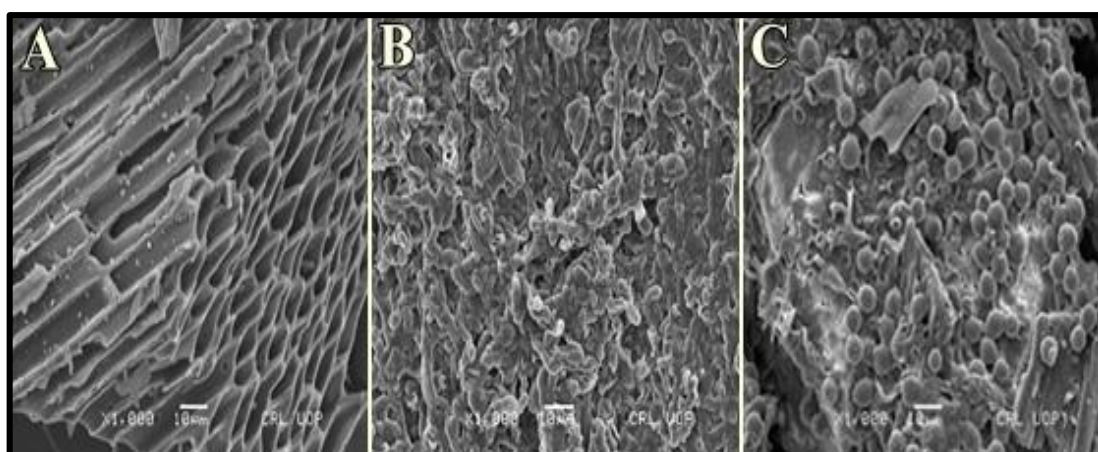


**Fig. 3.40** SEM images of pure biochar (A), *T. harzianum* (B), and *T. harzianum* loaded biochar (C).



#### 3.4.4 Fluctuations in Soil pH

Application of both MB and MBT raised the pH of treated soil at the initial phases of incubation (day 7), particularly with a dosage rate of 5%. During 90-day incubation, the soil pH changed in all treatments (Fig. 3.41). Less variation in the pH of all the amendments was perceived with the increasing incubation time. Both MB and MBT changed the soil pH at 1% and 5% concentrations. After the addition of 1% MB1 and MBT1, the pH was changed from 7.2 (control soil pH) to 7.8 and 8.0, respectively. After the addition of 5% MB5 and MBT5 biochar, the pH values in the treated soils increased to 8.3 and 8.7, respectively. These studies have revealed that the rapid rise in the soil pH was because of the breakdown of alkaline material (like carbonate), present in the biochar. At later stages, soil pH is decreased due to the depletion of alkaline substances. In this study, MBT treatment showed more decline in pH than MB treatment. Specifically, BT5 treatment ominously declined the soil pH after 42-days of incubation.

These findings proposed that the higher concentration of MBT can meritoriously intervene in soil. This may be due to the secretion of some organic acids by *T. harzianum* to reduce soil. Still, in this experiment, the pH of the soil was in the neutral-alkaline range after MBT treatment. The pH buffering capability of MBT is a fascinating episode, which is commendable for more research on the speciation and liability of Cu and Cd in contaminated soil, particularly in soil having acidic pH. About the similar pattern of results was found by some other researcher at similar application rate of biochar (Tu et al., 2020).

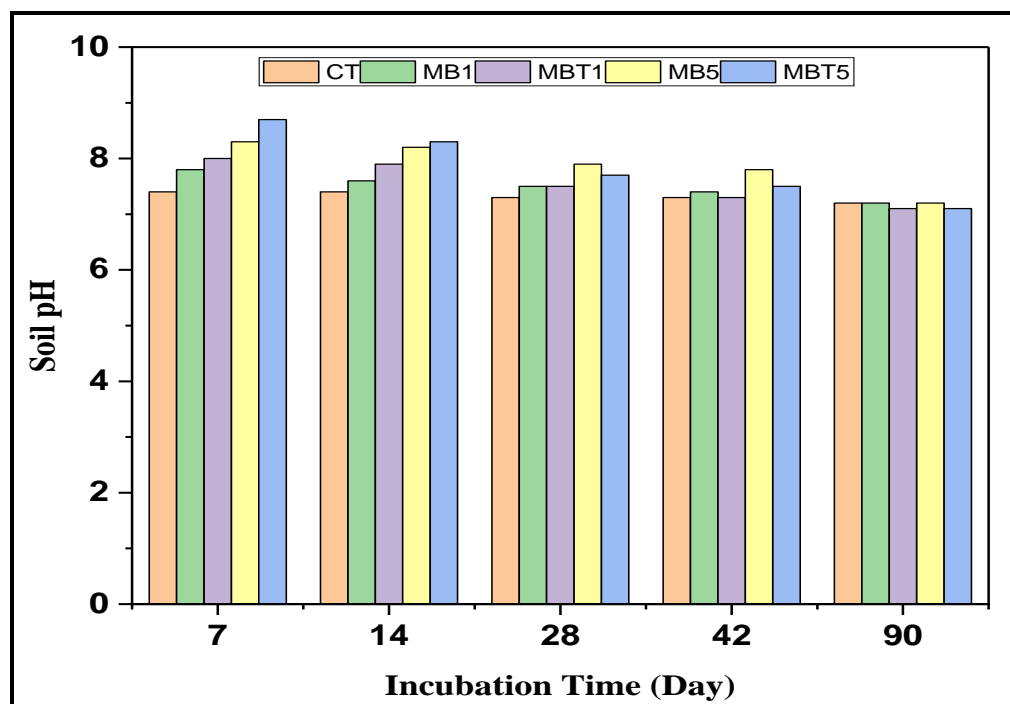


**Fig. 3.41** Fluctuations in soil pH after the addition of maize biochar (MB) and fungus-loaded biochar (MBT). CT shows control sample; MB1, MB5, MBT1 and MBT5 indicates the soil samples treated with 1% MB, 5% MB, 1% MBT and 5% MBT, respectively.

### 3.4.5 Cd and Cu Fractionation in a Treated Soil

Cd and Cu proportion in contaminated soil were interrupted by the application of biochar treatments (Fig. 3.42). At the start (0-day), the major Cd fraction in control sample (untreated soil) was exchangeable Cd (59.10%), sequentially carbonate bound Cd (27.2%), residual bound fraction (8.10%), Fe-Mn oxide Cd (4.80%), and organic matter bound fraction (>1.0%). After 90 days of incubation period, the fraction of exchangeable Cd in treated soil decreased to various marks and changed to additional components. In comparison with CT sample, the exchangeable fraction of Cd in MB1 and MBT1, FB1 amendment was reduced by 2.0% and 3.1%, respectively. Fe-Mn oxide Cd raised by 1.90 % and 2.11 %, respectively, whereas the residual bound fraction of Cd was improved by 1.1 % and 1.9 %, respectively. MB5 and MBT5 amendments showed decline in the exchangeable portion of Cd by 6.73% and 15.33%, respectively. In the interim, an enhance in the Fe-Mn oxide portion was observed, by 5.23% and

9.30%, respectively and in the residual bound fraction of Cd, an increase of 2.0% and 6.31% was seen, correspondingly.

Very small changes in organic matter binding fraction were observed in all treatments and the highest amount of organic matter bound Cd was observed in MB5 (0.65%) and MBT5 (0.75%). No significant differences in carbonates bound Cd fraction were observed in all amendments. It was observed that the amendment of biochar considerably changed the speciation of HMs in the soil (Fig. 3.42). In current study, Cd exchangeable contents progressively reduced with the increase of biochar dosage rate. Previous research also claimed that the exchangeable fraction of Cd is the major part of the whole Cd concentration in the soil (Huang et al., 2019; Lu et al., 2017). In our findings, no reduction was observed in carbonate bound portion which might be due to the increased pH of biochar amendments. The change in pH have been reported to promote carbonate precipitation like  $\text{CdCO}_3$  (Yang et al., 2018). In the current study, a rise in residual bound fraction and Fe-Mn bound fraction was observed. Some previous researchers documented that the used of biochar to the soil can substantially lessen the reducible Cd concentration and increase the oxidizable and residual Cd concentration (Jiang et al., 2012).

Different from Cadmium, Copper in the control sample (CT, 0 days) was mostly in the carbonate bound form (50.70%), followed by residual Cu (27.33%), Fe-Mn oxide Cu (16.50%), organic matter bound fraction (3.30%) and exchangeable Cu (2.44%). On the 90<sup>th</sup> day of the experiment, the exchangeable Cu fraction decreased up to 2.0% in MB1, 1.96% in MBT1, 1.70% in MB5, and 1.20% in MBT5. In comparison to CT amendment, the carbonate bound Cu portions of MB5 and MBT5 amendments were notably decreased to 38.80% and 34.64%, respectively. The residual Cu fraction was increased by 7.47%, 9.37%, 13.63%, and 19.65% in MB1, MBT1, MB5, and MBT5 respectively. In this study, Fe-Mn oxide Cu portion was reduced which may be changed to organic matter Cu portion, within 90 days of incubation, as it increased in all treatments (MB1, MBT1, MB5, and MBT5). Many researchers reported that the appliance of biochar increases the fraction of organic bound Cu (Park et al., 2011; Rinklebe and Shaheen, 2015).

The biochar surface has numerous oxygen-containing functional groups that may result in increased oxidizable fraction to form organic-bound Cu by reacting with Cu (Park et al., 2011). Gholami and Rahimi (2021) reported that the biochar can elevate the organic matter-bound Cu ratio. Though, current results displayed improved organic bound fraction with biochar treatments, the soil organic matter Cu fraction was not elevated, proportionately. The carbonate-bound Cu fraction in the current work was increased to transform to the residual bound Cu fractions (most recalcitrant fractions). The carbonate and exchangeable bound content indicate the most available component, whereas the Fe-Mn oxide, residual fractions, and organic matter bound fraction can be recognized as the recalcitrant portion. Both the recalcitrant and liable proportions can be applied to determine the efficiency of *in-situ* stabilization (He et al., 2019b; Rinklebe et al., 2016; Jiang et al., 2012).

In the current work, we find out that both bioavailable Cd and Cu contents of MB5 amendment were considerably lesser than MB1 amendment (Fig. 3.42 A and B). Additionally, in comparison to MB treatment, MBT could efficiently diminish the bioavailable Cu and Cd in the contaminated soil; hence increasing the immobility of Cu and Cd, particularly with 5% application rate. Both MB and MBT could encourage the changes of Cu and Cd from bioavailable portion to less bioavailable form. Though, the fraction disseminations of Cu and Cd in the amended soils are different. Particularly, the soil exchangeable Cu fraction is clearly lesser as compared to Cd, whereas the soil organic matter bond Cu is distinctly greater than that of Cd. This might be because of the Cu greater affinity sequence and greater sorption potential to organic matters (e.g., biochar and humic acid) and soil inorganic matter (Ding et al., 2019; Sellaoui et al., 2018; Sipos et al., 2019). Hence, the appliance of biochar to the soil can condense heavy metals into a greater stable form and decrease their environmental threat.

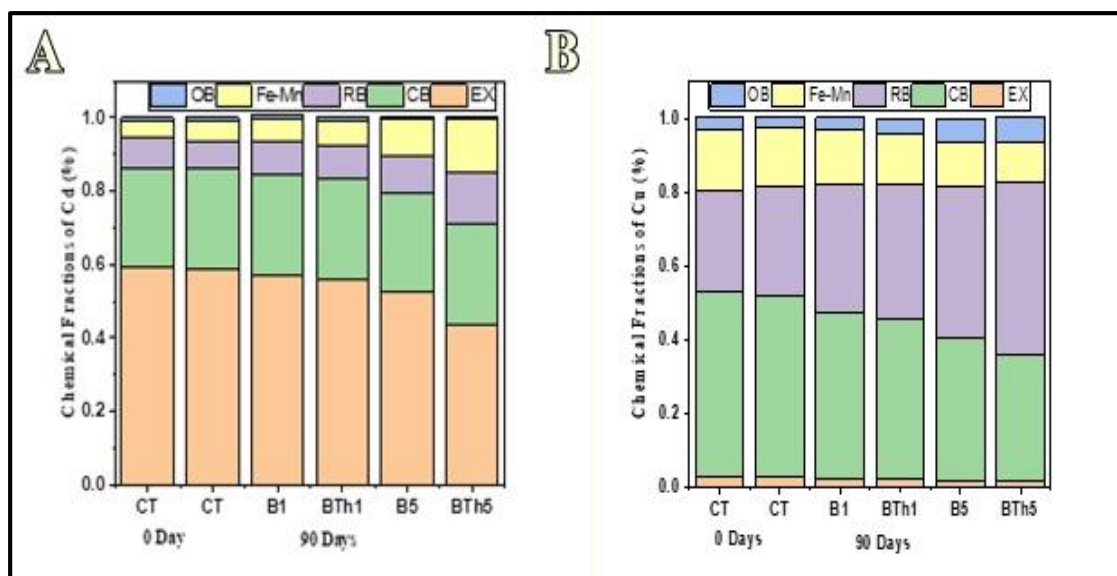


**Fig. 3.42** Cd (A) and Cu (B) speciation in the contaminated soil.

### 3.4.6 Phyto-availability of Cu and Cd

The finding of our study revealed that the DTPA extractable Cu and Cd concentration (i.e., DTPA-Cu, DTPA-Cd) in the amended soil gradually decreased with an increase in incubation duration (Fig. 3.43). After 90 days, the DTPA-Cd contents lowered from  $45 \text{ mg kg}^{-1}$  in CT to  $38 \text{ mg kg}^{-1}$  in MB1,  $36 \text{ mg kg}^{-1}$  in MBT1,  $31.1 \text{ mg kg}^{-1}$  in MB5 and  $25.3 \text{ mg kg}^{-1}$  in MBT5. In comparison to control, a decline in DTPA-Cu concentration was observed in all treatments. Though, variable results have been described in some other studies (Fellet et al., 2014). Some other workers have also perceived an escalation in the phyto-availability of Cu (Mendez et al., 2012). This increase might be because of an amplified proportion of dissolved organic matter present in biochar. Dissolved organic matter produced from biochar have various hydroxyl and carboxylate functional groups which can interact with Cu cations and elevate their mobility and bioavailability (Wei et al., 2019). Biochar has been reported to produce minimum amount of dissolved organic matter (Liu et al., 2017). As shown in Fig. 3.43, in comparison to the individual MB amendment, the MBT amendment with an equal dose rate had lesser concentration of DTPA-Cu and DTPA-Cd. Specifically, on the 90<sup>th</sup> day, the DTPA-Cd contents was  $23.2$  and  $16.7 \text{ mg kg}^{-1}$  in MBT1 and MBT5; whereas the DTPA-Cu level was  $104.2$  and  $62.3 \text{ mg kg}^{-1}$  in MBT1 and MBT5, correspondingly. These findings showed that MBT creates a momentous

impact in declining the phyto-availability of Cu and Cd in soil, particularly at treatment dose of the 5%.

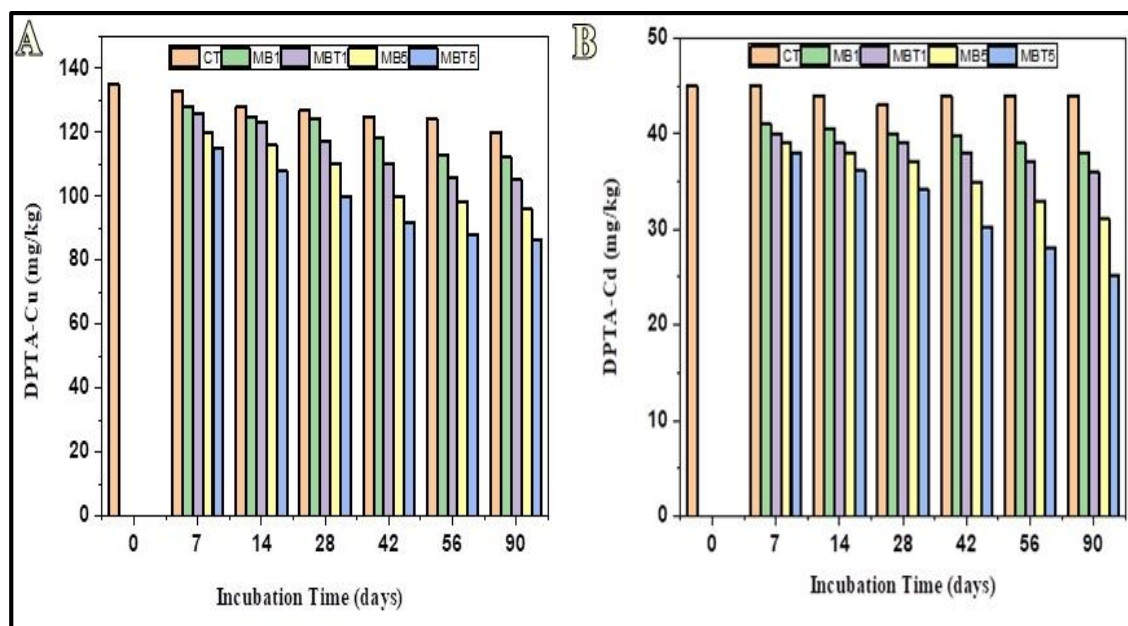


**Fig. 3.43** Fluctuations in DTPA-Cu (A) and DTPA-Cd (B) in a treated soil.

### 3.4.7 Bio-accessibility of Cd and Cu

In this study, a unified bio-accessibility test was successfully implemented to see bio-accessible Cu and Cd proportions from the contaminated soil (Fig. 3.44). This test is cost-effective and quick, while other animal studies are costly, difficult in management and care, and time-consuming. It is always desirable to shift from *in vivo* studies approaches to *in vitro* approaches (Ruby et al., 1996); though, a consistently reproducible extraction protocol for several soils is still needed. Additionally, this procedure will be easily applied by various research laboratories. Artificial biofluids have been applied in different physiological tests, for the expectation of drug uptake, nutritional analysis (Miller et al., 1981), and metal solubility of orthodontic applications (Fusayama et al., 1963; Katz and Samitz, 1975).

Like DTPA-phyto-availability, Cu and Cd bioavailability of the amended soil was reduced to different percentages with the application of two treatments of biochar at various doses (Fig. 3.44 A, B). In the CT samples, the bioavailable Cd and Cu percentages were 80.6% and 75.4%, respectively, showing a high discharging threat

under extraordinary gastric phase. After the completion of 90 days incubation experiment, Cd bio-accessibility of gastric juice was somewhat reduced in all treatments including MB1 (77%), MBT1 (75.2%), MB5 (70.4%), and MBT5 (68.1%). Gastrointestinal fractions at the various treatments were recorded to be 73% (MB1), 71.1% (MBT1), 67.4% (MB5), and 63.5% (MBT5). In comparison, an obvious reduction in Cu bio-accessibility was perceived in all four amendments, viz. MB1 (72.5%), MBT1 (69.6%), MB5 (65.1%), and MBT5 (61.4%) in gastric solution. Similarly, after 90 days of incubation, reduction in Cu was analyzed in the intestinal juice for all four amendments, including MB1 (66.4%), MBT1 (60.1%), MB5 (58%), and MBT5 (54.4%). Different studies have reported the potential of biochar to decrease metal bioavailability, even at small doses (Bashir et al., 2018b; Yoo et al., 2018). Though, the majority of researchers used acidic soils (Janus et al., 2018). Some studies have assessed the effect of three types of biochar on the oral bioavailability of Cd, Zn, and Pb in basic soil (pH 7.6). The addition of acid biochar (pH 3.2) had no impact on the bioavailability of Cd in two different basic soils (pH 7.91 and 8.5), though, the neutral biochar was proficient of declining the bioavailability of Cd (Qi et al., 2018).

In amended soil, Cd and Cu bioavailability in the intestinal juice was notably lesser, in comparison to gastric fractions (Fig. 3.44 C, D), which is parallel with the previously published studies (Fu and Cui, 2013; Pelfrêne et al., 2015). This could be credited to elevated pH and the application of organic components like pancreatin and bile extract in the intestinal juice. The change in pH (from 1.5 to 7.0 in the intestinal phase) may cause precipitation of part of the solubilized Cd (Mounicou et al., 2002). Other studies also proved that Cd may produce insoluble complexes with the phytate that exist in the diet of human (Versantvoort et al., 2005).

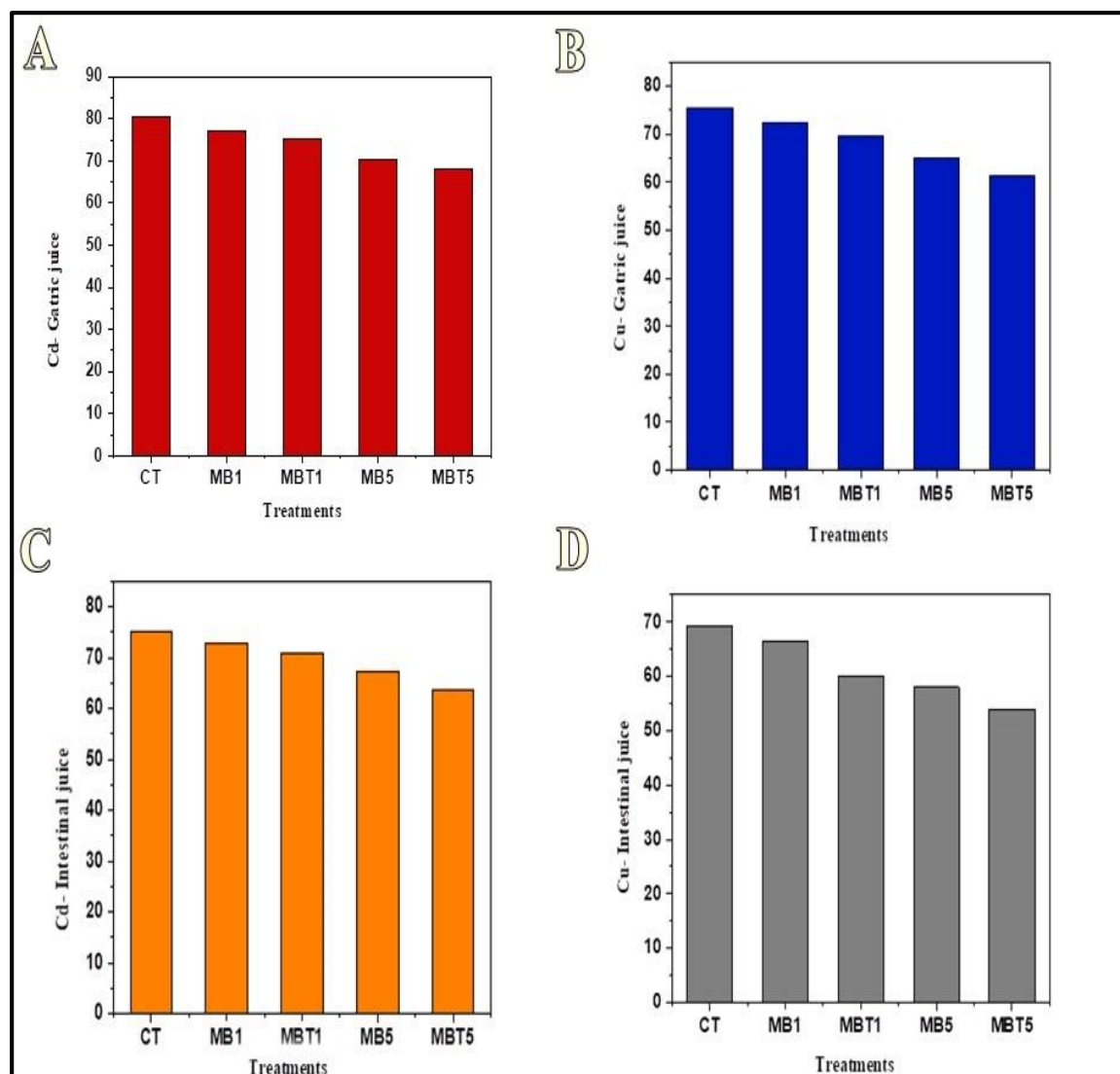


**Fig. 3.44** Bio-accessibility of Cd (A) and Cu (B) in stomach phase, and Cd (C) and Cu (D) in intestinal phase after 90 days of incubation.

### 3.4.8 Effect of Biochar Amendments on Enzymatic Activities of Soil

During the incubation, significant variations of soil enzymatic potential (catalase and urease) were observed (Fig. 3.45). Heavy metal pollution can have bad effects on the biological functions of soil microorganisms (Jiang et al., 2010; Pan and Yu, 2011). Soil enzymes especially urease and catalase activities worked as sensitive bioindicators to HMs and they are usually studied to analyze the influence of soil treatment on the biological activities of soil (He et al., 2019b; Tu et al., 2018). Some researchers described that biochar affect enzymatic activities in polluted soil adversely,



which may be due to biochar properties and soil ecology (Bashir et al., 2018a; Nie et al., 2018; Zhu et al., 2017).

At the start of incubation, both urease and catalase functions slowly declined in all amendments, and later recovered at the final phase of the experiment. The decline of the enzyme activities at an initial phase may be due to the inhibitory effects of high amount of Cd ( $60 \text{ mg kg}^{-1}$ ) and Cu ( $258 \text{ mg kg}^{-1}$ ) in the contaminated soil. Gong et al. (2019) reported the same pattern for urease activity after the application of biochar in Cd-polluted sediment. Remarkably, during the first two weeks, soil treated with MBT5 displayed maximum catalase activity, among all amendments (Fig. 3.45 A), which is probably because of the survival of fungus in the porous structure of biochar (Quilliam et al., 2013). During 4<sup>th</sup>, 6<sup>th</sup>, and 8<sup>th</sup> week, almost similar catalase activity was observed, in all amendments. But on the 90<sup>th</sup> day, the catalase activity of the MB and MBT treatments were higher than untreated soil. Similar trend of catalase activity has been studied earlier (Tu et al., 2020).

Urease performs a noteworthy part in the conversion of soil nitrogen. In our study, application of biochar reduced soil urease activity during the first 42 days, which was later elevated, and the maximum activity was observed at 90<sup>th</sup> day of incubation (Fig. 3.45 B). Previous studies have also documented the same trend of results after applying high doses of biochar, probably owing to the damaging role of biochar to microorganisms in the soil (Bhaduri et al., 2016; Gong et al., 2019; Huang et al., 2017). Application of MBT resulted in the decline of soil urease activity at the initial phase but later this activity was increased after 42<sup>nd</sup> days of incubation. These results showed a quick and greater self-restoring ability of soil activities in polluted soil. Former studies have also proposed the effect of heavy metals on soil enzymatic activities (Yang et al., 2016), which ultimately reveals the capability of polluted soil to self-purify with MBT (Cui et al., 2019). Previous studies have also proposed the effect of heavy metals on soil enzymatic activities (Yang et al., 2016), which ultimately reveals the capability of polluted soil to self-purify (Cui et al., 2019).

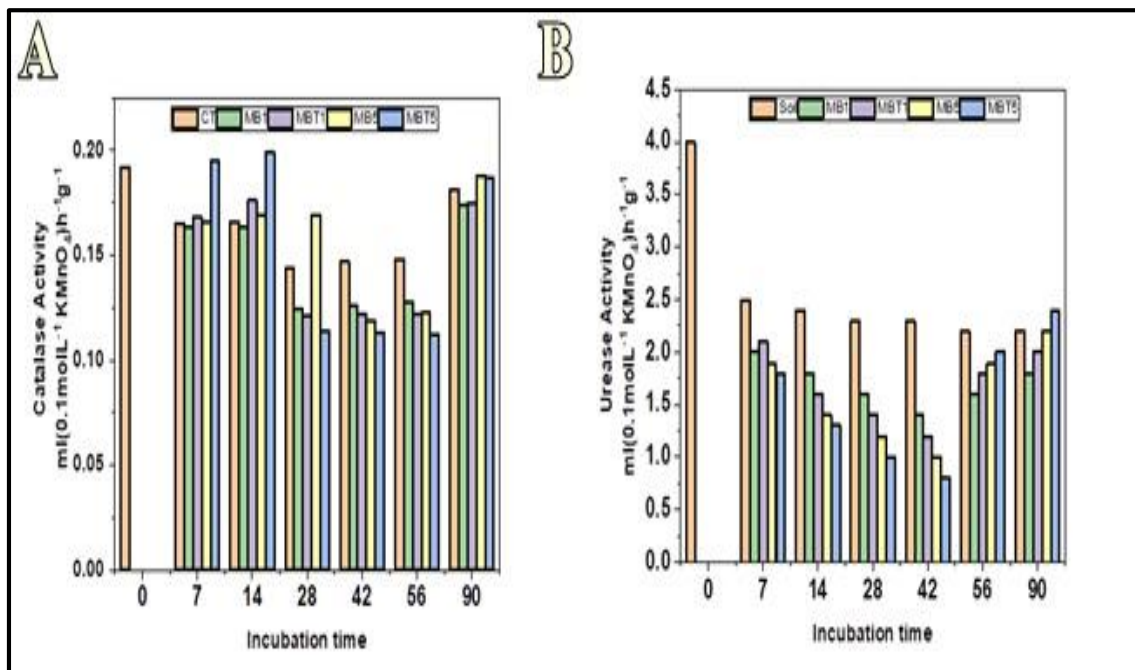


**Fig. 3.45** Impact of MB and MBT on the activities of urease (A) and catalase (B) in the soil.

### 3.4.9 Mechanisms and Effects

According to the findings of our study, the bioavailable portions of Cu and Cd were clearly declined in both MB and MBT-treated soils. These declines decreased adverse impacts on microorganisms and subsequently stimulated the enzymatic activities of soil microorganisms. Among these multiple amendments, the application of MBT5 resulted in optimal activity for the heavy metals stabilization and restoration of soil. In previous studies, biochar has been reported to stabilize soil heavy metals (Hamid et al., 2019; Igalavithana et al., 2019; Rechberger et al., 2019). MBT exhibited great tolerance to Cu and Cd in the polluted soil, and this tolerance increased at later stages of incubation due to long-lasting effect on the immobilization of Cu and Cd.

### 3.5. EXPERIMENT 5

#### 3.5.1 Graphical Abstract

For initial understanding, schematic representation of the experiment has been presented in Figure (3.46).

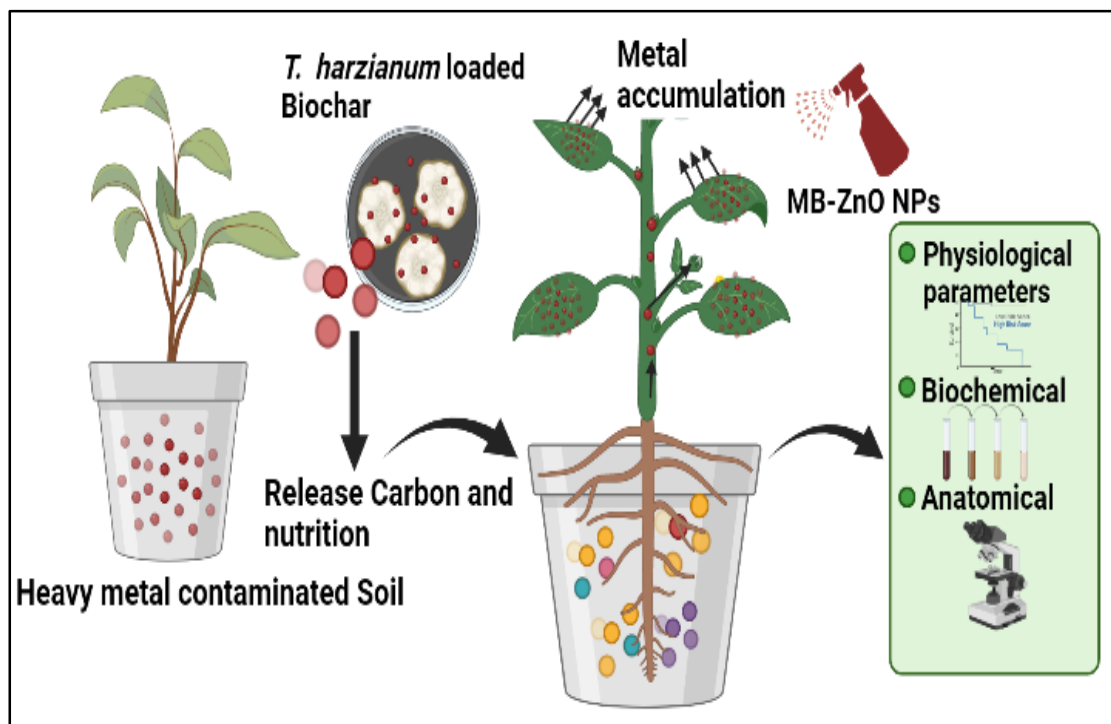


Fig. 3.46 Schematic Depiction of Complete Experiment.

#### 3.5.2 Physiological Parameters

Following physiological and biochemical parameters assisted us to recognize the response of *Sesbania* under different treatments.

##### 3.5.2.1 Root and Shoot Length

The results revealed that the application of MBT and MB-ZnO notably enhanced root length of *Sesbania* in Cd-Cu stressed soil (Fig. 3.47). The root length of plants with the application of MBT and MB-ZnO was significantly enhanced (up to 30%) at 100 mg L<sup>-1</sup> of Cd-Cu stress, in comparison to un-inoculated plants. The shoot length of uninoculated plants was also significantly reduced under Cd-Cu stress. By the

inoculation of MBT and MB-ZnO, an enhanced plant shoot length (33.33%) was observed at 100 mg L<sup>-1</sup> stress, then control (Fig. 3.47).

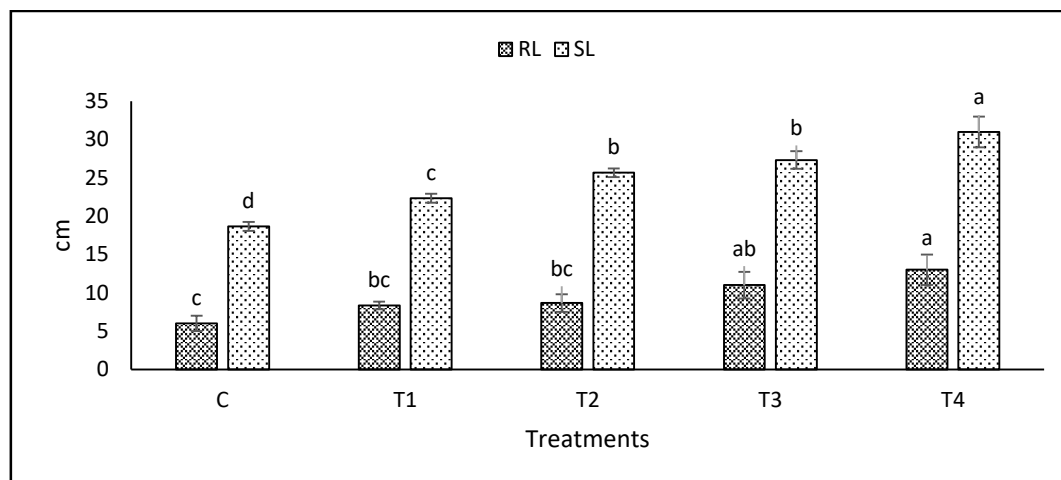


**Fig. 3.47** Effects of MB-ZnO on Root and Shoot of *S. sesban* in Cd-Cu stressed soil; C (Control), T1 (0 mg/L), T2 (50 mg/L), T3 (75 mg/L), T4 (100 mg/L).

### 3.5.2.2 Fresh and Dry Weight

The fresh weight of un-inoculated *Sesbania* plants was significantly reduced under Cd-Cu stressed soil in comparison to treated plants (Fig. 3.41). The use of MBT and MB-ZnO nanocomposite maintained up to 60 % higher fresh weight at 100 mg L<sup>-1</sup>, as compared to un-treated plants grown in the same growth conditions. The dry mass of the plants was also higher at elevated concentration of MB-ZnO nanocomposite (Fig. 3.48).

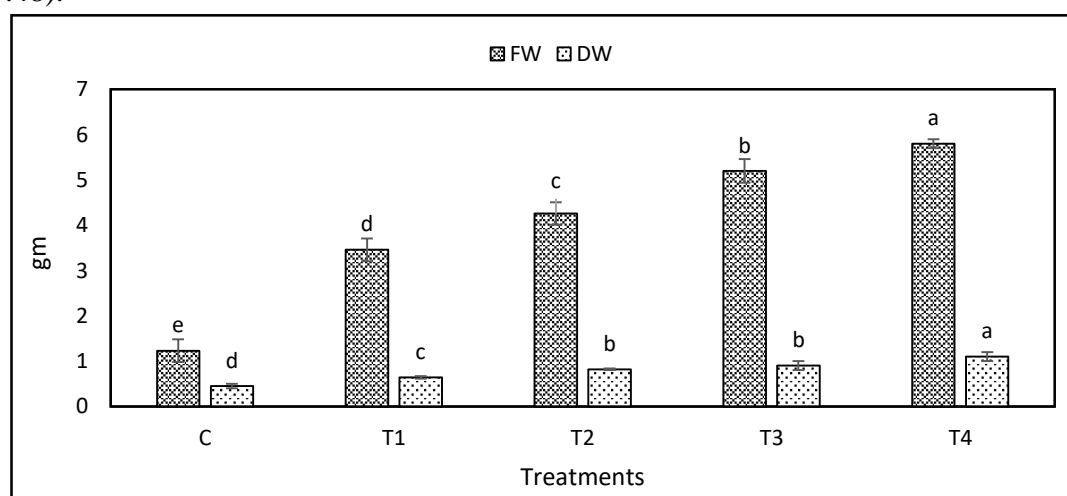


**Fig. 3.48** Effects of MB-ZnO on Fresh and Dry weight of *S. sesban* in Cd-Cu stressed soil. C (Control), T1 (0 mg/L), T2 (50 mg/L), T3 (75 mg/L), (100 mg/L).

### 3.5.3 Biochemical Parameters

#### 3.5.3.1 Chlorophyll a,b and Carotenoids

Metal toxicity affects chlorophyll a, b and carotenoid contents in the body of *S. Sesbania* (Fig. 3.49). Findings of our study revealed a positive effect of MBT and MB-ZnO nanocomposite on the chlorophyll contents of *Sesbania* leaves (Fig. 3.49). The NPs foliar treatments and biochar soil addition were greatly capable in increasing photosynthetic pigment in *Sesbania* leaves. When compared with control, enhanced concentrations of chlorophyll a (48%), chlorophyll b (57%) and carotenoids (32.43%) were examined at concentration of 100 mg/L of NPs.

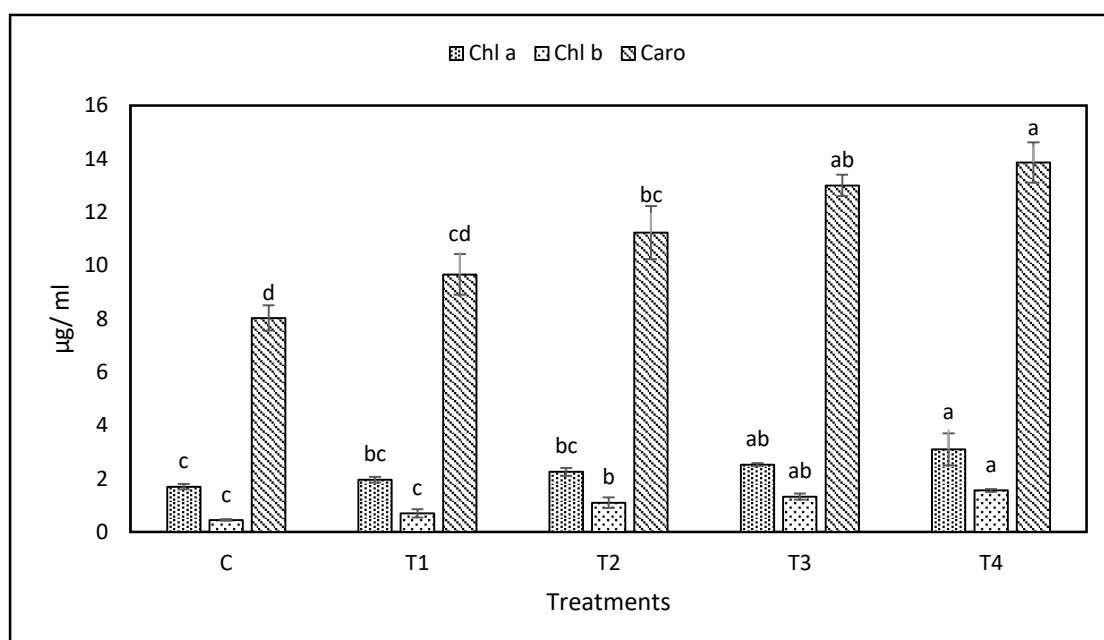


**Fig. 3.49** Effects of MB-ZnO on Chlorophyll a, Chlorophyll b, and Carotenoids contents of *S. sesban* in Cd-Cu stressed soil. C (Control), T1 (0 mg/L), T2 (100 mg/L), T3 (150 mg/L), (200 mg/L).

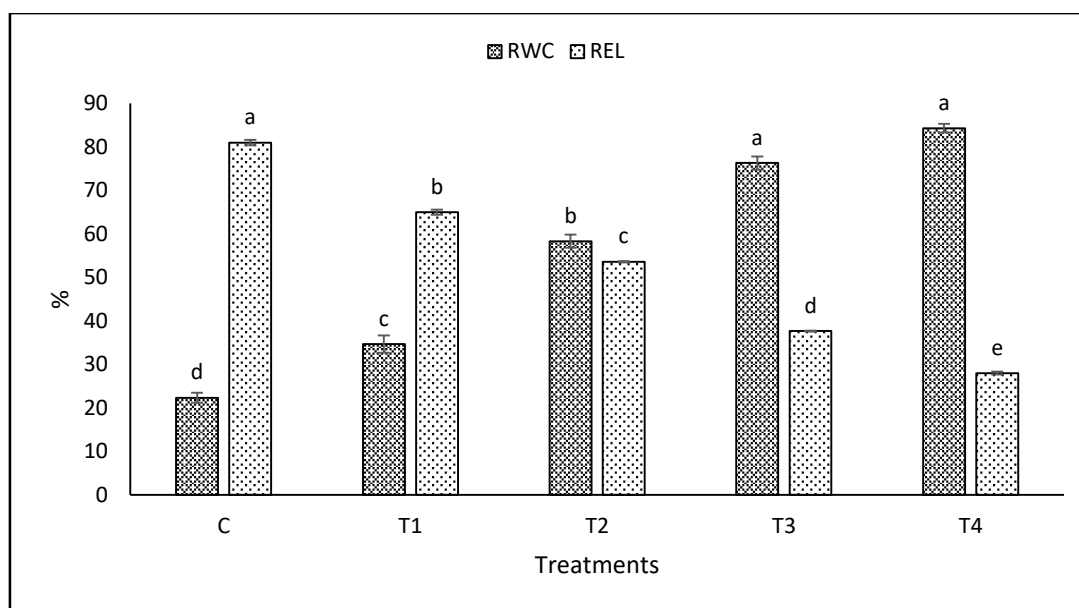


**Fig. 3.50** Effects of MB-ZnO on RWC, and REL of *S. sesban* in Cd-Cu stressed soil. C (Control), T1 (0 mg/L), T2 (50 mg/L), T3 (75 mg/L), T4 (100 mg/L).

### 3.5.3.2 Relative Water Contents (RWC) and Relative Electrolyte Leakage (REL)

RWC of *Sesbania* plants declined significantly in un-inoculated plants. Application of engineered biochar significantly maintained RWC under Cd-Cu stressed condition (Fig 3.43). Plants without inoculation showed lowered RWC. The membrane electrolyte leakage in *S. sesban* plant growing in Cd-Cu stressed soil increased significantly (Fig. 3.50). Inoculation of MBT and MB-ZnO to *Sesbania* plant protected them from damage, significantly.

### 3.5.3.3 Malondialdehyde (MDA) and Hydrogen peroxide (H<sub>2</sub>O<sub>2</sub>)

Under the influence of metals stress, plants produce excessive levels of MDA, due to lipid peroxidation. Application of engineered biochar helped plants to stabilize under stress conditions and in these plants, low MDA contents were produced than control plants (Fig. 3.51). Similarly, application of engineered biochar also decreased the concentration of H<sub>2</sub>O<sub>2</sub> in treated plants, in comparison to control plants (Fig. 3.51). NPs has been well accepted to decrease the levels of lipid peroxidation, hydrogen peroxide, superoxide anions, and enhance the mechanism of defense (Gupta et al., 2017).

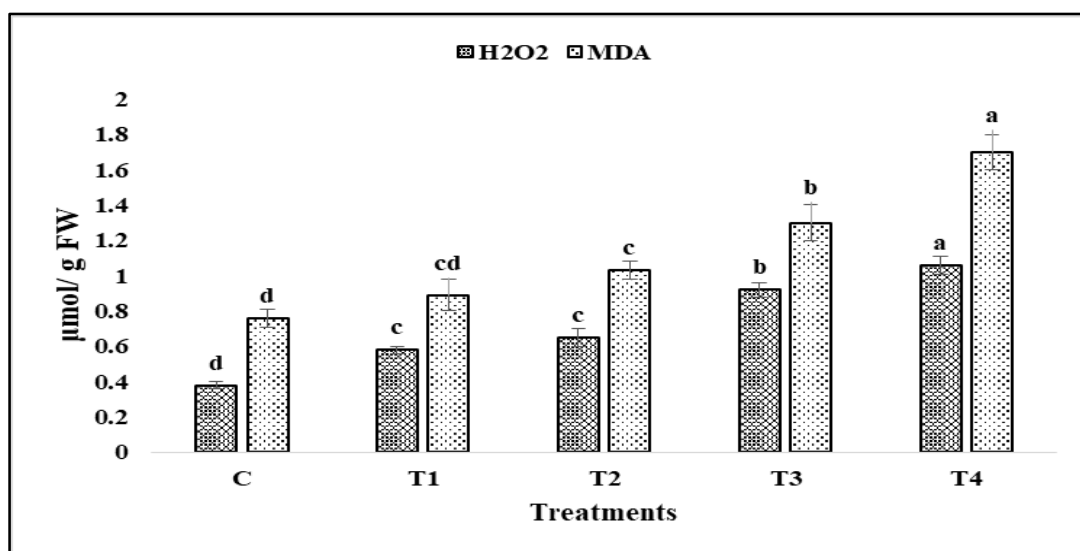


**Fig. 3.51** Effects of MB-ZnO on MDA, and H<sub>2</sub>O<sub>2</sub> of *S. sesban* in Cd-Cu stressed soil.

C (Control), T1 (0 mg/L), T2 (50 mg/L), T3 (75 mg/L), (100 mg/L).

#### 3.5.3.4 Total soluble sugar, leaf protein contents and Proline Content

Application of engineered biochar maintained higher sugar, protein, and proline contents in treated plants, when compared with uninoculated plants (Fig. 3.52). These results show the positive impact of our treatments. Previous studies have also highlighted the importance of higher levels of sugar, protein and proline contents, in plant defense (Singh and Jha, 2017).

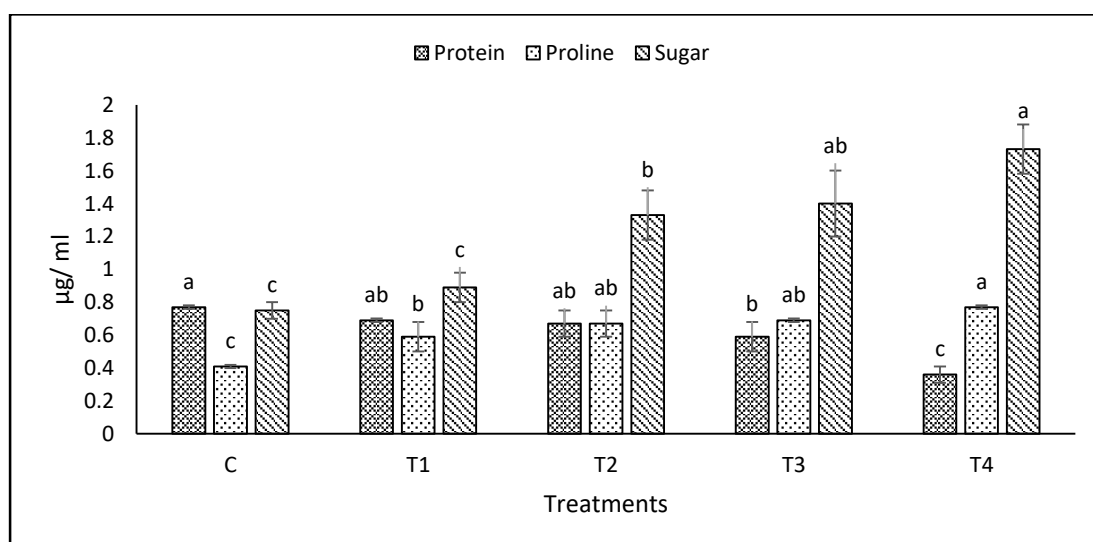


**Fig. 3.52** Effects of MB-ZnO on Sugar, Proline and H<sub>2</sub>O<sub>2</sub> of *S. sesban* in Cd-Cu stressed soil. C (Control), T1 (0 mg/L), T2 (50 mg/L), T3 (75 mg/L), (100 mg/L).

### 3.5.3.5 Cadmium and Copper Level in *Sesbania*

The tested MBT soil amendment and MB-ZnO nanocomposite were very effective in declining the Cd and Cu concentrations in *Sesbania* roots and aerial parts (Fig. 3.53; Fig. 3.54). Variable fraction of both Cd and Cu were detected in below ground and aboveground parts of *Sesbania* plant. The Cd and Cu levels were the highest in the control plants, while these were decreased significantly by the application of NPs (100 mg/L) with biochar.

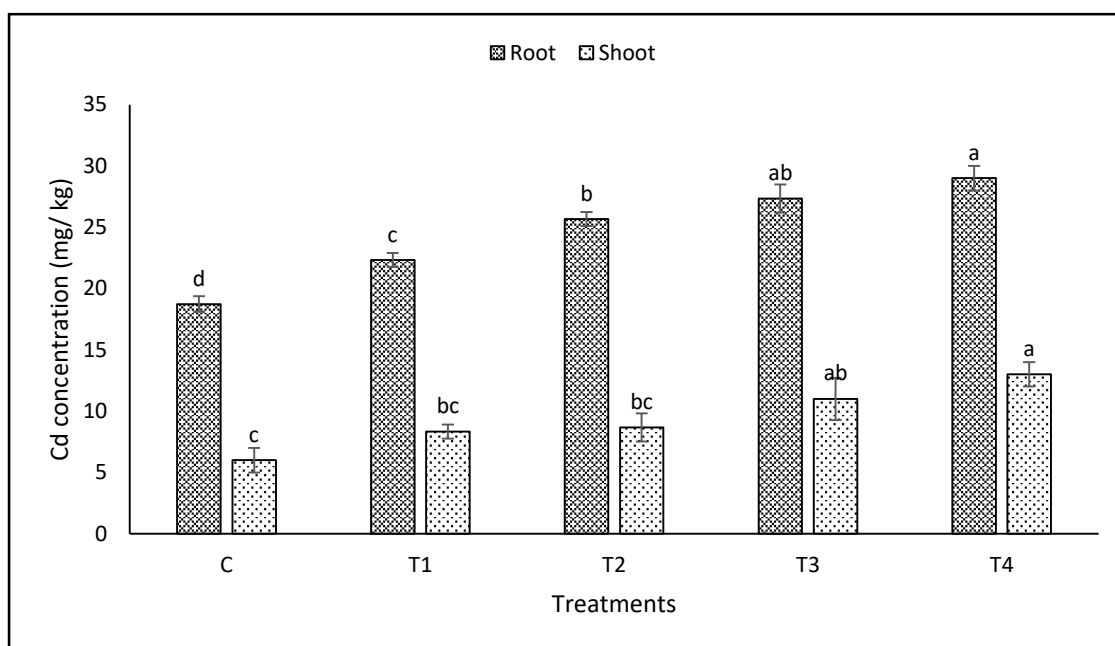


**Fig. 3.53** Effects of MB-ZnO on Cd concentration in Roots and Shoots of *S. sesban* in Cd-Cu stressed soil. C (Control), T1 (0 mg/L), T2 (50 mg/L), T3 (75 mg/L), (100 mg/L).

### 3.5.4 Antioxidant Enzyme Assays

Significant enhancement of antioxidant enzyme activity (SOD, POD and CAT) was examined in plants under Cd-Cu stress with MBT and MB-ZnO inoculation, as compared to un-inoculated plants, at same levels of stresses. The application of MB-ZnO significantly enhanced SOD (33.33%), and POD (37.5%) activity at 100 mg /L concentration in treated plants, I comparison to control plants (Fig. 3.55). A moderate increase in CAT activity (22.5%) was also observed at 100 mg /L stress level (Fig. 3.55).



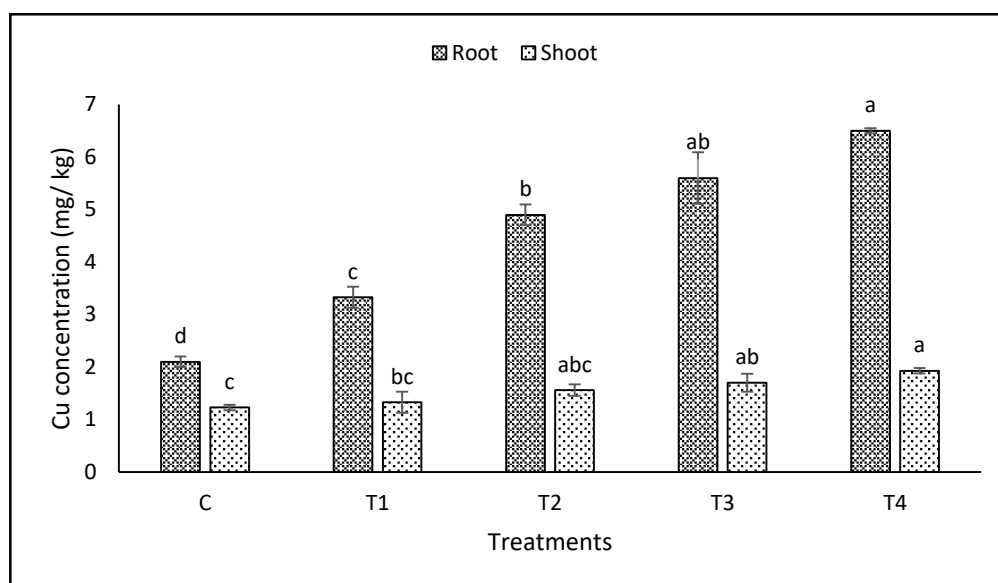


**Fig. 3.54** Effects of MB-ZnO on Cu concentration in Roots and Shoots of *S. sesban* in Cd-Cu stressed soil. C (Control), T1 (0 mg/L), T2 (50 mg/L), T3 (75 mg/L), (100 mg/L).

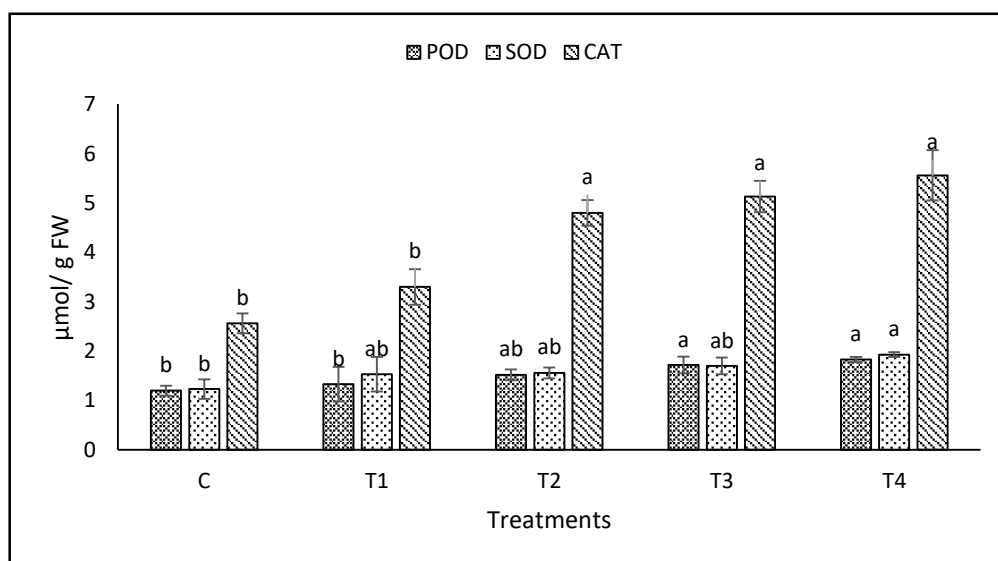


**Fig. 3.55** Effects of MB-ZnO on POD, SOD and CAT of *S. sesban* in Cd-Cu stressed soil. C (Control), T1 (0 mg/L), T2 (50 mg/L), T3 (75 mg/L), (100 mg/L).

#### 3.5.4. Anatomical Assay

The leaf epidermal anatomy of *S. sesban* was studied. The epidermal cells with regular symmetry were observed with curved anticlinal wall pattern. The shape of epidermal cells was similar on both surfaces. Anomocytic type of stomata was observed, with significant variation in their number after foliar application of MB-ZnO NPs (Fig. 3.56). However, the increase in stomata number was dose dependent and the highest number was examined at concentration of 100 mg/ L dose of NPs.

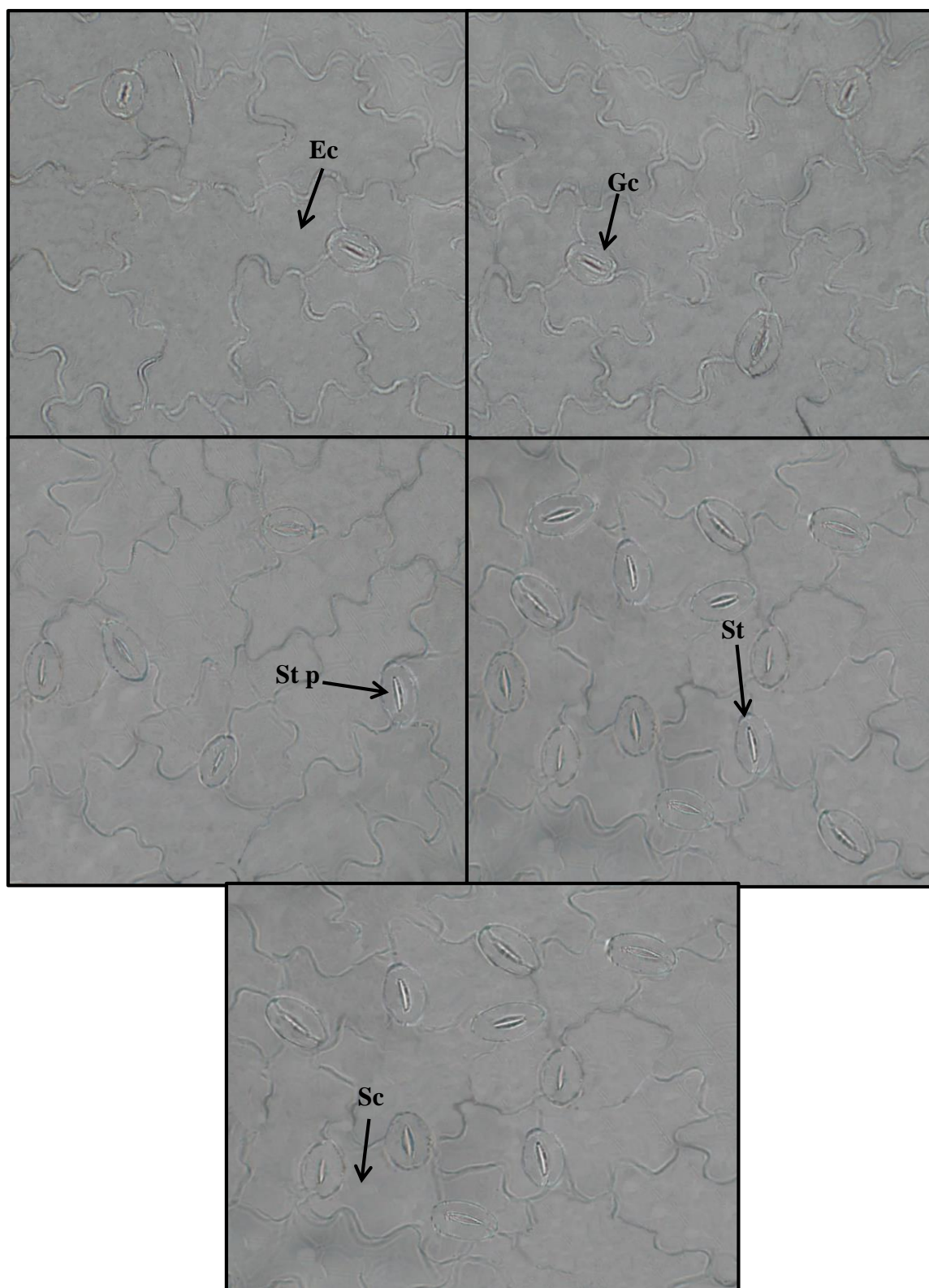


**Fig. 3.56** Effects of MB-ZnO on leaf anatomy of *S. sesban* in Cd-Cu stressed soil; C (Control), T1 (0 mg/L), T2 (50 mg/L), T3 (75 mg/L), (100 mg/L).

# CHAPTER 4

# DISCUSSION

#### 4. DISCUSSION

This study described the successful ball-mill synthesis of MB-ZnO nanocomposite and its application under a variety of stress conditions. The findings of this study confirmed the existence of ZnO in the porous structure of biochar. The detection of ZnO and the porosity of biochar are the defining characteristics of any zinc nanocomposite (Yu et al., 2021). Different elements (including C and O) were observed in the EDX spectrum of the MB-ZnO nanocomposite, which is revealed as the main components in MB-ZnO, mainly carbon, as it rises with rising pyrolysis temperature (Aup-Ngoen and Noipitak, 2020; Selvarajoo and Oochit, 2020). In addition, other elements were examined including K, P, Si, Cl, and Zn with various concentrations. All these elements are regarded as the principal plant constituents (Basu, 2018; Selvarajoo and Oochit, 2020).

The XRD spectra of MB-ZnO nanocomposite were similar to earlier reported studies of biochar/ZnO nanocomposite (Lourenço et al., 2021). The average size of a particle of MB-ZnO nanocomposite (47 nm) established its nano-size (Gholami et al., 2019). These findings are similar to previous studies of biochar-ZnO (Yu et al., 2021). In the FTIR study, nine different peaks were examined stretching from 500-4000  $\text{cm}^{-1}$ . These different peaks confirmed the presence of multiple functional groups in the MB-ZnO nanocomposite. Most of the functional groups observed in the MB-ZnO spectrum perform a significant part in the reduction and capping of nanocomposite (Sajjad et al., 2018). Previously, the phytochemical of *P. salicifolia*, such as alkaloids, flavonoids, terpenoids, and glycosides, present in biochar has been documented to be participated in the stabilization and reduction of ZnO nanoparticles, present on the skeleton of biochar (Calis et al., 1999). Therefore, the FTIR results of this study established the formation of MB-ZnO nanocomposite successfully.

Findings of this study confirmed the decent thermal properties of both pure biochar and MB-ZnO. The attained result is aligned with previously documented research related to the thermal constancy of biochar by amending it with carbon nanotubes (Calis et al., 1999). Thus, the over-all weight loss of MB-ZnO nanocomposite was lower in comparison to the pure biochar that could be related to the zinc oxide ability of resisting thermal

decaying. The UV-Vis peak of MB-ZnO was examined at 400 nm and these results are very close to previously published findings (Saedi et al., 2021). The synthesized MB-ZnO exhibited a band gap of almost 1.71 eV which looks superior to that of previous studies (Duo et al., 2018). The researchers have reported a band gap energy of Ag-ZnO nanocomposite (3.22 eV) and our results are superior to that which might be because of the preparation of biochar at high temperatures. The deposition of ZnO NPs on the biochar surface reduces the bandgap energy of the biochar and assists the establishment of new energy states in MB-ZnO produced via Zn-C bonds, formed due to the association of ZnO NPs with carbon contents present in the biochar (Cheraghcheshm and Javanbakht, 2021).

Normally, photocatalytic ability of the ZnO-biochar nanocomposite can be enhanced by means of numerous factors: surface morphology, particle size, crystallographic structure of particles, and adsorption potential (Didehban et al., 2018; Ma et al., 2021). The photocatalytic potential of pure ZnO is narrow (Ma et al., 2021; Zhong et al., 2012;). A greater surface area causes a durable oxidation-reduction reaction; it emanates more electrons and holes, enhance the band gap; decline particle size, which strongly contribute in the photocatalytic activity; and increase the rate of degradation (Gnanasekaran et al., 2017). Purposefully, ZnO has been combined with alkaline earth metals (Etacheri et al., 2012; Vickers, 2017), transition metals (Sriram et al., 2017), noble metals (Ren et al., 2010; Vickers, 2017), non-metals (Zhang et al., 2015b), rare earth metals (Raza et al., 2016; Zhang et al., 2015b), co-doping (Sirakov, 2009) and semiconductor coupling (Ma et al., 2008) to enhance photocatalytic process (Li et al., 2014). Combination of these metals is favorable for the improvement of photocatalytic activity (Ma et al., 2008).

Sanakousar et al. (2022) documented the preparation of ZnO-Fe-nanocomposite ZnO by hydrothermal process and evaluated its photocatalytic potential against rhodamine B degradation in an aqueous condition under UV and visible light at 410 nm. The Fe-doped ZnO composite showed better photodegradation (84%) of Rh B, in visible light for 180 min. Min et al. (2011) prepared Cu-ZnO nanocomposite via a sol-gel technique and evaluated their photocatalytic activity (Fu et al., 2011). Several other scientists applied various methods including co-precipitation, simple chemical method and facile wet

chemical method, respectively to prepare ZnO–Cu– nanoparticles and analyzed their photocatalytic competency driven by UV–visible-light (Goswami and Suresh, 2020; Kuriakose et al., 2015). According to Guy et al. (2016), Pd-ZnO NPs were successfully prepared by means of photoreduction, borohydride reduction, and microwave irradiation technique and documented the highest photocatalytic efficacy up to 80%. Ahmed et al. (2019) applied the sol-gel technique for the synthesis of Au-doped ZnO, which showed 82.1% degradation ability after 180 min in UV irradiation.

In comparison to overall results of various researchers, our synthesized MB-ZnO showed excellent degradation ability. The supreme decay of Saf (84%) was perceived after 60 min under visible light. In case of MC, 57% photocatalytic degradation was observed under visible light source which is better in comparison of UV light and dark environment in the equal duration (50 mins). Majority of scientists have used chemical methods for the nanocomposite formation which have their own limitations such as lethal nature, harmful to environment, time consuming and costly nature. Our prepared nanocomposite showed degradation ability against all types of pollutants including organic and inorganic in a very short time in all conditions, without releasing any harmful agents to surroundings and without expenditure of any high amount of energy. For indulgent, the mechanisms of pollutant degradation (Saf and MC) Kinetics were applied. The photo-catalytic degradation tracks the Langmuir–Hinshelwood (L-H) pseudo-first-order kinetic model. It can be noticed that the apparent rate constant enhanced ominously for MB-ZnO nanocomposite. i.e.,  $0.93 \text{ min}^{-1}$ ,  $0.94 \text{ min}^{-1}$ , and  $0.95 \text{ min}^{-1}$  in dark, UV and Visible light respectively against Saf. For MC, degradation rate constant was maximum ( $0.882 \text{ min}^{-1}$ ) under visible light, followed by UV ( $0.884 \text{ min}^{-1}$ ), and dark conditions ( $0.920 \text{ min}^{-1}$ ). This also proved that MB-ZnO performed in all conditions, without effecting rate of reaction.

In the present work, along with photocatalysis, the prepared nanocomposite was tested for various biological activities at different concentration. The MB-ZnO performed differently in different experiment. Antioxidant assays were measured at various doses ranges from 1.95 to 200  $\mu\text{g/ml}$ . MB-ZnO nanocomposite has never been explored for antioxidant assays, formerly. From the antioxidant results of this findings, it is determined that MB-ZnO nanocomposite displays good antioxidant potential which make them useful

in provoking oxidative stress, which are aligned to previous results (Shanmugam et al., 2021). The highest growth inhibition of MB-ZnO nanocomposite was determined at 1000  $\mu\text{g}/\text{mL}$  concentration (76%). Previous studies also proved ZnO loaded biochar, works as an excellent anti-inflammatory medicine (Shanmugam et al., 2021).

In the current work, PK inhibition can be acknowledged as a possible cancer therapeutic site. The better protein kinase inhibition (19 mm) was verified at 1000  $\mu\text{g}/\text{ml}$  concentration. Previous study has found the bald zone of 12 mm by at 4 mg/mL by using ZnO nanoparticles (Mohamed et al., 2020). These results may be due to the additive role of MB and ZnO. Our findings are aligned with the available literature on ZnO-NP kinase inhibition enzymes potential (Faisal et al., 2021). These results confirmed that MB-ZnO can be used as chemical inhibitors. Due to admirable Protein Kinase inhibition, MB-ZnO nanocomposite may play some definite role in cancer treatment.

Alpha-amylase show a valuable part in the breakdown of polysaccharides (starch) into monosaccharides (glucose) (Oyedemi et al., 2017). This inhibiting potential of this enzyme can decrease level of glucose, hence create new research area to treat diabetes by nano-size ingredients (Dobrovolskaia et al., 2008). In diabetic persons, regulatory blood glucose concentration after meal is one of the most key feature for control of disease (Apostolidis et al., 2008). Alpha amylase is one of the vital enzymes in the digestive carbohydrate metabolism and its inhibitors decrease the AA enzyme activity of, thus decreasing the glucose amount created in the small intestine and ultimately decrease glucose level in blood. Numerous compounds have been explored that are actively participated in the inhibition of  $\alpha$ -amylase enzyme (Moorthy et al., 2012). Comparing the level of  $\alpha$ -amylase inhibition in the different studies, there are huge variations in the enzyme inhibition, in term of percentage. In the present study, the prepared MB-ZnO revealed huge alpha-amylase inhibition (45%) at the maximum concentration (1,000  $\mu\text{g}/\text{ml}$ ). In the former research work by Dhobale et al. (2008), the inhibitory effect of ZnO NPs was enhanced by thioglycerol. Shaik and Kumar (2016) established that 30  $\mu\text{g}/\text{mL}$  ZnO nanoparticles caused highest  $\alpha$ -amylase inhibition of 58% along with thioglycerol, while 30  $\mu\text{g}/\text{mL}$  of acarbose coated ZnO nanoparticles caused 75% inhibition (Shaik and Kumar, 2016). These findings confirmed that ZnO NPs, have their own  $\alpha$ -amylase enzyme



inhibition. The mechanism of inhibition is not clear, though it can be predicted that the NPs attach to reactive carboxyl or amine groups adjacent to the enzymes active site (Dhobale et al., 2008). By comparing the results to those of previously published research, some variations are observed. These difference are may be due to the type of solvent used for extraction , as it might also change the level of  $\alpha$ -amylase inhibition.

The biocompatibility of NPs is a prerequisite for any clinical trial. When a new nanomaterial arises, its cytotoxic effect, i.e., the potential alteration of physiological characteristics is generally evaluated at priority. Though, a lack of cytotoxicity does not convene these materials an implicit biocompatibility. This must be assessed as a separate criterion. The biocompatibility idea depends upon the suitable interaction between the nanomaterial and its biological system; i.e., the lack of toxic or immune response from the treated biological system (cell, tissue, organ or organism) (Song et al., 2019). The possible cytotoxicity of MB-ZnO nanocomposite was measured against the red blood cells. Highest erythroblastosis (28%) was perceived at the highest dose (200  $\mu\text{g/ml}$ ). It has been observed that different factors such as size, morphology , and particles charge perform active roles in the blood compatibility (Iqbal et al., 2018). For further assessment of the biocompatible behavior of MB-ZnO nanocomposite, an MTT assay was performed against macrophages of human blood. This study confirmed that MB-ZnO nanocomposite is non-toxic at a small application rate (2  $\mu\text{g/ml}$ ), whereas it is a slight toxic at 5–100  $\mu\text{g/ml}$  concentration.

Antileishmanial efficiency was increased with increase in dose concentration. A dose-based effect of different concentrations of MB-ZnO nanocomposite was perceived. Higher concentration (100  $\mu\text{g ml}^{-1}$ ) of MB-ZnO nanocomposite revealed maximum percentage inhibition of parasites, as compared to lower doses. A concentration -dependent enhancement in potential have also been documented previously in several studies (Jan et al., 2020). There is a little difference in the Antileishmanial efficiency of various nanoparticles. This may be due to variations in their morphology, size, dimensions, stabilizing and capping agents. In alignment with our findings, different research have confirmed that the smaller size nanoparticles, have the better antileishmanial potential by creating more ROS (Allahverdiyev et al., 2011). Various types of nanoparticles are documented to produce high amount of ROS, which enhance the apoptosis process (Ahmad

et al., 2020; Khan et al., 2019). It has been proven that the Leishmania parasites are very subtle to ROS and any agent that could produce ROS would be a capable antileishmanial contestant (Abbasi et al., 2017). ZnO NPs act as large reservoir of ROS ( $\text{OH}^-$ ,  $\text{H}_2\text{O}_2$ ,  $\text{O}^{2-}$  etc) and free  $\text{Zn}^{2+}$  ions, and NB provide large surface area for them which could result to intracellular destruction of Leishmania parasites.

In the present study, the antifungal potential was assessed against a novel fungus isolated from Kiwi plant. For the identification of the fungus previously reported ITS sequences from *R. oryzae* strains were involved for reference (Hiol et al., 2000). In the phylogenetic tree, the current isolate was placed within a clade comprising *R. oryzae* references isolates. Leaf spot caused by *R. oryzae* has not been documented in Pakistan. BLAST study of the resultant ITS1-ITS4 sequence revealed >99% similarity with *R. oryzae* strain RAA internal transcribed spacer 1, partial sequence; 5.8S ribosomal RNA gene and internal transcribed spacer 2, complete sequence; and large subunit ribosomal RNA gene, partial sequence (MT603964.1), while EF-1 $\alpha$  sequence showed 100% resemblance with *R. oryzae* translation elongation factor-1 $\alpha$  gene (MK510718.1). Based on the mycological appearance, molecular analysis, and pathogenicity testing, the fungus was recognized as *R. oryzae* Went & Prisen Geerligs (Kwon et al., 2012). This is the first study of *R. oryzae* on kiwi leaf in Pakistan. The morphological appearance growth pattern, and color were similar to previously documented features of *R. oryzae* (Zhang et al., 2013).

During the past few years, researchers have successfully applied ZnO NPs to control the growth of several pathogenic fungi like *Fusarium graminearum*, *Candida albicans*, and *Aspergillus niger* (Nguyen et al., 2019; Omar et al., 2016; Thaya et al., 2016). For the antifungal activity, a novel fungus isolated from kiwi leaves was used. The obtained results of the antifungal assay clearly reveal that the growth of *R. oryzae* was inhibited at low concentrations (6 mg/ml) of the prepared nanocomposite. The highest antifungal inhibition via the MB-ZnO nanocomposite was observed at 19 mg/ml. All these findings are parallel to the previous results (Zafar et al., 2020). Such findings are in an similar with the earlier published article considering the influence of the stabilization of nanoparticles on their antimicrobial potential (Cho et al., 2005). The interaction with

proteins existing in the cell wall of the fungus, prevents the functions of different enzymes such as cholesterol acyltransferase activity and ATPase (Panáček et al., 2009).

The present study also explained the principal *in-vitro* method for the HMs immobilization in polluted soil. For the stabilization of HMs in the polluted soil, different microorganisms were inoculated into the contaminated soil as microbial agents by attaching to the biochar surface due to excellent growth-enhancing microorganisms carrier. In the present study, MB and metal tolerant fungus (*Trichoderma harzianum*) loaded biochar (MBT) have been used at various rates in the Cd-Cu dual polluted soil to elaborate their effects on the physiochemical properties. *Trichoderma* has been validated to boost up the growth of the plants (Dimitriou and Aronsson, 2005). The growth enhancing characteristics of the *Trichoderma* along with its own physiological features make it worthy choice for metal remediation (Ezzi and Lynch, 2002; Harman et al., 2004b). In current research, *T. harzianum* adherence to the surface of biochar was examined by scanning electron microscope. In accordance with previous studies, our findings have described the successful colonization of fungi on biochar surface (Jaafar et al., 2014).

Application of both MB and MBT raised the pH of treated soil at the initial phases of incubation. Similar variations in soil pH during different incubation periods have been reported earlier (Wu et al., 2017; Yuan et al., 2011). In the current work, we find out that both bioavailable Cd and Cu contents of the MB5 amendment were considerably lesser than MB1 amendment. Additionally, in comparison to MB treatment, MBT could efficiently diminish the bioavailable Cu and Cd in the polluted soil; hence increasing the immobility of Cu and Cd, particularly with 5% application rate. Both MB and MBT could encourage the changes of Cu and Cd from bioavailable portions to less bioavailable forms. Nie et al. (2018) established that the bioavailable portions of Cu and Cd in contaminated soil decline with increasing biochar amendment, whereas their recalcitrant proportion raises. Similar kind of findings has been reported earlier (Tu et al., 2020).

DTPA-Cu and DTPA-Cd in the amended soil gradually decreased with an increase in incubation duration. Previous researchers found similar trends by using bamboo biochar at a 5% dosage rate for DTPA-Cu and DTPA-Cd in polluted soil (Lu et al., 2017). Alike DTPA-Phyto-availability, Cu and Cd bioavailability of the amended soil was reduced to

different percentages with the application of two treatments of biochar at various doses. These findings suggest the potential of MBT to minimize the danger of Cd and Cu to human health.

Similar to previous studies, catalase and urease activities significantly elevated with increased dose of biochar, in this study (Leszczuk et al., 2019). Joško et al. (2019) described that biochar may have an impact on enzymatic activities by enhancing water retaining capacity and promoting the porosity and texture of the soil. This study also highlighted that the rise in CEC of soil had a constructive effect on the enzymatic activities of soil. The increase in enzymatic activity has been credited to surge in soil organic materials and a reduction in the loss of nutrients, as well as the heavy metals stabilization, owing to the use of biochar (Xu et al., 2017).

This study was also focused on the role of MBT and MB-ZnO nanocomposite individually and combined in the Cd- Cu induced stress in *Sesbania* plant. Although nanoparticles and biochar could be applied in reducing metal toxicity in plants, the joint application of these treatments on accumulation of metal by plants is not well recognized. The findings of the experiment revealed that nanoparticles enhancing chlorophyll concentration, carotenoids, enhance relative water contents, antioxidant enzymes, anatomical characters and metal stress tolerance and reducing electrolyte leakage and Cd, Cu concentrations in plants and bioavailable. The lower biomass in the control treatment may be because of the greater Cd and Cu concentration in these plants. The metals stress (Cd and Cu) has been proved to reduce growth of plants when its grown in metals stressed soil in different experimental set up as documented in the earlier studies (Ali et al., 2015; Rizwan et al., 2016a). The metals interceded minimization in plant growth may be related with the disruption of numerous processes in plants including chlorophyll synthesis, water deficit, and internal changes in plant body (Ali et al., 2013). The enhanced root and shoot length, height of plant, biomass with nanoparticles evidently show that MB-ZnO are taking part in improving *Sesbania* growth by eliciting metals tolerance in *Sesbania* plant. These findings are parallel to the documented reports signifying that NPs stimulated the plants growth in metal induce stress (Hussain et al., 2018; Liu et al., 2015b; Rizwan et al., 2019b). Previous findings also showed that zinc oxide nanoparticles NPs enhanced the root and

shoot length, plant height and biomass of plant in Cd and Cu stress (Venkatachalam et al., 2017).

The enhanced *Sesbania* biomass with the applications of MB-ZnO nanocomposite might be because of the falling of stress level in plants body, as documented in *Leucaena leucocephala* seedlings with the application of ZnO nanoparticles in metals stress (Venkatachalam et al., 2017). The biochar has been reported to enhance the plants growth in metal stresses including Cd and other metals (Abbas et al., 2018; Rizwan et al., 2016b). The biochar can enhance the plant growth by providing essential nutrients to the plant (i.e., Zn and Mn) together with declining toxic metals in body of plant (Abbas et al., 2017). Some researchers reported that biochar enhanced plant growth by enhancing nutrient competition with metals at the roots surface, and metals immobilization in the contaminated soil (Abbas et al., 2017). The greater biomass in the combined application might be because of the dual effects of treatments on the plants such as rise in amount of Zn in plants with MB-ZnO nanocomposite and the reduced bioavailable portion of Cd and Cu in the soil with the *Trichoderma* loaded biochar amply in the soil which declined Cd and Cu in different parts of *Sesbania* plants.

Previously study reported that biochemical compounds in leaves are used very sensitive indicators of HMs induced stress (Rizwan et al., 2017). The current findings revealed that MB-ZnO nanocomposite enhanced the chlorophyll a, chlorophyll b, carotenoids concentrations, sugar, protein contents and relative water contents and control the production of MDA, proline and electrolytes leakage attributes in leaves of *Sesbania*. ZnO nanoparticles increased the chlorophyll contents in a plants grown in a metal-stressed soil (Rizwan et al., 2019a; Venkatachalam et al., 2017). Application of SiO<sub>2</sub> nanoparticles increased the Chloro a, Chloro b, and carotenoids under Cr-stressed pea plant (Tripathi et al., 2015). The improved photosynthetic pigments in leaves of rice by the ZnO nanoparticles treatments may be the result of the condensed oxidative stress in rice plants with treatments as earlier documented by scientists (Hussain et al., 2018; Venkatachalam et al., 2017) antioxidant enzymes, and metal stress tolerance. The soluble sugar and leaf protein contents were increased in treated plants even more than the control plants. MB-ZnO enhance exopolysaccharides, which help in increasing soluble sugar and protein

contents of leaves (Khan et al., 2018). The decrease in relative water content is at par with previous studies (Menhas et al., 2021). The antioxidant enzymes like SOD, POD, and CAT were boosted in treated *Sesbania* plants. Similar pattern of enzymes activity previously have been reported to control oxidative stresses (Bortoloti and Baron, 2022).

The decreased values of proline, MDA and H<sub>2</sub>O<sub>2</sub> content in the inoculated *sesbania* plants, was the indication of stress tolerance potential of plant in response to various environmental factors (Akhtar et al., 2017). Proline is a ROS scavenger, osmo-protectant and metal chelator (Hayat et al., 2020). It was predicted that the heavy metal ions induce raise in lipid peroxidation, because of the removal of hydrogen from the fatty acids through ROS which then result in lipid radical production. This mechanism then generates reaction cascade – producing short chain alkanes and aldehydes that deform the lipid structure (Khanna et al., 2019). ROS are important component of cellular free radicals that cause oxidative stress. These ROS cause disruption of cellular proteins, nucleic acids, pigments and lipids that leads to membrane damage, lipid peroxidation and enzyme inactivation, which then affects cell's viability (Jan et al., 2022). MDA is the final product after lipid peroxidation in plants that accumulates under stressed conditions.

Under stress, H<sub>2</sub>O<sub>2</sub> is also harmful for plants. The antioxidant enzymes particularly SOD and POD convert H<sub>2</sub>O<sub>2</sub> into harmless water and oxygen and CAT prevents the accumulation of H<sub>2</sub>O<sub>2</sub> in cells (Bali et al., 2019). The upsurge in the electrolyte leakage content in un-inoculated plants might be because of bio-membrane damage under heavy metal stress. The application of MBT and MB-ZnO helps to decrease membrane damage. Electrolyte leakage decrease was also documented previously while working on plant in metals stress (Ahmad et al., 2018). MB-ZnO NPs exhibit positive effects on leaf. Dimkpa et al. (2020) showed the useful effect of ZNO NPs on leaf anatomy. Adrees et al. (2021) confirmed the positive effect of foliar application of ZNO NPs. In our results it was observed that number of stomata was increase in combined application of MBT and MB-ZnO. The former studies also reported the increase in stomatal index and density and increase in a number of leaf xylem vessels while working on ZnO NPs (Magdaleno-Garcia et al., 2022).

The amount of Cd and Cu in tissues of *Sesbania* plants were lesser in treated *Sesbania* plants in comparison to untreated plants. Previous researchers reported that biochar-ZnO nanocomposite decrease the Cd and Cu level in wheat plant (Hussain et al., 2018) and foliar application of ZnSO<sub>4</sub> reduced the Cd amount in rice plant (Wang et al., 2018). These reduced Cd and Cu concentrations in *Sesbania* plant can be credited, to MB-ZnO due to the antagonistic effects with Cd and Cu (Javed et al., 2016b; Wang et al., 2018). The Cd and Cu concentrations has negative correlation with Zn concentration in plants tissues. The negative correlation of Cd and Cu with Zn has been described previously (Wang et al., 2018). It can be proposed that the enhanced Zn concentration after the foliar application of MB-ZnO nanocomposite might inhibit the function of Zn transporters molecules present in the roots, resulting in reduced Cd accumulation in roots. The mutual effect of foliar sprayed MB-ZnO nanocomposite and *Trichoderma* loaded biochar has better potential in reducing Cd and Cu concentration in *Sesbania* in comparison to MB-ZnO applied alone. This huge reduction in Cd and Cu concentration in *Sesbania* plants might due to the dual effects of treatments on Cd and Cu accretion by changing different factors increase in soil pH, reduce Cd and Cu bioavailable fraction in the soil via biochar application, and enhanced Zn nutrition through the NPs treatments. Li et al. (2018) proved that the application of biochar to the soil amendments was a likely factor in immobilizing the accessible Cd fraction for the wheat plant in the soil. Hence, the combined practice of biochar along the foliar spray of MB-ZnO nanocomposite can be applied for declining Cd and Cu concentrations in crops and eventually in food chain.

Many studies have revealed that exogenous application of Zn prevents the metals accretion by plants. Foliar use of Zn is assimilated via plants which can reduce Cd and Cu amassing by plants. Earlier studies also confirmed that Zn level enhance in crops with the foliar application of Zn (Javed et al., 2016b; Rizwan et al., 2017). High level of Zn can compete at root surface with Cd and Cu as both the metals are being carried by same transporters present in roots surface (Pandey, 2012). It might be possible that high concentration of Zn in the roots can block the Zn transporters. The foliar spray of MB-ZnO nanocomposite reduced the bioavailable Cd in the soil (Hussain et al., 2018). Similarly The ability of biochar to adsorb heavy metals is also linked to a number of factors,

including ion exchange between the protons on the surface of the biochar and the metallic cations and electrostatic interactions between the metal cations and carbon's negative charge (Machida et al., 2006). The increased biomass of the *Sesbania*, which accumulated the higher Cd concentrations in the plant biomass, may be the cause of the lower Cd and Cu levels in the soil with foliar spray of nanocomposite.

ZnO NPs exhibit positive effects on flowering, increased root and stem growth and chlorophyll content in leaf (Srivastav et al., 2021). It is concluded from our results that MB-ZnO has positive effect on the anatomy (stomata number). Magdaleno-Garcia et al. (2022) also reported the increase in stomatal index and density and increase in number of leaf xylem vessels due to ZnO NPs. The study of Bernal-Azlate et al. (2016) highlighted the significance of Zinc nano-fertilizer application that promotes the growth of plant as it increases the photosynthesis because it is known co-factor for enzymes that are involved in photosynthesis, and it maintains the integrity of plant cell membrane. ZnO and ZnS NPs has proved a novel promising fertilizer nutrient for plants. ZnO NPs foliar application improves the stomatal conductance and maintains the leaf water potential level (Kolencik et al., 2022).

It remains provocative about the nano-fertilizer in field of agriculture because of the dissimilarities in the properties of nanoparticles with size, shape, synthesis methods, and application timing. In the upcoming, the application of nanoparticles in agriculture might only be conceivable if the nanoparticles are synthesized in a price effective method. Generally, biofortification of nanoparticles in plants may be one of the strategies for declining the Cd, Cu or possibly other metals in polluted soil.

## 5. CONCLUSION AND FUTURE PROSPECTS

### 5.1 CONCLUSION

Ball-milling is a powerful and environmental friendly method for the preparation of MB-ZnO nanocomposite. This nanocomposite can efficiently perform catalytic activity against both Saf and MC both in light and dark. The photocatalytic activity revealed that the MB-ZnO has higher photocatalytic potential under visible light in case of both organic



and inorganic pollutants. MB-ZnO showed greater photocatalytic efficacy against Saf (83.5%) in just one hour and against MC (57%) in 50 min of reaction time. Most notably, the MB-ZnO nanocomposite can perform well in different light sources at constant temperatures and pH. Therefore, we believe that MB-ZnO can be effectively used for degradation. To the best of our study, this is the first study in which MB-ZnO nanocomposite has been investigated in different *in-vitro* biological assays. The inimitable characteristics of MB-ZnO like low toxicity, antifungal activity, and biocompatibility analyses nominate them as appropriate tools for biomedical and agricultural uses.

MB-ZnO can also be used as a useful fungicide. This study confirmed its usage as a fungicide against *R. oryzae*, to control leaf spot of kiwi. This is the first study of *R. oryzae* to report as a causing leaf spot disease of kiwi in Pakistan. Due to its health-friendly nature, the MB-ZnO can be sprayed on fruits and vegetables as an alternate to toxic chemical fungicides.

Findings of this study proved that biochar can effectively be used in soil stress. MBT can efficiently decline the phyto-availability and bio-accessibility of both Cu and Cd, particularly at greater dose levels. MBT also stabilizes the soil pH quickly as compared to MB. Additionally, MBT significantly increases enzymatic activities of soil microorganism in Cd and Cu polluted soils. In comparison to the amendment of individual biochar (MB), the MBT more efficiently immobilized heavy metals to improve soil environment. Findings of this study suggest that the combination of functional microbial pathogens and a biochar treatment could work as an auspicious tool for the reclamation of contaminated soil. Foliar application of MB-ZnO nanocomposite with or without biochar increased the pH of the soil and decrease the bioaccessible Cd and Cu in the soil. The unique properties of NPs make them able to be used in agriculture and plant growth.

Treatments MB-ZnO nanocomposite enhanced the underground and aboveground biomass of *Sesbania* and reduced the Cd and Cu level in the aforementioned parts. The combined application of MB-ZnO and biochar was more effective in shrinking Cd and Cu level in *Sesbania* roots. The decrease in metals bioaccessibility and other changes to the soil made using MB-ZnO and biochar might be useful for the formation of green cover on the top of soil to help in remediation and diminish risks associated with environment of

polluted matter. So, the combined use of MB-ZnO NPs and biochar could be used for metals polluted soils. Though, prior to endorsement of ZnO nanoparticles and biochar application in *Sesbania* plant, more research is needed to authenticate these results in different soil pollution levels, type of soil, crop species, along with various climatic conditions.

## 5.2 FUTURE PROSPECTUS

- There is a need to study the practical application of biochar in different fields. More research is required to study reactors scheme, fabrication methods, the effectiveness of the light source, multi-pollutants elimination efficacy, waste water treatment technology and sludge management.
- Regardless of several developments in application of nanomaterial in agriculture and the safety of nanomaterial, there is a vast gap in the interaction of nanomaterial with plants and the destiny of various nanomaterial in ecosystem. To understand the safety of nanoparticles decisively, an extensive term study in all aspects is needed.
- The application and prescription of material in the field of agriculture is needed to enable farmers and consumers for the utilization of this technology, on a large-scale.

# CHAPTER 5

# **REFERENCES**

## REFERENCES

- Abbas, T., Rizwan, M., Ali, S., Zia-ur-Rehman, M., Qayyum, M.F., Abbas, F., Hannan, F., Rinklebe, J., Ok, Y.S., 2017. Effect of biochar on cadmium bioavailability and uptake in wheat (*Triticum aestivum* L.) grown in a soil with aged contamination. *Ecotoxicology and Environmental Safety* 140, 37-47.
- Abbas, T., Rizwan, M., Ali, S., Adrees, M., Mahmood, A., Zia-ur-Rehman, M., Ibrahim, M., Arshad, M., Qayyum, M.F., 2018. Biochar application increased the growth and yield and reduced cadmium in drought stressed wheat grown in an aged contaminated soil. *Ecotoxicology and Environmental Safety* 148, 825-833.
- Abbasi, B.H., Anjum, S., Hano, C., 2017. Differential effects of in vitro cultures of *Linum usitatissimum* L. (Flax) on biosynthesis, stability, antibacterial and antileishmanial activities of zinc oxide nanoparticles: A mechanistic approach. *RSC Advances* 7(26), 15931-15943.
- Abe, A., Asano, K., Sone, T., 2010. A molecular phylogeny-based taxonomy of the genus *Rhizopus*. *Bioscience, Biotechnology, and Biochemistry* 74(7), 1325-1331.
- Abukhadra, M.R., Mohamed, A.S., 2019. Adsorption removal of safranin dye contaminants from water using various types of natural zeolite. *Silicon* 11(3), 1635-1647.
- Adrees, M., Khan, Z.S., Hafeez, M., Rizwan, M., Hussain, K., Asrar, M., Alyemeni, M.N., Wijaya, L., Ali, S., 2021. Foliar exposure of zinc oxide nanoparticles improved the growth of wheat (*Triticum aestivum* L.) and decreased cadmium concentration in grains under simultaneous Cd and water deficient stress. *Ecotoxicology Environmental Safety* 208(35), 111627.
- Ahmad, M., Rajapaksha, A.U., Lim, J.E., Zhang, M., Bolan, N., Mohan, D., Vithanage, M., Lee, S.S., Ok, Y.S., 2014. Biochar as a sorbent for contaminant management in soil and water: a review. *Chemosphere* 99(09), 19-33.
- Ahmad, A., Syed, F., Imran, M., Khan, A.U., Tahir, K., Khan, Z.U.H., Yuan, Q., 2016. Phytosynthesis and antileishmanial activity of gold nanoparticles by *Maytenus Royleanus*. *Journal of Food Biochemistry* 40(4), 420-427.

- Ahmad, I., Akhtar, M.J., Mehmood, S., Akhter, K., Tahir, M., Saeed, M.F., Hussain, M.B., Hussain, S., 2018. Combined application of compost and *Bacillus* sp. CIK-512 ameliorated the lead toxicity in radish by regulating the homeostasis of antioxidants and lead. *Ecotoxicology and Environmental Safety* 148, 805-812.
- Ahmed, M., Abou-Gamra, Z., Alshakhanbeh, M., Medien, H., 2019. Control synthesis of metallic gold nanoparticles homogeneously distributed on hexagonal ZnO nanoparticles for photocatalytic degradation of methylene blue dye. *Environmental Nanotechnology, Monitoring & Management* 12, 100217.
- Ahmad, A., Ullah, S., Syed, F., Tahir, K., Khan, A.U., Yuan, Q., 2020. Biogenic metal nanoparticles as a potential class of antileishmanial agents: mechanisms and molecular targets. *Nanomedicine* 15(08), 809-828.
- Ahmed, S., Ahmad, M., Swami, B.L., Ikram, S., 2016. A review on plants extract mediated synthesis of silver nanoparticles for antimicrobial applications: a green expertise. *Journal of Advanced Research* 7(1), 17-28.
- Ahmet, T., Vedat, Z., 2009. Estimation of certain chemical constituents of fruits of selected tomato genotypes grown in Turkey. *African Journal of Agricultural Research* 4(10), 1086-1092.
- Ahmaruzzaman, M., 2021. Biochar based nanocomposites for photocatalytic degradation of emerging organic pollutants from water and wastewater. *Materials Research Bulletin* 140(27), 111262.
- Ahn, K.S., Yan, Y., Lee, S.H., Deutsch, T., Turner, J., Tracy, C.E., Perkins, C.L., Al-Jassim, M., 2007. Photoelectrochemical properties of N-incorporated ZnO films deposited by reactive RF magnetron sputtering. *Journal of the Electrochemical Society* 154(9), 956.
- Ajmal, A., Majeed, I., Malik, R.N., Idriss, H., Nadeem, M.A., 2014. Principles and mechanisms of photocatalytic dye degradation on TiO<sub>2</sub> based photocatalysts: a comparative overview. *RSC Advances* 4(70), 37003-37026.
- Akhtar, N., Khan, S., Malook, I., Rehman, S.U., Jamil, M., 2017. Pb-induced changes in roots of two cultivated rice cultivars grown in lead-contaminated soil mediated by smoke. *Environmental Science Pollution Research* 24(5), 21298-21310.

- Akir, S., Hamdi, A., Addad, A., Coffinier, Y., Boukherroub, R., Omrani, A.D., 2017. Facile synthesis of carbon-ZnO nanocomposite with enhanced visible light photocatalytic performance. *Applied Surface Science* 400, 461-470.
- Akinmoladun, A.C., Obuotor, E.M., Farombi, E.O., 2010. Evaluation of antioxidant and free radical scavenging capacities of some Nigerian indigenous medicinal plants. *Journal of Medicinal Food* 13(2), 444-451.
- Albuquerque, J.A., Salazar, P., Barrón, V., Torrent, J., del Campillo, M.d.C., Gallardo, A., Villar, R., 2013. Enhanced wheat yield by biochar addition under different mineral fertilization levels. *Agronomy for Sustainable Development* 33(3), 475-484.
- Ali, B., Tao, Q., Zhou, Y., Gill, R.A., Ali, S., Rafiq, M.T., Xu, L., Zhou, W., 2013. 5-Aminolevulinic acid mitigates the cadmium-induced changes in *Brassica napus* as revealed by the biochemical and ultra-structural evaluation of roots. *Ecotoxicology Environmental Safety* 92, 271-280.
- Ali, B., Gill, R.A., Yang, S., Gill, M.B., Farooq, M.A., Liu, D., Daud, M.K., Ali, S., Zhou, W., 2015. Regulation of cadmium-induced proteomic and metabolic changes by 5-aminolevulinic acid in leaves of *Brassica napus* L. *PLoS One* 10(4), e0123328.
- Ali, A., Ambreen, S., Javed, R., Tabassum, S., Ul Haq, I., Zia, M., 2017. ZnO nanostructure fabrication in different solvents transforms physio-chemical, biological and photodegradable properties. *Materials Science and Engineering* 74, 137-145.
- Ali, S., Rizwan, M., Noureen, S., Anwar, S., Ali, B., Naveed, M., Abd\_Allah, E.F., Alqarawi, A.A., Ahmad, P., 2019. Combined use of biochar and zinc oxide nanoparticle foliar spray improved the plant growth and decreased the cadmium accumulation in rice (*Oryza sativa* L.) plant. *Environmental Science and Pollution Research* 26(11), 11288-11299.
- Ali, M., Iqbal, R., Safdar, M., Murtaza, S., Mustafa, M., Sajjad, M., Bukhari, S.A., Huma, T., 2021. Antioxidant and antibacterial activities of *Artemisia absinthium* and *Citrus paradisi* extracts repress viability of aggressive liver cancer cell line. *Molecular Biology Reports* 48(12), 7703-7710.

- Als bou, E.M.E., Al-Khashman, O.A., 2018. Heavy metal concentrations in roadside soil and street dust from Petra region, Jordan. *Environmental Monitoring and Assessment* 190(1), 1-13.
- Allahverdiyev, A.M., Abamor, E.S., Bagirova, M., Ustundag, C.B., Kaya, C., Kaya, F., Rafailovich, M., 2011. Antileishmanial effect of silver nanoparticles and their enhanced antiparasitic activity under ultraviolet light. *International Journal of Nanomedicine* 6, 2705-2714.
- Amara, H., Nelayah, J., Creuze, J., Chmielewski, A., Alloyeau, D., Ricolleau, C., Legrand, B., 2022. Effect of size on the surface energy of noble metal nanoparticles from analytical and numerical approaches. *Physical Review* 105(16), 165403.
- Amacher, M.C., 1996. Nickel, cadmium, and lead. *Methods of Soil Analysis: Part 3 Chemical Methods* 5, 739-768.
- Ansari, S.A., Khan, M.M., Ansari, M.O., Cho, M.H., 2016. Nitrogen-doped titanium dioxide (N-doped TiO<sub>2</sub>) for visible light photocatalysis. *New Journal of Chemistry* 40(4), 3000-3009.
- Antal, M.J., Wade, S.R., Nunoura, T., 2007. Biocarbon production from Hungarian sunflower shells. *Journal of Analytical and Applied Pyrolysis* 79(1-2), 86-90.
- Antoniadis, V., Shaheen, S.M., Levizou, E., Shahid, M., Niazi, N.K., Vithanage, M., Ok, Y.S., Bolan, N., Rinklebe, J., 2019. A critical prospective analysis of the potential toxicity of trace element regulation limits in soils worldwide: Are they protective concerning health risk assessment?-A review. *Environment International* 127, 819-847.
- Arfin, T., Rangari, S.N., 2018. Graphene oxide–ZnO nanocomposite modified electrode for the detection of phenol. *Analytical Methods* 10(3), 347-358.
- Arif, S., Liaquat, F., Khizar, M., Shah, I.H., Inam, W., Chaudhary, H.J., Farooq, A.B.U., Munis, M.F.H., 2017. First report of *Rhizopus oryzae* causing fruit rot of yellow oleander in Pakistan. *Canadian Journal of Plant Pathology* 39(3), 361-364.
- Arif, S., Munis, M.F.H., Liaquat, F., Shah, I.H., Zhang, Y., 2019. Leaf rot caused by *Rhizopus oryzae* on pak choy (*Brassica campestris* ssp. *chinensis*) in China. *Phytopathologia Mediterranea* 58(1), 213-217.

- Arkaan, M.F., Ekaputri, R.F., Fatimah, I., Kamari, A., 2020. Physicochemical and photocatalytic activity of hematite/biochar nanocomposite prepared from Salacca skin waste. *Sustainable Chemistry and Pharmacy* 16(6), 100261.
- Aup-Ngoen, K., Noipitak, M., 2020. Effect of carbon-rich biochar on mechanical properties of PLA-biochar composites. *Sustainable Chemistry and Pharmacy* 15(5), 100204.
- Ayllon, M., Aznar, M., Sánchez, J., Gea, G., Arauzo, J., 2006. Influence of temperature and heating rate on the fixed bed pyrolysis of meat and bone meal. *Chemical Engineering Journal* 121(2-3), 85-96.
- Azizullah, A., Khattak, M.N.K., Richter, P., Häder, D.P., 2011. Water pollution in Pakistan and its impact on public health—a review. *Environment International* 37(2), 479-497.
- Azmi, M.A., Naqvi, S., Azmi, M.A., Aslam, M., 2006. Effect of pesticide residues on health and different enzyme levels in the blood of farm workers from Gadap (rural area) Karachi—Pakistan. *Chemosphere* 64(10), 1739-1744.
- Bajpai, R., Chitale, S., Upadhyay, S., Urkurkar, J., 2006. Long-term studies on soil physico-chemical properties and productivity of rice-wheat system as influenced by integrated nutrient management in Inceptisol of Chhattisgarh. *Journal of the Indian Society of Soil science* 54(1), 24-29.
- Bakr, A., Sayed, N., Salama, T., Ali, I.O., Gayed, R.A., Negm, N., 2018. Potential of Mg–Zn–Al layered double hydroxide (LDH)/montmorillonite nanocomposite in remediation of wastewater containing manganese ions. *Research on Chemical Intermediates* 44(1), 389-405.
- Bali, S., Jamwal, V.L., Kohli, S.K., Kaur, P., Tejpal, R., Bhalla, V., Ohri, P., Gandhi, S.G., Bhardwaj, R., Al-Huqail, A.A., 2019. Jasmonic acid application triggers detoxification of lead (Pb) toxicity in tomato through the modifications of secondary metabolites and gene expression. *Chemosphere* 235, 734-748.
- Baqi, A., Tareen, R.B., Mengal, A., Khan, N., Behlil, F., Achakzai, A.K.K., Anwer, M., Faheem, M., 2018. Determination of antioxidants in two medicinally important plants, *Haloxylon griffithii* and *Convolvulus leiocalycinus*, of Balochistan. *Pure and Applied Biology* 7(1), 296-308.
- Bashir, S., Hussain, Q., Akmal, M., Riaz, M., Hu, H., Ijaz, S.S., Iqbal, M., Abro, S., Mehmood, S., Ahmad, M., 2018a. Sugarcane bagasse-derived biochar reduces



- the cadmium and chromium bioavailability to mash bean and enhances the microbial activity in contaminated soil. *Journal of Soils Sediments* 18(3), 874-886.
- Bashir, S., Hussain, Q., Shaaban, M., Hu, H., 2018b. Efficiency and surface characterization of different plant derived biochar for cadmium (Cd) mobility, bioaccessibility and bioavailability to Chinese cabbage in highly contaminated soil. *Chemosphere* 211, 632-639.
- Batra, N., Tomar, M., Gupta, V., 2012. Realization of an efficient cholesterol biosensor using ZnO nanostructured thin film. *Analyst* 137(24), 5854-5859.
- Bandara, T., Franks, A., Xu, J., Bolan, N., Wang, H., Tang, C., 2020. Chemical and biological immobilization mechanisms of potentially toxic elements in biochar-amended soils. *Critical Reviews in Environmental Science and Technology* 50(9), 903-978.
- Basu, P., 2018. Biomass gasification, pyrolysis and torrefaction: practical design and theory. Academic press.
- Battaglia, E., Benoit, I., van den Brink, J., Wiebenga, A., Coutinho, P.M., Henrissat, B., de Vries, R.P., 2011. Carbohydrate-active enzymes from the zygomycete fungus *Rhizopus oryzae*: a highly specialized approach to carbohydrate degradation depicted at genome level. *BMC Genomics* 12(1), 1-12.
- Baxter, J.B., Aydil, E.S., 2005. Nanowire-based dye-sensitized solar cells. *Applied Physics Letters* 86(5), 053114.
- Beauchamp, C., Fridovich, I., 1971. Superoxide dismutase: improved assays and an assay applicable to acrylamide gels. *Analytical Biochemistry* 44(1), 276-287.
- Benítez, T., Rincón, A.M., Limón, M.C., Codon, A.C., 2004. Biocontrol mechanisms of *Trichoderma* strains. *International Microbiology* 7(4), 249-260.
- Bernal-Alzate, J., Grimaldo-Juarez, O., Gonzalez-Mendoza, D., Cervantes-Díaz, L., Rueda-Puente, E.O., CeceñaDurán, C., 2016. El injerto como alternativa para mejorar el rendimiento en la producción de frijol ejotero (*Phaseolus vulgaris* L.). *Idesia* 34(2), 43-46.
- Beveridge, T.J., 2001. Use of the Gram stain in microbiology. *Biotechnic & Histochemistry* 76(3), 111-118.

- Bhaduri, D., Saha, A., Desai, D., Meena, H., 2016. Restoration of carbon and microbial activity in salt-induced soil by application of peanut shell biochar during short-term incubation study. *Chemosphere* 148, 86-98.
- Bhat, S.A., Bashir, O., Haq, S.A.U., Amin, T., Rafiq, A., Ali, M., Américo-Pinheiro, J.H.P., Sher, F., 2022. Phytoremediation of heavy metals in soil and water: An eco-friendly, sustainable and multidisciplinary approach. *Chemosphere* 303(2), 134788.
- Bhatnagar, A., Sillanpää, M., 2010. Utilization of agro-industrial and municipal waste materials as potential adsorbents for water treatment—a review. *Chemical Engineering Journal* 157(2-3), 277-296.
- Bortoloti, G.A., Baron, D., 2022. Phytoremediation of toxic heavy metals by *Brassica* plants: A biochemical and physiological approach. *Environmental Advances* 8, 100204.
- Borkar, A., 2015. Studies on some physicochemical parameters of soil samples in Katol Taluka District Nagpur (MS), India. *Research Journal of Agriculture and Forestry Sciences* 3(1), 16-18.
- Bouabidi, Z.B., El-Naas, M.H., Zhang, Z., 2019. Immobilization of microbial cells for the biotreatment of wastewater: a review. *Environmental Chemistry Letters* 17(1), 241-257.
- Bouyoucos, G.J., 1962. Hydrometer method improved for making particle size analyses of soils. *Agronomy Journal* 54(5), 464-465.
- Brennan, M.J., Subrahmanyam, A., 1996. Market microstructure and asset pricing: On the compensation for illiquidity in stock returns. *Journal of Financial Economics* 41(3), 441-464.
- Brillas, E., Martínez-Huitle, C.A., 2015. Decontamination of wastewaters containing synthetic organic dyes by electrochemical methods. An updated review. *Applied Catalysis B: Environmental* 166, 603-643.
- Brito, S.M.D.O., Andrade, H.M.C., Soares, L.F., De Azevedo, R.P., 2010. Brazil nut shells as a new biosorbent to remove methylene blue and indigo carmine from aqueous solutions. *Journal of Hazardous Materials* 174(1-3), 84-92.
- Cakmak, I., Kutman, U.á., 2018. Agronomic biofortification of cereals with zinc: A review. *European Journal of Soil Science* 69(1), 172-180.

- Calis, I., Kuruüzüm, A., Demirezer, L.Ö., Sticher, O., Ganci, W., Rüedi, P., 1999. Phenylvaleric Acid and Flavonoid Glycosides from *Polygonum salicifolium*. *Journal of Natural Products* 62(8), 1101-1105.
- Carnovale, C., Bryant, G., Shukla, R., Bansal, V., 2019. Identifying trends in gold nanoparticle toxicity and uptake: size, shape, capping ligand, and biological corona. *ACS Omega* 4(1), 242-256.
- Cha, J.S., Park, S.H., Jung, S.C., Ryu, C., Jeon, J.K., Shin, M.C., Park, Y.K., 2016. Production and utilization of biochar: A review. *Journal of Industrial and Engineering Chemistry* 40, 1-15.
- Chen, G., Andries, J., Luo, Z., Spliethoff, H., 2003. Biomass pyrolysis/gasification for product gas production: the overall investigation of parametric effects. *Energy Conversion and Management* 44(11), 1875-1884.
- Chen, W.H., Zhuang, Y.Q., Liu, S.H., Juang, T.T., Tsai, C.M., 2016. Product characteristics from the torrefaction of oil palm fiber pellets in inert and oxidative atmospheres. *Bioresource Technology* 199, 367-374.
- Chen, L., Yang, S., Zuo, X., Huang, Y., Cai, T., Ding, D., 2018. Biochar modification significantly promotes the activity of  $\text{Co}_3\text{O}_4$  towards heterogeneous activation of peroxymonosulfate. *Chemical Engineering Journal* 354, 856-865.
- Chen, H., Zhang, J., Tang, L., Su, M., Tian, D., Zhang, L., Li, Z., Hu, S., 2019. Enhanced Pb immobilization via the combination of biochar and phosphate solubilizing bacteria. *Environment International* 127(2), 395-401.
- Chen, J., Ran, F., Shi, J., Chen, T., Zhao, Z., Zhang, Z., He, L., Li, W., Wang, B., Chen, X., 2022. Identification of the Causal Agent of Brown Leaf Spot on Kiwifruit and Its Sensitivity to Different Active Ingredients of Biological Fungicides. *Pathogens* 11(6), 673.
- Cheraghcheshm, F., Javanbakht, V., 2021. Surface modification of brick by zinc oxide and silver nanoparticles to improve performance properties. *Journal of Building Engineering* 34, 101933.
- Chiou, B.S., Valenzuela-Medina, D., Bilbao-Sainz, C., Klamczynski, A.P., Avena-Bustillos, R.J., Milczarek, R.R., Du, W.X., Glenn, G.M., Orts, W.J., 2016. Torrefaction of almond shells: Effects of torrefaction conditions on properties of solid and condensate products. *Industrial Crops and Products* 86, 40-48.

- Cho, K.H., Park, J.E., Osaka, T., Park, S.G., 2005. The study of antimicrobial activity and preservative effects of nanosilver ingredient. *Electrochimica Acta* 51(5), 956-960.
- Cho, D.W., Kwon, G., Yoon, K., Tsang, Y.F., Ok, Y.S., Kwon, E.E., Song, H., 2017. Simultaneous production of syngas and magnetic biochar via pyrolysis of paper mill sludge using CO<sub>2</sub> as reaction medium. *Energy Conversion and Management* 145, 1-9.
- Chonokhuu, S., Batbold, C., Chuluunpurev, B., Battsengel, E., Dorjsuren, B., Byambaa, B., 2019. Contamination and health risk assessment of heavy metals in the soil of major cities in Mongolia. *International Journal of Environmental Research and Public Health* 16(14), 2552.
- Chu, C.C., White, K.L., Liu, P., Zhang, X., Sue, H.J., 2012. Electrical conductivity and thermal stability of polypropylene containing well-dispersed multi-walled carbon nanotubes disentangled with exfoliated nanoplatelets. *Carbon* 50(12), 4711-4721.
- Cochrane, V., 1958. Inc. New York. *Physiology of fungi*. 415p. John Wiley & Sons.
- Committee, F.O.C.E., 2014. *Flora of China*. St. Louis, Missouri and Cambridge, Massachusetts, USA: Missouri Botanical Garden and Harvard University Herbaria.
- Conder, J.M., Lanno, R.P., Basta, N.T., 2001. Assessment of metal availability in smelter soil using earthworms and chemical extractions. *Journal of Environmental Quality* 30(4), 1231-1237.
- Connell, D.W., Connell, D.W., Vowles, P.D., Warne, M.S.J., Hawker, D.W., 2005. *Basic Concepts of Environmental Chemistry*. CRC/Taylor & Francis 2<sup>nd</sup> Ed. 480p.
- Cui, L., Noerpel, M.R., Scheckel, K.G., Ippolito, J.A., 2019. Wheat straw biochar reduces environmental cadmium bioavailability. *Environment International* 126(6), 69-75.
- Cullings, K., 1992. Design and testing of a plant-specific PCR primer for ecological and evolutionary studies. *Molecular ecology* 1(4), 233-240.
- Dande, P.R., Talekar, V.S., Chakraborty, G.S., 2010. Evaluation of crude saponins extract from leaves of *Sesbania sesban* (L.) Merr. for topical anti-inflammatory

- activity. *International Journal of Research in Pharmaecutical Sciences* 1(3), 269-299.
- Dapkekar, A., Deshpande, P., Oak, M.D., Paknikar, K.M., Rajwade, J.M., 2018. Zinc use efficiency is enhanced in wheat through nanofertilization. *Scientific Reports* 8(1), 1-7.
- Das, R., Panda, S.N., 2022. Preparation and applications of biochar based nanocomposite: A review. *Journal of Analytical and Applied Pyrolysis* 167, 105691.
- Dash, B.C., Réthoré, G., Monaghan, M., Fitzgerald, K., Gallagher, W., Pandit, A., 2010. The influence of size and charge of chitosan/polyglutamic acid hollow spheres on cellular internalization, viability and blood compatibility. *Biomaterials* 31(32), 8188-8197.
- Dehghani, M., Kazemi Shariat Panahi, H., Guillemain, G.J., 2019. Microorganisms, tryptophan metabolism, and kynurenine pathway: A complex interconnected loop influencing human health status. *International Journal of Tryptophan Research* 12, 1178646919852996.
- Demirbas, A., 2004. Effects of temperature and particle size on bio-char yield from pyrolysis of agricultural residues. *Journal of Analytical and Applied Pyrolysis* 72(2), 243-248.
- Deng, Y., Wang, M., Tian, T., Lin, S., Xu, P., Zhou, L., Dai, C., Hao, Q., Wu, Y., Zhai, Z., 2019. The effect of hexavalent chromium on the incidence and mortality of human cancers: a meta-analysis based on published epidemiological cohort studies. *Frontiers in Oncology* 9, 24.
- Dhobale, S., Thite, T., Laware, S.L., Rode, C.V., Koppikar, S.J., Ghanekar, R.K., Kale, S.N., 2008. Zinc oxide nanoparticles as novel alpha-amylase inhibitors. *Journal of Applied Physics* 104(9), 094907.
- Didehban, A., Zabihi, M., Shahrouzi, J.R., 2018. Experimental studies on the catalytic behavior of alloy and core-shell supported Co-Ni bimetallic nano-catalysts for hydrogen generation by hydrolysis of sodium borohydride. *International Journal of Hydrogen Energy* 43(45), 20645-20660.
- Dimitriou, I., Aronsson, P., 2005. Willows for energy and phytoremediation in Sweden. *Unasylva* 56(2), 47.

- Dimkpa, C.O., Andrews, J., Fugice, J., Singh, U., Bindraban, P.S., Elmer, W.H., Gardea-Torresdey, J.L., White, J.C., 2020. Facile coating of urea with low-dose ZnO nanoparticles promotes wheat performance and enhances Zn uptake under drought stress. *Frontiers in Plant Science* 11, 168.
- Ding, Y., Liu, M., Peng, S., Li, J., Liang, Y., Shi, Z., 2019. Binding characteristics of heavy metals to humic acid before and after fractionation by ferrihydrite. *Chemosphere* 226, 140-148.
- Dobrovolskaia, M.A., Clogston, J.D., Neun, B.W., Hall, J.B., Patri, A.K., McNeil, S.E., 2008. Method for analysis of nanoparticle hemolytic properties in vitro. *Nano Letters* 8(8), 2180-2187.
- Do Minh, T., Song, J., Deb, A., Cha, L., Srivastava, V., Sillanpää, M., 2020. Biochar based catalysts for the abatement of emerging pollutants: A review. *Chemical Engineering Journal* 394(2), 124856.
- Dragland, S., Senoo, H., Wake, K., Holte, K., Blomhoff, R., 2003. Several culinary and medicinal herbs are important sources of dietary antioxidants. *The Journal of Nutrition* 133(5), 1286-1290.
- Duo, S., Zhong, R., Liu, Z., Wang, J., Liu, T., Huang, C., Wu, H.J.J.o.P., Solids, C.o., 2018. One-step hydrothermal synthesis of ZnO microflowers and their composition-/hollow nanorod-dependent wettability and photocatalytic property. *Journal of Physics and Chemistry of Solids* 120, 20-33.
- Ebrahiminezhad, A., Zare-Hoseinabadi, A., Sarmah, A.K., Taghizadeh, S., Ghasemi, Y., Berenjian, A., 2018. Plant-mediated synthesis and applications of iron nanoparticles. *Molecular Biotechnology* 60(2), 154-168.
- Ekka, B., Sahu, M.K., Patel, R.K., Dash, P., 2019. Titania coated silica nanocomposite prepared via encapsulation method for the degradation of Safranin-O dye from aqueous solution: Optimization using statistical design. *Water Resources and Industry* 22, 100071.
- El-Berry, M.F., Sadeek, S.A., Abdalla, A.M., Nassar, M.Y., 2021. Microwave-assisted fabrication of copper nanoparticles utilizing different counter ions: An efficient photocatalyst for photocatalytic degradation of safranin dye from aqueous media. *Materials Research Bulletin* 133, 111048.
- El-Sharkawy, R.M., Allam, E.A., El-Taher, A., Shaaban, E.R., Mahmoud, M.E., 2021. Synergistic effect of nano-bentonite and nanocadmium oxide doping

- concentrations on assembly, characterization, and enhanced gamma-rays shielding properties of polypropylene ternary nanocomposites. *International Journal of Energy Research* 45(6), 8942-8959.
- Esfandyari-Manesh, M., Ghaedi, Z., Asemi, M., Khanavi, M., Manayi, A., Jamalifar, H., Dinarvand, R., 2013. Study of antimicrobial activity of anethole and carvone loaded PLGA nanoparticles. *Journal of Pharmacy Research* 7(4), 290-295.
- Etacheri, V., Roshan, R., Kumar, V., 2012. Mg-doped ZnO nanoparticles for efficient sunlight-driven photocatalysis. *ACS Applied Materials & Interfaces* 4(5), 2717-2725.
- Evans, D.O., Macklin, B., 1990. Perennial *Sesbania* production and use. Nitrogen Fixing Tree Association.
- Ezzi, M.I., Lynch, J.M., 2002. Cyanide catabolizing enzymes in *Trichoderma spp.* *Enzyme and Microbial Technology* 31(7), 1042-1047.
- Fahmi, F., Abidin, C., Rahmat, N., 2010. Multi-stage ozonation and biological treatment for removal of azo dye industrial effluent. *International Journal of Environmental Science and Development* 1(2), 193-198.
- Faisal, S., Jan, H., Shah, S.A., Shah, S., Khan, A., Akbar, M.T., Rizwan, M., Jan, F., Wajidullah, Akhtar, N., 2021. Green synthesis of zinc oxide (ZnO) nanoparticles using aqueous fruit extracts of *Myristica fragrans*: their characterizations and biological and environmental applications. *ACS Omega* 6(14), 9709-9722.
- Faris, D., Singh, U., 1990. Pigeonpea: nutrition and products. *Pigeonpea: nutrition and products.*, 401-433. Fatima, H., Khan, K., Zia, M., Ur-Rehman, T., Mirza, B., Haq, I.-u., 2015. Extraction optimization of medicinally important metabolites from *Datura innoxia* Mill.: an in vitro biological and phytochemical investigation. *BMC Complementary and Alternative Medicine* 15(1), 1-18.
- Fazal, T., Razzaq, A., Javed, F., Hafeez, A., Rashid, N., Amjad, U.S., Rehman, M.S.U., Faisal, A., Rehman, F., 2020. Integrating adsorption and photocatalysis: A cost effective strategy for textile wastewater treatment using hybrid biochar-TiO<sub>2</sub> composite. *Journal of Hazardous Materials* 390, 121623.
- Fellet, G., Marmiroli, M., Marchiol, L., 2014. Elements uptake by metal accumulator species grown on mine tailings amended with three types of biochar. *Science of the Total Environment* 468(1), 598-608.

- Filipiak-Szok, A., Kurzawa, M., Szłyk, E., 2015. Determination of toxic metals by ICP-MS in Asiatic and European medicinal plants and dietary supplements. *Journal of Trace Elements in Medicine and Biology* 30, 54-58.
- Fito, J., Kefeni, K.K., Nkambule, T.T.I., 2022. The potential of biochar-photocatalytic nanocomposites for removal of organic micropollutants from wastewater. *The Science of the Total Environment* 829, 154648.
- Fu, M., Li, Y., Wu S, Lu P, Liu J., Dong, F., 2011. Sol-gel Preparation and enhanced photocatalytic performance of Cu-doped ZnO nanoparticles. *Applied Surface Science* 258(4), 1587-1591.
- Fu, D., Han, G., Meng, C., 2012. Size-controlled synthesis and photocatalytic degradation properties of nano-sized ZnO nanorods. *Materials Letters* 72(72), 53-56.
- Fusayama, T., Katayori, T., Nomoto, S., 1963. Corrosion of gold and amalgam placed in contact with each other. *Journal of Dental Research* 42(5), 1183-1197.
- García-Gómez, C., García, S., Obrador, A.F., González, D., Babín, M., Fernández, M.D., 2018. Effects of aged ZnO NPs and soil type on Zn availability, accumulation and toxicity to pea and beet in a greenhouse experiment. *Ecotoxicology and Environmental Safety* 160, 222-230.
- Gholami, P., Dinpazhoh, L., Khataee, A., Orooji, Y., 2019. Sonocatalytic activity of biochar-supported ZnO nanorods in degradation of gemifloxacin: synergy study, effect of parameters and phytotoxicity evaluation. *Ultrasonics Sonochemistry* 55, 44-56.
- Gholami, L., Rahimi, G., 2021. Chemical fractionation of copper and zinc after addition of carrot pulp biochar and thiourea-modified biochar to a contaminated soil. *Environmental Technology* 42(22), 3523-3532.
- Ghosh, D., Sinha, M., Purkait, M.J.D., 2013. A comparative analysis of low-cost ceramic membrane preparation for effective fluoride removal using hybrid technique. *Desalination* 327, 2-13.
- Gomase, P.V., 2012. *Sesbania sesban* Linn: a review on its ethnobotany, phytochemical and pharmacological profile. *Asian Journal of Biomedical and Pharmaceutical Sciences* 2(12), 11-14.
- Gnanasekaran, L., Hemamalini, R., Saravanan, R., Ravichandran, K., Gracia, F., Agarwal, S., Gupta, V.K., 2017. Synthesis and characterization of metal oxides



- (CeO<sub>2</sub>, CuO, NiO, Mn<sub>3</sub>O<sub>4</sub>, SnO<sub>2</sub> and ZnO) nanoparticles as photo catalysts for degradation of textile dyes. *Journal of Photochemistry and Photobiology B: Biology* 173, 43-49.
- Gong, X., Huang, D., Liu, Y., Zeng, G., Chen, S., Wang, R., Xu, P., Cheng, M., Zhang, C., Xue, W., 2019. Biochar facilitated the phytoremediation of cadmium contaminated sediments: Metal behavior, plant toxicity, and microbial activity. *Science of the Total Environment* 666, 1126-1133.
- Gonçalves, M.G., Veiga, P.A.D.S., Fornari, M.R., Peralta-Zamora, P., Mangrich, A.S., Silvestri, S., 2020. Relationship of the physicochemical properties of novel ZnO/biochar composites to their efficiencies in the degradation of sulfamethoxazole and methyl orange. *Science of the Total Environment* 748, 141381.
- Goswami, M., Suresh, D., 2020. Plant growth-promoting rhizobacteria—alleviators of abiotic stresses in soil: a review. *Pedosphere* 30(1), 40-61.
- Guagliardi, I., Cicchella, D., De Rosa, R., 2012. A geostatistical approach to assess concentration and spatial distribution of heavy metals in urban soils. *Water, Air, & Soil Pollution* 223(9), 5983-5998.
- Günes, A., Inal, A., Alpaslan, M., 1996. Effect of salinity on stomatal resistance, proline, and mineral composition of pepper. *Journal of Plant Nutrition* 19(2), 389-396.
- Gupta, R., Singh, A., Ajayakumar, P., Pandey, R., 2017. Microbial interference mitigates *Meloidogyne incognita* mediated oxidative stress and augments bacoside content in *Bacopa monnieri* L. *Microbiological Research* 199, 67-78.
- Güy, N., Özacar, M., 2016. The influence of noble metals on photocatalytic activity of ZnO for Congo red degradation. *International Journal of Hydrogen Energy* 41(44), 20100-20112.
- Hamid, Y., Tang, L., Sohail, M.I., Cao, X., Hussain, B., Aziz, M.Z., Usman, M., He, Z.I., Yang, X., 2019. An explanation of soil amendments to reduce cadmium phytoavailability and transfer to food chain. *Science of The Total Environment* 660, 80-96.
- Hamed, J., Mohammadipanah, F., Panahi, H.K.S., 2015. Biotechnological exploitation of Actinobacterial members, Halophiles. Springer, pp. 57-143.

- Han, T.U., Kim, Y.M., Watanabe, A., Teramae, N., Park, Y.K., Kim, S., 2017. Pyrolysis kinetic analysis of poly (methyl methacrylate) using evolved gas analysis-mass spectrometry. *Korean Journal of Chemical Engineering* 34(4), 1214-1221.
- Haque, S., Faidah, H., Ashgar, S.S., Abujamel, T.S., Mokhtar, J.A., Almuhayawi, M.S., Harakeh, S., Singh, R., Srivastava, N., Gupta, V.K., 2022. Green Synthesis of Zn (OH)<sub>2</sub>/ZnO-Based Bionanocomposite using Pomegranate Peels and Its Application in the Degradation of Bacterial Biofilm. *Nanomaterials* 12(19), 3458.
- Harman, G.E., Howell, C.R., Viterbo, A., Chet, I., Lorito, M., 2004a. *Trichoderma* species—opportunistic, avirulent plant symbionts. *Nature Reviews Microbiology* 2(1), 43-56.
- Harman, G., Lorito, M., Lynch, J., 2004b. Uses of *Trichoderma* spp. to alleviate or remediate soil and water pollution. *Advances in Applied Microbiology* 56, 313-330.
- Hashmi, I., Farooq, S., Qaiser, S., 2009. Chlorination and water quality monitoring within a public drinking water supply in Rawalpindi Cantt (Westridge and Tench) area, Pakistan. *Environmental Monitoring and Assessment* 158(1), 393-403.
- Hayat, K., Gondal, M., Khaled, M., Yamani, Z., Ahmed, S., 2011. Laser induced photocatalytic degradation of hazardous dye (Safranin-O) using self synthesized nanocrystalline WO<sub>3</sub>. *Journal of Hazardous Materials* 186(2-3), 1226-1233.
- Hayat, K., Menhas, S., Bundschuh, J., Zhou, P., Niazi, N.K., Amna, Hussain, A., Hayat, S., Ali, H., Wang, J., 2020. Plant growth promotion and enhanced uptake of Cd by combinatorial application of *Bacillus pumilus* and EDTA on *Zea mays* L. *International Journal of Phytoremediation* 22(13), 1372-1384.
- He, X., Fang, J., Chen, X., Zhao, Z., Li, Y., Meng, Y., Huang, L., 2019a. *Actinidia chinensis* Planch.: A review of chemistry and pharmacology. *Frontiers in Pharmacology* 10, 1236.
- He, L., Zhong, H., Liu, G., Dai, Z., Brookes, P.C., Xu, J., 2019b. Remediation of heavy metal contaminated soils by biochar: Mechanisms, potential risks and applications in China. *Environmental Pollution* 252, 846-855.

- He, Y., Wang, D., Li, X., Fu, Q., Yin, L., Yang, Q., Chen, H., 2021. Photocatalytic degradation of tetracycline by metal-organic frameworks modified with Bi<sub>2</sub>WO<sub>6</sub> nanosheet under direct sunlight. *Chemosphere* 284, 131386.
- Hinrichsen, D., Tacio, H., 2002. The coming freshwater crisis is already here. The linkages between population and water. Washington, DC: Woodrow Wilson International Center for Scholars, 1-26.
- Hiol, A., Jonzo, M.D., Rugani, N., Druet, D., Sarda, L., Comeau, L.C., 2000. Purification and characterization of an extracellular lipase from a thermophilic *Rhizopus oryzae* strain isolated from palm fruit. *Enzyme and Microbial Technology* 26(5-6), 421-430.
- Hoseinzadeh, A., Habibi-Yangjeh, A., Davari, M., 2016. Antifungal activity of magnetically separable Fe<sub>3</sub>O<sub>4</sub>/ZnO/AgBr nanocomposites prepared by a facile microwave-assisted method. *Progress in Natural Science: Materials International* 26(4), 334-340.
- Howell, S., Barnard, R., Humphreys, F., 1999. Application of molecular typing methods to dermatophyte species that cause skin and nail infections. *Journal of Medical Microbiology* 48(1), 33-40.
- Huang, D., Liu, L., Zeng, G., Xu, P., Huang, C., Deng, L., Wang, R., Wan, J., 2017. The effects of rice straw biochar on indigenous microbial community and enzymes activity in heavy metal-contaminated sediment. *Chemosphere* 174, 545-553.
- Huang, Y., Wang, L., Wang, W., Li, T., He, Z., Yang, X., 2019. Current status of agricultural soil pollution by heavy metals in China: A meta-analysis. *Science of the Total Environment* 651, 3034-3042.
- Huang, J., Zimmerman, A.R., Chen, H., Gao, B., 2020. Ball milled biochar effectively removes sulfamethoxazole and sulfapyridine antibiotics from water and wastewater. *Environmental Pollution* 258, 113809.
- Hui, T.S., Zaini, M.A.A., 2015. Potassium hydroxide activation of activated carbon: a commentary. *Carbon Letters* 16(4), 275-280.
- Hussain, R., Sattar, S., Khan, M.H., Nafees, M., 2013. Low Cost Wastewater Treatment at Beverage Industry, Hattar Industrial Estate, Pakistan-A Case Study. *International Journal of Environmental Protection* 3(11), 23.

- Hussain, A., Ali, S., Rizwan, M., Rehman, M.Z., Javed, M.R., Imran, M., Chatha, S.A.S., Nazir, R., 2018. Zinc oxide nanoparticles alter the wheat physiological response and reduce the cadmium uptake by plants. *Environmental Pollution* 242, 1518-1526.
- Hussain, A., Rizwan, M., Ali, Q., Ali, S., 2019. Seed priming with silicon nanoparticles improved the biomass and yield while reduced the oxidative stress and cadmium concentration in wheat grains. *Environmental Science and Pollution Research* 26(8), 7579-7588.
- Ifijen, I.H., Maliki, M., Anegebe, B., 2022. Synthesis, Photocatalytic Degradation and Antibacterial Properties of Selenium or Silver Doped Zinc Oxide Nanoparticles: A Detailed Review. *OpenNano* 8, 100082.
- Igalavithana, A.D., Kwon, E.E., Vithanage, M., Rinklebe, J., Moon, D.H., Meers, E., Tsang, D.C., Ok, Y.S., 2019. Soil lead immobilization by biochars in short-term laboratory incubation studies. *Environment International* 127, 190-198.
- Inguanzo, M., Menendez, J., Fuente, E., Pis, J., 2001. Reactivity of pyrolyzed sewage sludge in air and CO<sub>2</sub>. *Journal of Analytical and Applied Pyrolysis* 58, 943-954.
- Inyang, M.I., Gao, B., Yao, Y., Xue, Y., Zimmerman, A., Mosa, A., Pullammanappallil, P., Ok, Y.S., Cao, X., 2016. A review of biochar as a low-cost adsorbent for aqueous heavy metal removal. *Critical Reviews in Environmental Science and Technology* 46(4), 406-433.
- Iqbal, J., Abbasi, B.A., Ahmad, R., Mahmood, T., Kanwal, S., Ali, B., Khalil, A.T., Shah, S.A., Alam, M.M., Badshah, H., 2018. Ursolic acid a promising candidate in the therapeutics of breast cancer: Current status and future implications. *Biomedicine Pharmacotherapy* 108, 752-756.
- Iqbal, J., Abbasi, B.A., Ahmad, R., Batool, R., Mahmood, T., Ali, B., Khalil, A.T., Kanwal, S., Shah, S.A., Alam, M.M., 2019. Potential phytochemicals in the fight against skin cancer: Current landscape and future perspectives. *Biomedicine & Pharmacotherapy* 109, 1381-1393.
- Jaafar, N.M., Clode, P.L., Abbott, L.K., 2014. Microscopy observations of habitable space in biochar for colonization by fungal hyphae from soil. *Journal of Integrative Agriculture* 13(3), 483-490.
- Jan, H., Shah, M., Usman, H., Khan, M.A., Zia, M., Hano, C., Abbasi, B.H., 2020. Biogenic synthesis and characterization of antimicrobial and antiparasitic zinc

- oxide (ZnO) nanoparticles using aqueous extracts of the Himalayan Columbine (*Aquilegia pubiflora*). *Frontiers in Materials* 7, 249.
- Jan, S.U., Rehman, M., Gul, A., Fayyaz, M., Rehman, S.U., Jamil, M., 2022. Combined application of two *Bacillus* species enhance phytoremediation potential of *Brassica napus* in an industrial metal-contaminated soil. *International Journal of Phytoremediation* 24(6), 652-665.
- Janus, A., Waterlot, C., Heymans, S., Deboffe, C., Douay, F., Pelfrène, A., 2018. Do biochars influence the availability and human oral bioaccessibility of Cd, Pb, and Zn in a contaminated slightly alkaline soil? *Environmental Monitoring Assessment* 190(4), 218.
- Javanbakht, S., Pooresmaeil, M., Namazi, H., 2019. Green one-pot synthesis of carboxymethylcellulose/Zn-based metal-organic framework/graphene oxide bio-nanocomposite as a nanocarrier for drug delivery system. *Carbohydrate Polymers* 208, 294-301.
- Javed, R., Usman, M., Tabassum, S., Zia, M., 2016a. Effect of capping agents: structural, optical and biological properties of ZnO nanoparticles. *Applied Surface Science* 386, 319-326.
- Javed, H., Naeem, A., Rengel, Z., Dahlawi, S., 2016b. Timing of foliar Zn application plays a vital role in minimizing Cd accumulation in wheat. *Environmental Science Pollution Research* 23, 16432-16439.
- Jennessen, J., Nielsen, K.F., Houbraeken, J., Lyhne, E.K., Schnürer, J., Frisvad, J.C., Samson, R.A., 2005. Secondary metabolite and mycotoxin production by the *Rhizopus microsporus* group. *Journal of Agricultural and Food Chemistry* 53(5), 1833-1840.
- Jiang, J., Wu, L., Li, N., Luo, Y., Liu, L., Zhao, Q., Zhang, L., Christie, P., 2010. Effects of multiple heavy metal contamination and repeated phytoextraction by *Sedum plumbizincicola* on soil microbial properties. *European Journal of Soil Biology* 46(1), 18-26.
- Jiang, J., Xu, R.K., Jiang, T.Y., Li, Z., 2012. Immobilization of Cu (II), Pb (II) and Cd (II) by the addition of rice straw derived biochar to a simulated polluted Ultisol. *Journal of Hazardous Materials* 229, 145-150.

- Jin, X., Liu, Y., Qiao, X., Guo, R., Liu, C., Wang, X., Zhao, X., 2019. Risk assessment of organochlorine pesticides in drinking water source of the Yangtze River. *Ecotoxicology and Environmental Safety* 182, 109390.
- Joško, I., Oleszczuk, P., Dobrzyńska, J., Futa, B., Joniec, J., Dobrowolski, R., 2019. Long-term effect of ZnO and CuO nanoparticles on soil microbial community in different types of soil. *Geoderma* 352, 204-212.
- Jung, S.H., Kim, J.S., 2014. Production of biochars by intermediate pyrolysis and activated carbons from oak by three activation methods using CO<sub>2</sub>. *Journal of Analytical and Applied Pyrolysis* 107, 116-122.
- Jung, K.W., Choi, B.H., Dao, C.M., Lee, Y.J., Choi, J.W., Ahn, K.H., Lee, S.H., 2018. Aluminum carboxylate-based metal organic frameworks for effective adsorption of anionic azo dyes from aqueous media. *Journal of Industrial Engineering Chemistry* 59, 149-159.
- Jyske, T., 2008. The effects of thinning and fertilisation on wood and tracheid properties of Norway spruce (*Picea abies*): the results of long-term experiments. *Dissertationes Forestales* 55, 1-59.
- Kamal, A., Haroon, U., Manghwar, H., Alamer, K.H., Alsudays, I.M., Althobaiti, A.T., Iqbal, A., Akbar, M., Anar, M., Nazish, M., 2022b. Biological Applications of Ball-Milled Synthesized Biochar-Zinc Oxide Nanocomposite Using Zea mays L. *Molecules* 27(16), 5333.
- Kamal, A., Saleem, M.H., Alshaya, H., Okla, M.K., Chaudhary, H.J., Munis, M.F.H., 2022a. Ball-milled synthesis of maize biochar-ZnO nanocomposite (MB-ZnO) and estimation of its photocatalytic ability against different organic and inorganic pollutants. *Journal of Saudi Chemical Society* 26(3), 101445.
- Kamal, A., Ali, M., Farraj, D.A.A., Al-Zaidi, E.M., Khizar, M., Aljaaidi, R.A., Elshikh, M.S., Munis, M.F.H.J.C., 2023. Diagnosis and Control of Brown Leaf Spot of Kiwi (*Actinidia deliciosa*) Using Biochar-Zinc Oxide Nanocomposite (MB-ZnO) as a Non-Toxic Bio-Fungicides. *Crystals* 13(1), 98.
- Kamunda, C., Mathuthu, M., Madhuku, M., 2016. Health risk assessment of heavy metals in soils from Witwatersrand Gold Mining Basin, South Africa. *International Journal of Environmental Research and Public Health* 13(7), 663.

- Kapoor, D., Singh, S., Kumar, V., Romero, R., Prasad, R., Singh, J., 2019. Antioxidant enzymes regulation in plants in reference to reactive oxygen species (ROS) and reactive nitrogen species (RNS). *Plant Gene* 19, 100182.
- Kappler, A., Wuestner, M.L., Ruecker, A., Harter, J., Halama, M., Behrens, S., 2014. Biochar as an electron shuttle between bacteria and Fe (III) minerals. *Environmental Science Technology Letters* 1(8), 339-344.
- Karimi, B., Cahurel, J.Y., Gontier, L., Charlier, L., Chovelon, M., Mahé, H., Ranjard, L., 2020. A meta-analysis of the ecotoxicological impact of viticultural practices on soil biodiversity. *Environmental Chemistry Letters* 18(6), 1947-1966.
- Karlsson, I., Friberg, H., Steinberg, C., Persson, P., 2014. Fungicide effects on fungal community composition in the wheat phyllosphere. *PLOS One* 9(11), e111786.
- Katz, S., Samitz, M., 1975. Leaching of nickel from stainless steel consumer commodities. *Acta Dermato-Venereologica* 55(2), 113-115.
- Kathiresh, M., Suganya, P., Saravanakumar, M., 2011. Antioxidant effect of *Sesbania sesban* flower extract. *International Journal of Pharmaceutical Sciences* 3(2), 1307-1312.
- Khalil, A.T., Ovais, M., Ullah, I., Ali, M., Shinwari, Z.K., Hassan, D., Maaza, M., 2018. *Sageretia thea* (Osbeck.) modulated biosynthesis of NiO nanoparticles and their in vitro pharmacognostic, antioxidant and cytotoxic potential. *Artificial cells, Nanomedicine, and Biotechnology* 46(4), 838-852.
- Khan, N., Zandi, P., Ali, S., Mehmood, A., Adnan Shahid, M., Yang, J., 2018. Impact of salicylic acid and PGPR on the drought tolerance and phytoremediation potential of *Helianthus annuus*. *Frontiers in Microbiology* 9, 2507.
- Khan, T., Ullah, N., Khan, M.A., Nadhman, A., 2019. Plant-based gold nanoparticles; a comprehensive review of the decade-long research on synthesis, mechanistic aspects and diverse applications. *Advances in Colloid and Interface Science* 272, 102017.
- Khanna, K., Jamwal, V.L., Kohli, S.K., Gandhi, S.G., Ohri, P., Bhardwaj, R., Abd\_Allah, E.F., Hashem, A., Ahmad, P., 2019. Plant growth promoting rhizobacteria induced Cd tolerance in *Lycopersicon esculentum* through altered antioxidative defense expression. *Chemosphere* 217(3), 463-474.

- Kigkr, R.W., 1971. Epidermal and cuticular mounts of plant material obtained by maceration. *Stain Technology* 46(2), 71-75.
- Kolenčík, M., Ernst, D., Komár, M., Urík, M., Šebesta, M., Ďurišová, Ľ., Bujdos, M., Cerny, I., Chlpik, J., Juriga, M., Illa, R., Qian, Y., Feng, H., Kratosova, G., Barabaszova, K.C., Ducsay, L., Aydın, E., 2022. Effects of Foliar Application of ZnO Nanoparticles on Lentil Production, Stress Level and Nutritional Seed Quality under Field Conditions. *Nanomaterials* 12(3), 310.
- Konwar, L.J., Mäki-Arvela, P., Salminen, E., Kumar, N., Thakur, A.J., Mikkola, J.-P., Deka, D., 2015. Towards carbon efficient biorefining: multifunctional mesoporous solid acids obtained from biodiesel production wastes for biomass conversion. *Applied Catalysis B: Environmental* 176, 20-35.
- Kredics, L., Antal, Z., Manczinger, L., Nagy, E., 2001. Breeding of mycoparasitic *Trichoderma* strains for heavy metal resistance. *Letters in Applied Microbiology* 33(2), 112-116.
- Kumar, V., Sharma, A., Thukral, A., Bhardwaj, R., 2016. Assessment of soil enzyme activities based on soil samples from the Beas river bed, India using multivariate techniques. *Malaysian Journal of Soil Science* 20, 135-145.
- Kumar, S., Loganathan, V.A., Gupta, R.B., Barnett, M.O., 2011. An assessment of U (VI) removal from groundwater using biochar produced from hydrothermal carbonization. *Journal of Environmental Management* 92(10), 2504-2512.
- Kuriakose, S., Satpati, B., Mohapatra, S., 2015. Highly efficient photocatalytic degradation of organic dyes by Cu doped ZnO nanostructures. *Physical Chemistry Chemical Physics* 17(38), 25172-25181.
- Kwon, YI., Apostolidis, E., Shetty, K.J.B.T., 2008. In vitro studies of eggplant (*Solanum melongena*) phenolics as inhibitors of key enzymes relevant for type 2 diabetes and hypertension. *Bioresource Technology* 99, 2981-2988.
- Kwon, J.H., Kang, D.W., Ha, J.S., Kim, J.W., Kwak, Y.S., 2012. Soft rot on peach caused by *Rhizopus oryzae* in Korea. *The Korean Journal of Mycology* 40(1), 65-68.
- Lanoiselet, V., Cother, E., Ash, G.J., 2007. Aggregate sheath spot and sheath spot of rice. *Crop Protection* 26(6), 799-808.



- Law, Z.X., 2020. A Comparative Study on the Photocatalytic Degradation of Organic Dye in the Presence of Biochar Composites Using Various Oxidants. *UTAR* 1-112.
- Lee, M.S., Chan, J.Y.W., Kong, S.K., Yu, B., Eng-Choon, V.O., Nai-Ching, H.W., Mak Chung-Wai, T., Fung, K.P., 2005. Effects of polyphyllin D, a steroidal saponin in *Paris polyphylla*, in growth inhibition of human breast cancer cells and in xenograft. *Cancer Biology & Therapy* 4(11), 1248-1254.
- Lee, K.M., Lai, C.W., Ngai, K.S., Juan, J.C., 2016a. Recent developments of zinc oxide based photocatalyst in water treatment technology: a review. *Water Research* 88, 428-448.
- Lee, E.H., Park, R.S., Kim, H., Park, S.H., Jung, S.C., Jeon, J.K., Kim, S.C., Park, Y.K., 2016b. Hydrodeoxygenation of guaiacol over Pt loaded zeolitic materials. *Journal of Industrial and Engineering Chemistry* 37, 18-21.
- Lehmann, J., Joseph, S., 2015. Biochar for environmental management: an introduction, *Biochar for environmental management*. Routledge, pp. 1-13.
- Leichtweis, J., Silvestri, S., Carissimi, E., 2020. New composite of pecan nutshells biochar-ZnO for sequential removal of acid red 97 by adsorption and photocatalysis. *Biomass and Bioenergy* 140, 105648.
- Leszczuk, A., Chylińska, M., Zdunek, A., 2019. Enzymes and vitamin C as factors influencing the presence of arabinogalactan proteins (AGPs) in *Solanum lycopersicum* fruit. *Plant Physiology Biochemistry* 139, 681-690.
- Li, D., Huang, J.F., Cao, L.Y., Jia-Yin, L., Ouyang, H.B., Yao, C.Y., 2014. Microwave hydrothermal synthesis of Sr<sup>2+</sup> doped ZnO crystallites with enhanced photocatalytic properties. *Ceramics International* 40(2), 2647-2653.
- Li, H., Ye, X., Geng, Z., Zhou, H., Guo, X., Zhang, Y., Zhao, H., Wang, G., 2016. The influence of biochar type on long-term stabilization for Cd and Cu in contaminated paddy soils. *Journal of Hazardous Materials* 304, 40-48.
- Li, P., Lin, K., Fang, Z., Wang, K., 2017. Enhanced nitrate removal by novel bimetallic Fe/Ni nanoparticles supported on biochar. *Journal of Cleaner Production* 151, 21-33.
- Li, S., Wang, M., Zhao, Z., Li, X., Han, Y., Chen, S., 2018. Alleviation of cadmium phytotoxicity to wheat is associated with Cd re-distribution in soil aggregates as affected by amendments. *RSC Advances* 8(31), 17426-17434.

- Li, J., Wang, S.-L., Zhang, J., Zheng, L., Chen, D., Wu, Z., Shaheen, S.M., Rinklebe, J., Ok, Y.S., Wang, H., 2020. Coconut-fiber biochar reduced the bioavailability of lead but increased its translocation rate in rice plants: elucidation of immobilization mechanisms and significance of iron plaque barrier on roots using spectroscopic techniques. *Journal of Hazardous Materials* 389, 122117.
- Liang, F., Liu, Z., Jiang, X., Li, J., Xiao, K., Xu, W., Chen, X., Liang, J., Lin, Z., Li, M., 2023. NaOH-modified biochar supported Fe/Mn bimetallic composites as efficient peroxymonosulfate activator for enhance tetracycline removal. *Chemical Engineering Journal* 454(5), 139949.
- Lichtenthaler, H.K., 1987. Chlorophylls and carotenoids: pigments of photosynthetic biomembranes, *Methods in Enzymology* 148, 350-382.
- Lisowski, P., Colmenares, J.C., Masek, O., Lisowski, W., Lisovytskiy, D., Kamińska, A., Łomot, D., 2017. Dual functionality of TiO<sub>2</sub>/biochar hybrid materials: photocatalytic phenol degradation in the liquid phase and selective oxidation of methanol in the gas phase. *ACS Sustainable Chemistry & Engineering* 5(7), 6274-6287.
- Liu, X.Y., Huang, H., Zheng, R.Y., 2007. Molecular phylogenetic relationships within *Rhizopus* based on combined analyses of ITS rDNA and pyrG gene sequences. *Sydowia-horn* 59(2), 235.
- Liu, X., Song, Q., Tang, Y., Li, W., Xu, J., Wu, J., Wang, F., Brookes, P.C., 2013. Human health risk assessment of heavy metals in soil–vegetable system: a multi-medium analysis. *Science of the Total Environment* 463, 530-540.
- Liu, J., Cai, H., Mei, C., Wang, M., 2015b. Effects of nano-silicon and common silicon on lead uptake and translocation in two rice cultivars. *Frontiers of Environmental Science Engineering* 9(5), 905-911.
- Liu, Q., Liu, B., Zhang, Y., Lin, Z., Zhu, T., Sun, R., Wang, X., Ma, J., Bei, Q., Liu, G., 2017. Can biochar alleviate soil compaction stress on wheat growth and mitigate soil N<sub>2</sub>O emissions? *Soil Biology Biochemistry* 104, 8-17.
- Lonappan, L., Rouissi, T., Das, R.K., Brar, S.K., Ramirez, A.A., Verma, M., Surampalli, R.Y., Valero, J.R., 2016. Adsorption of methylene blue on biochar microparticles derived from different waste materials. *Waste Management* 49, 537-544.

- Lourenço, M.A., Zeng, J., Jagdale, P., Castellino, M., Sacco, A., Farkhondehfal, M.A., Pirri, C.F., 2021. Biochar/zinc oxide composites as effective catalysts for electrochemical CO<sub>2</sub> reduction. *ACS Sustainable Chemistry Engineering* 9(15), 5445-5453.
- Lowry, O.H., Rosebrough, N.J., Farr, A.L., Randall, R.J., 1951. Protein measurement with the Folin phenol reagent. *Journal of Biological Chemistry* 193(1), 265-275.
- Lu, G., Low, J., Liu, C., Lua, A., 1995. Surface area development of sewage sludge during pyrolysis. *Fuel* 74(3), 344-348.
- Lu, K., Yang, X., Gielen, G., Bolan, N., Ok, Y.S., Niazi, N.K., Xu, S., Yuan, G., Chen, X., Zhang, X., 2017. Effect of bamboo and rice straw biochars on the mobility and redistribution of heavy metals (Cd, Cu, Pb and Zn) in contaminated soil. *Journal of Environmental Management* 186, 285-292.
- Luo, Q., Cai, Y., Yan, J., Sun, M., Corke, H., 2004. Hypoglycemic and hypolipidemic effects and antioxidant activity of fruit extracts from *Lycium barbarum*. *Life Sciences* 76(2), 137-149.
- Lutts, S., Kinet, J., Bouharmont, J., 1996. Effects of salt stress on growth, mineral nutrition and proline accumulation in relation to osmotic adjustment in rice (*Oryza sativa* L.) cultivars differing in salinity resistance. *Plant Growth Regulation* 19(3), 207-218.
- Lyu, H., Tang, J., Shen, B., Siddique, T., 2018. Development of a novel chem-bio hybrid process using biochar supported nanoscale iron sulfide composite and *Corynebacterium variabile* HRJ4 for enhanced trichloroethylene dechlorination. *Water Research* 147, 132-141.
- Ma, Y., Ye, X., Hao, Y., Xu, G., Xu, G., Liu, D., 2008. Ultrasound-assisted extraction of hesperidin from Penggan (*Citrus reticulata*) peel. *Ultrasonics Sonochemistry* 15(3), 227-232.
- Ma, B., Chaudhary, J.P., Zhu, J., Sun, B., Chen, C., Sun, D., 2021. Construction of silver nanoparticles anchored in carbonized bacterial cellulose with enhanced antibacterial properties. *Colloids and Surfaces A: Physicochemical and Engineering Aspects* 611, 125845.
- Machida, M., Mochimaru, T., Tatsumoto, H., 2006. Lead (II) adsorption onto the graphene layer of carbonaceous materials in aqueous solution. *Carbon* 44(13), 2681-2688.

- Magdaleno-Garcia, G., Peralta-Manjarrez, R.M., Benavides-Mendoza, A., Juarez-Maldonado, A., Sandoval, A., 2022. Effects of zinc oxide nanoparticles on growth, micromorphology and histology of grafted eggplant (*Solanum Melongena*). *Pakistan Journal of Botany* 54(4), 1285-1293.
- Malagoli, D., 2007. A full-length protocol to test hemolytic activity of palytoxin on human erythrocytes. *Invertebrate Survival Journal* 4(2), 92-94.
- Malakootian, M., Heidari, M.R., 2018. Removal of phenol from steel wastewater by combined electrocoagulation with photo-Fenton. *Water Science and Technology* 78(6), 1260-1267.
- Manocha, S.A., Patel, H., Manocha, L.A., 2010. Effect of steam activation parameters on characteristics of pine based activated carbon. *Carbon Letters* 11(3), 201-205.
- Mehta, A., Shaha, C., 2006. Mechanism of metalloid-induced death in *Leishmania* spp.: role of iron, reactive oxygen species,  $Ca^{2+}$ , and glutathione. *Free Radical Biology and Medicine* 40(10), 1857-1868.
- Mench, M., Lepp, N., Bert, V., Schwitzguébel, J.P., Gawronski, S.W., Schröder, P., Vangronsveld, J., 2010. Successes and limitations of phytotechnologies at field scale: outcomes, assessment and outlook from COST Action 859. *Journal of Soils and Sediments* 10(6), 1039-1070.
- Mendez, A., Gomez, A., Paz-Ferreiro, J., Gasco, G., 2012. Effects of sewage sludge biochar on plant metal availability after application to a Mediterranean soil. *Chemosphere* 89(11), 1354-1359.
- Menhas, S., Hayat, K., Niazi, N.K., Zhou, P., Amna, Bundschuh, J., Naeem, M., Munis, M.F.H., Yang, X., Chaudhary, H.J., 2021. Microbe-EDTA mediated approach in the phytoremediation of lead-contaminated soils using maize (*Zea mays* L.) plants. *International Journal of Phytoremediation* 23(6), 585-596.
- Miller, D.D., Schrickler, B.R., Rasmussen, R.R., Van Campen, D., 1981. An *in vitro* method for estimation of iron availability from meals. *The American Journal of Clinical Nutrition* 34(10), 2248-2256.
- Min, S. K., Zhang, X., Zwiers, F. W., Hegerl, G.C., 2011. Human contribution to more-intense precipitation extremes. *Nature* 470(7334), 378-381.

- Mo, J., Yang, Q., Zhang, N., Zhang, W., Zheng, Y., Zhang, Z., 2018. A review on agro-industrial waste (AIW) derived adsorbents for water and wastewater treatment. *Journal of Environmental Management* 227, 395-405.
- Mohammadipanah, F., Dehghani, M., 2017. Classification and taxonomy of Actinobacteria, *Biology and biotechnology of Actinobacteria*. Springer 51-77.
- Mohamed, F., Abukhadra, M.R., Shaban, M., 2018. Removal of safranin dye from water using polypyrrole nanofiber/Zn-Fe layered double hydroxide nanocomposite (Ppy NF/Zn-Fe LDH) of enhanced adsorption and photocatalytic properties. *Science of the Total Environment* 640, 352-363.
- Mohamed, H.E.A., Afridi, S., Khalil, A.T., Zia, D., Shinwari, Z.K., Dhlamini, M.S., Maaza, M., 2020. Structural, morphological and biological features of ZnO nanoparticles using *Hyphaene thebaica* (L.) Mart. fruits. *Journal of Inorganic and Organometallic Polymers and Materials* 30, 3241-3254.
- Mohan, D., Sarswat, A., Ok, Y.S., Jr, C.U.P., 2014. Organic and inorganic contaminants removal from water with biochar, a renewable, low cost and sustainable adsorbent—a critical review. *Bioresource technology* 160, 191-202.
- Moharram, A., Mansour, S., Hussein, M., Rashad, M., 2014. Direct precipitation and characterization of ZnO nanoparticles. *Journal of Nanomaterials* 2014, 20-20.
- Monticone, S., Tufeu, R., Kanaev, A., 1998. Complex nature of the UV and visible fluorescence of colloidal ZnO nanoparticles. *The Journal of Physical Chemistry B* 102(16), 2854-2862.
- Mounicou, S., Szpunar, J., Andrey, D., Blake, C., Lobinski, R., 2002. Development of a sequential enzymolysis approach for the evaluation of the bioaccessibility of Cd and Pb from cocoa. *Analyst* 127(12), 1638-1641.
- Moussavi, G., Hossaini, H., Jafari, S.J., Farokhi, M., 2014. Comparing the efficacy of UVC, UVC/ZnO and VUV processes for oxidation of organophosphate pesticides in water. *Journal of Photochemistry Photobiology A: Chemistry* 290(1), 86-93.
- Moustafa, H., Youssef, A.M., Darwish, N.A., Abou-Kandil, A.I., 2019. Eco-friendly polymer composites for green packaging: Future vision and challenges. *Composites Part B: Engineering* 172, 16-25.
- Nagajyothi, P., Cha, S.J., Yang, I.J., Sreekanth, T., Kim, K.J., Shin, H.M., 2015. Antioxidant and anti-inflammatory activities of zinc oxide nanoparticles

- synthesized using *Polygala tenuifolia* root extract. Journal of Photochemistry and Photobiology B: Biology 146, 10-17.
- Naik, N., Tare, H., Sherikar, A., Deore, S., Dama, G., 2011. Central nervous system stimulant effect of extracts obtained from the barks of *Sesbania sesban*. International Journal of Pharmaceutical and Life Sciences 1(1), 77-92.
- Najar, G.R., Ganie, M.A., Tahir, A., 2015. Biochar for sustainable soil health: a review of prospects and concerns. Pedosphere 25(5), 639-653.
- Namazi, H., Belali, S., 2016. Starch-g-lactic acid/montmorillonite nanocomposite: Synthesis, characterization and controlled drug release study. Starch-Stärke 68(3), 177-187.
- Naraginti, S., Li, Y., 2017. Preliminary investigation of catalytic, antioxidant, anticancer and bactericidal activity of green synthesized silver and goldnanoparticles using *Actinidia deliciosa*. Journal of Photochemistry Photobiology B: Biology 170, 225-234.
- Naz, H., Gul, S., Chaudhary, H., Munis, M., 2015. First report of *Rhizopus oryzae* causing fruit rot of *Citrus medica* L. in Pakistan. Journal of Plant Pathology 97(1), 209-220.
- Ndiaye, E., Sandeno, J., McGrath, D., Dick, R., 2000. Integrative biological indicators for detecting change in soil quality. American Journal of Alternative Agriculture 15(1), 26-36.
- Nenavathu, B.P., Kandula, S., Verma, S., 2018. Visible-light-driven photocatalytic degradation of safranin-T dye using functionalized graphene oxide nanosheet (FGS)/ZnO nanocomposites. RSC Advances 8(35), 19659-19667.
- Ngole-Jeme, V.M., Fantke, P., 2017. Ecological and human health risks associated with abandoned gold mine tailings contaminated soil. PloS one 12(2), e0172517.
- Nguyen, V.T., Vu, V.T., Nguyen, T.H., Nguyen, T.A., Tran, V.K., Nguyen-Tri, P., 2019. Antibacterial activity of TiO<sup>2</sup>-and ZnO-decorated with silver nanoparticles. Journal of Composites Science 3(2), 61.
- Nie, C., Yang, X., Niazi, N.K., Xu, X., Wen, Y., Rinklebe, J., Ok, Y.S., Xu, S., Wang, H., 2018. Impact of sugarcane bagasse-derived biochar on heavy metal availability and microbial activity: a field study. Chemosphere 200, 274-282.

- Nigam, N., Kumar, S., 2022. Contamination of water resources: With special reference to groundwater pollution. In *Current Directions in Water Scarcity Research*. Elsevier 5, 169-186.
- Nunoura, T., Wade, S.R., Bourke, J.P., Antal, M.J., 2006. Studies of the flash carbonization process. 1. Propagation of the flaming pyrolysis reaction and performance of a catalytic afterburner. *Industrial & Engineering Chemistry Research* 45(2), 585-599.
- O'Connor, D., Peng, T., Zhang, J., Tsang, D.C., Alessi, D.S., Shen, Z., Bolan, N.S., Hou, D., 2018. Biochar application for the remediation of heavy metal polluted land: a review of in situ field trials. *Science of the Total Environment* 619, 815-826.
- Omar, K., Meena, B.I., Muhammed, S.A., 2016. Study on the activity of ZnO-SnO<sub>2</sub> nanocomposite against bacteria and fungi. *Physicochemical Problems of Mineral Processing* 52(2), 754-766.
- Ong, S.T., Keng, P.S., Lee, W.N., Ha, S.T., Hung, Y.T., 2011. Dye waste treatment. *Water* 3(1), 157-176.
- Orwa, C., Mutua, A., Kindt, R., Jamnadass, R., Simons, A., 2009. *Agroforestry Database: a tree reference and selection guide. Version 4.* Agroforestry Database: a tree reference and selection guide. Version 4.
- Otomo, P.V., Owojori, O., Reinecke, S., Daniels, S., Reinecke, A., 2011. Using estimates of metal bioavailability in the soil and genetic variation of allozymes to investigate heavy metal tolerance in the earthworm *Eisenia fetida* (Oligochaeta). *Ecotoxicology and Environmental Safety* 74(7), 2070-2074.
- Oyedemi, S.O., Oyedemi, B.O., Ijeh, I.I., Ohanyerem, P.E., Cooposamy, R.M., Aiyegoro, O.A., 2017. Alpha-amylase inhibition and antioxidative capacity of some antidiabetic plants used by the traditional healers in Southeastern Nigeria. *The Scientific World Journal* 2017(3), 3592491.
- Pakistan, W., 2007. Pakistan's water at risk, water and health related issues and key recommendations. *Freshwater & Toxics Programme, Communications Division, WWF Pakistan.*
- Palansooriya, K.N., Yang, Y., Tsang, Y.F., Sarkar, B., Hou, D., Cao, X., Meers, E., Rinklebe, J., Kim, K.H., Ok, Y.S., 2020. Occurrence of contaminants in drinking water sources and the potential of biochar for water quality

- improvement: A review. *Critical Reviews in Environmental Science and Technology* 50(6), 549-611.
- Panáček, A., Kolář, M., Večeřová, R., Pucek, R., Soukupová, J., Kryštof, V., Hamal, P., Zbořil, R., Kvítek, L., 2009. Antifungal activity of silver nanoparticles against *Candida spp.* *Biomaterials* 30(31), 6333-6340.
- Pandey, V.C., 2012. Phytoremediation of heavy metals from fly ash pond by *Azolla caroliniana*. *Ecotoxicology and Environmental Safety* 82, 8-12.
- Pandhare, R.B., Sangameswaran, B., Mohite, P.B., Khanage, S.G., 2011. Antidiabetic activity of aqueous leaves extract of *Sesbania sesban* (L) Merr. in streptozotocin induced diabetic rats. *Avicenna Journal of Medical Biotechnology* 3(1), 37.
- Park, J.H., Choppala, G.K., Bolan, N.S., Chung, J.W., Chuasavathi, T., 2011. Biochar reduces the bioavailability and phytotoxicity of heavy metals. *Plant and Soil* 348, 439-451.
- Park, J.H., Cho, S.E., Kim, B.S., Shin, H.D., 2014. First report of postharvest root rot caused by *Rhizopus oryzae* on *Codonopsis lanceolata*. *Australasian Plant Disease Notes* 9(1), 1-3.
- Patel, G.M., Rohit, J.V., Singhal, R.K., Kailasa, S.K., 2015. Recognition of carbendazim fungicide in environmental samples by using 4-aminobenzenethiol functionalized silver nanoparticles as a colorimetric sensor. *Sensors and Actuators B: Chemical* 206, 684-691.
- Partovinia, A., Rasekh, B., 2018. Review of the immobilized microbial cell systems for bioremediation of petroleum hydrocarbons polluted environments. *Critical Reviews in Environmental Science and Technology* 48(1), 1-38.
- Pavlovic, I., Knez, Z., Skerget, M., 2013. Hydrothermal reactions of agricultural and food processing wastes in sub-and supercritical water: a review of fundamentals, mechanisms, and state of research. *Journal of Agricultural and Food Chemistry* 61(34), 8003-8025.
- Paz, A., Carballo, J., Pérez, M.J., Domínguez, J.M., 2017. Biological treatment of model dyes and textile wastewaters. *Chemosphere* 181, 168-177.
- Pelfrêne, A., Waterlot, C., Guerin, A., Proix, N., Richard, A., Douay, F., 2015. Use of an *in vitro* digestion method to estimate human bioaccessibility of Cd in vegetables grown in smelter-impacted soils: the influence of cooking. *Environmental Geochemistry Health* 37(4), 767-778.



- Peñuelas, J., Filella, I., Biel, C., Serrano, L., Save, R., 1993. The reflectance at the 950–970 nm region as an indicator of plant water status. *International Journal of Remote Sensing* 14(10), 1887-1905.
- Pereira, L., Dias, N., Carvalho, J., Fernandes, S., Santos, C., Lima, N., 2014. Synthesis, characterization and antifungal activity of chemically and fungal-produced silver nanoparticles against *Trichophyton rubrum*. *Journal of Applied Microbiology* 117(6), 1601-1613.
- Pietro, M., Paola, C., 2004. Thermal analysis for the evaluation of the organic matter evolution during municipal solid waste aerobic composting process. *Thermochimica Acta* 413(1-2), 209-214.
- Pooresmaeil, M., Namazi, H., 2023. Positively charged covalent organic framework modified magnetic chitosan as a smart device for efficient diclofenac sodium removal from water. *Chemical Engineering Journal* 452, 139557.
- Premarathna, K., Rajapaksha, A.U., Adassoriya, N., Sarkar, B., Sirimuthu, N.M., Cooray, A., Ok, Y.S., Vithanage, M., 2019. Clay-biochar composites for sorptive removal of tetracycline antibiotic in aqueous media. *Journal of Environmental Management* 238, 315-322.
- Priya, G., Saravanan, K., Renuka, C., 2012. Medicinal plants with potential antifertility activity-A review of sixteen years of herbal medicine research (1994-2010). *International Journal of PharmTech Research* 4(1), 481-494.
- Pudęłko, A., Postawa, P., Stachowiak, T., Malińska, K., Drózd, D., 2021. Waste derived biochar as an alternative filler in biocomposites-mechanical, thermal and morphological properties of biochar added biocomposites. *Journal of Cleaner Production* 278, 123850.
- Pueyo, M., López-Sánchez, J., Rauret, G., 2004. Assessment of CaCl<sub>2</sub>, NaNO<sub>3</sub> and NH<sub>4</sub>NO<sub>3</sub> extraction procedures for the study of Cd, Cu, Pb and Zn extractability in contaminated soils. *Analytica Chimica Acta* 504(2), 217-226.
- Qadir, A., Malik, R.N., 2011. Heavy metals in eight edible fish species from two polluted tributaries (Aik and Palkhu) of the River Chenab, Pakistan. *Biological Trace Element Research* 143(3), 1524-1540.
- Qi, F., Lamb, D., Naidu, R., Bolan, N.S., Yan, Y., Ok, Y.S., Rahman, M.M., Choppala, G., 2018. Cadmium solubility and bioavailability in soils amended with acidic and neutral biochar. *Science of the Total Environment* 610, 1457-1466.

- Qi, G., Pan, Z., Zhang, X., Miao, X., Xiang, W., Gao, B., 2022. Effect of ball milling with hydrogen peroxide or ammonia hydroxide on sorption performance of volatile organic compounds by biochar from different pyrolysis temperatures. *Chemical Engineering Journal* 450, 138027.
- Quilliam, R.S., Glanville, H.C., Wade, S.C., Jones, D.L., 2013. Life in the 'charosphere'—Does biochar in agricultural soil provide a significant habitat for microorganisms. *Soil Biology Biochemistry* 65, 287-293.
- Radich, E.J., Krenselewski, A.L., Zhu, J., Kamat, P.V., 2014. Is graphene a stable platform for photocatalysis. Mineralization of reduced graphene oxide with UV-irradiated TiO<sub>2</sub> nanoparticles. *Chemistry of Materials* 26(15), 4662-4668.
- Rajapaksha, A.U., Chen, S.S., Tsang, D.C., Zhang, M., Vithanage, M., Mandal, S., Gao, B., Bolan, N.S., Ok, Y.S.J.C., 2016. Engineered/designer biochar for contaminant removal/immobilization from soil and water: potential and implication of biochar modification. *Chemosphere* 148, 276-291.
- Ramadan, M.M., Abd-Elsalam, K.A., 2020. Micro/Nano biochar for sustainable plant health: Present status and future prospects. *Carbon Nanomaterials for Agriculture and Environmental Applications* 323-357.
- Ramakrishnan, M., Nagarajan, S., 2009. Utilization of waste biomass for the removal of basic dye from water. *World Applied Sciences Journal* 5, 114-120.
- Ranjith, R., Ravikumar, S., Pandiyan, V., Rajaji, U., Abualnaja, K.M., Alomar, T.S., AlMasoud, N., Ouladsmne, M., 2022. Synergistic photocatalytic removal of organic pollutants in the aqueous medium using TiO<sub>2</sub>-Co<sub>3</sub>O<sub>4</sub> decorated graphene oxide nanocomposite. *Journal of Materials Science: Materials in Electronics* 33, 9438–9447.
- Raul, P.K., Devi, R.R., Umlong, I.M., Banerjee, S., Singh, L., Purkait, M., 2012. Removal of fluoride from water using iron oxide-hydroxide nanoparticles. *Journal of Nanoscience and Nanotechnology* 12(5), 3922-3930.
- Raza, W., Faisal, S.M., Owais, M., Bahnemann, D., Muneer, M., 2016. Facile fabrication of highly efficient modified ZnO photocatalyst with enhanced photocatalytic, antibacterial and anticancer activity. *RSC Advances* 6(82), 78335-78350.
- Rechberger, M.V., Kloss, S., Wang, S.L., Lehmann, J., Rennhofer, H., Ottner, F., Wriessnig, K., Daudin, G., Lichtenegger, H., Soja, G., 2019. Enhanced Cu and

- Cd sorption after soil aging of woodchip-derived biochar: what were the driving factors. *Chemosphere* 216, 463-471.
- Ren, C., Yang, B., Wu, M., Xu, J., Fu, Z., Lv, Y.; Guo, T.; Zhao, Y.; Zhu, C., 2010. Synthesis of Ag/ZnO nanorods array with enhanced photocatalytic performance. *Journal of Hazardous Material* 182(1-3), 123-129.
- Rinklebe, J., Shaheen, S.M., 2015. Miscellaneous additives can enhance plant uptake and affect geochemical fractions of copper in a heavily polluted riparian grassland soil. *Ecotoxicology and Environmental Safety* 119, 58-65.
- Rinklebe, J., Shaheen, S.M., Schröter, F., Rennert, T., 2016. Exploiting biogeochemical and spectroscopic techniques to assess the geochemical distribution and release dynamics of chromium and lead in a contaminated floodplain soil. *Chemosphere* 150, 390-397.
- Rizwan, M., Ali, S., Adrees, M., Rizvi, H., Zia-ur-Rehman, M., Hannan, F., Qayyum, M.F., Hafeez, F., Ok, Y.S., 2016a. Cadmium stress in rice: toxic effects, tolerance mechanisms, and management: a critical review. *Environmental Science Pollution Research* 23, 17859-17879.
- Rizwan, M., Ali, S., Qayyum, M.F., Ibrahim, M., Zia-ur-Rehman, M., Abbas, T., Ok, Y.S., 2016b. Mechanisms of biochar-mediated alleviation of toxicity of trace elements in plants: a critical review. *Environmental Science Pollution Research* 23, 2230-2248.
- Rizwan, M., Ali, S., Hussain, A., Ali, Q., Shakoor, M.B., Zia-ur-Rehman, M., Farid, M., Asma, M., 2017. Effect of zinc-lysine on growth, yield and cadmium uptake in wheat (*Triticum aestivum* L.) and health risk assessment. *Chemosphere* 187, 35-42.
- Rizwan, M., Ali, S., Ali, B., Adrees, M., Arshad, M., Hussain, A., ur Rehman, M.Z., Waris, A.A., 2019a. Zinc and iron oxide nanoparticles improved the plant growth and reduced the oxidative stress and cadmium concentration in wheat. *Chemosphere* 214, 269-277.
- Rizwan, M., Ali, S., ur Rehman, M.Z., Adrees, M., Arshad, M., Qayyum, M.F., Ali, L., Hussain, A., Chatha, S.A.S., Imran, M., 2019b. Alleviation of cadmium accumulation in maize (*Zea mays* L.) by foliar spray of zinc oxide nanoparticles and biochar to contaminated soil. *Environmental Pollution* 248, 358-367.

- RK, L., 1999. Analysis method of soil agricultural chemistry. China Agricultural Science and Technology Press, Beijing.
- Ruby, M.V., Davis, A., Schoof, R., Eberle, S., Sellstone, C.M., 1996. Estimation of lead and arsenic bioavailability using a physiologically based extraction test. *Environmental Science Technology* 30(2), 422-430.
- Ryu, U.J., Kim, S.J., Lim, H.-K., Kim, H., Choi, K.M., Kang, J.K., 2017. Synergistic interaction of Re complex and amine functionalized multiple ligands in metal-organic frameworks for conversion of carbon dioxide. *Scientific Reports* 7(1), 1-8.
- Saedi, S., Shokri, M., Kim, J.T., Shin, G.H., 2021. Semi-transparent regenerated cellulose/ZnONP nanocomposite film as a potential antimicrobial food packaging material. *Journal of Food Engineering* 307, 110665.
- Saha, I., Kumar, G.S., 2011. Spectroscopic characterization of the interaction of phenosafranin and safranin O with double stranded, heat denatured and single stranded calf thymus DNA. *Journal of Fluorescence* 21(1), 247-255.
- Saha, S., Chakrabarty, P.K., Banerjee, K., 2022. Producing Crops without Mancozeb. Perspectives on Recent Regulatory Dilemmas and Ways Out. *ACS Agricultural Science & Technology* 2(2), 272-275.
- Sajjad, M., Ullah, I., Khan, M., Khan, J., Khan, M.Y., Qureshi, M.T., 2018. Structural and optical properties of pure and copper doped zinc oxide nanoparticles. *Results in Physics* 9, 1301-1309.
- Sajedi, H., Mohammadipanah, F., Shariat Panahi, H.K., 2018. An image analysis-aided method for redundancy reduction in differentiation of identical Actinobacterial strains. *Future Microbiology* 13(3), 313-329.
- Saleh, T.A., Adio, S.O., Asif, M., Dafalla, H., 2018. Statistical analysis of phenols adsorption on diethylenetriamine-modified activated carbon. *Journal of Cleaner Production* 182, 960-968.
- Sanakousar, F., Vidyasagar, C., Jiménez-Pérez, V., Prakash, K., 2022. Recent progress on visible-light-driven metal and non-metal doped ZnO nanostructures for photocatalytic degradation of organic pollutants. *Materials Science in Semiconductor Processing* 140, 106390.
- Sánchez-Olmos, L., Sánchez-Cárdenas, M., Sathish-Kumar, K., Tirado-González, D., Rodríguez-Valadez, F., 2020. Sulfonated rim rubber used as a solid catalyst for

- the biodiesel production with oleic acid and optimized by Box-Behnken method. *Revista Mexicana De Ingeniería Química* 19, 429-444.
- Saravanan, R., Karthikeyan, S., Gupta, V., Sekaran, G., Narayanan, V., Stephen, A., 2013. Enhanced photocatalytic activity of ZnO/CuO nanocomposite for the degradation of textile dye on visible light illumination. *Materials Science Engineering* 33(1), 91-98.
- Sawai, J., Kawada, E., Kanou, F., Igarashi, H., Hashimoto, A., Kokugan, T., Shimizu, M., 1996. Detection of active oxygen generated from ceramic powders having antibacterial activity. *Journal of Chemical Engineering of Japan* 29(4), 627-633.
- Sawai, J., Yoshikawa, T., 2004. Quantitative evaluation of antifungal activity of metallic oxide powders (MgO, CaO and ZnO) by an indirect conductimetric assay. *Journal of Applied Microbiology* 96(4), 803-809.
- Schmitz, N., Laverty, S., Kraus, V., Aigner, T., 2010. Basic methods in histopathology of joint tissues. *Osteoarthritis and Cartilage* 18(3), 113-116.
- Selvarajoo, A., Oochit, D., 2020. Effect of pyrolysis temperature on product yields of palm fibre and its biochar characteristics. *Materials Science for Energy Technologies* 170(3), 575-583.
- Sellaoui, L., Mendoza-Castillo, D.I., Reynel-Ávila, H.E., Bonilla-Petriciolet, A., Lamine, A.B., Erto, A., 2018. A new statistical physics model for the ternary adsorption of  $\text{Cu}^{2+}$ ,  $\text{Cd}^{2+}$  and  $\text{Zn}^{2+}$  ions on bone char: experimental investigation and simulations. *Chemical Engineering Journal* 343, 544-553.
- Setia, R., Dhaliwal, S.S., Kumar, V., Singh, R., Kukal, S.S., Pateriya, B., 2020. Impact assessment of metal contamination in surface water of Sutlej River (India) on human health risks. *Environmental Pollution* 265, 114907.
- Sewu, D.D., Boakye, P., Woo, S.H., 2017. Highly efficient adsorption of cationic dye by biochar produced with Korean cabbage waste. *Bioresource Technology* 224, 206-213.
- Shn Moorthy, N., Ramos, M.J., Fernandes, P.A., 2012. Studies on  $\alpha$ -glucosidase inhibitors development: magic molecules for the treatment of carbohydrate mediated diseases. *Mini reviews in medicinal chemistry* 12(8), 713-720.
- Shafaghat, H., Rezaei, P.S., Daud, W.M.A.W., 2016. Catalytic hydrodeoxygenation of simulated phenolic bio-oil to cycloalkanes and aromatic hydrocarbons over

- bifunctional metal/acid catalysts of Ni/HBeta, Fe/HBeta and NiFe/HBeta. *Journal of Industrial and Engineering Chemistry* 35, 268-276.
- Shah, K., Patel, S., Halder, P., Kundu, S., Marzbali, M.H., Hakeem, I.G., Pramanik, B.K., Chiang, K., Patel, T., 2022. Conversion of pyrolytic non-condensable gases from polypropylene co-polymer into bamboo-type carbon nanotubes and high-quality oil using biochar as catalyst. *Journal of Environmental Management* 301, 113791.
- Shaik, F., Kumar, A., 2017. ZnO nanoparticles and their acarbose-capped nanohybrids as inhibitors for human salivary amylase. *IET nanobiotechnology* 11(3), 329-335.
- Shanmugam, R., Subramaniam, R., Kathirason, S.G., Ali, D., Balusamy, S.R., Gurusamy, A., Arunachalam, K., Sellami, H., 2021. Curcumin-chitosan nanocomposite formulation containing *Pongamia pinnata*-mediated silver nanoparticles, wound pathogen control, and anti-inflammatory potential. *BioMed Research International* 2021(3), 1-10.
- Shen, Y., 2015. Chars as carbonaceous adsorbents/catalysts for tar elimination during biomass pyrolysis or gasification. *Renewable and Sustainable Energy Reviews* 43, 281-295.
- Shen, Z., Chen, Y., Xu, D., Li, L., Zhu, Y., 2020. Interactions between heavy metals and other mineral elements from soil to medicinal plant Fengdan (*Paeonia ostii*) in a copper mining area, China. *Environmental Science and Pollution Research* 27(27), 33743-33752.
- Sial, R., Chaudhary, M., Abbas, S., Latif, M., Khan, A., 2006. Quality of effluents from Hattar industrial estate. *Journal of Zhejiang University Science* 7(12), 974-980.
- Silvestri, S., Goncalves, M.G., da Silva Veiga, P.A., da Silva Matos, T.T., Peralta-Zamora, P., Mangrich, A.S., 2019. TiO<sub>2</sub> supported on *Salvinia molesta* biochar for heterogeneous photocatalytic degradation of Acid Orange 7 dye. *Journal of Environmental Chemical Engineering* 7(1), 102879.
- Singh, K.K., Chen, G., McCarter, J.B., Meentemeyer, R.K., 2015. Effects of LiDAR point density and landscape context on estimates of urban forest biomass. *ISPRS Journal of Photogrammetry and Remote Sensing* 101, 310-322.

- Singh, P., Kim, Y.J., Zhang, D., Yang, D.C., 2016a. Biological synthesis of nanoparticles from plants and microorganisms. *Trends in Biotechnology* 34(7), 588-599.
- Singh, S., Singh, N., Kumar, V., Datta, S., Wani, A.B., Singh, D., Singh, K., Singh, J., 2016b. Toxicity, monitoring and biodegradation of the fungicide carbendazim. *Environmental Chemistry Letters* 14(3), 317-329.
- Singh, R.P., Jha, P.N., 2017. The PGPR *Stenotrophomonas maltophilia* SBP-9 augments resistance against biotic and abiotic stress in wheat plants. *Frontiers in Microbiology* 8, 1945.
- Sipos, P., Tóth, A., Kis, V.K., Balázs, R., Kovács, I., Németh, T., 2019. Partition of Cd, Cu, Pb and Zn among mineral particles during their sorption in soils. *Journal of Soils Sediments* 19, 1775-1787.
- Sirakov, B., 2009. Some estimates and maximum principles for weakly coupled systems of elliptic PDE. *Nonlinear Analysis, Theory, Methods and Applications* 70(8), 3039-3046.
- Sokhal, G.S., Gangacharyulu, D., Bulasara, V.K., 2018. Influence of copper oxide nanoparticles on the thermophysical properties and performance of flat tube of vehicle cooling system. *Vacuum* 157, 268-276.
- Solaymani, E., Ghaedi, M., Karimi, H., Ahmadi Azqhandi, M.H., Asfaram, A., 2017. Intensified removal of Malachite green by AgOH-AC nanoparticles combined with ultrasound: Modeling and optimization. *Applied Organometallic Chemistry* 31(12), 3857.
- Song, J., Zhou, J., Wang, Z.L., 2006. Piezoelectric and semiconducting coupled power generating process of a single ZnO belt/wire. A technology for harvesting electricity from the environment. *Nano Letters* 6(8), 1656-1662.
- Song, J.Y., Kim, B.S., 2009. Rapid biological synthesis of silver nanoparticles using plant leaf extracts. *Bioprocess and Biosystems Engineering* 32(1), 79-84.
- Song, W.J., Jeong, M.S., Choi, D.M., Kim, K.N., Wie, M.B., 2019. Zinc oxide nanoparticles induce autophagy and apoptosis via oxidative injury and pro-inflammatory cytokines in primary astrocyte cultures. *Nanomaterials* 9(7), 1043.
- Song, C., Chen, K., Chen, M., Jin, X., Liu, G., Du, X., Chen, D., Huang, Q., 2022. Sequential combined adsorption and solid-phase photocatalysis to remove

- aqueous organic pollutants by H<sub>3</sub>PO<sub>4</sub>-modified TiO<sub>2</sub> nanoparticles anchored on biochar. *Journal of Water Process Engineering* 45, 102467.
- Sriram, S., Lalithambika, K., Thayumanavan, A., 2017. Experimental and theoretical investigations of photocatalytic activity of Cu doped ZnO nanoparticles. *Optik* 139, 299-308.
- Srivastav, A., Ganjewala, D., Singhal, R.K., Rajput, V.D., Minkina, T., Voloshina, M., Srivastav, S., Shrivastava, M., 2021. Effect of ZnO Nanoparticles on Growth and Biochemical Responses of Wheat and Maize. *Plants* 10(12), 2556.
- Stocks-Fischer, S., Galinat, J.K., Bang, S.S., 1999. Microbiological precipitation of CaCO<sub>3</sub>. *Soil Biology and Biochemistry* 31(11), 1563-1571.
- Sturikova, H., Krystofova, O., Huska, D., Adam, V., 2018. Zinc, zinc nanoparticles and plants. *Journal of Hazardous Materials* 349, 101-110.
- Sun, L., Wan, S., Yuan, D., Yu, Z., 2019. Adsorption of nitroimidazole antibiotics from aqueous solutions on self-shaping porous biomass carbon foam pellets derived from *Vallisneria natans* waste as a new adsorbent. *The Science of the Total Environment* 664, 24-36.
- Tabatabai, M. A., & Bremner, J. M. (1972). Assay of urease activity in soils. *Soil biology and Biochemistry*, 4(4), 479-487.
- Takaya, C., Fletcher, L., Singh, S., Anyikude, K., Ross, A., 2016. Phosphate and ammonium sorption capacity of biochar and hydrochar from different wastes. *Chemosphere* 145, 518-527.
- Talhok, R., Karam, C., Fostok, S., El-Jouni, W., Barbour, E., 2007. Anti-inflammatory bioactivities in plant extracts. *Journal of Medicinal Food* 10(1), 1-10.
- Tamer, T.M., Alsehli, M.H., Omer, A.M., Afifi, T.H., Sabet, M.M., Mohy-Eldin, M.S., Hassan, M.A., 2021. Development of polyvinyl alcohol/kaolin sponges stimulated by marjoram as hemostatic, antibacterial, and antioxidant dressings for wound healing promotion. *International Journal of Molecular Sciences* 22(23), 13050.
- Tan, X.F., Liu, Y.G., Gu, Y.L., Xu, Y., Zeng, G.M., Hu, X.J., Liu, S.B., Wang, X., Liu, S.M., Li, J., 2016. Biochar-based nano-composites for the decontamination of wastewater: a review. *Bioresource Technology* 212, 318-333.



- Teo, E.Y.L., Muniandy, L., Ng, E.P., Adam, F., Mohamed, A.R., Jose, R., Chong, K.F., 2016. High surface area activated carbon from rice husk as a high performance supercapacitor electrode. *Electrochimica Acta* 192, 110-119.
- Tessier, A., Campbell, P.G., Bisson, M., 1979. Sequential extraction procedure for the speciation of particulate trace metals. *Analytical Chemistry* 51(7), 844-851.
- Thaya, R., Malaikozhundan, B., Vijayakumar, S., Sivakamavalli, J., Jeyasekar, R., Shanthi, S., Vaseeharan, B., Ramasamy, P., Sonawane, A., 2016. Chitosan coated Ag/ZnO nanocomposite and their antibiofilm, antifungal and cytotoxic effects on murine macrophages. *Microbial Pathogenesis* 100, 124-132.
- Tripathi, D.K., Singh, V.P., Prasad, S.M., Chauhan, D.K., Dubey, N.K., 2015. Silicon nanoparticles (SiNp) alleviate chromium (VI) phytotoxicity in *Pisum sativum* (L.) seedlings. *Plant Physiology Biochemistry* 96, 189-198.
- Tripathi, M., Sahu, J.N., Ganesan, P., 2016. Effect of process parameters on production of biochar from biomass waste through pyrolysis: A review. *Renewable and Sustainable Energy Reviews* 55, 467-481.
- Tu, C., Guan, F., Sun, Y., Guo, P., Liu, Y., Li, L., Scheckel, K.G., Luo, Y., 2018. Stabilizing effects on a Cd polluted coastal wetland soil using calcium polysulphide. *Geoderma* 332, 190-197.
- Tu, C., Wei, J., Guan, F., Liu, Y., Sun, Y., Luo, Y., 2020. Biochar and bacteria inoculated biochar enhanced Cd and Cu immobilization and enzymatic activity in a polluted soil. *Environment International* 137, 105576.
- Tulkova, E., Kabashnikova, L., 2022. Malondialdehyde content in the leaves of small-leaved linden *tilia cordata* and Norway maple *acer platanoides* under the influence of volatile organic compounds. *Plant Biosystems* 156(3), 619-627.
- Ul-Haq, I., Ullah, N., Bibi, G., Kanwal, S., Ahmad, M.S., Mirza, B., 2012. Antioxidant and cytotoxic activities and phytochemical analysis of *Euphorbia wallichii* root extract and its fractions. *Iranian Journal of Pharmaceutical Research* 11(1), 241-249.
- Varun, M., Ogunkunle, C.O., D'Souza, R., Favas, P., Paul, M., 2017. Identification of *Sesbania sesban* (L.) Merr. as an efficient and well adapted phytoremediation tool for Cd polluted soils. *Bulletin of Environmental Contamination and Toxicology* 98(6), 867-873.

- Venkatachalam, P., Jayaraj, M., Manikandan, R., Geetha, N., Rene, E.R., Sharma, N., Sahi, S., 2017. Zinc oxide nanoparticles (ZnONPs) alleviate heavy metal-induced toxicity in *Leucaena leucocephala* seedlings: a physiochemical analysis. *Plant Physiology Biochemistry* 110, 59-69.
- Versantvoort, C.H., Oomen, A.G., Van de Kamp, E., Rompelberg, C.J., Sips, A.J., 2005. Applicability of an in vitro digestion model in assessing the bioaccessibility of mycotoxins from food. *Food Chemical Toxicology* 43(1), 31-40.
- Vetter, J., Steinberg, M., Nelson, A., 1958. Enzyme assay, quantitative determination of peroxidase in sweet corn. *Journal of Agricultural and Food Chemistry* 6(1), 39-41.
- Vickers, N.J., 2017. Animal communication: when i'm calling you, will you answer too? *Current Biology* 27(14), 713-715.
- Walkley, A., Black, I.A., 1934. An examination of the Degtjareff method for determining soil organic matter, and a proposed modification of the chromic acid titration method. *Soil Science* 37(1), 29-38.
- Wang, Z.L., 2004. Functional oxide nanobelts: materials, properties and potential applications in nanosystems and biotechnology. *Annual Review of Physical Chemistry* 55, 159-196.
- Wang, R., Gao, B., Chen, S., Ma, J., Li, X., Xue, C., 2017. First Report of *Rhizopus oryzae* Causing Soft Rot on Storage Roots of Sweetpotato in China. *Plant Disease* 101(6), 1039.
- Wang, S., Zhou, Y., Han, S., Wang, N., Yin, W., Yin, X., Gao, B., Wang, X., Wang, J.J.C., 2018. Carboxymethyl cellulose stabilized ZnO/biochar nanocomposites: Enhanced adsorption and inhibited photocatalytic degradation of methylene blue. *Chemosphere* 197, 20-25.
- Wang, H., Xu, C., Luo, Z.C., Zhu, H.H., Wang, S., Zhu, Q.H., Huang, D.Y., Zhang, Y.Z., Xiong, J., He, Y.B., 2018. Foliar application of Zn can reduce Cd concentrations in rice (*Oryza sativa* L.) under field conditions. *Environmental Science Pollution Research* 25, 29287-29294.
- Wang, C., Huang, R., Sun, R., Yang, J., Sillanpaa, M., 2021. A review on Persulfates activation by functional biochar for organic contaminants removal: Synthesis,

- characterizations, radical determination, and mechanism. *Journal of Environmental Chemical Engineering*, 9(5), 106267.
- Wei, B., Yang, L., 2010. A review of heavy metal contaminations in urban soils, urban road dusts and agricultural soils from China. *Microchemical Journal* 94(2), 99-107.
- Wei, J., Tu, C., Yuan, G., Bi, D., Wang, H., Zhang, L., Theng, B.K., 2019. Pyrolysis temperature-dependent changes in the characteristics of biochar-borne dissolved organic matter and its copper binding properties. *Bulletin of Environmental Contamination Toxicology* 103(1), 169-174.
- White, T.J., Bruns, T., Lee, S., Taylor, J., 1990. Amplification and direct sequencing of fungal ribosomal RNA genes for phylogenetics. *PCR Protocols: A Guide to Methods and Applications* 18(1), 315-322.
- Williams, J., Clarkson, J.M., Mills, P.R., Cooper, R.M., 2003. Saprotrophic and mycoparasitic components of aggressiveness of *Trichoderma harzianum* groups toward the commercial mushroom *Agaricus bisporus*. *Applied and Environmental Microbiology* 69(7), 4192-4199.
- Wink, J., Mohammadipanah, F., Hamed, J., 2017. *Biology and biotechnology of actinobacteria*. Springer. Cham, Switzerland, Springer International Publishing.
- Wragg, J., Cave, M., Basta, N., Brandon, E., Casteel, S., Denys, S., Gron, C., Oomen, A., Reimer, K., Tack, K., 2011. An inter-laboratory trial of the unified Barge bioaccessibility method for arsenic, cadmium and lead in soil. *Science of the Total Environment* 409(19), 4016-4030.
- Wu, J., Zhao, Y., Qi, H., Zhao, X., Yang, T., Du, Y., Zhang, H., Wei, Z., 2017. Identifying the key factors that affect the formation of humic substance during different materials composting. *Bioresource Technology* 244, 1193-1196.
- Wu, B., Wang, Z., Zhao, Y., Gu, Y., Wang, Y., Yu, J., Xu, H., 2019. The performance of biochar-microbe multiple biochemical material on bioremediation and soil micro-ecology in the cadmium aged soil. *Science of the Total Environment* 686, 719-728.
- Xu, Z., Yu, G., Zhang, X., He, N., Wang, Q., Wang, S., Wang, R., Zhao, N., Jia, Y., Wang, C., 2017. Soil enzyme activity and stoichiometry in forest ecosystems along the North-South Transect in eastern China (NSTEC). *Soil Biology Biochemistry* 104, 152-163.

- Xu, X., Zheng, Y., Gao, B., Cao, X., 2019. N-doped biochar synthesized by a facile ball-milling method for enhanced sorption of CO<sub>2</sub> and reactive red. *Chemical Engineering Journal* 368, 564-572.
- Yang, X., Liu, J., McGrouther, K., Huang, H., Lu, K., Guo, X., He, L., Lin, X., Che, L., Ye, Z., 2016. Effect of biochar on the extractability of heavy metals (Cd, Cu, Pb, and Zn) and enzyme activity in soil. *Environmental Science Pollution Research* 23, 974-984.
- Yang, Q., Li, Z., Lu, X., Duan, Q., Huang, L., Bi, J., 2018. A review of soil heavy metal pollution from industrial and agricultural regions in China: Pollution and risk assessment. *Science of the Total Environment* 642, 690-700.
- Yang, B., Zhang, M., Wu, M., Zhang, H., Song, Q., Yu, S., 2019. Synthesis of biochar-based Cu<sub>2</sub>O nanoparticles and their antibacterial activity against *Escherichia coli*. *Inorganic Nano-Metal Chemistry* 49(1), 12-16.
- Yao, Y., Zhang, Y., Gao, B., Chen, R., Wu, F., 2018. Removal of sulfamethoxazole (SMX) and sulfapyridine (SPY) from aqueous solutions by biochars derived from anaerobically digested bagasse. *Environmental Science and Pollution Research* 25(26), 25659-25667.
- Yari, K., Seidmohammadi, A., Khazaei, M., Bhatnagar, A., Leili, M., Engineering, 2019. A comparative study for the removal of imidacloprid insecticide from water by chemical-less UVC, UVC/TiO<sub>2</sub> and UVC/ZnO processes. *Journal of Environmental Health Science and Engineering* 17(1), 337-351.
- Ye, S., Zeng, G., Wu, H., Liang, J., Zhang, C., Dai, J., Xiong, W., Song, B., Wu, S., Yu, J., 2019. The effects of activated biochar addition on remediation efficiency of co-composting with contaminated wetland soil. *Resources, Conservation and Recycling* 140, 278-285.
- Yi, G.C., Wang, C., Park, W.I., 2005. ZnO nanorods: synthesis, characterization and applications. *Semiconductor Science and Technology* 20(20), 22-34.
- Yoo, J.C., Beiyuan, J., Wang, L., Tsang, D.C., Baek, K., Bolan, N.S., Ok, Y.S., Li, X.D., 2018. A combination of ferric nitrate/EDDS-enhanced washing and sludge-derived biochar stabilization of metal-contaminated soils. *Science of the Total Environment* 616, 572-582.
- Youssef, A.M., El-Sayed, S.M., El-Sayed, H.S., Salama, H.H., Assem, F.M., Abd El-Salam, M.H., 2018. Novel bionanocomposite materials used for packaging

- skimmed milk acid coagulated cheese (Karish). *International Journal of Biological Macromolecules* 115, 1002-1011.
- Yu, F., Zhou, Y., Gao, B., Qiao, H., Li, Y., Wang, E., Pang, L., Bao, C., 2016. Effective removal of ionic liquid using modified biochar and its biological effects. *Journal of the Taiwan Institute of Chemical Engineers* 67, 318-324.
- Yu, F., Tian, F., Zou, H., Ye, Z., Peng, C., Huang, J., Zheng, Y., Zhang, Y., Yang, Y., Wei, X., 2021. ZnO/biochar nanocomposites via solvent free ball milling for enhanced adsorption and photocatalytic degradation of methylene blue. *Journal of Hazardous Materials* 415, 125511.
- Yuan, J.H., Xu, R.K., Zhang, H., 2011. The forms of alkalis in the biochar produced from crop residues at different temperatures. *Bioresource Technology* 102(3), 3488-3497.
- Zafar, S., Aqil, F., Ahmad, I., 2007. Metal tolerance and biosorption potential of filamentous fungi isolated from metal contaminated agricultural soil. *Bioresource Technology* 98(13), 2557-2561.
- Zafar, N., Madni, A., Khalid, A., Khan, T., Kousar, R., Naz, S.S., Wahid, F., 2020. Pharmaceutical and biomedical applications of green synthesized metal and metal oxide nanoparticles. *Current Pharmaceutical Design* 26(45), 5844-5865.
- Zhang, Q., Chang, J., Wang, T., Xu, Y., 2007. Review of biomass pyrolysis oil properties and upgrading research. *Energy Conversion and Management* 48(1), 87-92.
- Zhang, Y., Zhang, N., Tang, Z.R., Xu, Y.J., 2012. Graphene transforms wide band gap ZnS to a visible light photocatalyst. The new role of graphene as a macromolecular photosensitizer. *ACS Nano* 6(11), 9777-9789.
- Zhang, X., Yao, Z., Zhao, S., Xie, H., Yang, M., 2013. Rizopus Stem Rot of *Orobanche aegyptiaca* caused by *Rizopus oryzae* in China. *Journal of Phytopathology* 161(10), 745-748.
- Zhang, L.J., Yang, M.Y., Sun, Z.H., Tan, C.X., Weng, J.Q., Wu, H.K., Liu, X.H., 2014a. Synthesis and antifungal activity of 1, 3, 4-thiadiazole derivatives containing pyridine group. *Letters in Drug Design Discovery* 11(9), 1107-1111.
- Zhang, Y., Chang, T.R., Zhou, B., Cui, Y.T., Yan, H., Liu, Z., Schmitt, F., Lee, J., Moore, R., Chen, Y., 2014b. Direct observation of the transition from indirect

- to direct bandgap in atomically thin epitaxial MoSe<sub>2</sub>. *Nature Nanotechnology* 9(2), 111-115.
- Zhang, J., Liu, J., Liu, R., 2015a. Effects of pyrolysis temperature and heating time on biochar obtained from the pyrolysis of straw and lignosulfonate. *Bioresource Technology* 176, 288-291.
- Zhang, X., Qin, J., Hao, R., Wang, L., Shen, X., Yu, R., Limpanart, S., Ma, M., Liu, R., 2015b. Carbon-doped ZnO nanostructures: facile synthesis and visible light photocatalytic applications. *The Journal of Physical Chemistry C* 119(35), 20544-20554.
- Zhang, X.F., Liu, Z.G., Shen, W., Gurunathan, S., 2016. Silver nanoparticles: synthesis, characterization, properties, applications, and therapeutic approaches. *International Journal of Molecular Sciences* 17(9), 1534.
- Zhang, A., Li, X., Xing, J., Xu, G., 2020. Adsorption of potentially toxic elements in water by modified biochar: A review. *Journal of Environmental Chemical Engineering* 8(4), 104196.
- Zheng, H., Wang, Z., Deng, X., Herbert, S., Xing, B., 2013. Impacts of adding biochar on nitrogen retention and bioavailability in agricultural soil. *Geoderma* 206, 32-39.
- Zhong, J.B., Li, J.Z., Lu, Y., He, X.Y., Zeng, J., Hu, W., Shen, Y.C., 2012. Fabrication of Bi<sup>3+</sup>-doped ZnO with enhanced photocatalytic performance. *Applied Surface Science* 258(11), 4929-4933.
- Zhong, M.S., Jiang, L., 2017. Refining health risk assessment by incorporating site-specific background concentration and bioaccessibility data of Nickel in soil. *Science of the Total Environment* 581, 866-873.
- Zhou, Y., Liu, X., Xiang, Y., Wang, P., Zhang, J., Zhang, F., Wei, J., Luo, L., Lei, M., Tang, L., 2017. Modification of biochar derived from sawdust and its application in removal of tetracycline and copper from aqueous solution: adsorption mechanism and modelling. *Bioresource Technology* 245, 266-273.
- Zhou, Y., Cheng, G., Chen, K., Lu, J., Lei, J., Pu, S., 2019. Adsorptive removal of bisphenol A, chloroxylenol, and carbamazepine from water using a novel  $\beta$ -cyclodextrin polymer. *Ecotoxicology and Environmental Safety* 170, 278-285.

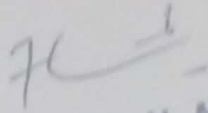
Zhu, X., Chen, B., Zhu, L., Xing, B., 2017. Effects and mechanisms of biochar-microbe interactions in soil improvement and pollution remediation: a review. *Environmental Pollution* 227, 98-115.

# Turnitin Originality Report

Photocatalytic and Biological Activities of Engineered Maize Biochar to Remove Aqueous Pollutants,  
Immobilize Soil Metals and Improve Plant Growth by Asif Kamal.

From PhD (PhD DRSMML)

- Processed on 10-Jul-2023 11:44 PKT
- ID: 2128983483
- Word Count: 32390

  
Dr. M. Farooq H. Munis  
Professor  
Department of Plant Sciences  
Quaid-i-Azam University  
Islamabad, PAKISTAN

Similarity Index

13%

Similarity by Source

Internet Sources:

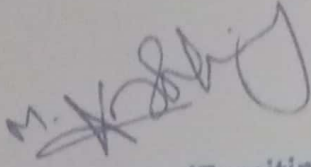
8%

Publications:

10%

Student Papers:

2%

  
Focal Person (Turnitin)  
Quaid-i-Azam University  
Islamabad

## sources:

- 1 2% match (Chen Tu, Jing Wei, Feng Guan, Ying Liu, Yuhuan Sun, Yongming Luo. "Biochar and bacteria inoculated biochar enhanced Cd and Cu immobilization and enzymatic activity in a polluted soil", Environment International, 2020)  
Chen Tu, Jing Wei, Feng Guan, Ying Liu, Yuhuan Sun, Yongming Luo. "Biochar and bacteria inoculated biochar enhanced Cd and Cu immobilization and enzymatic activity in a polluted soil". Environment International, 2020
- 2 1% match (Internet from 16-Feb-2023)  
<https://www.researchgate.net/publication/232738022> Realization of an efficient cholesterol biosensor using ZnO nanostructured thin film
- 3 1% match (Jemal Fito, Kebede K. Kefeni, Thabo T.I. Nkambule. "The potential of biochar-photocatalytic nanocomposites for removal of organic micropollutants from wastewater", Science of The Total Environment, 2022)  
Jemal Fito, Kebede K. Kefeni, Thabo T.I. Nkambule. "The potential of biochar-photocatalytic nanocomposites for removal of organic micropollutants from wastewater". Science of The Total Environment, 2022
- 4 < 1% match (Chen Tu, Jing Wei, Feng Guan, Ying Liu, Yuhuan Sun, Yongming Luo. "Biochar and bacteria inoculated biochar enhanced Cd and Cu immobilization and enzymatic activity in a polluted soil", Environment International, 2020)  
Chen Tu, Jing Wei, Feng Guan, Ying Liu, Yuhuan Sun, Yongming Luo. "Biochar and bacteria inoculated biochar enhanced Cd and Cu immobilization and enzymatic activity in a polluted soil". Environment International, 2020
- 5 < 1% match (Internet from 17-Sep-2022)  
[https://www.researchgate.net/figure/SEM-images-of-pure-biochar-a-and-MB-ZnO-nanocomposite-b-fig9\\_358873714](https://www.researchgate.net/figure/SEM-images-of-pure-biochar-a-and-MB-ZnO-nanocomposite-b-fig9_358873714)
- 6 < 1% match (Internet from 17-Sep-2022)  
[https://www.researchgate.net/figure/Thermogravimetric-analysis-of-pristine-biochar-a-and-MB-ZnO-nanocomposites-b-fig4\\_358873714](https://www.researchgate.net/figure/Thermogravimetric-analysis-of-pristine-biochar-a-and-MB-ZnO-nanocomposites-b-fig4_358873714)





ORIGINAL ARTICLE

# Ball-milled synthesis of maize biochar-ZnO nanocomposite (MB-ZnO) and estimation of its photocatalytic ability against different organic and inorganic pollutants



Asif Kamal<sup>a</sup>, Muhammad Hamzah Saleem<sup>b</sup>, Huda Alshaya<sup>c</sup>, Mohammad K. Okla<sup>d</sup>, Hassan Javed Chaudhary<sup>a</sup>, Muhammad Farooq Hussain Munis<sup>a,\*</sup>

<sup>a</sup> Department of Plant Sciences, Faculty of Biological Sciences, Quaid-i-Azam University, Islamabad 45320, Pakistan

<sup>b</sup> College of Plant Science and Technology, Huazhong Agricultural University, Wuhan 430070, China

<sup>c</sup> Cell and Molecular Biology Program, University of Arkansas, Fayetteville, NC 72701, USA

<sup>d</sup> Botany and Microbiology Department, College of Science, King Saud University, Riyadh 11451, Saudi Arabia

Received 18 November 2021; revised 17 February 2022; accepted 20 February 2022

Available online 25 February 2022

## KEYWORDS

Biochar-ZnO;  
Ball-milled;  
Photocatalysis;  
Safranin;  
Mancozeb

**Abstract** Different industrial and agricultural practices release a variety of dyes and pesticides in soil and water. Degradation of these pollutants is very important to avoid health and environmental issues. In this study, the photocatalysis technique has been optimized and adopted to degrade organic and inorganic pollutants. First of all, biochar with distinctive physicochemical properties, like high specific surface, highly carbonaceous property, and the electron-conductive nature was prepared in a vacuum furnace from maize straw. These properties depicted the effective absorbance ability of prepared biochar. Using a solvent-free ball-milling method, ZnO loaded maize biochar nanocomposite (MB-ZnO) was synthesized from this biochar and used as a photocatalyst to degrade aqueous pollutants, under different light sources. The adsorption and photocatalytic activity of MB-ZnO was assessed against Safranin O (Saf) and Mancozeb (MC) within a closed system using different light conditions including dark, UV and visible light. To understand the mechanism of Saf and MC removal from aqueous solution, reaction kinetics was calculated according to the pseudo-first-order kinetic model. MB-ZnO composite exhibited variable photocatalytic performances to degrade Saf under visible light (83.5%), UV radiations (81.0%) and dark conditions (78%) in 60 min. Similarly, maximum MC degradation by MB-ZnO nanocomposite was exhibited

\* Corresponding author.

E-mail addresses: [kamal@bs.qau.edu.pk](mailto:kamal@bs.qau.edu.pk) (A. Kamal), [saleemhamza312@webmail.hzau.edu.cn](mailto:saleemhamza312@webmail.hzau.edu.cn) (M.H. Saleem), [hmalshay@uark.edu](mailto:hmalshay@uark.edu) (H. Alshaya), [Malokla@ksu.edu.sa](mailto:Malokla@ksu.edu.sa) (M.K. Okla), [munis@qau.edu.pk](mailto:munis@qau.edu.pk) (M.F.H. Munis).

Peer review under responsibility of King Saud University.



## Article

# Biological Applications of Ball-Milled Synthesized Biochar-Zinc Oxide Nanocomposite Using *Zea mays* L.

Asif Kamal <sup>1</sup>, Urooj Haroon <sup>1</sup>, Hakim Manghwar <sup>2</sup>, Khalid H. Alamer <sup>3</sup>, Ibtisam M. Alsudays <sup>4</sup>, Ashwaq T. Althobaiti <sup>5</sup>, Anila Iqbal <sup>6</sup>, Mahnoor Akbar <sup>1</sup>, Farhana <sup>1</sup>, Maryam Anar <sup>1</sup>, Moona Nazish <sup>7</sup>, Hassan Javed Chaudhary <sup>1</sup> and Muhammad Farooq Hussain Munis <sup>1,\*</sup>

<sup>1</sup> Department of Plant Sciences, Faculty of Biological Sciences, Quaid-i-Azam University, Islamabad 45320, Pakistan

<sup>2</sup> Lushan Botanical Garden, Chinese Academy of Sciences, Jiujiang 332000, China

<sup>3</sup> Biological Sciences Department, Faculty of Science and Arts, King Abdulaziz University, Rabigh 21911, Saudi Arabia

<sup>4</sup> Department of Biology, College of Science and Arts, Qassim University, Unaizah 56452, Saudi Arabia

<sup>5</sup> Department of Biology, College of Science, Taif University, P.O. Box 11099, Taif 21944, Saudi Arabia

<sup>6</sup> National Center for Physics, Quaid-i-Azam University Islamabad Campus, Shahdra Valley Road, Islamabad 45320, Pakistan

<sup>7</sup> Department of Botany, Faculty of Biological Sciences, Rawalpindi Women University, Rawalpindi 46000, Pakistan

\* Correspondence: munis@qau.edu.pk; Tel.: +92-341-2005434



**Citation:** Kamal, A.; Haroon, U.; Manghwar, H.; Alamer, K.H.; Alsudays, I.M.; Althobaiti, A.T.; Iqbal, A.; Akbar, M.; Farhana; Anar, M.; et al. Biological Applications of Ball-Milled Synthesized Biochar-Zinc Oxide Nanocomposite Using *Zea mays* L. *Molecules* **2022**, *27*, 5333. <https://doi.org/10.3390/molecules27165333>

Academic Editor: Artur J. M. Valente

Received: 27 July 2022

Accepted: 15 August 2022

Published: 22 August 2022

**Publisher's Note:** MDPI stays neutral with regard to jurisdictional claims in published maps and institutional affiliations.



**Copyright:** © 2022 by the authors. Licensee MDPI, Basel, Switzerland. This article is an open access article distributed under the terms and conditions of the Creative Commons Attribution (CC BY) license (<https://creativecommons.org/licenses/by/4.0/>).

**Abstract:** Nanotechnology is one of the vital and quickly developing areas and has several uses in various commercial zones. Among the various types of metal oxide-based nanoparticles, zinc oxide nanoparticles (ZnO NPs) are frequently used because of their effective properties. The ZnO nanocomposites are risk-free and biodegradable biopolymers, and they are widely being applied in the biomedical and therapeutics fields. In the current study, the biochar-zinc oxide (MB-ZnO) nanocomposites were prepared using a solvent-free ball-milling technique. The prepared MB-ZnO nanocomposites were characterized through scanning electron microscopy (SEM), energy-dispersive X-ray (EDX) *spectroscopy*, X-ray powder diffraction (XRD), and thermogravimetric analysis (TGA), Fourier-transform infrared spectroscopy (FTIR), and ultraviolet–visible (UV) spectroscopy. The MB-ZnO particles were measured as 43 nm via the X-ray line broadening technique by applying the Scherrer equation at the highest peak of 36.36°. The FTIR spectroscopy results confirmed MB-ZnO's formation. The band gap energy gap values of the MB-ZnO nanocomposites were calculated as 2.77 eV by using UV–Vis spectra. The MB-ZnO nanocomposites were tested in various *in vitro* biological assays, including biocompatibility assays against the macrophages and RBCs and the enzymes' inhibition potential assay against the protein kinase, alpha-amylase, cytotoxicity assays of the leishmanial parasites, anti-inflammatory activity, antifungal activity, and antioxidant activities. The maximum TAC (30.09%), TRP (36.29%), and DPPH radicals' scavenging potential (49.19%) were determined at the maximum dose of 200 µg/mL. Similarly, the maximum activity at the highest dose for the anti-inflammatory (76%), at 1000 µg/mL, alpha-amylase inhibition potential (45%), at 1000 µg/mL, antileishmanial activity (68%), at 100 µg/mL, and antifungal activity (73 ± 2.1%), at 19 mg/mL, was perceived, respectively. It did not cause any potential harm during the biocompatibility and cytotoxic assay and performed better during the anti-inflammatory and antioxidant assay. MB-ZnO caused moderate enzyme inhibition and was more effective against pathogenic fungus. The results of the current study indicated that MB-ZnO nanocomposites could be applied as effective catalysts in various processes. Moreover, this research provides valuable and the latest information to the readers and researchers working on biopolymers and nanocomposites.

**Keywords:** nanotechnology; MB-ZnO nanocomposite; ball-milling; SEM; XRD

## Article

# Diagnosis and Control of Brown Leaf Spot of Kiwi (*Actinidia deliciosa*) Using Biochar-Zinc Oxide Nanocomposite (MB-ZnO) as a Non-Toxic Bio-Fungicides

Asif Kamal<sup>1</sup>, Musrat Ali<sup>1</sup>, Dunia A. Al Farraj<sup>2</sup>, Enshad M. Al-Zaidi<sup>2</sup>, Maria Khizar<sup>1</sup>, Reem Amer Aljaaidi<sup>2</sup>,  
Mohmed S. Elshikh<sup>2</sup>  and Muhammad Farooq Hussain Munis<sup>1,\*</sup> 

<sup>1</sup> Department of Plant Sciences, Faculty of Biological Sciences, Quaid-i-Azam University, Islamabad 45320, Pakistan

<sup>2</sup> Department of Botany and Microbiology, College of Science, King Saud University, P.O. Box 2455, Riyadh 11451, Saudi Arabia

\* Correspondence: munis@qau.edu.pk

**Abstract:** Kiwi is one of the best natural sources of vitamin C and has wide applications. During October–November 2021, small brown spots were examined on the Kiwi leaves. The diseased leaf samples were collected and placed on potato dextrose agar nutrient media for diagnosis. Morphological, anatomical, and molecular studies revealed this disease-causing agent to be *Rhizopus oryzae*. Molecular characterizations of the isolated pathogen were performed by using actin translation elongation factor (EF-1 $\alpha$ ) and ribosomal deoxyribose nucleotide inter transcribed sequence (rDNA ITS ITS1/ITS4) and elongation factors (EF1-F/EF1-R) primers. A BLAST study of the resultant ITS1/ITS4 sequence showed > 99% resemblance with *R. oryzae* (MT603964.1), while the EF-1 $\alpha$  sequence revealed 100% similarity with translation elongation factor-1 $\alpha$  gene of *R. oryzae* (MK510718.1). The obtained ITS1/ITS4 sequence was submitted to NCBI (MW603842.1). Koch's postulates established the pathogenicity of isolated *R. oryzae* and proved it to be the brown spot pathogen of Kiwi. For the environmentally-friendly management of Kiwi leaf spot, maize biochar-Zinc Oxide (MB-ZnO) nanocomposite was used. The prepared nanocomposite was characterized by Fourier transform infrared (FTIR) spectroscopy, thermo gravitational analysis (TGA), X-ray diffraction (XRD) analysis, scanning electron microscopy (SEM), and energy dispersive X-ray (EDX) analysis. After successful preparation, MB-ZnO was assessed for its possible antifungal potential against *R. oryzae*. MB-ZnO displayed substantial growth inhibition, and the highest growth inhibition (79%) was observed at a 19 mg/mL dose rate of nanoparticles. These excellent findings propose that Ball-milled synthesis is a fast, economical, and environmentally friendly method for nanocomposite in the near future. The nanocomposite is used as a nominal substitute for chemical fungicides.

**Keywords:** *Rhizopus oryzae*; Kiwi; ITS region; EF-1 $\alpha$  gene; MB-ZnO



**Citation:** Kamal, A.; Ali, M.; Farraj, D.A.A.; Al-Zaidi, E.M.; Khizar, M.; Aljaaidi, R.A.; Elshikh, M.S.; Munis, M.F.H. Diagnosis and Control of Brown Leaf Spot of Kiwi (*Actinidia deliciosa*) Using Biochar-Zinc Oxide Nanocomposite (MB-ZnO) as a Non-Toxic Bio-Fungicides. *Crystals* **2023**, *13*, 98. <https://doi.org/10.3390/cryst13010098>

Academic Editor: Eamor M. Woo

Received: 12 November 2022

Revised: 6 December 2022

Accepted: 19 December 2022

Published: 5 January 2023



**Copyright:** © 2023 by the authors. Licensee MDPI, Basel, Switzerland. This article is an open access article distributed under the terms and conditions of the Creative Commons Attribution (CC BY) license (<https://creativecommons.org/licenses/by/4.0/>).

## 1. Introduction

Kiwi (*Actinidia chinensis*) is a perennial vine, and it is usually known by several other names, such as Chinese gooseberry, monkey peach, and sheep peach. Kiwi contains more "Vitamin C" than citrus and is delightful in taste. In the 1950s, Kiwi was first introduced in New Zealand [1]. In recent times, Italy has been the leading Kiwi-producing country (415,877 tons yield); second on the list is New Zealand (378,500 tons production) [2]. Other countries, such as Japan, Iran, Canada, France, Chile, and the USA also produce Kiwis in a great amount. Because of its distinct flavor and high nutritional value, efforts are being made to increase Kiwi production and its utilization in various traditional medicines [3,4]. Its different plant parts, including the root, stem, and leaves contain different health-friendly bioactive compounds [5]. More than 70 species of Kiwi have been grown in the world. Kiwi is considered a tropical plant as it has no tolerance to lower than 10 °C temperature [5].